TRNSYS Modeling of the NIST Net Zero Energy Residential Test Facility

by

Brian P. Leyde

A thesis submitted in partial fulfillment of
the requirements for the degree of

MASTER OF SCIENCE
(MECHANICAL ENGINEERING)

at the

UNIVERSITY OF WISCONSIN – MADISON

2014

Blank

Approved by

_____

Professor Sanford A. Klein

_____

Professor Gregory F. Nellis

Date:_____

Blank

Abstract

The objective of this research was to investigate energy saving equipment configurations and control strategies for high efficiency residential buildings. It is based on the National Institute of Standards and Technology's (NIST) Net Zero Energy Residential Test facility (NZERTF) which is designed to produce more electricity over the course of a year than it consumes.

In order to meet this objective, the NZERTF was modelled in the transient system simulation program TRNSYS 17. This model was compared with an EnergyPlus model of the Test Facility and experimental data from Test Facility. The TRNSYS simulation predicted that the total electrical energy consumed by the Test Facility would be 6.84% less than predicted by the Energy Plus Model and 3.42% less than recorded by the Test Facility. The TRNSYS model predicted that the total electricity generated by the Test Facility would be 3.35% less than predicted by the EnergyPlus simulation and 19.91% greater than recorded by the Test Facility. The reasons for these differences in total consumption and generation, as well as differences observed in subsystems, were investigated and documented.

The TRNSYS model was used as a basis to test variations of the Test Facility HVAC and domestic hot water systems. The most successful model variations involved changes to the HVAC controls due to decreased use of an auxiliary electric heater resulting in a 9.2% decrease in predicted total electrical consumption. The next most successful variation was the use of a large ground source heat pump system which resulted in an 8.5% decrease in the predicted total electrical consumption. The least successful model change was the replacement of a solar hot water and heat pump hot water heater system with a tankless

electric resistance hot water heater which resulted in a 38.7% increase in the predicted total electrical consumption.

In addition, several separate models were created to investigate the vertical ground loop heat exchanger (GLHX) at the Test Facility. An investigation into GLHX model parameter determination resulted in the development of a parametric optimization and visualization technique dubbed the Crossed Contour Method. It was also found that there was significant uncertainty in model parameter estimates made from Thermal Response Tests and that this has implications for ground source heat pump performance.

Acknowledgments

Though I have done this work and written these words, without many others I would not have had the opportunity to start, the direction to continue, or the ability to finish.

First, I would like to thank my advisers Dr. Sanford A. Klein and Dr. Gregory F. Nellis. They have challenged and supported me in every aspect of this project and their contribution extends far beyond providing ideas, critical feedback, analysis, and focus. They have taught me more about engineering, problem solving, professionalism, and life than I have yet realized. Working with them and taking their classes has been a privilege.

Second, I would like to thank Dr. Harrison Skye who was my main contact at NIST. Without his work, insight, and questions this project would not have been possible. The help of Harrison and the HVAC&R Equipment Performance Group has been invaluable.

I would also like to thank Dr. Franklin Miller who served as the third member of my thesis committee. His teaching and our diverse conversations have always been enlightening.

Many others have also contributed to my ability to complete this project. Jeff Thornton and Matt Duffy of TESS were helpful both in my initial TRNSYS training and in answering any questions about ground loop modeling. My lab mates Amanda Pertzborn and Russell Knudsen provided insights into TRNSYS, geology, heat-pumps, HVAC systems, and why someone would take the stairs to get to an office on the 13th floor.

Lastly, I would like to thank those who have supported me and helped me keep things in perspective over the last few years. Amir Jahromi found many of my sign errors. Kasia made

sure I stopped to have some ice cream. Some of the other class and SEL mates who have made Madison more enjoyable, interesting, and educational: Qi, Yerzhigit, Nathan, Renzhuo, Brad, Erik, Rogelio, John, Wenjie, Diego, Fritz, Kelsey, Joe, Avi, Evan, Alle, and many others I won't list here. I am glad that I have met each and every one of you.

Table of Contents

List of Figures

List of Tables

Nomenclature

Symbol	Units	Definition
$\boldsymbol{a}$	m^2/s	Thermal Diffusivity
$\boldsymbol{\alpha_f}$	m^2/s	Predicted effective thermal diffusivity of the geological formation
$\boldsymbol{b_x}$	varies	In the hybrid map derivation. Represents a linear offset.
C_f	kJ/m^3	Predicted effective volumetric heat capacity of the geological formation
$\boldsymbol{H_b}$	m	Depth of the borehole
K_f	W/m-K	Effective thermal conductivity of the geological formation
$\dot{\boldsymbol{Q}}$	W	The steady heat input rate to the borehole
$\boldsymbol{r}$	m	Radius from center of borehole
$\boldsymbol{R_{bt}}$	W/m-K	Borehole Resistance
$\boldsymbol{r_b}$	m	Borehole Radius
s	K/ln(s)	the slope of the linear regression of temperature with the natural log of time
$\boldsymbol{t}$	s	Time from begging of TRT
$\boldsymbol{t_{init}}$	s	Time at the beginning of the analysis relative to TRT start time
$\boldsymbol{T(r,t)}$	K	Temperature of the formation as a function of radius and time
T_0	K	Effective undisturbed temperature of the geological formation
$\boldsymbol{T_b}$	K	Mean borehole surface temperature
$\boldsymbol{T_f(t)}$	K	Mean working fluid temperature in the borehole
$\boldsymbol{T_{f,in}}$	K	Working Fluid Temperature at GHX inlet
$\boldsymbol{T_{f,out}}$	K	Working Fluid Temperature at GHX outlet
$\boldsymbol{u}$	-	Independent variable (placeholder in integration)
$\boldsymbol{\gamma}$	-	Euler's constant: 0.5772

Acronyms

%RH	Percent Relative Humidity
AHU	Air Handling Unit
CSM	Cylindrical Source Model
DBT	Dry Bulb Temperature
DHW	Domestic Hot Water
DHW HP	Domestic Hot Water Heater Heat Hump
GLHX	Ground Loop Heat Exchanger
HRV	Heat Recovery Ventilator
HVAC	Heating Ventilation and Air-conditioning
HVAC HP	Heating and Air-conditioning Heat Pump
ID	Indoor
LSM	Line Source Model
LSM	Infinite Line Source Model
NIST	National Institute of Standards and Technology
NZERTF	Net Zero Residential Test Facility
OD	Outdoor
PV	Solar Photo Voltaic
SHW	Solar Hot Water
TMY	Typical Meteorological Year
TRT	Thermal Response Test
TRT	Thermal Response Test
WBT	Wet Bulb Temperature
Z1	Zone 1 (basement)
Z2	Zone 2 (1^{st} floor)
Z3	Zone 3 (2^{nd} floor)
Z4	Zone 4 (attic)

Chapter 1: Project Background and Purpose

1.1 Building Energy Use

The overall objective of this project is to investigate energy saving equipment configurations and control strategies for high efficiency residential buildings. This research is motivated by the need for improved building energy efficiency while maintaining current standards of living and building performance. This reduction in energy consumption is necessary both to reduce the use of fossil fuels, which are problematic due to their limited reserves and environmental impacts, and to provide energy cost savings and economic benefits. The Department of Energy (DOE) reports that in 2009, the residential housing sector accounted for 22% of the primary energy used in the U.S and that 49% of this energy was lost as heat to the environment during electrical generation, transmission, and distribution rather than being supplied to the residential end use. The nature of transmission and distribution losses makes end use conservation and generation in residential settings an extremely effective method of primary energy reduction. The DOE also forecasts that residential energy consumption will continue to increase with the increasing population but expects the increase to be partially ameliorated by "projected improvements in building and appliance efficiency" (U.S. DOE, 2012). Advances in residential housing efficiency could, and are in fact expected, to contribute substantially to the overall reduction in the use of fossil fuels.

While reduced energy consumption and distributed renewable energy generation both contribute to reducing the use of fossil fuels, they do not necessarily result in net zero energy houses. The term 'Net Zero Energy' requires clarification as it has several possible meanings. In this project it will be defined as a site that "produces as much electricity as it consumes

over an entire year" (Kneifel, Sep. 2012) and also does not rely upon any off site energy source other than the electrical grid, such as natural gas or coal. This definition averages out the extremely variable demand and generation profiles of individual sites and shifts daily and seasonal storage considerations to the grid operators and utility power generators. As most existing infrastructure and new construction are grid-connected, this definition is also the most likely operating regime for a future net-zero house in a cooling-dominated location.

1.2 Building Energy Efficiency

Building energy efficiency measures start with the building structure itself. The building envelope provides thermal insulation as well as structural support and determines the amount and quality of sunlight entering the building. In regions where heating loads are large (e.g., the American Northeast and Midwest) and/or cooling loads are large (e.g., the American Southeast and Southwest), the building envelope has a large effect on the total HVAC energy use. The equipment used inside a structure is another major driver of the buildings energy use. This equipment is used to provide heating, ventilation, and air conditioning (HVAC), domestic hot water (DHW), lighting, and appliance services such as cooking and refrigeration. There are numerous options available and ratings such as Energy Star or LEED to aid in decision making processes. However, what is feasible from an engineering stand point is not necessarily economically competitive and the most efficient technology varies depending on the building, climate, and internal loads. Thus each scenario requires a specific solution.

1.3 Building Energy Modeling

Building energy modeling is the process of creating a model of a building's energy consumption, use and efficiency. These models are then used to predict building energy use

and economics in order to better match structures, equipment, and control strategies to different scenarios and desired outcomes. This process allows details of implementation and economics to be explored before the much more expensive construction process begins.

There are numerous software packages specifically for building energy modeling. The program used for this project is TRNSYS 17 (Thermal Energy System Specialists LLC, 2012) which is a flexible transient system simulation program that has many built in models of building, HVAC, and energy generation equipment. Another prominent building energy simulation software is EnergyPlus, which is a rate controlled building energy simulation software derived from DOE2 and maintained by the Department of Energy. EnergyPlus was used to create the "Annual Whole Building Energy Simulation of the NIST NetZero Energy Residential Test Facility Design" (Kneifel, 2012a) and was used to perform initial analysis of the Test Facility Design. TRNSYS and EnergyPlus are both effective modeling packages, however TRNSYS offers more flexibility both in terms of simulation type but also simulation equipment and parameters. Thus it was decided that a TRNSYS simulation of the Test Facility would provide added utility.

1.4 NIST Net Zero Energy Residential Test Facility

The National Institute of Standards and Technology (NIST) built and began operation of the Net Zero Energy Residential Test Facility (NZERTF or Test Facility) in order to demonstrate that net-zero energy residential homes could maintain the appearance and comfort levels of a typical suburban home and to provide a Test Facility for further investigations into residential energy efficiency and economics. The Test Facility was completed in 2012 and features a wide array of energy efficiency measures, energy efficient equipment, and

instrumentation for recording the results of yearlong experimental runs. The building envelope includes increased insulation, triple paned windows, and extremely tight construction to reduce thermal energy transfer and unwanted air infiltration. The structure is also situated in such a way as to maximize winter solar input and shaded to reduce summer solar input.

The HVAC systems include heat recovery ventilation, provided by a Venmar AVS HRV EKO 1.5, in order to reduce heating and cooling energy while meeting the ventilation requirements. For heating, cooling and dehumidification the Test facility uses an AAON F1-B-024-1-V-B air source heat pump. The domestic hot water is provided by 4 Heliodyne GOBI 406 001 flat plate solar hot water collectors, a Heliodyne HPAK heat-exchanger and storage tank, and a Hubbell PBX 50SL air-to-water heat pump hot water heater. The internal equipment, appliances, water fixtures, and lighting systems were selected to be highly energy efficient while maintaining expected performance levels. To provide electricity generation and allow the facility to meet its net zero energy goals, 32 SunPower SPR-320E-WHT-U solar PV panels were installed on the roof connected to two SunPower SPR-5000m inverters which were installed in the attic space.

1.5 The Goals of this Project

The overall objective of this project is to investigate energy saving equipment configurations and control strategies for high efficiency residential buildings and specifically for the NZERTF. The transient system simulation tool, TRNSYS, was used to model the NIST Net Zero Energy Residential Test Facility and predict the thermal and electrical energy demands of the Test Facility as a whole and of each individual subsystem and component.

Modeling a single house very accurately will not necessarily yield results that translate to a neighboring structure and therefore it is more useful to do comparative studies of changes to a representative structure. As the purpose is to reduce the influence of the exact structure involved on the conclusions about the impacts of the changes being modeled, it is of less importance to precisely match a specific structure. While efforts were made to match the TRNSYS Model to data collected from the NZERTF using the TRNSYS model, the project focused on relative comparisons. These comparisons involve running control and test cases for different equipment configurations and control strategies in a similar manner to the work previously done by Greg Marsicek on heat pump sizing and economics (Marsicek, 2012). This method allows recommendations to be made about both the Test Facility and its configuration for future experimental runs and about building energy efficiency measures in general.

Chapter 2: House Envelope and Load Model

2.1 House Envelope Model Development

2.1.1 Purpose of the House Envelope and Load Model

The main reasons for trying to match the model specifically to the Test Facility were to allow for the model to be verified with experimental data and to provide the ability to predict the performance of the facility with different equipment installed. This capability can then be used to aid experiment selection and design, equipment selection, and the simulation of systems that would be difficult or impossible to implement in the actual Test Facility. However, for these purposes the TRNSYS full house model's ability to very precisely match the EnergyPlus model or the Test Facility based upon nominal design parameters is less important than its ability to produce accurate building loads behavior as long as it properly predicts trends. If the TRNSYS full house model captures the general behavior of the Test Facility, it can be used to aid ongoing efforts and it can be calibrated to more precisely match test data as the project proceeds.

The TRNSYS Full House Model was initially split into a house envelope and load model and an HVAC system model. The purpose of separating the models was to allow the thermal performance of the TRNSYS simulated house geometry, envelope, and loads to be evaluated independently of the HVAC, water heating and solar equipment models.

The utility of modeling the envelope and gain schedule of the Net Zero Energy Residential Test Facility, NZERTF, using TRNSYS is to provide a more accurate base for evaluating

HVAC equipment and control system changes as well as allowing variations in the climate, construction quality, and building design. Though it is possible to feed modeled loads from the NIST EnergyPlus model or measured loads from the Test Facility directly into TRNSYS, a prerecorded load profile would not account for feedback from the TRNSYS equipment model and consequent changes in the house load due to alterations in temperature or air flow. Accounting for this feedback is particularly important as the TRNSYS simulations and the Test Facility itself would then not precisely follow the temperature set points. In fact failing to precisely follow the temperature set points may even be desirable for energy conservation if reasonable comfort levels can be maintained. It is thus necessary that the model be able to take into account the changes in temperature and load due to the equipment explicitly modeled in the TRNSYS full house model.

2.2 Design and Implementation of the House Envelope and Load Model

The House Envelope and Load model used a TRNSYS3d model of the NZERTF along with modified versions of the resident occupancy schedule, the temperature set point schedule, and the internal electrical gain and water demand schedule used in planning the operation of the Test Facility: "Narrative Schedule for a Typical Monday V2.xlsx" (Harrison? Skye & NIST, 2012). Infiltration was handled by an Infiltration Model component using the equivalent leakage areas as reported in J. Kneifel's documentation of the NIST EnergyPlus model (Kneifel, 2012a) and the Building Science Corporation's note on Advanced Construction Documentation (Building Science Corporation, 2011). All of the components were then linked together into a larger TRNSYS Envelope and Load model which is provided in the electronic supplement and is shown in Figure 2-1. This model was run with

the TMY3 data file for Washington DC Dulles International Airport (file name: 'Washington Dc Dulles Int'l Ar [Sterling - ISIS]_724030TY.csv') (NREL, n.d.). The TRNSYS Envelope and Load model output the total thermal energy gain per month from electric appliances, occupants, and infiltration. The model also output the water consumption per month, and the temperatures of the 1st and 2nd floors. The energy required to meet a temperature set point schedule was calculated assuming that the nominal HVAC equipment capacities were available and that some deviation from the temperature set points was acceptable.

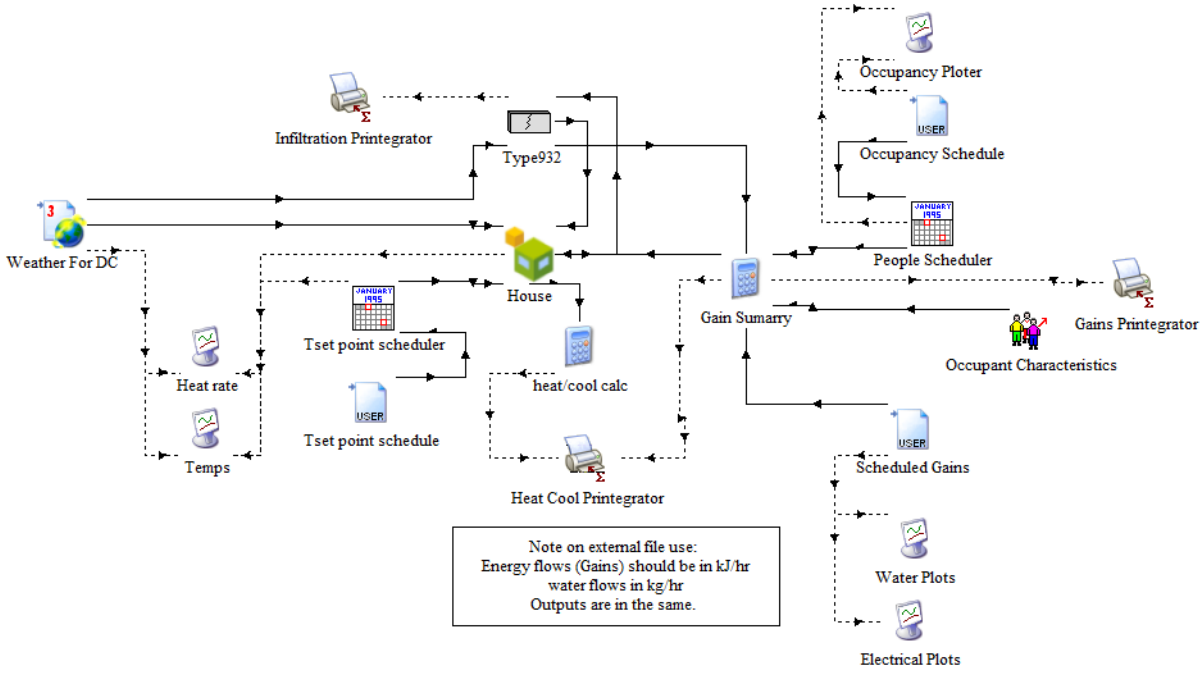

Figure 2-1: Diagram of TRNSYS Initial House Envelope and Load Model

2.3 House Structure and Envelope Modeling

A CAD model of the Test Facility was created using the TRNSYS3d plug-in for Google SketchUp. The CAD model, shown in Figure 2-2, was based on the Building Science Corporation's NIST Net Zero Energy Residential Test Facility As Built Architectural Plans (Building Science Corporation, 2009). Because the objective of this research is more to

investigate equipment configurations and control schemes than the building structure itself, a fairly simple model of the Test Facility was considered to be sufficient to provide simulated loads and responses.

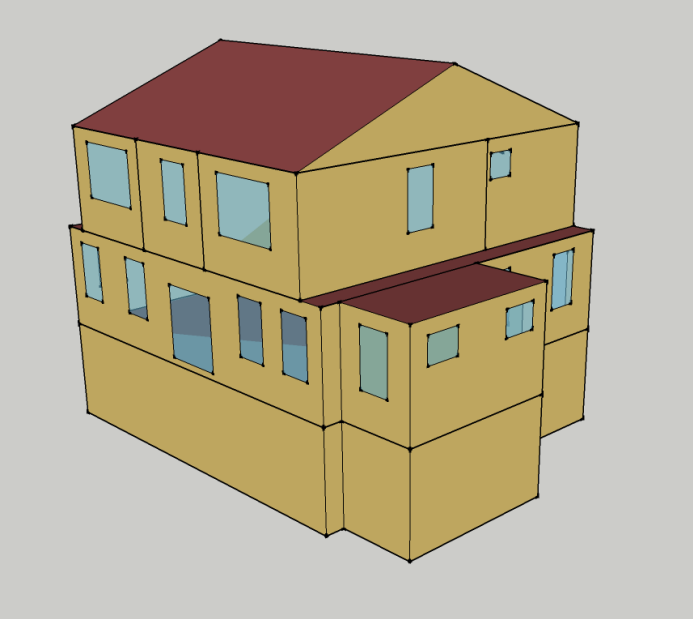

Figure 2-2: TRNSYS3d model of the Test Facility rendered in Google SketchUp

2.3.1 Zone Choices

The CAD model built in TRNSYS3d follows the EnergyPlus model and the Test Facility temperature control system in dividing the house into four vertical zones: **Basement, Main Floor, Second Floor, and Roof/Attic space**. These zones are labeled throughout the project as Z1, Z2, Z3, and Z4 respectively. The Basement and Attic space are both unoccupied and, in the TRNSYS Envelope and Load model, currently unconditioned. The basement contains much of the HVAC and hot water equipment and the attic contains solar equipment that adds to the thermal loads in each zone.

The basement is open and usually closed off from the rest of the house which should result in a uniform temperature. The **Basement** zone in the TRNSYS Envelope and Load model is entirely open allowing air to circulate freely. The Basement alcove**,** along with the Main Floor Alcove and Stair Well**,** were originally not modeled in order to maintain compatibility with the more detailed radiative heat transfer model available in TRNSYS. It was later decided that the simpler radiative heat transfer model is more than sufficiently accurate and the Basement and Main Floor Alcoves were added.

The **1st Floor** is a mostly open design with the only isolatable areas, not including closets, being a small bedroom/office and the bathroom. As such it was decided a single zone model should be sufficient to capture most of the thermal behavior. In order to account for the mass of unmodeled interior walls, the thermal mass per unit area of 'furniture' specified in the TRNBuild program was increased from the furniture mass specified in the EnergyPlus model documentation. The total thermal mass of the unmodeled interior walls is thus distributed evenly across the first floor.

The **2nd Floor** was also modeled as a single zone. Though the second floor is less open than the 1st Floor, it was decided to consider it as a single zone in the model to match the existing temperature control zones. If detailed occupant comfort measurements become more important in the future, it would be possible to separate the 2nd Floor into sub zones as the bedrooms are occupied and likely to be closed for more time than most of the other rooms. As with the first floor, the thermal mass per unit area of 'furniture' was increased from the estimated mass of just the furniture in order to account for unmodeled interior walls.

The main **Roof/Attic** space was modeled as a single open unconditioned zone. **The lower eves** and resultant alcove spaces were left out of the current model as they added little area to the zone being modeled, resulted in a large number of small connected zones which are problematic when using the high detail radiation model. For purposes of mechanical system modeling, the eves and alcove spaces are most likely an unnecessary level of detail. The change in surface area was made up for by shifting the modeled **outside walls** 6 [in] out from their actual positions.

Table 2-1 gives the parameters for the four zones and

Table 2-2: Area Differences between Models and NZERTF

	Total Floor Area [m2]	Difference [m2]	% Difference (a-b)/b*100
NZERTF	252	-	-
EnergyPlusModel	285	33	13.1%
TRNSYS Envelope and Load model	256	4	1.7%

compares the total conditioned floor area for the Test Facility, EnergyPlus Model, and the TRNSYS Envelope and Load model.

Table 2-1: Improved TRNSYS Envelope and Load model Zone Statistics

Zone Number	Name	Floor Area [m^2]	Volume [m^2]	Exterior Surface Area [m^2]	Adjacent Surface Area [m^2]	Window Area [m^2]	Interior Thermal Capacitance [kJ/K]
Z1	**Basement**	142	432	295	142	0	519

Z2	**First Floor**	142	447	186	256	30	13796
Z3	**Second Floor**	114	360	135	229	17	12538
Z4	**Attic**	114	122	147	114	0	147

Table 2-2: Area Differences between Models and NZERTF

	Total Floor Area [m^2]	**Difference [m^2]**	**% Difference (a-b)/b*100**
NZERTF	252	-	-
EnergyPlusModel	285	33	13.1%
TRNSYS Envelope and Load model	256	4	1.7%

2.3.2 Surfaces Properties

All of the layers used in the construction of the various surfaces (wall, floors, ceilings, windows etc) were input in the TRNBuild utility program during the TRNSYS building model component generation process. The layers were matched to the construction details specified in the as built NZERTF construction plans (Building Science Corporation, 2009). Thin layers such as vapor barriers and sealing tar have very small thermal capacitance and result in TRNSYS failing to converge during simulations and have been omitted. Infiltration rates are being adapted from empirical data and moisture penetration of wall layers is currently not of interest in this project. The basement floor was modeled without the radiant heating system as it does not greatly change the passive thermal characteristics of the floor. If the radiant heating system is modeled later, it will need to be added as a layer in the TRNBuild utility and then integrated as part of the hydronic system in the TRNSYS Envelope and Load model. The properties of each material were taken from the TRNBuild default library and Engineering Toolbox (Engineering Toolbox, 2009). Tables of the layer

materials, material properties, and layer thicknesses are included in 'Wall Construction.xlsx' in the electronic supplement.

The majority of the material properties (ex: gypsum board, fiberglass) are already included in TRNBuild libraries. Details on the foil faced Polyisocyanurate and expanded foam insulations used on the construction were taken from the Building Science Corporation's Guide to Insulating Sheathing (Building Science Corporation, 2007).

A significant point of deviation from the specified wall structure is the current model of frame bridging. An equivalent thermal resistance for the wall layer which included the framing was calculated based on the thermal resistances for insulation and framing components and the fraction of the area of each wall composed of these components. A conservative estimate for the average percentage of framing of 20% was used for all above ground walls and 6% for the basement walls. The basement wall framing area is much lower because structural support is provided by concrete slabs and the wooden frame serves only to support the insulating panels and dry wall.

The window specifications were not in the as built documentation so the heat transfer property values were taken from the EnergyPlus model file provided by J. Kneifel and matched to windows in the TRNSYS window library. The window properties specified were a very close match to the TRNBuild model of the Saint Gobain CLIMAPLUS FUTUR KR (TRNBuild ID 13003) which was then used in the TRNBuild model. The change from the default window implementation had a noticeable and expected effect in lowering thermal losses and solar gains. The doors were modeled as windows, as is any penetration in a TRNBuild wall, and were set to the same parameters as the windows.

2.3.3 Infiltration Model

A TRNSYS TYPE 932 Infiltration Model component was used to set infiltration rates into the first and second floors. This component implements the same infiltration model used in the EnergyPlus simulation: the Sherman Grimsrud model recommended by ASRAE (Grimsrud, 1980). The TYPE 932 allows the Stack and Wind coefficients to be set manually from a lookup table of building heights and wind shielding classes. To match the EnergyPlus model the Stack Coefficients and Wind Coefficients for both floors were set to constants taken from the EnergyPlus simulation file, yielding values of 0.00029 [1/K] and 0.000325 [-] respectively. These values are recommended for a two story building with light site shielding as would be provided by a shed or a few trees. Kneifel's method of partitioning the equivalent leakage area by floor area was used. The preliminary blower door test value of 69 [ft^3/min] at –50 [Pa] to outside (Building Science Corporation, 2011) was converted to an equivalent leakage area at 5 [Pa] and split by floor area leading to ELAs of 103 [cm^2] for the 1st Floor and 86 [cm^2] for the second 2nd Floor (Kneifel, 2012a).

2.3.4 Thermal Capacitance and Internal Convection

TRNSYS includes thermal mass of the wall and floor construction in the zone boundary walls and floors but it does not include the thermal capacitance of unmodeled interior partitions (interior to a modeled zone) or of occupant's furniture and possessions. The thermal capacitances were already estimated for the EnergyPlus model (Kneifel, 2012b) and are reused here as the zone shapes are similar and the assumptions behind them are equally applicable. The estimated capacitances were input in TRNBuild. The first and second floor capacitances were estimated as 13,448 [kJ/K] and 12,273 [kJ/K] respectively. The thermal capacitances of the basement and attic spaces due to interior contents were calculated by

multiplying the volume of the spaces by the heat capacity of enclosed air and were 471 and 143 [kJ/K] respectively. It is important to note that the thermal capacity of the walls, floors, and ceilings of the zones are calculated separately by the TRNBuild program. Thus the actual thermal capacitance of any given zone is significantly higher than just the air and material within it. For the Attic and Basement the majority of the thermal capacity is found in the zone surfaces.

TRNSYS is capable of running an internal convection model for building zones. However this option does not work in conjunction with geometrically unspecified thermal inputs of the sort used to specify the electrical and occupational gains. Because of this limitation, the internal convective heat transfer coefficients have been left at the default value of 11 [W/m^2-K].

2.3.5 Temperature Set Points

The temperature set point schedule used in the TRNSYS Envelope and Load model is a modified version of the one used in the EnergyPlus model. The same temperature values were used for heating and cooling and the schedule is the same except for Tuesday and Thursday for which the unoccupied time was extended to match the rest of the work week for use with the TRNSYS Type 41a Load Profile Sequencer. Figure 2-3 shows the heating and cooling set points for the first week of the simulation as well as the temperatures calculated for each of the zones during a sample week.

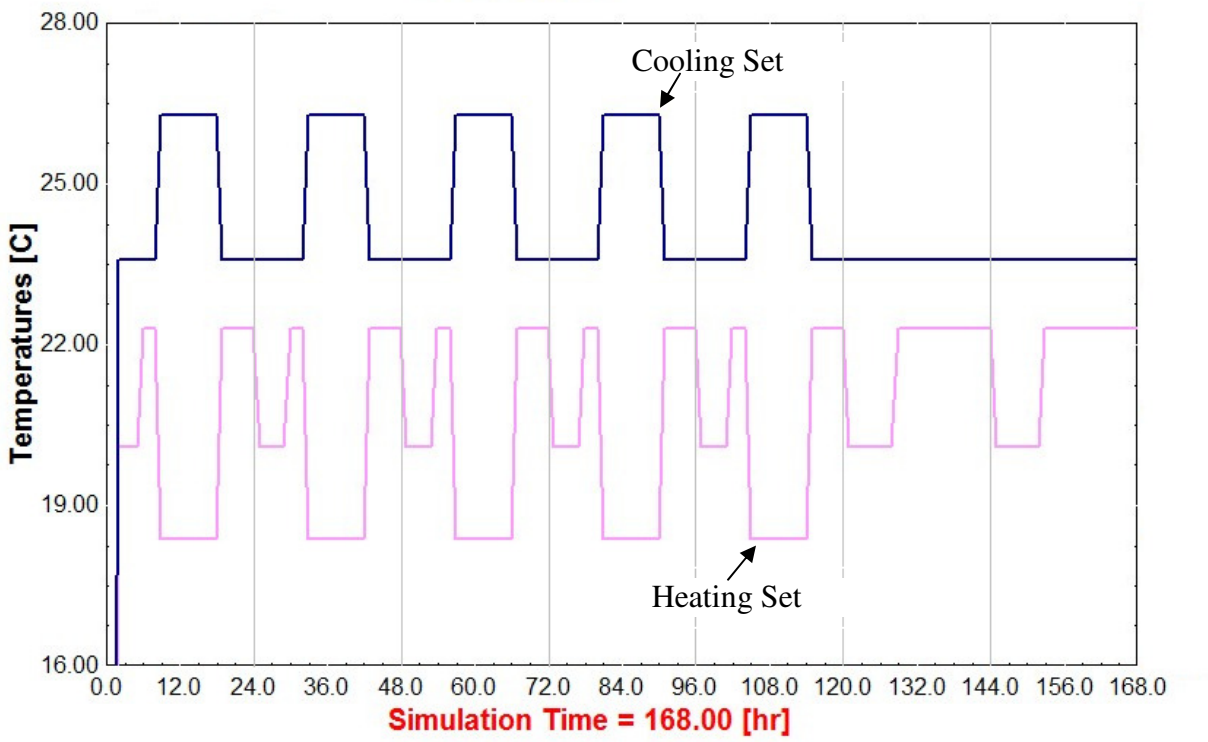

Figure 2-3: Weekly Set Point Temperature Schedule

2.3.6 Placeholder HVAC System

For the initial Building Envelope and Load Model, there was some concern that the use the use of square wave temperature set points in the preliminary house load model would result in unrealistic hourly heating and cooling requirements. To avoid this problem, the maximum capacities of the placeholder HVAC system were set to the anticipated capacities of the equipment in the As Built Diagrams. In the Baseline models this place holder HVAC system has been replaced by the system documented in Chapter 4. The anticipated nominal heating and cooling capacities for the primary air handling unit (AHU-1) as outlined in the As Built documentation are 25.6 MBH (7.5 [kW], 27 [MJ/hr]) and 36.6 MBH (10.7 [kW], 38.5 [MJ/hr]). The maximum heating and cooling values of the simple placeholder HVAC system were set to the anticipated nominal equipment capabilities to ensure that the load outputs

were reasonable for any independently modeled equipment and to allow the zone temperatures to deviate in a more realistic manner.

2.3.7 Electrical and Water Use Schedule

The electrical and water use schedules used were generated from the gain schedule included in a "Narrative Schedule for a Typical Monday V2" (Harrison? Skye & NIST, 2012). To generate the TRNSYS schedules, the zone in which an activity occurs was entered into an EXCEL sheet and then a MATLAB function was used to integrate the data into minute and hourly water and power consumption schedules for each zone. The schedules were recorded to '.csv' files which TRNSYS reads during the simulation. The MATLAB function used was 'schedule_integrator.m' and is documented in Electronic Supplement. The typical Monday schedule was reused for each day of the simulation. The use of a single daily load profile provides a good estimate of utility consumption for weekdays but typically underestimates consumption for weekends.

The lighting schedule and an unknown difference in internal equipment electrical use are included as continuous electrical loads and thermal gains. In order to facilitate testing of other parts of the model, constant heat inputs were added to match the EnergyPlus models monthly contributions from these sources.

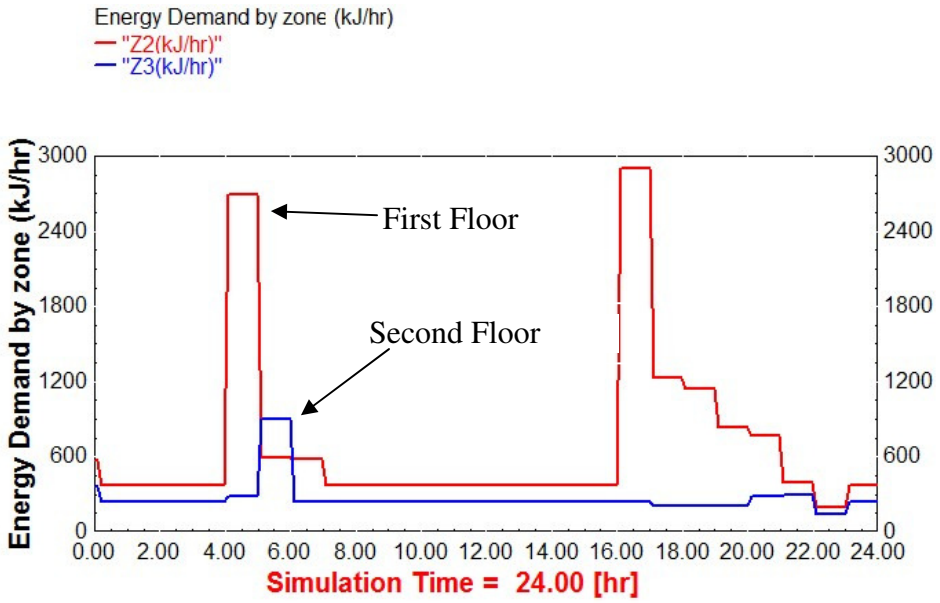

Figure 2-4: Daily Electrical Demand Schedule

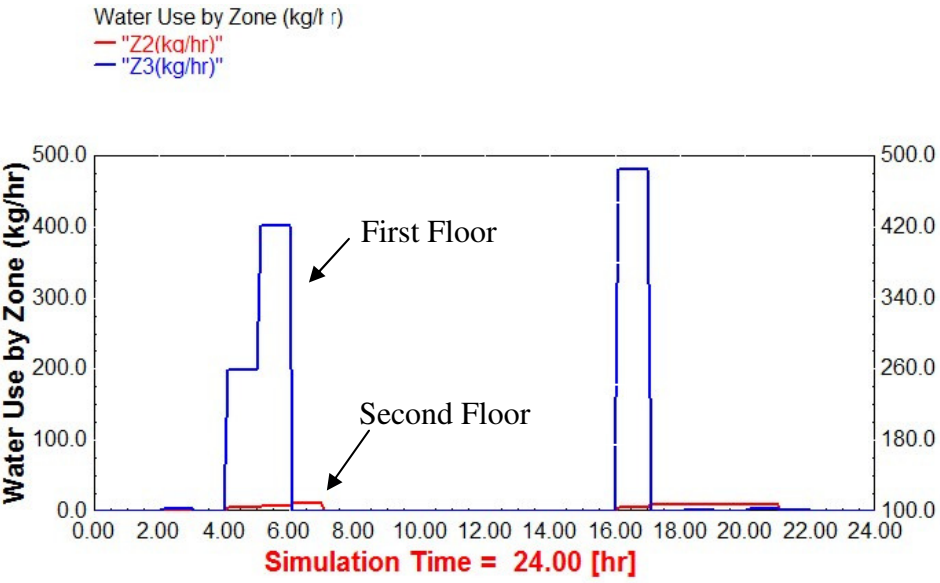

Figure 2-5: Daily Water Use Schedule

2.3.8 Occupancy Schedules

An occupancy schedule was created based on 'Figure 4.1 Occupancy Density' in the NIST technical note (Kneifel, 2012a). The occupied times were split between the two conditioned zones with the second floor being occupied during all expected sleep times and the ground

floor for the remainder of the occupied time. As with the temperature set point schedule, the Tuesday and Thursday schedules were made identical to those for the rest of the work week. The occupant thermal loading per person per unit time was set to the levels used in the EnergyPlus model.

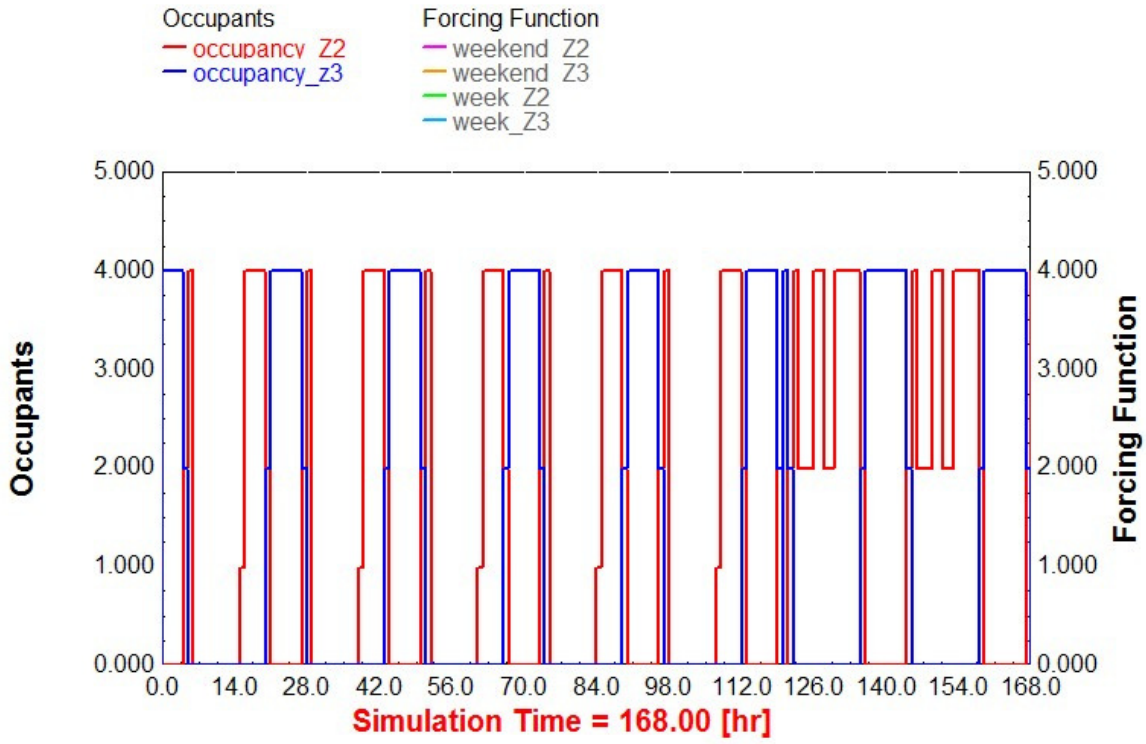

Figure 2-6: Weekly Occupant Schedule by Zone

2.4 Initial House Envelope and Load Model comparison with the EnergyPlus Model

The combination of the simple house model and the modified load schedules yielded results similar to, but notably different, from the results reported for the EnergyPlus NZERTF model. These results are reported here as this model was used to generate the load file for the subsequent geothermal heat pump investigation.

The internal heat gains for the 1st floor of the EnergyPlus NZERTF model and the TRNSYS Envelope and Load model are shown in Figure 2-7. The top figure is "Figure 5.13 Internal Heat Gains by Category (kWh) – 1st Floor" (Kneifel, 2012a). The overall values of the heat gains are quite close: the EnergyPlus model averages 323 [kWh/month] and the TRNSYS Envelope and Load model averages about 2.8% higher at 332 [kWh/month]. The differences in gains are due to the TRNSYS Envelope and Load model using a different electric gain schedule that does not include variations for the different days of the week and particularly the relatively energy intense weekend. This missing electrical load is made up for with an equivalent base load.

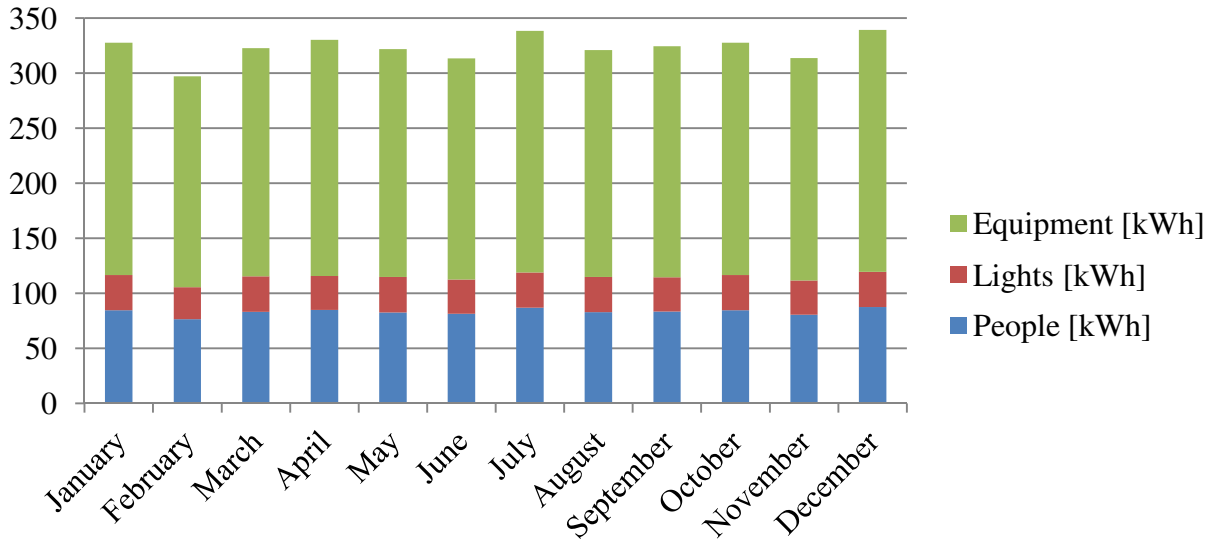

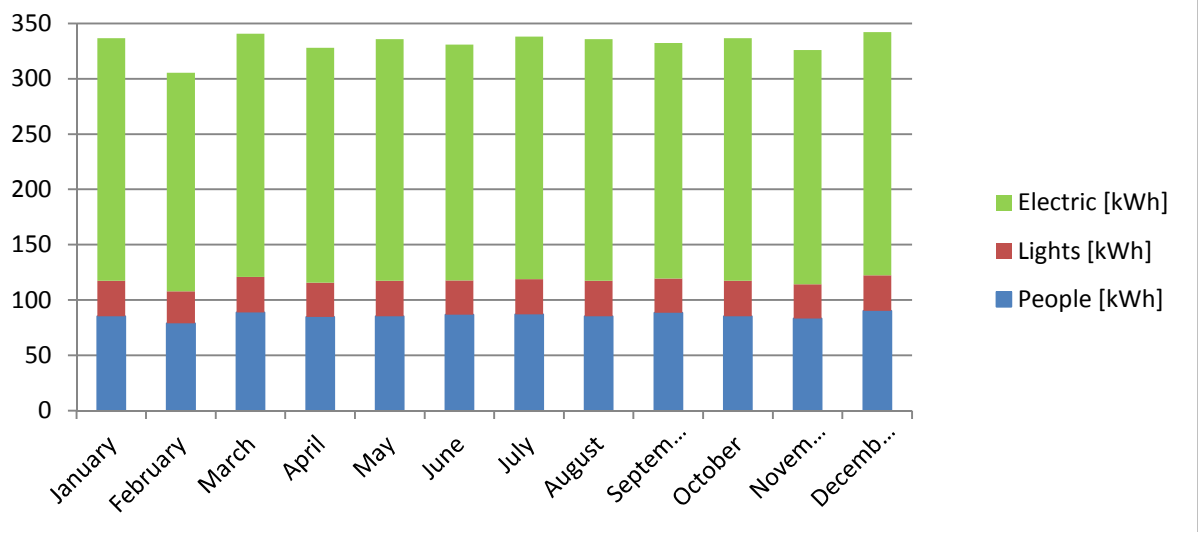

Figure 2-7: Comparison of Internal Heat Gains 1st Floor. The top graph is "Figure 5 13 Internal Heat Gains by Category (kWh) – 1st Floor" (Kneifel, Sep. 2012) and the bottom figure are results of the TRNSYS Envelope and Load model.

The internal heat gains for the 2nd floor of the EnergyPlus NZERTF model and the TRNSYS Envelope and Load model are shown below in Figure 2-8. The top figure is "Figure 5.14 Internal Heat Gains by Category (kWh) – 2nd Floor" (Kneifel, 2012a). The overall values of the heat gains are very close with the EnergyPlus model averaging around 200[kWh/month] and the TRNSYS Envelope and Load model averaging 205 [kWh/month]. The similarity of the models on the second floor despite the difference in schedules reflects the nearly constant nature of most of the second floors electrical gains that are not significantly affected by the day of the week, the consistency of the assumed heat gains for minimally active and sleeping occupants, and the unchanging nature of their sleep schedule.

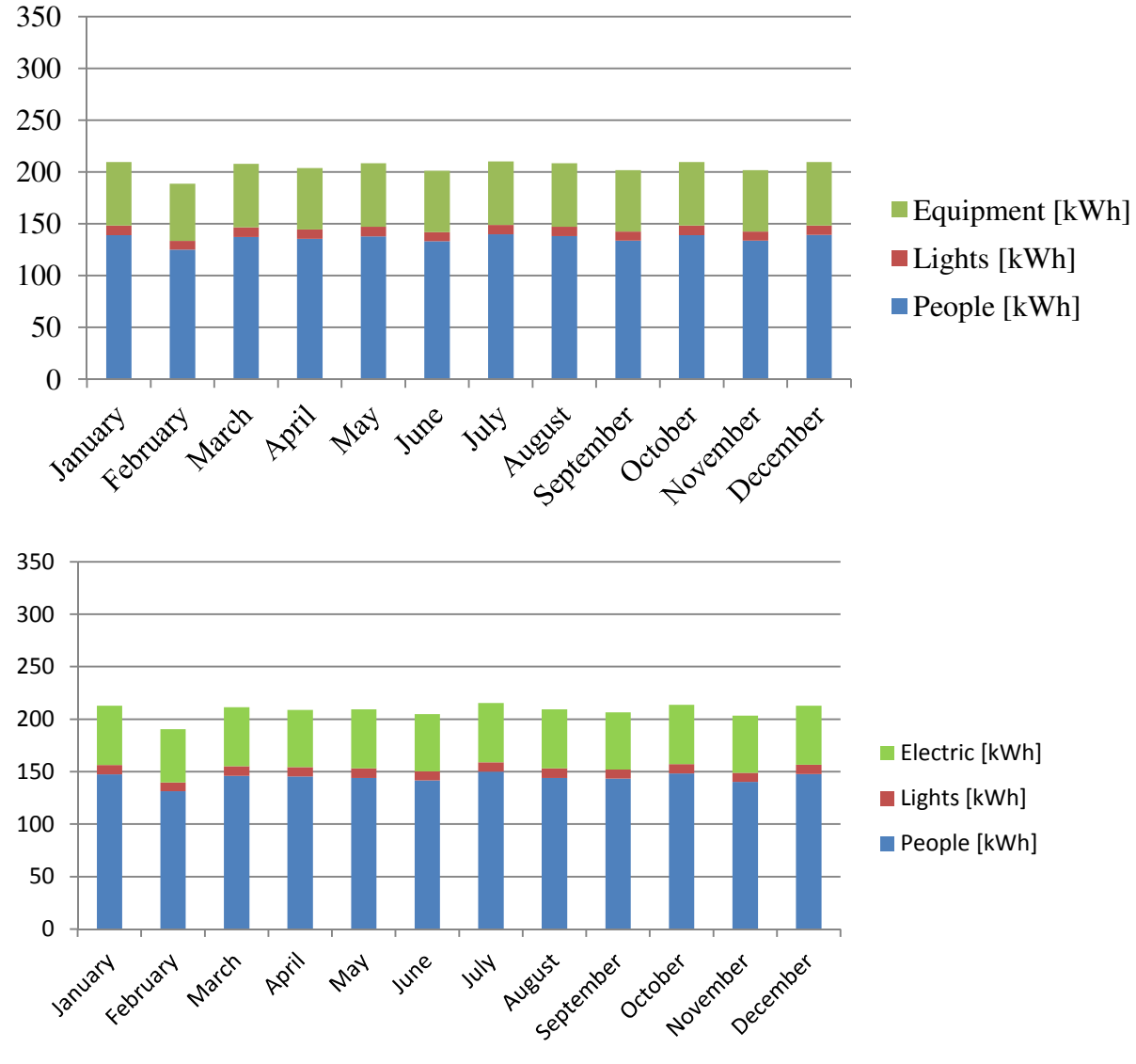

Figure 2-8: Comparison of Internal Heat Gains 1st Floor. The top graph is "Figure 5.14 Internal Heat Gains by Category (kWh) – 2nd Floor" (Kneifel, Sep. 2012) and the bottom figure is from the results of the TRNSYS Envelope and Load model.

The monthly average infiltration rate for the 1st and 2nd floors of the EnergyPlus NZERTF model and the TRNSYS Envelope and Load model are shown in Figure 2-9. The top graph is "Figure 5.27 Infiltration Rate by Floor - ACH" (Kneifel, 2012a). The TRNSYS Envelope and Load model results were quite similar in shape but were consistently 0.2 air changes per hour greater than the EnergyPlus results. Identical wind shielding and stack coefficients were provided to the TRNSYS infiltration model indicating that the difference is caused either by

the infiltration model itself or differences in an interaction between other elements of the models such as increases in internal pressure due to the HVAC system.

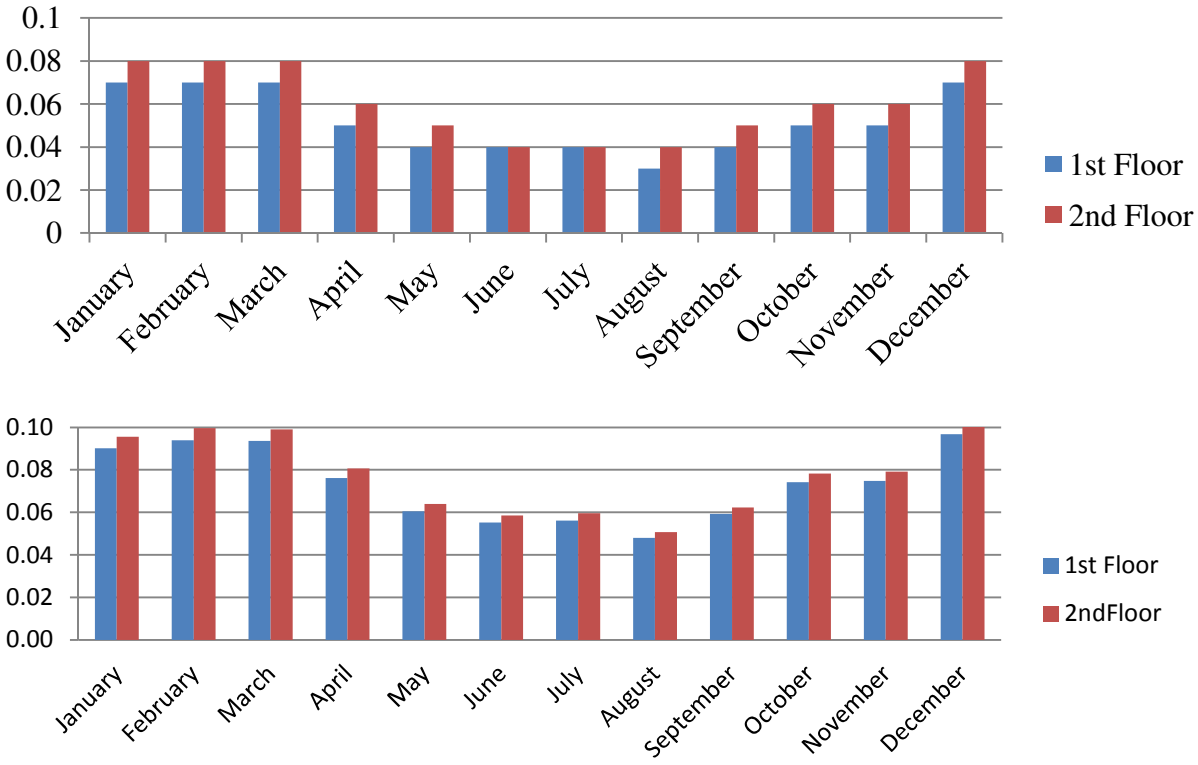

Figure 2-9: Comparison of Monthly Average Infiltration Rate in Air changes/hr
The top graph is "Figure 5.27 Infiltration Rate by Floor - ACH" (Kneifel, Sep. 2012) and the bottom figure is from the results of the TRNSYS Envelope and Load model.

The sensible heat transfer due to infiltration for the 1st floor of the EnergyPlus NZERTF model and the TRNSYS Envelope and Load model are shown below in Figure 2-10. The top figure is "Figure 5.28 Infiltration Sensible Heat Transfer – 1st Floor (kWh)" (Kneifel, 2012a). The TRNSYS Envelope and Load model results in greater infiltration heat losses (50-75%) during winter months than were reported for the EnergyPlus model. The heat gains during summer months are almost identical. The differences appear to be the result of differences in infiltration rates and the household temperature set point schedules.

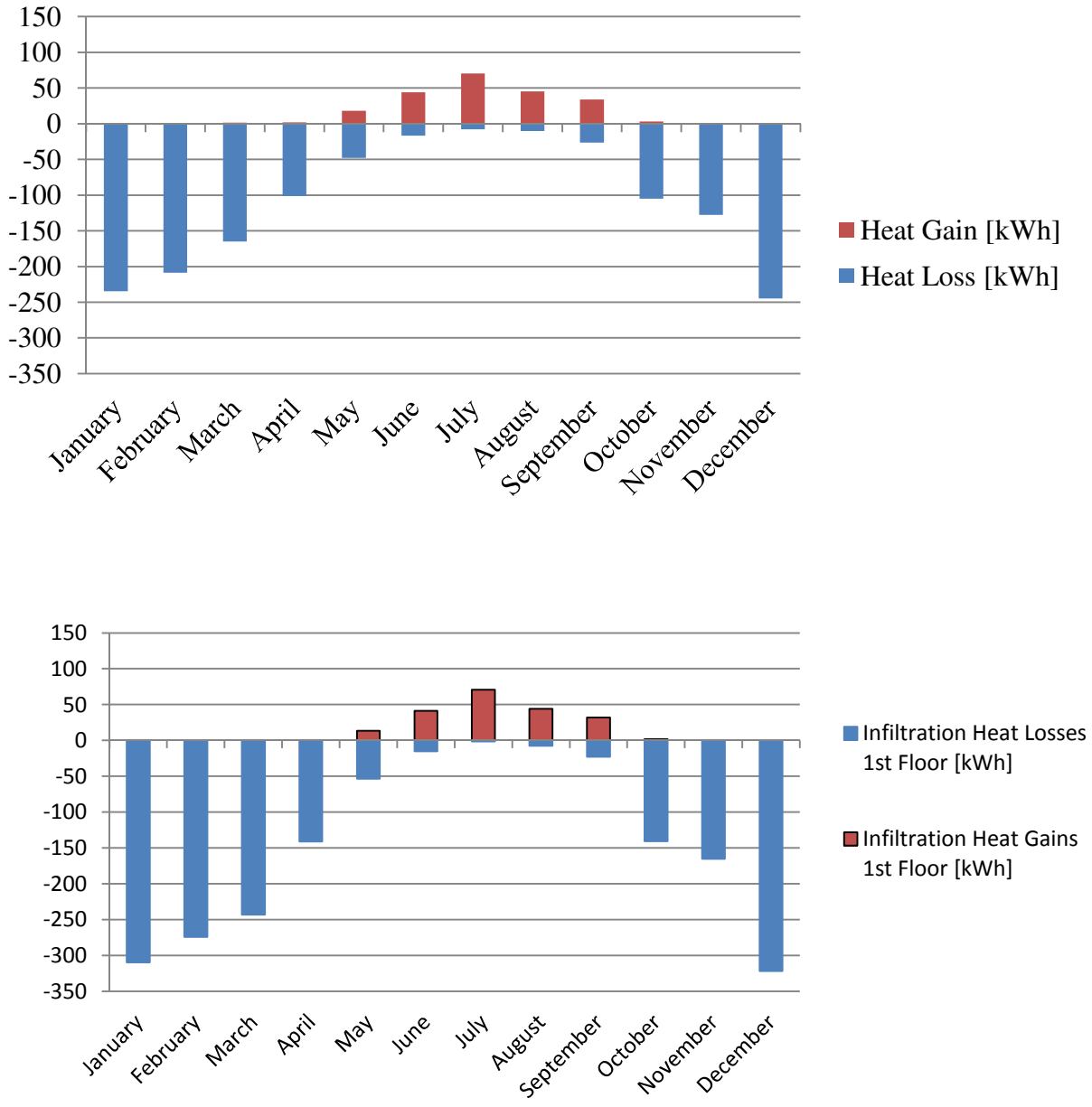

Figure 2-10: Comparison of Infiltration Heat Gains and loses 1st Floor.
The top graph is "Figure 5.28 Infiltration Sensible Heat Transfer – 1st Floor (kWh)" (Kneifel, Sep. 2012) and the bottom figure is from the results of the TRNSYS Envelope and Load model.

The monthly cooling and heating loads for the EnergyPlus NZERTF model and the TRNSYS Envelope and Load model are shown below in Figure 2-11. The top figure is from "Figure 5.10 HVAC Energy Load by Coil (kWh) – Monthly" (Kneifel, 2012a). In line with what

would expected from the relative internal energy gains and monthly infiltration gains/losses, the TRNSYS Envelope and Load model had slightly higher heating requirements during winter than the EnergyPlus model. However the cooling requirements during summer months are unexpectedly lower in the TRNSYS Envelope and Load model. The difference in heating and cooling requirements may be a result of lower internal gains due to electrical and HVAC equipment gains that are not currently included in the TRNSYS Envelope and Load model. These out of season loads are a result of the model assuming that all equipment is always available to meet the temperature set points as opposed to turning heating and cooling equipment off when they are not expected to be in use. The HVAC model addresses this by locking out heating and cooling during inappropriate seasons.

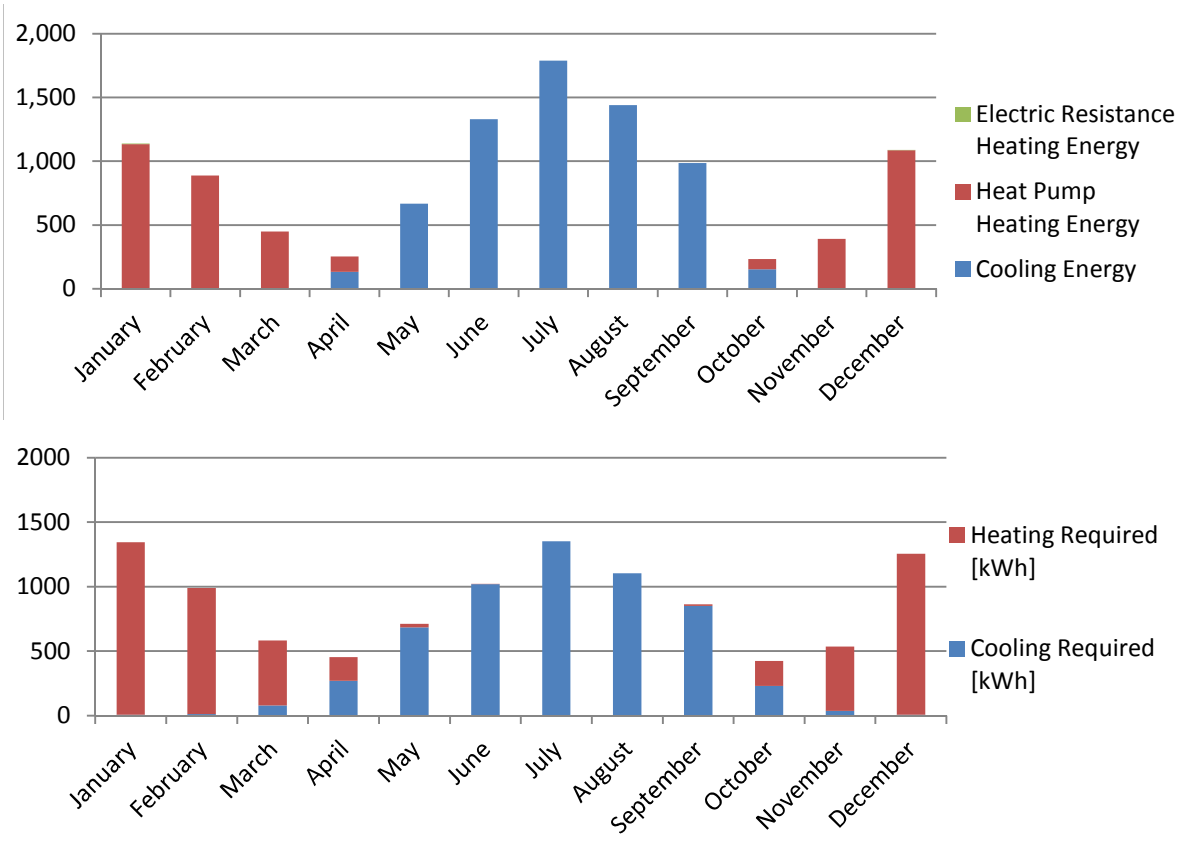

Figure 2-11: Comparison of Heating and Cooling Loads 1st Floor
The top graph is "Figure 5.10 HVAC Energy Load by Coil (kWh) – Monthly" (Kneifel, Sep. 2012) and the bottom figure is from the results of the TRNSYS Envelope and Load model.

Table 2-3: Comparison of Required Heating and Cooling

	EnergyPlus Model		Initial TRNSYS Envelope and Load model	
Month	**Heating [kWh]**	**Cooling [kWh]**	**Heating [kWh]**	**Cooling [kWh]**
Jan	1134	0	1337	6
Feb	888	0	979	11
Mar	449	0	504	80
Apr	121	133	183	271
May	0	667	28	685
Jun	0	1329	1	1019
Jul	0	1788	0	1352
Aug	0	1440	0	1104
Sep	0	985	13	850
Oct	79	154	192	231
Nov	392	0	499	37
Dec	1085	0	1249	7
Annual	4148	6496	4986	5654

Note that the results from table Table 2-3 were generated using the Placeholder HVAC System and are not the results from the full house model.

The heating and cooling rates required to maintain the set point temperature ranges in for the 1st and 2nd Floor of the TRNSYS model are shown in below in Figure 2-12 and Figure 2-13. The sum of these rates is currently limited to the primary air handling unit's nominal capacities. The capacity dedicated to each zone was determined by the ratio of the zones floor areas.

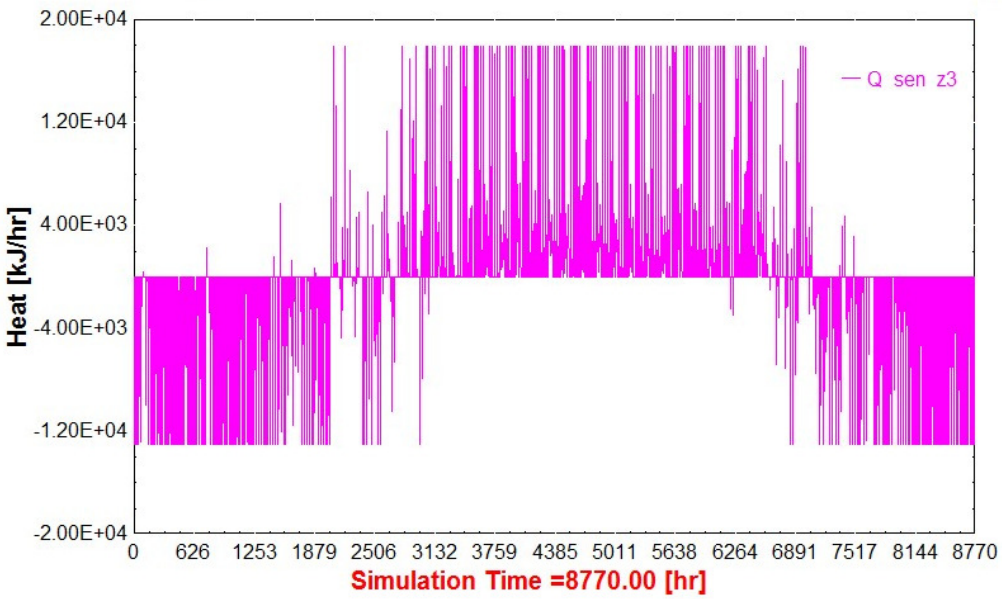

Figure 2-12: Annual Heat Requirements 1st Floor

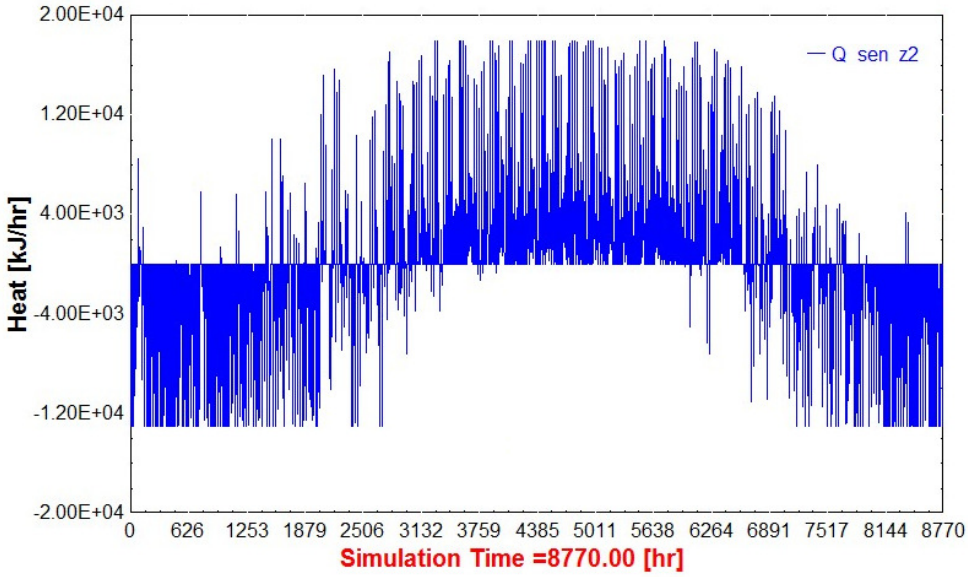

Figure 2-13: Annual Heat Requirements 2nd Floor.

2.5 Use and Later Modification of the Initial House Envelope and Load Model

The Initial House Envelope and Load Model was able to come fairly close to the EnergyPlus model's predictions for house thermal requirements without the inclusion of any of the HVAC equipment. These thermal requirement predictions were used to provide a simulated load profile for a series of investigations into ground loop heat exchangers which are documented in Chapter 3. While useful, the initial house envelope and load model was insufficient for the desired full house simulations and comparative studies. The initial model was updated and modified, as documented in Chapter 4, for use in the Full House Model. The Full House Model includes all of the components of the House Envelope and Load Model but also includes the Test Facilities HVAC, Electrical, and Water systems.

Chapter 3: Ground Loop Heat Exchanger Modeling

3.1 Background on Ground Loop Heat Exchanger Thermal Properties

3.1.1 Purpose of the Ground Loop Heat Exchanger Studies

The ground loop studies were necessary to accurately model the ground loop heat exchangers for use with a ground source heat pump HVAC system which will be implemented in the Test Facility. This modeling resulted in an extensive study of geothermal borehole modeling, ground formation thermal property determination, model parameter optimization techniques, and the impacts of long term operation of ground loop heat exchangers.

3.1.2 Methods for the Determination of Ground Thermal Properties

This review briefly covers methods of determining ground thermal properties. It focuses on the most common method, the Thermal Response Test (TRT), and the estimation procedures for determining ground and borehole properties from the collected TRT data. It also reviews the predicted accuracy of such results and ends with a look at more powerful emerging techniques for both TRT data collection and analysis.

3.1.3 Importance of Accurate Property Measurements:

When used in space and water heating and cooling applications, ground source heat pumps have the potential to reduce energy consumption and carbon dioxide output while saving consumers money over the lifetime of the heat pump equipment (Liu, 2010). One of the main barriers to greater adoption of this technology is the high initial cost of the system relative to conventional heating and cooling systems. A large portion of the initial cost is the installation of the ground loop heat exchanger (Yang, Cui, & Fang, 2010). It is common for ground loops

to be made larger than necessary due to uncertainty about the ground properties and thus the available heating/cooling capacity of the loop. Reducing this uncertainty would reduce the need to overbuild loops, reducing the initial cost of the system and could also reduce instances of under built systems and increase the usable life of the ground loop as the geological formation temperature changes over time. Though they are a substantial investment, ground loops can last for multiple generations of heat pump equipment and it is therefore important to size them properly (Liu, 2010),

3.1.4 Methods of Ground Property Assessment

3.1.4.1 Which Properties are Assessed and Formation Variability

In geothermal applications the geological formation properties of greatest interest are the undisturbed temperature (T_0), the thermal conductivity (K_f), and the volumetric heat capacity (C_f). Knowing these properties allows accurate long time-scale modeling of the ground heat exchanger (GHX). It is also desirable to know the thermal properties of the borehole itself as these properties allow accurate modeling on shorter time-scales. It would be ideal to know all of these properties for every part of the ground volume near the GHX. However this ideal situation is currently impractical and therefore effective values for the entire formation are used. The actual ground properties may change with both position and time (due to weather, moisture content etc.) (Witte, 2013). In many models there is also an inherent and often incorrect assumption that ground water flow is a negligible heat transport mechanism. There is some research directed towards measuring the distribution of effective properties along the vertical axis of a borehole (Fujii et al., 2009) as well as the additional complexity of

convective heat transport within ground water flows (Signorelli, Bassetti, Pahud, & Kohl, 2007).

3.1.4.2 Ground Water Flow

One of the basic assumptions behind most geological formation property assessments is that an effective thermal conductivity and an effective heat capacity are capable of representing the thermal transport processes within the formation. This assumption may not be valid when there is significant groundwater at large borehole depths due to the associated natural and forced convection processes. Natural convection results from the establishment of vertical convective cells around the borehole and impacts borehole resistance measurements. Forced convection results from ground water flowing past the borehole and can result in significantly greater heat transfer from the borehole than conduction through the formation. Thus convection may result in a much higher predicted effective K_f and render conduction only models inaccurate. Signorelli et al. (2007) recommended looking at the stability of the K_f predicted by the most common analysis method, the line source model (LSM), to check for interference from ground water flow. The LSM stability was determined by plotting the LSM analysis results for different sections of data starting at 5 hours and varying the end time up to the end of the data set. If flow velocities are significantly higher than 1 m/day, then the K_f value given by varying starting points of the LSM analysis, after the initial data are discarded, will continue to vary, usually increasing. It should be noted that a varying K_f value will also occur if other non-uniform formation structures are present and thus this stability test is not a conclusive indicator of ground water flow. Though it is possible to model ground water flow, due to the heterogeneous nature of geological formation, it is often difficult to determine the actual flow patterns around the borehole.

3.1.4.3 Methods of Assessment

The current methods of ground property assessment involve either taking samples from the formation or using a borehole to measure the formation's properties in situ. Sampling involves drilling a hole and taking core samples and subjecting them to laboratory tests to determine their thermal properties. These properties are then averaged to yield effective formation properties. It is also possible to use the material brought up in the drilling fluid however it is usually not suitable for laboratory tests and is more often used to determine rock and material types to give an estimated range of properties. Taking core samples and running tests on them is relatively expensive, only provides information on the material in bore hole itself, and requires drilling a borehole. Due to these factors, an in-situ Thermal Response Test is more commonly used (Austin 2000).

3.1.4.4 Thermal Response Test

The thermal response test (TRT) involves drilling a borehole and setting up a ground loop heat exchanger (usually a single U-tube) within the bore. The hole is then backfilled with grout and allowed to return to the undisturbed ground temperature. For the test itself, a constant flow of working fluid is sent through the GHX and allowed to equilibrate with the ground temperature in order to measure T_0. Once equilibrium has been established, a constant heat input is applied to the fluid. In the most common version of the test, the temperatures going into and coming out of the borehole are monitored and analyzed to determine the average formation properties. The test is usually run for several days so that the thermally affected volume, and thus the measured formation volume, is relatively large. The current standard is to get average properties for the ground volume affected by a ~50

hour heat pulse. Under ideal conditions, this test duration also reduces the effects of the borehole geometry and resistances, which are important in transient behavior. Analytical techniques have been developed to extract some borehole properties from TRT data (Gehlin, 2002).

The ideal TRT is based upon the requirements for predicting ground properties using the line source model in the manner explained in the Line Source section. An ideal test is semi-steady state in that the working fluid flow rate, heat input rate to the ground loop, and thermal properties/resistances of the borehole and ground do not vary while the temperatures in the working fluid and ground increase. To this end it is undesirable to have fluctuations in the heat input to the working fluid, heat loss outside the GHX, or interruptions of any sort during the test.

3.1.4.5 Heat Extraction Tests

Standard TRTs only measure the response of the borehole/formation system to a steady heat input; however, it is also possible to use the borehole for heat extraction tests. A heat extraction test is identical to a heat input test only with heat being extracted from the working fluid by a heat pump in the testing apparatus. The use of a heat pump necessitates that the heat input/extraction rate be controlled using the measured working fluid temperatures. Performing both tests sequentially may also be beneficial in determining accurate properties when significant ground water flow is present (Gustafsson & Westerlund, 2011).

3.1.4.6 Problems with the Data Sets

The use of average properties and the associated assumption of a homogenous formation lead to inaccuracy when analyzing TRT data. However there are also difficulties with the testing, and consequently, the data itself. For example, it is often difficult to maintain a constant heat rate to the feed stream and there are problems with heat loss from the testing rig equipment to the surroundings. Errors in the temperature measurements, flow rate, and power measurements can also have large impacts on the formation properties determined from the data. Bandos et al. (2011) found that approximately 5% of the heat being generated by the heater in a well-insulated TRT testing rig was lost to the atmosphere. This heat loss corresponded to a 15% change in the predicted K_f values obtained by analyzing the data with the line source model.

Improving the quality of the test data can be done by improving sensor accuracy, improving power rate control, recording fluid temperatures from below the surface where they are not affected by atmospheric losses, and using the fluid temperatures to control power input rather than assuming all input power is going to the fluid. However physical modification of the test apparatus and improvement of the test data is relatively expensive compared to the value of the associated improvements of the models and analytical techniques. Thus, much research has been devoted to developing methods to deal with varying heat input rates, transient and early time data, heat loss the atmosphere, and varying borehole resistances (Bandos et al., 2011).

Ambient temperature variations can cause significant variations in the measured K_f regardless of the model used to analyze the data (Signorelli et al., 2007). This variation is

worse with poorly insulated testing rigs or with long stretches of shallowly buried or surface pipes. It can be partially corrected for by including additional heat loss paths in the model and using an iterative method such as that outlined by Bandos et al. (2011) to determine the additional heat loss.

3.1.5 Borehole Heat Exchanger Models

3.1.5.1 Analytical Models

Analytical models of the borehole define a series of differential equations that describe the heat transfer (typically conductive) for a simplified region of interest. The solution to these equations yields temperature profiles at a location and time. The difficulty in solving the equation sets limits this type of model to simplified cases such as steady heat input into an infinite homogenous formation (Taylor et al., 2011). However the use of superposition allows steady state solutions to be stacked to simulate transients (Lamarche & Beauchamp, 2007) and multiple boreholes (Katsura, Nagano, & Takeda, 2008). The models are still limited to homogenous formations including the borehole and are thus limited in potential accuracy.

3.1.5.2 Line and Cylindrical Source Models

Commercially, there are two main borehole heat exchanger models used for extracting ground thermal properties from TRT data: the Infinite Line Source Model (LSM) and the Cylindrical Source Model (CSM).

The current industry standard for modeling TRTs is the infinite line source model which is an analytical model that approximates the borehole as an infinitely long thin line with a constant

heat flux along its length. The surrounding geological formation is approximated as homogenous, isotropic, and infinite. Typically the average of the entering and exiting fluid temperatures at each time step is taken to be the temperature of the entire line (i.e. the borehole) temperature. Using these approximations it is possible to use Lord Kelvin's analytical solution for an infinite line heat source in an infinite medium with a constant heat flux (Warren Adam Austin, 1995) resulting in a temperature distribution following equation (3-1) in the derivation below (Roth, Georgiev, Busso, & Barraza, 2004).

$$T(r,t) - T_0 = \frac{\dot{Q}}{4\,\pi\,K_f H_b} \int_{r^2/4at}^{\infty} \frac{e^{-u}}{u} du \tag{3-1}$$

For large values of $a\ t/r^2 \geq 20$ for 2.5% maximum introduced error, Equation (3-1) reduces to:

$$T(r,t) - T_0 = \frac{\dot{Q}}{4\,\pi\,K_f H_b} \left[\ln\left(\frac{4at}{r^2}\right) - \gamma\right] \tag{3-2}$$

Evaluating equation (3-2) at $r = r_b$ and introducing the borehole resistance R_{bt} yields:

$$T_f(t) = \frac{\dot{Q}}{4\,\pi\,K_f H_b} \left[\ln\left(\frac{4at}{r_b^2}\right) - \gamma\right] + \dot{Q}\,R_{bt} + T_0 \tag{3-3}$$

As $\gamma,\ \dot{Q}\,R_{bt}, and\ T_0$ are constants (3-3) can be rewritten as:

$$T_f(t) = C_1 \ln(t) + C_2 \tag{3-4}$$

$$C_1 = \frac{\dot{Q}}{4\,\pi\,K_f H_b} \tag{3-5}$$

$$C_2 = \frac{\dot{Q}}{4\,\pi\,K_f H_b} \left[\ln\left(\frac{4a}{r_b^2}\right) - \gamma\right] + \dot{Q}\,R_{bt} + T_0 \tag{3-6}$$

Using s, the slope of the linear regression of temperature with the natural log of time starting at t_{init}, K_f is given by equation (3-7):

$$K_f = \frac{-(\dot{Q})}{4\pi H_b s} \quad (3\text{-}7)$$

where $\dot{Q}$ is equivalent to the average heat lost by the working fluid, ideally resulting in:

$$K_f = \frac{-(\dot{m} C_f (T_{out} - T_{in}))}{4\pi H_b s} \quad (3\text{-}8)$$

The line source model requires no actual knowledge of the borehole properties or geometry however it does require a minimum of approximately 20 hours of data and a very stable heat input rate. The actual length of testing required before the LSM model becomes useful is given by:

$$t_{init} \geq \frac{5\, r_b^2}{\alpha_f} \quad (3\text{-}9)$$

Data preceding t_{init} are discarded during analysis with the LSM in order to avoid the effects of the borehole thermal resistance and heat capacity which the LSM model does not account for. The data discarded usually corresponds to around 12 to 20 hours of the initial data and therefore overall test lengths of < 50 hours are recommended (Gelder, Spitler, and Witte 2002). The model is too simple to accurately account for large variations in ground properties or test data that deviates from semi-steady state. Any experimental deviation from the nominal heat input can yield large variations in K_f predictions.

The LSM model has been adapted to include the finite length of the borehole using numerically tabulated non-dimensional G functions as well as to include an equivalent borehole resistance term (Eskilson, 1987). However these improvements do not appear to be commonly used in commercial TRT analysis.

The cylindrical source model represents the borehole as an infinitely long cylindrical heat source with constant heat flux across its surface. Because the model includes equivalent thermal resistance (R'_{bt}) and capacitance (C_b) terms for the bore hole, this model is better able to simulate transients but requires more information about the borehole. It is still an imperfect representation of the borehole and the relation of some input parameters such as cylinder radius to the actual borehole measurements is a subject of investigation. The primary problem is that there are often multiple sets of parameters that yield results with very similar behavior (Warren Adam Austin, 1995).

3.1.5.3 Borehole Resistance Terms

Many of the geometric and thermal parameters of the borehole have similar effects on the boreholes performance. Due to the difficulty in teasing out which parameter is responsible for a change in the behavior of the borehole and the uncertain nature of a number of these parameters, they are often lumped into a single equivalent borehole thermal resistance term (R_{bt}). R_{bt} is defined as:

$$R_{bt} = \frac{H_b\,(T_f - T_b)}{\dot{Q}} \tag{3-10}$$

where T_b is the mean borehole surface temperature, q'_b is the heat transfer rate per unit length of the borehole, and T_f is the average fluid temperature as found by the following formula.

$$T_f = \frac{T_{f,in} + T_{f,out}}{2} \tag{3-11}$$

$T_{f,in}$ is the entering fluid temperature and $T_{f,out}$ is the exiting fluid temperature.

Because of its utility and wide use, significant effort has been put into determining and predicting the borehole thermal resistance based upon other parameters (Gustafsson and Westerlund 2011) (Borinaga-Treviño et al. 2013). Lamarche et al (2010) have conducted a review of five common methods of calculating the equivalent borehole resistance. They then compared the methods to detailed numerical models of boreholes using the COMSOL software in order to obtain quantitative measures of the deviation of these methods from the more accurate numerically calculated borehole resistance.

3.1.5.4 Numerical Models

There are numerous numerical models that have been developed in a variety of languages and simulation environments. These models can generally be split into two groups: low detail and high detail. Low detail models are usually used in TRT data analysis and long term simulations due to their relatively low computational intensity. High detail models are often used to generate simulated test data with controlled parameters in order to examine the sensitivity and accuracy of the other models and analysis methods. There are a few experimental data sets in which all of the parameters of interest were controlled in a laboratory, but the useful duration of these data sets are limited to the time required for the thermal wave to reach the edges of the test rig, which is often too short to be of use. They also do not include factors like water flow and non-homogenous formations. Due to these limitations and generally lower costs, the highly detailed numerical models are useful for generating ‘validation data’ and sensitivity data.

3.1.5.5 Hybrid Models

Hybrid models use superposition to combine numerical and analytical solutions for different parts of the heat transfer problem in order to calculate an overall solution. A popular hybrid model is the Duct Storage Model (DST) originally created by HellStrom (1989). The DST model has been implemented in the TRNSYS (Klein, S A, Beckman, W. A., Mitchell, J. W., Duffie, J. A., Thornton, J W, Mitchell, J. C., 2012) simulation environment as component TYPE 557: Borefield Ground Heat Exchanger and is commonly used in HVAC system simulations. As the DST model is being used in the bore-field simulations for this project, it is presented in more detail in the DST section.

3.1.5.6 TRNSYS DST Implementation

The TRNSYS Type557 borehole field component model is a full implementation of the Duct Ground Heat Storage Model (the DST model) first presented by HellStrom (1989). The TRNSYS implementation has some preset parameters and allows user input for the depth, number of boreholes, bore geometry, ground layers and heat transport properties.

The model sets up an axially symmetrical bore-field with the bores automatically distributed on a hexagonal pattern. The bore-field is designated as the storage volume and is assumed to be homogenous, isotropic, and lacking both flowing ground water and sufficient permeability to allow convective circulation. The ground surrounding the storage volume is assumed to be isolated from rapid transient effects in the borehole and the model allows multiple homogeneous, isotropic, horizontal layers to be modeled. Because the DST model was originally created with the intent to model ground thermal storage it was not seen as

important or practical to model ground water flow as any location with ground water flow would be a poor choice for storage.

In order to reduce computational intensity and calculation time, the model breaks the heat transfer relationships into three types of sub problems: global, steady flow, and local. The sub problems are then solved and superimposed to give an approximate solution.

The global problem employs an automatically generated 2D radial and vertical mesh centered on the center of the bore-field. This portion of the model handles the large scale, long time period, conduction between regions inside the storage volume, the coupling of the ground with the surface, and heat transfer in the ground surrounding the bore-field. Details of the temperature fields near individual boreholes and heat transfer to the fluid are dealt with by the local and steady flow problems.

The steady flow problem computes the change in temperature around the individual boreholes due to slowly varying heat pulses. The time variant temperature change in the pipes is converted to a series of superimposed step pulses and then the temperature distribution due to these pulses is solved analytically. This solution deals with the redistribution of heat within the storage volume due to the heat input/extraction of the individual boreholes over a long time period.

The local problem deals with heat transfer around a borehole due to short term transient effects. To conserve computational effort, the DST model sets up sub regions: radial cells of equal volume covering the entire storage volume. The number of sub regions is determined by the number of boreholes plumbed in series and each region contains an equal number of

bore holes. For example the model will use five concentric cylinders of equal volume to simulate a system with five boreholes in series. Within each sub region the boreholes are considered equivalent and the same solution is used for each. The solutions for the boreholes in a sub region are generated from a series of simple 1D radial meshes. These meshes are then solved for transient temperature changes in the storage volume near the borehole and heat transfer to and from the working fluid. The system is assumed to be conduction dependent and calculates the heat transfer coefficients for a given initial flow rate and temperature (for fluid properties) rather than calculating them for the inputs at each time step. The heat transferred to the ground and from the ground by this process is 'stored' for a given number of time steps and then added to the global solution. In TRNSYS, this results in spikes representing all of the heat transferred from the storage to the surrounding ground over a 24 hour time period. (Yavuzturk, 1999) (Pertzborn, 2012)

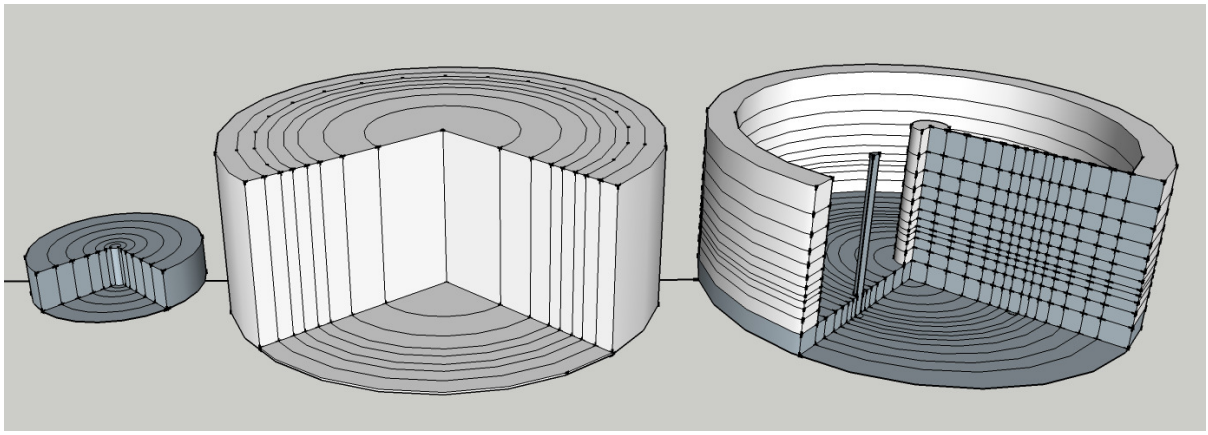

Figure 3-1: DST model mesh depictions. (Left) Local Mesh. (Middle) Sub Regions. (Right) Global Mesh.

Figure 3-1 is a visualization of the meshes involved in the DST model. The mesh on the left is a 1d mesh for the local problem, centered on a single borehole and stacked on top of each other for the length of the borehole. The middle figure shows a sample of how the sub regions are set up. The central cell contains the first boreholes in all of the borehole groups;

the second cell contains all of the second boreholes and so on outward. This model is optimized for storage where prevention of heat loss to the surroundings is the goal. The mesh on the right is a model of the global mesh. The mesh is 2D radial and vertical (as shown by the plane on the left). This represents ring shaped nodes with a rectangular cross section. The mesh is made finer near radii which contain boreholes (the projection left of the center) and near depths which mark property changes in the surrounding ground. It should be noted that separate ground layers are only modeled outside the storage volume.

3.1.5.7 Borehole Model Dimension: 1D, 2D, 3D

Many models are one dimensional and treat the borehole as infinitely long and axially symmetric. This assumption reduces the borehole to a radial heat transfer problem with a series of cylindrical nodes around the axis of the borehole. Two dimensional models take the borehole and assume that it has radial symmetry but conditions may vary in the vertical direction resulting in a series of ring shaped nodes centered on the borehole. Fully three dimensional models are more varied and range from a refinement of the two dimensional models to include radial asymmetry to fully computer generated tetrahedral meshes. The potential detail of the simulation, and thus the accuracy of the results, increases with the number of dimensions of the model.

3.1.5.8 Analysis of TRT Data

TRT tests do not directly measure ground or borehole properties. Instead they measure the heat transfer rate to the borehole and the temperature of the working fluid. The desired properties are then determined by matching a model to the measured data. For analytical models, matching the properties can be as simple as deriving an equation such as the LSM

equation discussed below. For more complex models multiple model runs and optimization methods such as parameter determination must be used.

3.1.5.9 Parameter Determination

Parameter determination works with any model that predicts a temperature distribution. The parameters to be determined are modified following an optimization algorithm until the desired error function (usually the sum of the squared errors of the average of the inlet and outlet temperatures for the test data and the modeled data) has been reduced below a set tolerance. This process will produce better results the more closely the model matches the physical situation. Using the LSM with this method would produce inaccurate parameter estimates due to the LSM's inability to simulate the short term behavior of the borehole. The optimizer will still attempt to match the inaccurate early time period LSM temperature predictions to the experimental data. If the initial data are discarded and if the actual test is close to the conditions that are assumed in the LSM then this method would produce similar results to typical LSM analysis. Likewise, when used with the DST model implementation in TRNSYS this method works better when the initial data are discarded. This improvement is a result of the fact that the DST model does not account for deviation of the borehole heat capacity from that of the surrounding ground. (Warren Adam Austin, 1995)

3.1.5.10 Two Step Parameter Determination

Two step parameter determination is an extension of parameter determination that is designed to improve speed and accuracy relative to standard parameter determination. This method works for situations involving multiple parameters with different periods of maximum impact on the simulation results. The advantage is that the early time series data

are more affected by borehole properties and the later time series data are ideally almost independent of them. This behavior allows the technique to estimate more parameters with higher accuracy than a single step parameter optimization. (Bozzoli, Pagliarini, Rainieri, & Schiavi, 2011)

The TRT data are broken into early and later time series. Parameter estimation is then used on the first series to predict parameters that will have a bigger impact on early time data. These parameters include borehole geometric and thermal properties. The calculated properties are then input into a second parameter determination using the late time data series. This parameter determination is used to predict formation properties, which have a larger impact on the late time series. These properties are then input back into the first parameter optimization and the process repeats until all of the properties being solved for converge to within a specified tolerance.

3.1.6 Error and Sensitivity Analysis of Resulting Parameters

The propagation and potential error involved in using the LSM model to analyze TRT data was determined by Witte (2013). The analysis assumed typical measurement precision and accurate measurements and did not including any variation of the ground from spatial and temporal homogeneity or deviation of the TRT test from ideal steady state. It was found that the resulting theoretical errors are expected to be on the order of 5% for the soil thermal conductivity and 10–15% for the borehole resistance.

A comparable sensitivity test of the LSM was done by Signorelli et al. (2007). This study looked at the sensitivity of the LSM to the test duration, heterogeneous subsurface

conditions, ground water movement, and variable data quality. The analysis was done with data sets generated using a numerical model created by the FRACTure geological modeling system. The numerical model was later validated with experimental test data and it was found that the expected error of the measured formation conductivity was about 10%.

3.1.7 Use of Laboratory Test Data for Validation

Validation of parameters measured using TRT tests can be done via laboratory measurements of the conductivity of samples taken from different sites around the formation. However this option is both expensive and only partially accurate due to the limited number of sampling sites. There are also other uncertain parameters in the borehole itself. To solve this problem, a full scale laboratory controlled borehole was constructed at the Oklahoma State University (Beier, Smith, & Spitler, 2011). This borehole test bed is modified to mimic various ground conditions and then subjected to thermal response tests. The resulting data are then used for validation of different models and analytical techniques.

3.1.8 Software TRT Data Analysis Tools

The GPM tool is an automated tool developed by Shonder and Beck at Oakridge National Lab. It uses a parameter estimation technique coupled with a simple numerical model to automatically estimate ground and borehole parameters from TRT data. The one dimensional numerical model approximates the borehole as an infinite cylinder in a similar manner as the cylindrical source model but allows the calculation of transients. The TRT data are input via a formatted text file and the parameters to be estimated are selected. The program then splits the parameters into sets and uses an initial guess for all but one set. This set is then estimated using parameter estimation techniques along with the numerical model and the measured heat

input rate. The algorithm, a Nelder-Mead optimization function, minimizes the sum of the squares error between the measured and modeled average fluid temperatures over the duration of the data set/simulation. The results of this calculation are input back into the model and a different set of parameters is calculated. Once all of the parameter sets have been calculated, the process starts over again with the initial set. The process iterates until the estimated values of all of the parameters have converged to within a specified tolerance.

The program outputs the estimated parameters, a plot of the residuals from the final run, plots of the sensitivity of the total error with respect to time for each thermal parameter, and a plot of how the parameter estimates change with the length of the data set included in the analysis. The plots are useful in determining whether there were inaccuracies in the model or errors in the data set. These inaccuracies include the presence of significant ground water flow or a geological formation with different thermal properties.

The algorithm and the program itself were tested in the same manner as the parameter estimation technique and found to yield conductivities within 2-3% of the line and cylindrical source models when analyzing ideal TRT data. (J A Shonder & Beck, 2000)

3.1.9 Future of Testing and Analysis

New test variants are coming into use to allow the collection of more or higher quality information using a similar set up. These newer tests include heat extraction tests, monitoring the return (recovery) of the borehole to T_0, and intentionally varying the heating rate. Though these techniques yield more information, it often takes longer to perform the initial test and

they require more complex modeling to determine the ground properties from the collected data. (Raymond, Therrien, Gosselin, & Lefebvre, 2011)

In order to improve the quality of the data, it has been suggested that the working fluid temperature sensors be fitted below the surface as close to the head of the borehole as possible. This placement ensures that the measured heat loss from the working fluid occurs only inside the borehole and not to the atmosphere or shallow soil around feed pipes (Gehlin, 2002).

Another new technique uses a fiber optic strand to monitor the temperature profile along the length of a borehole. A temperature dependent characteristic of Raman scattering allows the temperature of the cable to be measured with a spatial resolution of about 1 m and a temperature resolution of about 0.1 ºC (LIOS, 2013). The data collected allow borehole and formation properties to be calculated for the length of the borehole rather than simply averaged over the entire borehole. In some cases this technique can even determine the presence of water flow. Though the fiber optic cable used in the borehole is cheap enough that it could be left in place, the required laser equipment is currently more expensive than the standard thermocouple based testing setup (Fujii et al., 2009).

3.2 Ground Loop Model Development and Parameter Optimization

3.2.1 Description of the Site and Data Sets

The Test Facility has three ground loop heat exchangers (GLHX): horizontal, vertical, and slinky. A single deep, 300 ft, test borehole was drilled approximately at the site of borehole 1 of the vertical GLHX as shown in the bore-field diagram in Appendix A. Average heat

transfer properties of the geological formation were measured and estimated from the materials found in the bore hole by the drilling company on 4/7/2010. The results of cuttings analysis and the initial thermal response test are recorded in the Schnabel Geotechnical Report (SCHNABEL ENGINEERING, 2010c). The original data set from the conductivity test performed on the test borehole was provided by Harrison Skye at NIST and is referred to as the conductivity test, Ktest (SCHNABEL ENGINEERING, 2010a). Seven shallow soil test boreholes were also drilled to characterize the subsurface. The subsurface layering, ground water, and laboratory test results from these boreholes are documented in the Soil Test Report (SCHNABEL ENGINEERING, 2010b).

After construction activities on the Test Facility had been completed, two thermal response tests were conducted on the vertical GLHX on 1/25/2013 and 4/1/2013. These data sets were also provided by Harrison Skye and are referred to as Thermal Response Test One (TRT1) and Thermal Response Test Two (TRT 2) respectively (Harrison Skye, 2013). It should be noted that while the TRT test maintained a constant heat input to the bore field, each individual borehole did not receive a constant heat input making these tests non ideal for industry standard line source analysis.

The three test data sets available (the conductivity test and the first and second thermal response tests) provide data for four individual boreholes, three of which have two sets of measurements. Each of the seven data sets were run through parametric simulations and estimates of the ground formation thermal parameters were made using several methods.

Though the Ktest borehole and borehole 1 from the TRT data sets are at proximate locations, they are not actually replicate measurements since they were obtained using different

boreholes and therefore were presumably subject to small changes in some of the geometric properties of the bore holes. As will be shown here, the geometry of the bore holes can have a major impact on the predicted ground thermal properties.

3.2.1.1 Confirmation of Line Source Model Results

Analysis of borehole TRT data is typically done using the line source model. In this model it is assumed that the borehole is an infinitely thin line with heat rejection taking place uniformly along its length. Despite the many assumptions and potential inaccuracy of the line source model it is still widely used due to the simplicity of estimating thermal conductivity using equation (3-12).

$$K_f = \frac{-(\dot{m}C_f(T_{out} - T_{in}))}{4\pi H_b s} \quad (3\text{-}12)$$

Where s equals the slope of a linear regression of temperature with the natural log of time and H is the depth of the borehole (Gelder et al., 2002).

The original line source model analysis carried out by Western PA Geothermal Heating and Cooling Inc. (SCHNABEL ENGINEERING, 2010c) was repeated in order to confirm the predicted thermal properties and to compare the results of the original formation conductivity test and the ground response tests.

The line source formation thermal conductivity calculated from the conductivity test, 3.34 [W/m-C], was identical to that originally calculated by Western PA Geothermal Heating and Cooling Inc. When the line source model was applied to the data from TRT1, the calculated

formation conductivity was 2.438 [W/m-C]. This conductivity is a 27% decrease in the predicted formation conductivity. There are a number of possible reasons for the differences between these estimates, including greater ground water content at lower depths, differences in experimental setup, actual differences in the thermal properties at each location, and effects of the first borehole, which was drilled for the conductivity test and then sealed, on the second. Obviously this method of property estimation was inconsistent and it was decided to explore other models.

3.2.2 Ground Loop Modeling

3.2.2.1 Initial Modeling Effort

Models of the horizontal and vertical borehole ground loop heat exchangers were created using the thermal properties calculated by Western PA Geothermal Heating and Cooling Inc. The calculated conductivities and heat capacities were used for the vertical GLHX. The soil heat transfer properties near the surface were based on geological layer data from the Ground Test Report (SCHNABEL ENGINEERING, 2010c) in conjunction with The Encyclopedia of Solid earth Geophysics (Gupta, 2011). These properties were used to simulate the horizontal GLHX at the NIST site (buried at six feet) as well as the feed and return lines of the vertical GLHX (buried at 4 ft). These predicted ground properties were then used as a baseline to investigate the process of calibrating the TRNSYS models using the data gathered from the test site.

These properties did not result in TRNSYS accurately matching the TRT data from the vertical boreholes and it was determined that more analysis of the test data was necessary to determine appropriate properties to fit the TRNSYS simulations to the test data. The initial

vertical and horizontal GLHX models were then set aside in favor of modeling individual boreholes as explained in the next section.

3.2.2.2 First Individual Bore-hole Modeling Effort

The first model consisted of a simple single borehole simulation with parameters set to match the Ktest nominal geometry. The single borehole simulation depicted in Figure 3-2 reads an experimental data file using the Type9c data reader. The borehole inlet temperature and flow rates are then converted to TRNSYS native units, °C and kg/hr, and fed into the DST bore field component (Type557a). The bore field outlet temperature, the experimental inlet temperature, and the experimental outlet temperature are then output to a file and passed to an error calculation, Error1 in this diagram. The equation components along the top of the diagram set parameters in the bore field simulation so that they are accessible to TRNOPT (the TRNSYS interface for Lawrence Berkeley National Lab's GenOpt optimization library) and a MATLAB parametric run script. This change also makes it easier to adjust the parameters manually. All of the output temperatures are printed to a text file at the end of each time step.

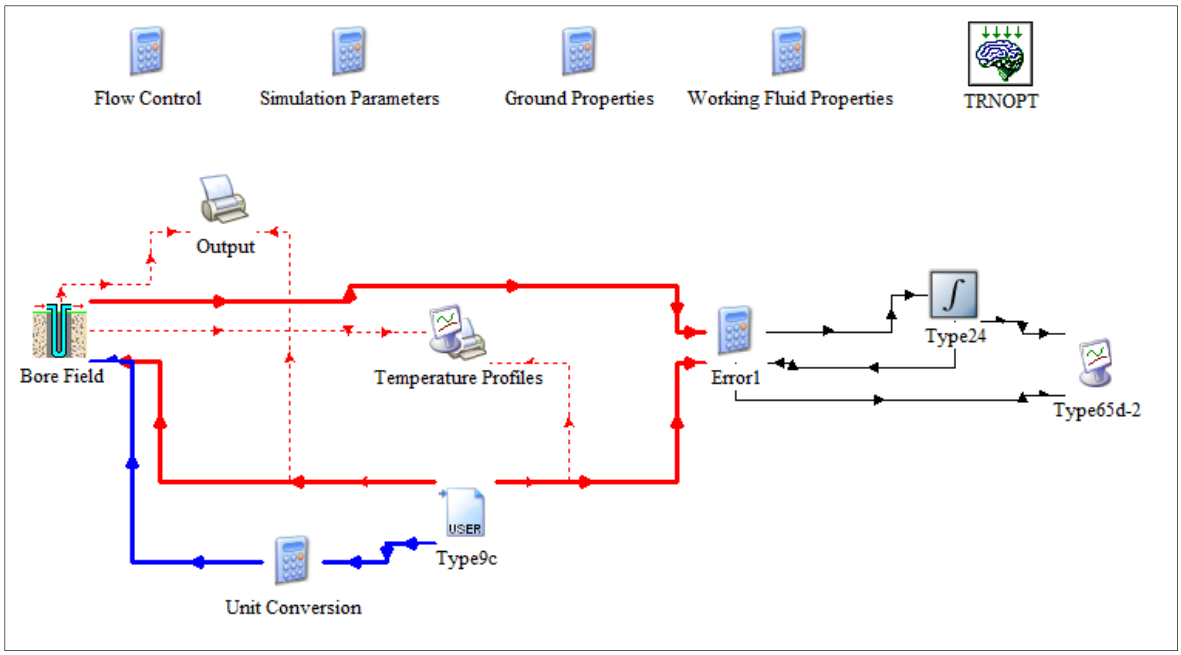

Figure 3-2: Diagram of TRNSYS simulation of a single borehole.

3.2.2.3 Time Lag Calculations

The physical borehole system has a time lag between the input temperature and the output temperature, which is a result of the time required for the working fluid to flow through the piping. The DST model in TRNSYS has does not simulate this effect. The time lag isn't a problem when the plug flow time of the physical system is much smaller than the time step of the simulation or when the temperature change per time step is small. However in this case, the plug flow time is on the order of the time step and we are specifically interested in the transient behavior. The plug flow time for the single bore hole during the conductivity test was 4.708 [min] and the time step of the Ktest data was 5 [min]. The plug flow time for an individual borehole during the TRT tests was 3.915 [min]. For the Ktest simulation a time delay of 1 time step, 5 min, was introduced in the modeled borehole outlet temperature data to more accurately replicate the estimated time lag of the actual test.

3.2.2.4 Uncertainty and Optimization of Borehole Model Parameters

It was originally assumed that a simple single parameter optimization fit of the borehole model would be sufficient for calibration. This approach used the nominal borehole geometry and varied the ground thermal properties in order to reduce the difference between the resulting temperature profiles. The original plan was to use the built-in TRNOPT tool to calibrate the formation thermal conductivity and specific heat to the experimental data by minimizing the RMS error between the modeled and experimental temperature drop over the borehole. Using TRNOPT proved problematic as the optimization output unrealistic ground properties when run with the nominal borehole geometry.

The possible uncertainty in the many of the parameters led to a situation in which there are multiple possible solutions that match the measured data. These uncertainties stem from a number of sources. The most obvious are inaccurate assumptions about the ground. Both the line source model and DST model (the TRNSYS default bore model) assume that ground properties are homogenous in time and space and that there is no mobile ground water or heat transport mechanism other than conduction (HellStrom, 1989). Other sources include measurement errors and uncertainty about the actual geometry of the borehole. In this situation measurement uncertainty has been minimized but the geometric parameters of the borehole are still uncertain by virtue of the nature of the construction process.

The borehole radius is of particular concern due to its large potential variability and the large impact that it has on simulation results. The radius is typically not measured but rather estimated based on the drill size and is expected to vary due to shifts in the drill and caving in of the borehole wall during drilling (Witte, 2013). These effects are evident in the

conductivity test bore drilling report which states “The bore diameter is to be no larger than 6 inches, with 4.5 inches being the target diameter” (SCHNABEL ENGINEERING, 2010b). It is also possible to have a varying radius with depth such that a single number is not representative of the entire length of the borehole. For instance, collapse of the borehole after insertion of the piping could result in direct soil contact at the base of the borehole and a greater radius at the location of collapse. This undesirable situation is protected against by filling the borehole with grout as soon as possible after drilling and pipe insertion.

After encountering difficulties matching the experimental and modeled results by varying only the ground thermal properties assuming the nominal borehole geometry, it was decided to vary the average bore hole radius as well. In this case the average borehole radius, was used as a proxy for a number of uncertain borehole geometric parameters such as the average U tube spacing and gap thickness. The properties are averaged over the length (i.e. depth) of the borehole. For the DST model all of these parameters affect the borehole resistance to heat transfer and thus changing any of them is effectively changing the resistance.

3.2.2.5 MATLAB Script Description

After the initial troubles with using TRNOPT to run parametric optimizations a series of MATLAB tools were created. The MATLAB code used to generate the parametric model runs consists of three functions called ‘deckWriter.m’, ‘outputReader.m’, ‘TRNSYScall2.m’, and a script file called ‘batchRunner.m’.

The first MATLAB function, deckWriter, modifies the values of an arbitrary number of variables in a TRNSYS deck file and saves it as a new deck file. It takes the name of the

TRNSYS deck file (.dck) containing the simulation to be run and vectors containing the names of any variables to be changed and the values to which they should be changed. The function reads the file, edits the variable values in the file and then resaves it with the addition of ' MLopt' before the '.dck' extension. It then returns a string with the new file name.

The second function, outputReader, reads a tab deliminated data output file and returns several sets of data for analysis. It takes in the name of the output file to be read, the column position of the experimental input temperature and output temperatures, and modeled output temperature that are to be analyzed. It also takes the number of header lines to be ignored when reading the file. It then returns vectors for measured borehole inlet temperature (T_{in}), measured borehole outlet temperature (T_{outExp}), modeled borehole outlet temperature (T_{outMod}), and a matrix of all of the data in the output file.

The third function, TRNSYScall2, generates a linear distribution of input values (2d grid for 2 variables, 3d grid for 3, etc) calls the other functions, runs TRNSYS, processes the output and the returns a matrix of values run and results. It takes in the names of the TRNSYS deck file to be run, a vector with the names of the variables to be changed, vectors of the minimum and maximum values for each variable and the number of divisions within that range to run. It also takes in the column positions of the desired data in the output file and the number of header lines. The function generates a series of all the combinations of the variable values. Each combination is then feed to the deckWriter and the resulting deck file run in TRNSYS. The TRNSYS output file is read using outputReader and the mean bias error (MBE) and root mean square error (RMS) of the modeled outlet temperatures is calculated. These errors,

along with the variable values used, are added to a matrix of all of the results. After all of the parameter combinations are run the function returns the results matrix. The calculation of mean bias error, MBE, and root mean square error, RMS, within TRNSYScall2 used equations (3-13) and (3-14).

$$MBE = \frac{\sum \left(Modeled - Measured \right)}{N} \tag{3-13}$$

$$RMS = \sqrt{\frac{\sum \left[\left(Modeled - MBE \right) - Measured \right]^2}{N}} \tag{3-14}$$

The script file, batchRunner, is used to set up a series of TRNSYScall2 runs. It takes a significant time to generate a large number of results for even relatively fast TRNSYS simulations so it is often useful to build a list of parametric runs and then leave it to run overnight. These MATLAB files, and later versions, are provided in the electronic supplement.

3.2.2.6 Results of Initial Bore-Field Modeling

Figure 3-3 through Figure 3-6 illustrate the Mean Bias Error and Root Mean Square Error (in ΔºC) for the conductivity test parametric simulations. Figure 3-3 and Figure 3-4 represent 40 variations of bore radius spaced linearly between 1.5 and 3.25 [in] and 120 variations of conductivity linearly spaced between 2 and 30 [W/m-K]. The high maximum value of conductivity was to show the values which corresponded to low error at a radius of 3 in. The specific heat used for these simulations was the estimated value of 2548.45 [kJ/m^3-K], based on the initial conductivity test report.

Figure 3-3 shows that conductivity and radius have competing effects on the MBE, where large radii and high conductivity produce essentially the same result as small radii and small conductivity. There are several things to note. The first is that at a radius of 3 [in], the required conductivity is well beyond the realm of possibility (solid rocks typically range from 2-7 and wet soils from 0.5-4 [W/m-K]) (Gupta, 2011). The thermal conductivity calculated using the line source model, 3.34 [W/m-K], yields a borehole radius of 1.98 [in] which is smaller than the target 2.25 [in] radius. Such a small radius is likely smaller than the drill size and is thus improbable. However this combination does result in a very good match between the experimental and modeled temperature profiles, as can be seen in Figure 9. The target radius of 2.25 [in] results in a required conductivity of 4.875 [W/m-K] , which is within the range of reported conductivity for the materials found within the borehole (Robertson, 1988).

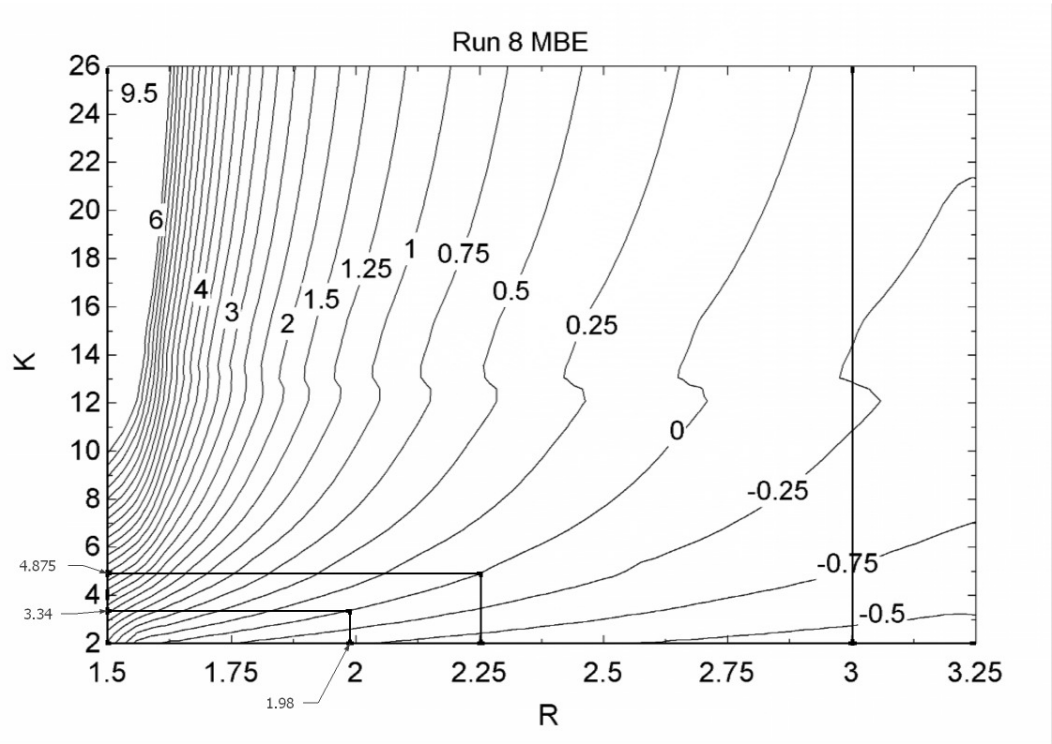

Figure 3-3: Mean Bias Error in ΔºC with varying borehole radius, R [in], and thermal conductivity, K [W/m-K], of the Ground Formation

Figure 3-4 shows that conductivity and radius have complex effects on the RMS, where several combinations of radii and conductivity produce minimums. As with the MBE results, the minimums of 0.67 and 0.71 at radii of 1.55 [in] and 1.60 [in] are unrealistic due to the required conductivities, 8.1 [W/m-K] and 14.9 [W/m-K], being beyond the realm of possibility (solid rocks typically range from 2-7 and wet soils from 0.5-4 [W/m-K]) (Gupta, 2011). These radii are also very small relative to the size of the tubing (1" diameter) and spacing within the borehole (2" center to center).

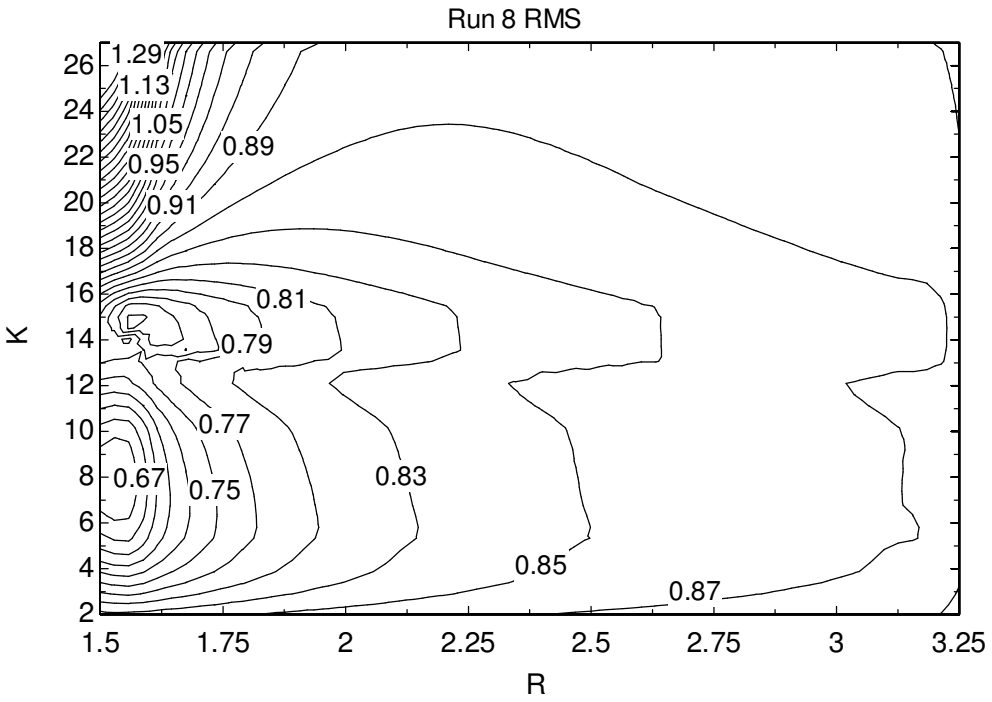

Figure 3-4: Root Mean Square Error in ΔºC with varying borehole radius, R [in], and thermal conductivity, K [W/m-K], of the Ground Formation

Figure 3-5 and Figure 3-6 (Run 9) represent 100 variations of specific heat capacity spaced linearly between 1250 and 5000 [kJ/m^3-K] and 300 variations of conductivity spaced linearly between 1 and 9 [W/m-K]. The borehole radius was left at the 2.25 [in] target specified in the conductivity test report.

As can be seen in Figure 3-5 and Figure 3-6 the temperature results and error are almost independent of volumetric heat capacity. Heat capacity is set with an estimate based on the ground composition as determined by materials retrieved during the bore drilling process. These horizontal slopes in the figures indicate that short duration tests are not useful for measuring the specific heat capacity. As test duration increases it is expected that the impact of specific heat capacity will become more important.

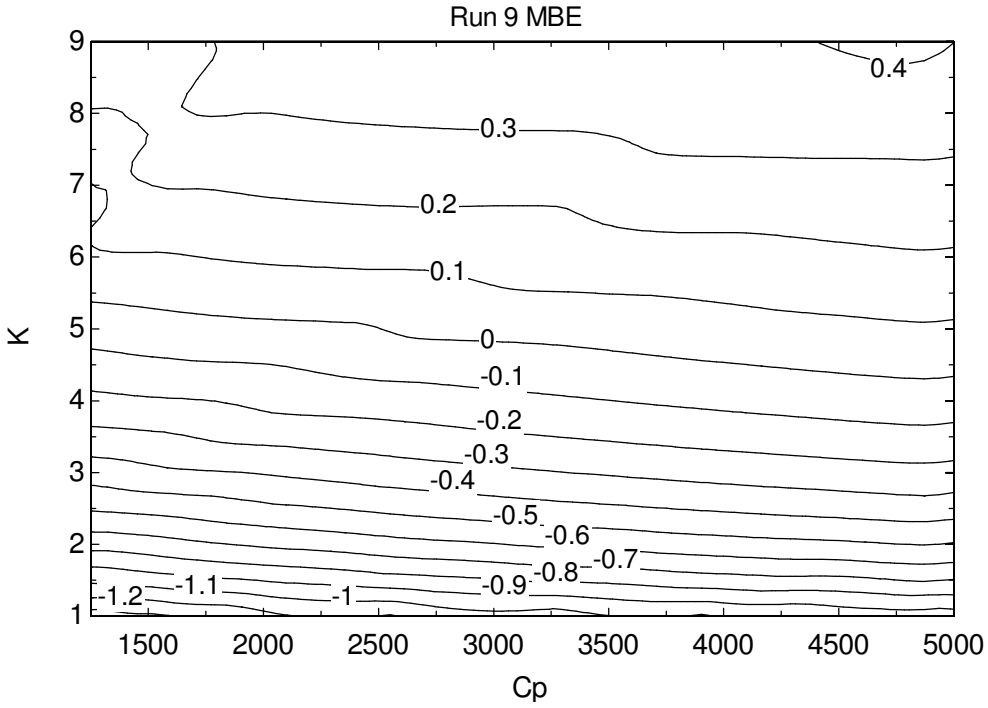

Figure 3-5: Mean Bias Error in ΔºC with varying volumetric specific heat, Cp [kJ/m^3-K]and thermal conductivity, K [W/m-K], of the Ground Formation

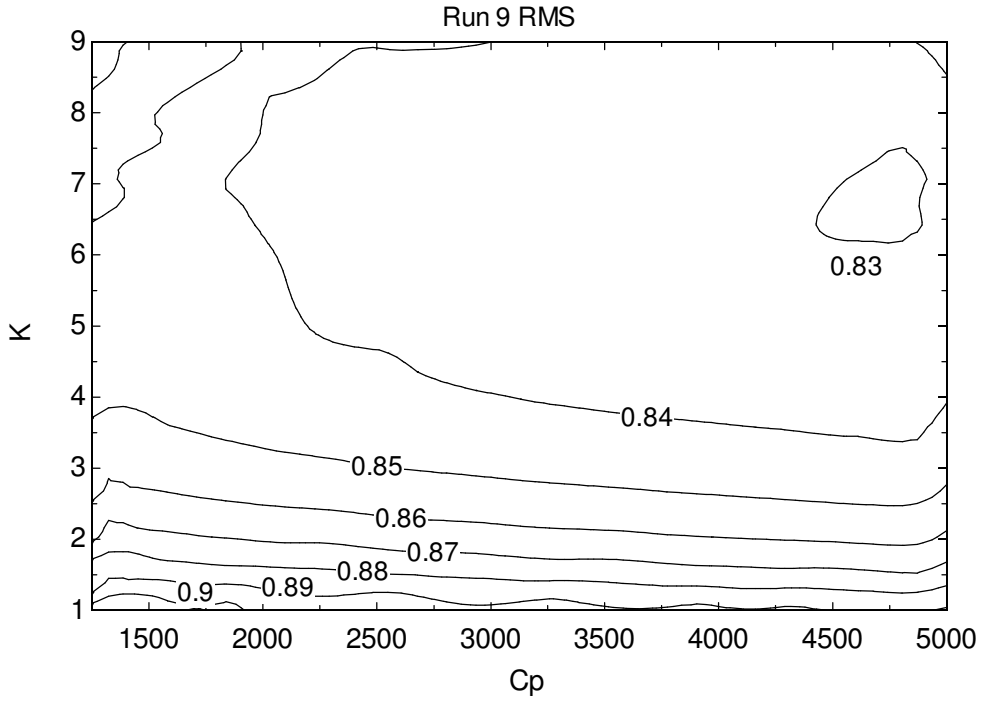

Figure 3-6: Root Mean Square Error in ΔºC with varying volumetric specific heat, Cp [kJ/m^3-K], and thermal conductivity, K [W/m-K], of the Ground Formation

The temperature profiles shown in Figure 3-7 through Figure 3-10 were generated using four different scenarios, all of which use the estimated heat capacity of 2549 [kJ/m^3-K]. The first (Figure 3-7) is a baseline case with a radius of 3 [in] and conductivity of 3.34 [W/m-K]. The second case (Figure 3-8) has a borehole radius of 3 [in] and a conductivity of 30 [W/m-K], which is the conductivity required to meet a 0 MBE requirement. The third (Figure 3-9) has the line source model thermal conductivity of 3.34 [W/m-K] and its corresponding radius of 1.98 [in]. The fourth (Figure 3-10) has the target radius of 2.25 and its corresponding conductivity of 4.875 [W/m-K].

Figure 3-9 and Figure 3-10 provide the best match between the modeled and experimental temperatures. However, as can be seen in Figure 3-3, there are multiple sets of model parameters that provide similar results. Increasing the radius beyond the 2.25 [in] target

radius very quickly increases the required formation conductivity outside the range of realistic values at around a radius of 2.5 [in].

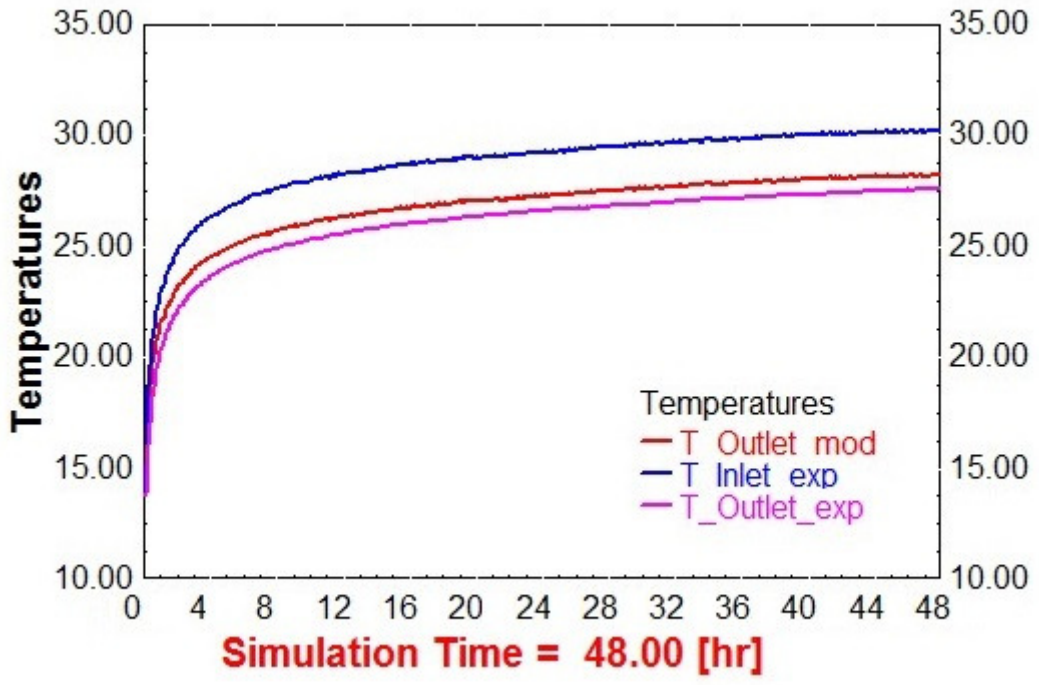

Figure 3-7: Temperature Profiles for Conductivity Test. Model Parameters: R = 3 [in], K = 3.34 [W/m-K], Cp =2549 [kJ/m^3-K]

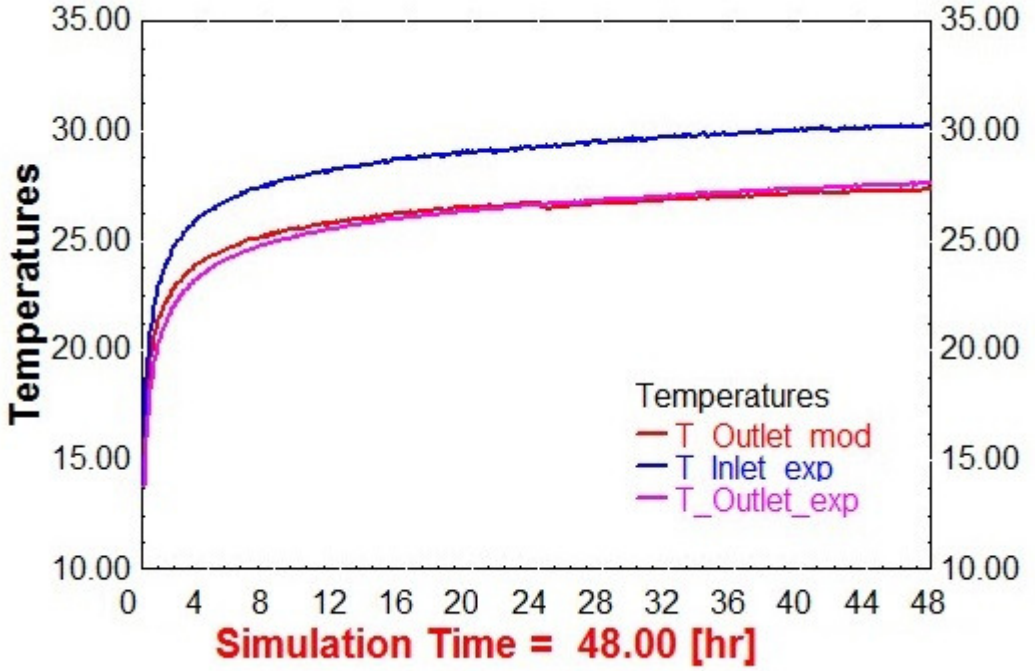

Figure 3-8: Temperature Profiles for Conductivity Test. Model Parameters: R = 3 [in], K = 30 [W/m-K], Cp =2549 [kJ/m^3-K]

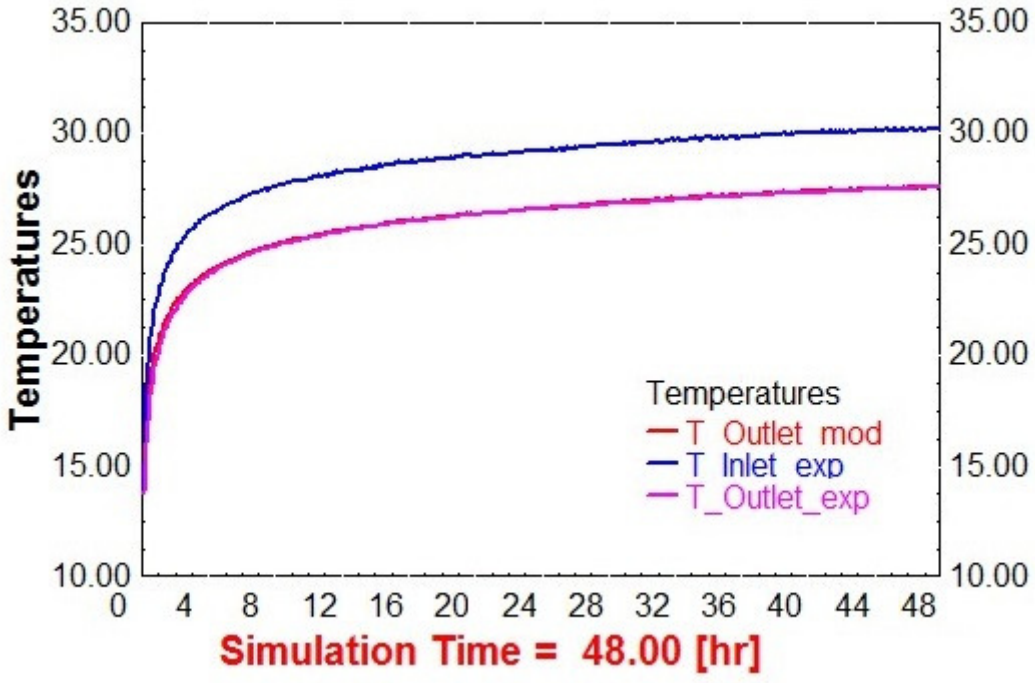

Figure 3-9: Temperature Profiles for Conductivity Test. Model Parameters: R = 1.98 [in], K = 3.34 [W/m-K], Cp =2549 [kJ/m^3-K]

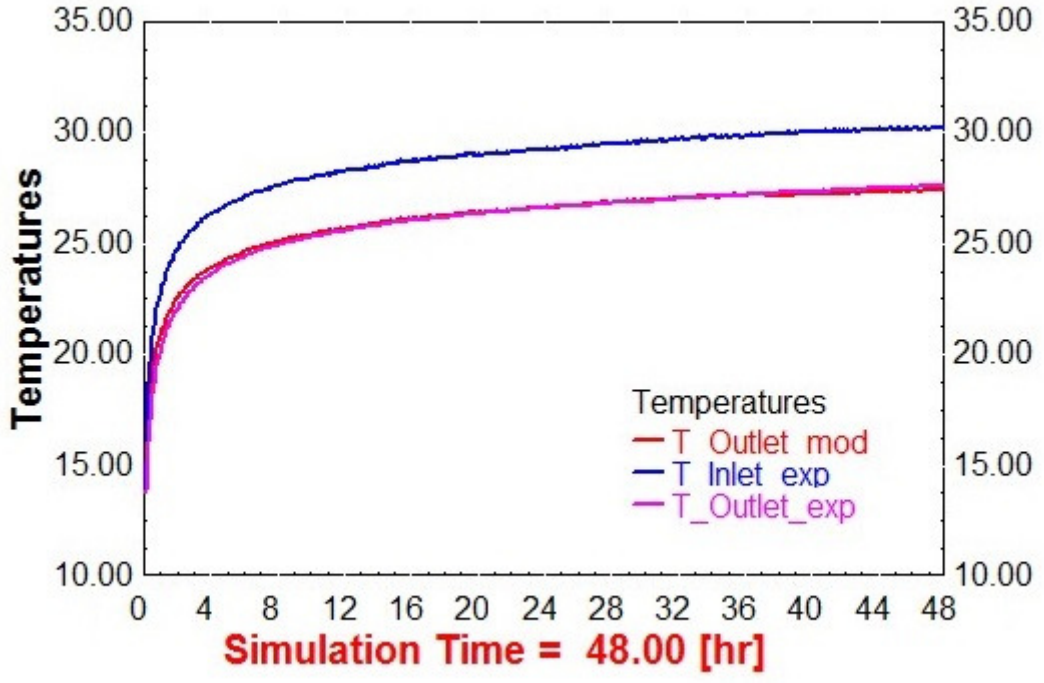

Figure 3-10: Temperature Profiles for Conductivity Test. Model Parameters: R = 2.25 [in], K = 4.875 [W/m-K], Cp =2549 [kJ/m^3-K]

3.2.3 The Second Bore-Field Modeling Effort

Following the initial bore-hole and bore-field modeling efforts, the TRNSYS models of the vertical borehole ground loop heat exchanger system were updated to make the simulations more easily adjustable via external program calls and more robust to variations in the time step of the experimental data. The variable names were also updated to match the temperature sensor labels in the NIST bore field documentation. The MATLAB code used to run parametric variations of TRNSYS simulations was modified and expanded to be more flexible. The three test data sets available (Ktest, TRT1, TRT2) provide data for four individual boreholes, three of which have two sets of measurements. Each of the seven borehole specific data sets were run using two parametric simulations based on feeding the model either experimental temperature data or experimental heat input data.

The error calculations previously done in the simulation and parametric MATLAB files were transferred and expanded into a new set of MATLAB files to form an analysis system. Similarly all of the analysis and plotting previously done in Excel, TRNSYS, and EES was implemented in MATLAB.

The borehole radius and formation thermal conductivity were then estimated by minimizing the error between the simulations and the experimental temperature profiles. The error minimization was done by finding the intersection of automatically determined contours of zero error for different time windows of data. Several other parameter estimation methods based on LSM, the Oakridge GPM tool, and a direct MATLAB optimization of TRNSYS simulation were also tested.

3.2.3.1 Data Processing Changes

In the initial borehole simulations, the data from the three tests was preprocessed before being fed into the simulations due to minor variations in sampling time and format. The resulting CSV file was then read directly into TRNSYS with one line being fed at each time step and then converted to the correct units in TRNSYS. In order to yield accurate predictions the model required that each line to be sampled at the required time step meaning that pauses in data collection or changes in the rate of data collection rendered data unusable. This requirement limited the available data and resulted in some additional error due to minor variations in the data collection rate.

For the second set of borehole simulations, the data were preprocessed to a set format and unit set by converting it into TRNSYS native units and saving it as a CSV file with a specific

column order. The data were then read into an interpolation table in which the simulation time is used to interpolate the values of the data. Like the simpler data reader, this method is most accurate when the simulation time step and sampling rate match and it is not subject to propagation of earlier timing errors through the rest of the simulation. This lack of error propagation also allows the simulation to use data with varying time stamps and missing data points though using such data will result in some loss of accuracy.

3.2.3.2 The Second Single Borehole Model

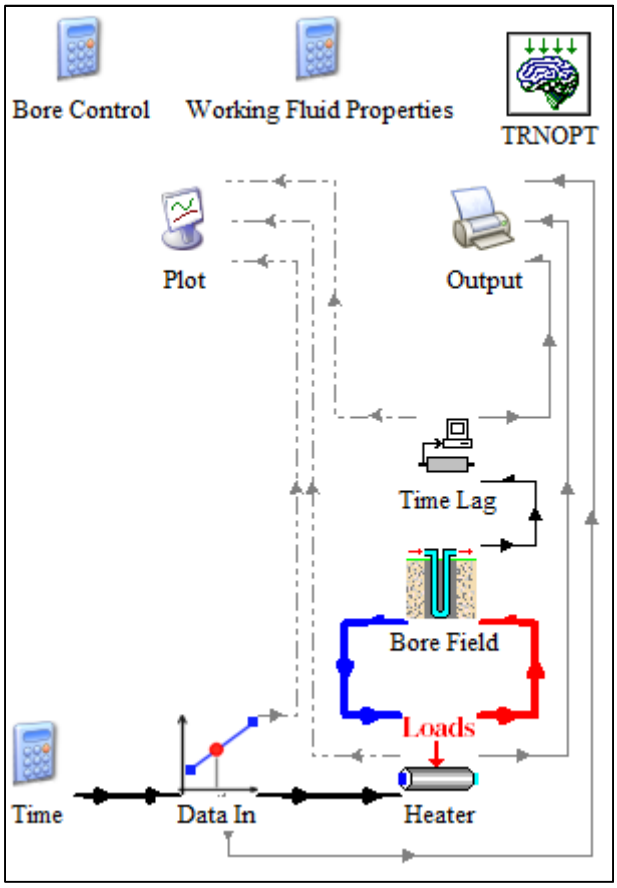

Figure 3-11: Diagram of TRNSYS simulation of a single borehole.

The single borehole simulation depicted in Figure 3-11 reads an experimental data file using the Type81 1D data file interpolator. The simulation time is output by the 'Time' equation

block and fed to the Interpolator. The interpolator then outputs the interpolated values for the inlet temperature, outlet temperature, mass flow rate, volumetric flow rate, and heating rate. If the simulation is set up as temperature feed the inlet temperature and mass flow rate are sent to the heater which then runs them through the borehole. If it is set up as heating rate feed then the heating rate and mass flow rate are sent to the heater which then applies them to the flow passing through the heater. The time lag adjust shifts the output to correspond with the time delay seen by the actual system. The equation components along the top of the diagram set parameters in the bore field simulation so that they are accessible to external programs in the text based TRNSYS simulation '.dck' file.

3.2.3.3 Temperature vs. Heating Rate Data Feed

Temperature data feed provides input temperature and mass flow rate to the load component which then passes them unchanged to the borehole model. The borehole model then provides output temperature. Temperature data feed provides a convenient way to compare the model with the experimental data using the Delta T. However it does not actually simulate a thermal response test except in the case where the model outputs the same temperature profile as the data because the heating rate is specified during a TRT. The heating rate required to bring the model output temperature up to the experimental input temperature is usually not constant and can be substantially different from the recorded heating data. This method is still useful for parameter optimization as, with a combination of input parameters matching the physical system, the model will recreate the test output temperature and the error measurements will approach zero.

Heating rate data feed provides the heating rate and mass flow rate to the load component which then applies it to a fluid loop running through the borehole allowing both the borehole input and output temperatures to change. Delta T error becomes useless as delta T is directly proportional to the heat input rate. Since this method uses the recorded (or a simulated constant) heat input rate, it is an actual simulation of the TRT. For comparisons between the simulation and the test data it is useful to use the slopes of the temperature profiles. Comparing these slopes has advantages over directly comparing temperatures, as with Delta T error or Mean Bias Error, because it is not be as strongly affected by initial temperature offsets in the modeled data. Thus in a situation where a large initial offset in the model is followed by behavior very similar to the test data, directly comparing temperatures will show the error associated with the initial offset at all time values after the offset while a measure of the slope will show the initial error only at the time of the offset followed by minimal error. As with the Temperature data feed set up, when the model parameters approach the 'correct' values all measures of error will approach zero.

After the comparison of temperature and heat rate data feed presented in Figure 3-12 through Figure 3-20 and in

Table 3-1 it was decided that there was insufficient difference in the predicted results to continue running both simulation types and heat rate data feed was used for the remaining studies.

3.2.3.4 MATLAB Script Description

The MATLAB scripts involved in determining ground loop heat exchanger parameters are diagramed in Appendix F and the scripts themselves are found in the electronic supplement. The scripts are separated into two branches: the first runs and records the TRNSYS simulations and the second analyses and plots the resulting data.

The first branch is controlled from the BatchRunner4 script, a follow up of the original 'batchRunner.m'. This script calls 'TRNSYScall3.m' to generate and run a parametric series of inputs in a TRNSYS simulation. TRNSYScall3 calls 'DeckWriter.m' to change the parameters in the TRNSYS '.dck' simulation file and then calls TRNSYS to run the simulation. 'OutputReader.m' then reads the simulation results and TRNSYScall3 collects them in a MATLAB data file.

The second branch is controlled by 'Predictor3.m'. Predictor3 calls 'Analysis3.m' which runs all of the error computations and stores them in another MATLAB data file. Predictor then calls the plotting scripts 'Plotter.m', which plots error contours and meshes, and 'PlotterTimeSeries.m', which plots 3D meshes of the Temperature profiles.

3.2.4 Analysis of Modeled Data

3.2.4.1 Types of Error Measurement Used in Analysis of Second set of Models

Two measures of the error in the slope of the average inlet and outlet temperature were implemented in addition to the root mean square (RMS) and mean bias error (MBE) used in the initial borehole modeling. The first is a direct measure of the difference between the experimental and modeled slopes. This method takes the average of the inlet and outlet temperature at each time step, calculates the slope of the averages, and then takes the difference between the slopes of the modeled and experimental data. The second method takes the average of the inlet and outlet temperature at each time step and then uses the inverse of the slope with respect to natural log of time and then calculates the difference. The second error method yields results which are proportional to the differences in the conductivity values calculated using the standard line source model. The methods have different scales with the second method resulting in more dramatic and easily read error plots. As both methods yield zero error in when the slopes are identical it doesn't matter which is used with the crossed contours method described below.

3.2.4.2 Crossed Contours Optimization Method

3.2.4.2.1 Use of Time Windows

Calculating error over an entire simulation run can result in the error from the initial, short, more rapidly changing, part of the simulation overshadowing better matching behavior during the rest of the simulation. In the case of mean bias error, this technique can also result in zero error even with poorly matched temperature profiles due to the initial error countering later errors. To counter these effects the error can be calculated separately for a series of time

windows. A set of parameters that results in minimum error for each time window, assuming that such a set exists, is close to the optimum parameters and will yield modeled temperature profiles that are very similar to the experimental ones over all time.

3.2.4.2.2 Contour Plot Overlays

For any given time window, a number of different values of radius and thermal conductivity will result in zero error. Thus, for a series of parametric runs there will be a contour of zero error for mean bias and delta slope error or near zero minimum for RMS error. For these borehole simulations, the contours do not flatten out as the length of a simulated experiment is increased. This effect has been tested out to 2000 hours and indicates that the sensitivity of the error to radius and other borehole geometric parameters does not disappear with time as is assumed in the Line Source Model. However the contours do change for different test lengths and different time windows. For a simulated experimental data set, it has been observed that the contours for all of the time windows cross at a single point corresponding to the "best" experimental parameters for radius and conductivity, as shown in Figure 3-12.

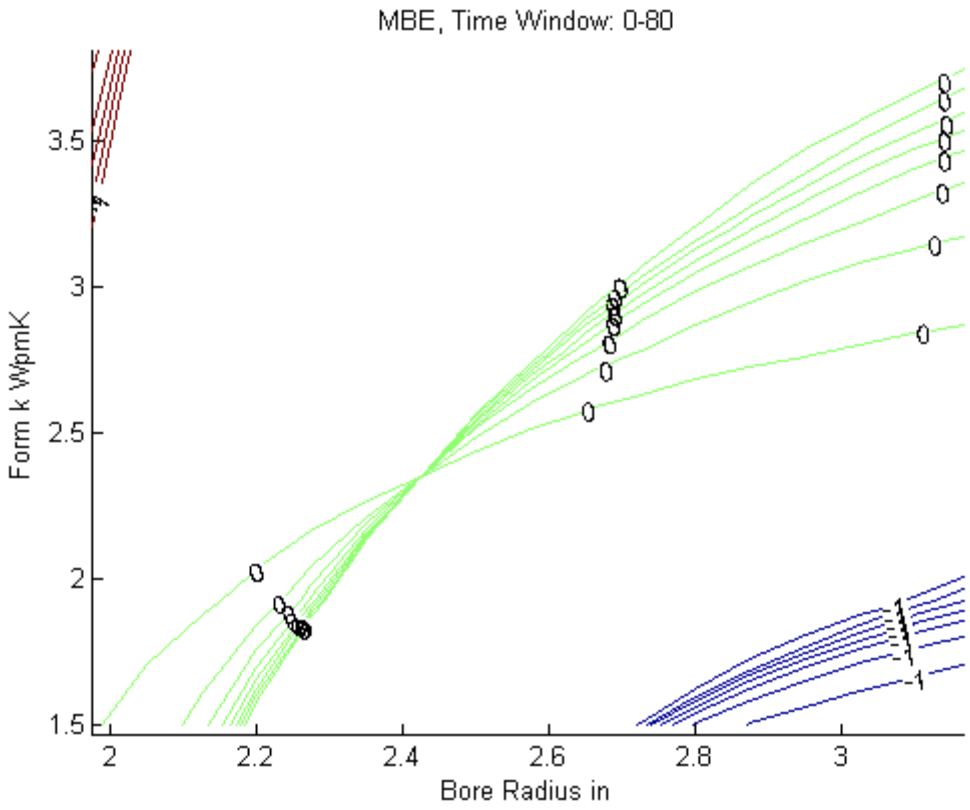

Figure 3-12: An example using the TRT1Leg1temeperature feed simulation. The simulated data was created using the parameters of R = 2.425 [in] and K = 2.35 [W/m-K]. The contours of zero error all cross at the point corresponding to the simulated parameters.

This method is effective as the radius and thermal conductivity have different effects on the temperature profiles at different time scales (and neither effect is really ever negligibly small). For experimental data sets this method still works, albeit not as cleanly. It is difficult to get close matching of the temperature profile in the earlier time windows while maintaining a match with the later time windows due to inaccuracies in the DST model being used to simulate the boreholes. To counter the trouble with early test data, the contour corresponding to the initial time window is ignored in the following analysis. Figure 3-13 and Figure 3-14 show the mean Bias and delta slope error contour plots for a simulation of the Ktest using temperature data feed. These two very different measures of error result in very similar sets of K and R values.

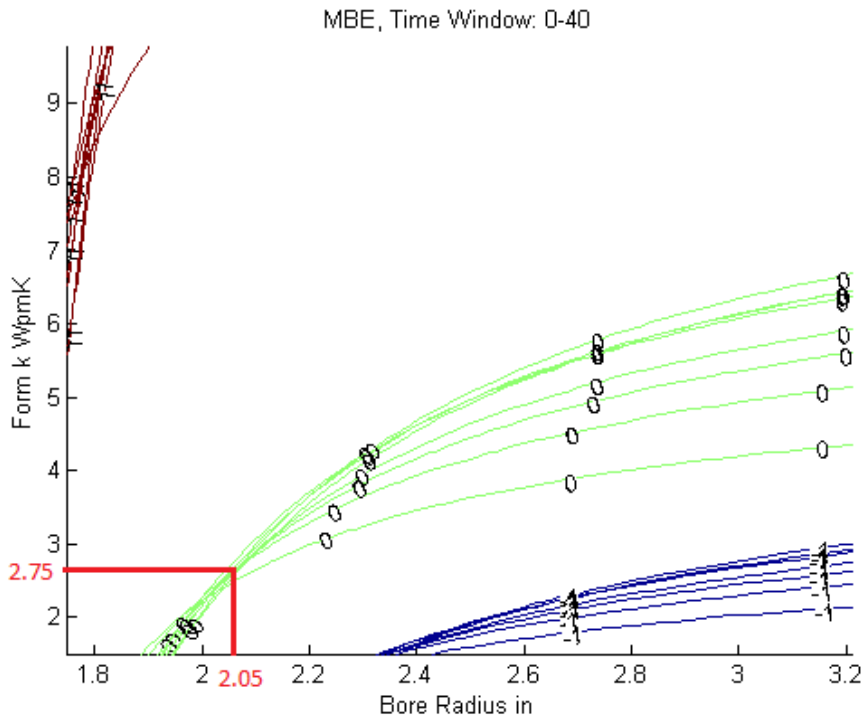

Figure 3-13: Example zero error contours for the mean bias error of the Ktest temperature feed simulation. The Point of intersection of the majority of the contours occurs at about 2.75 [W/m-K] and 2.05 [in].

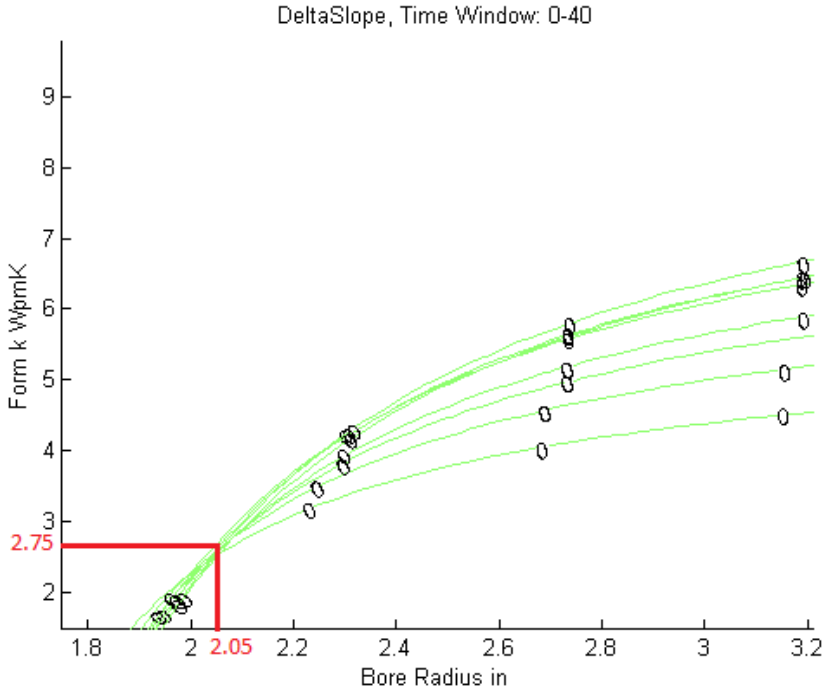

Figure 3-14: Example zero error contours for the delta slope error of the Ktest temperature feed simulation. The Point of intersection of the majority of the contours occurs at about 2.75 [W/m-K] and 2.05 [in] matching the parameters determined with the MBE contours.

3.2.4.3 Results of Second Bore-field Modeling and Parameter Determination

Table 3-1 documents the parameters determined using the Crossed Contour Method for all of the available individual borehole experimental data sets. The parameters vary significantly between data sets but are fairly consistent within the three measurements provided for each data set indicating that the results are fairly independent of whether the simulation is temperature or heat rate fed and which error measure is used to generate the contours.

Table 3-1: Comparison of Predicted Bore Radius and Formation Conductivity for Temperature and Heat Rate Data Feed

Data Set	Simulation Type	Error Type	Bore Radius [in]	Formation K [W/m-K]
Ktest	Temperature feed	MBE	2.05	2.75
\	\	Delta Slope	2.05	2.75
\	Heat rate feed	Delta Slope	2.05	2.75
TRT 1 Leg 1	Temperature feed	MBE	1.96	2.2
\	\	Delta Slope	1.97	2.3
\	Heat rate feed	Delta Slope	1.95	2.2
TRT 1 Leg 2	Temperature feed	MBE	2	2
\	\	Delta Slope	2.025	1.9
\	Heat rate feed	Delta Slope	1.96	1.9
TRT 1 Leg 3	Temperature feed	MBE	2.1	1.9
\	\	Delta Slope	2.1	2
\	Heat rate feed	Delta Slope	2.1	2
TRT 2 Leg 1	Temperature feed	MBE	2	2.5
\	\	Delta Slope	2	2.5
\	Heat rate feed	Delta Slope	1.98	2.75
TRT 2 Leg 2	Temperature feed	MBE	1.96	1.7
\	\	Delta Slope	1.97	1.75
\	Heat rate feed	Delta Slope	1.94	1.75
TRT 2 Leg 3	Temperature feed	MBE	2.08	1.8
\	\	Delta Slope	2.07	1.8
\	Heat rate feed	Delta Slope	2.05	1.7

Figure 3-15 and Figure 3-16 are the experimental and modeled temperature profiles for the temperature feed and heat rate feed simulations of the conductivity test using the values for R and K determined with the error contours. The temperature profiles match very well for the temperature feed simulation and are fairly good for the heat rate feed simulation.

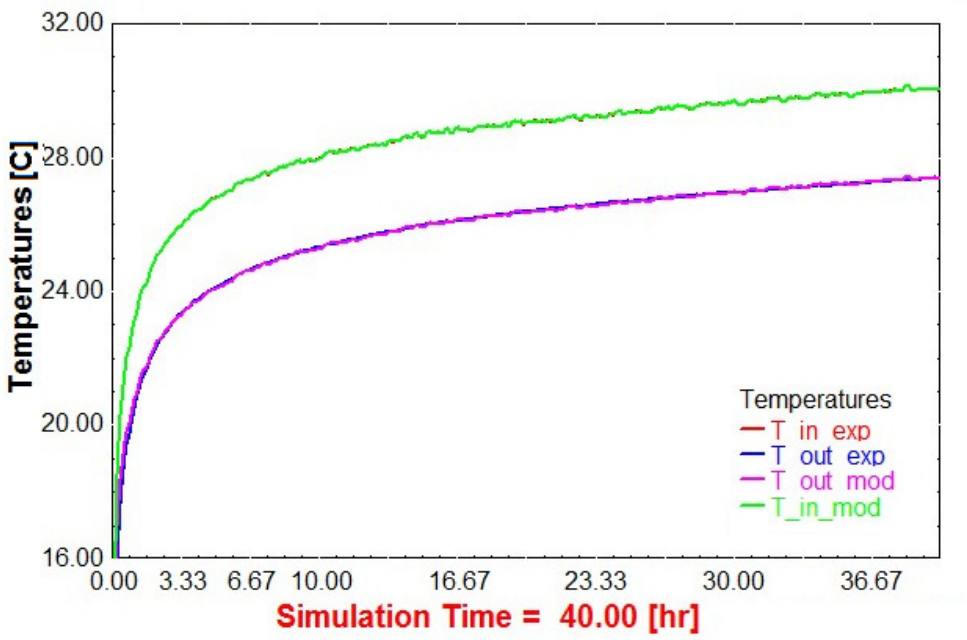

Figure 3-15: Temperature Profiles for Ktesttemeperature feed simulation using the determined values for K and R. Temperature in °C

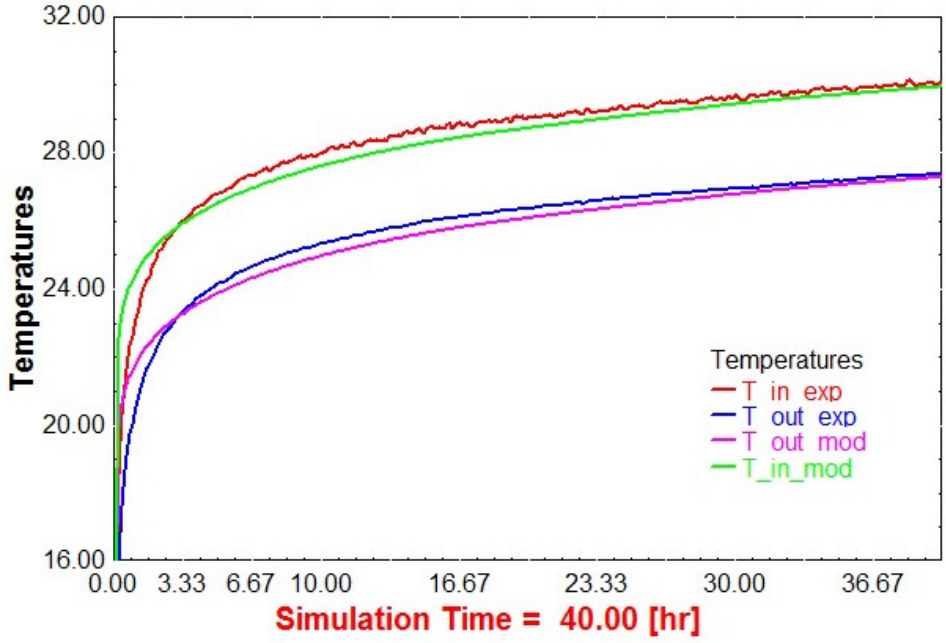

Figure 3-16: Temperature Profiles for Ktest Heat rate data feed simulation using the determined values for K and R. Temperature in °C

Figure 3-17 and Figure 3-18 are the experimental and modeled temperature profiles for the temperature feed and heat rate feed simulations of the first borehole during the first TRT

using the values for R and K determined with the error contours. Again the temperature profiles match very well for the temperature feed simulation and have the same early overshoot shown by the conductivity test plot.

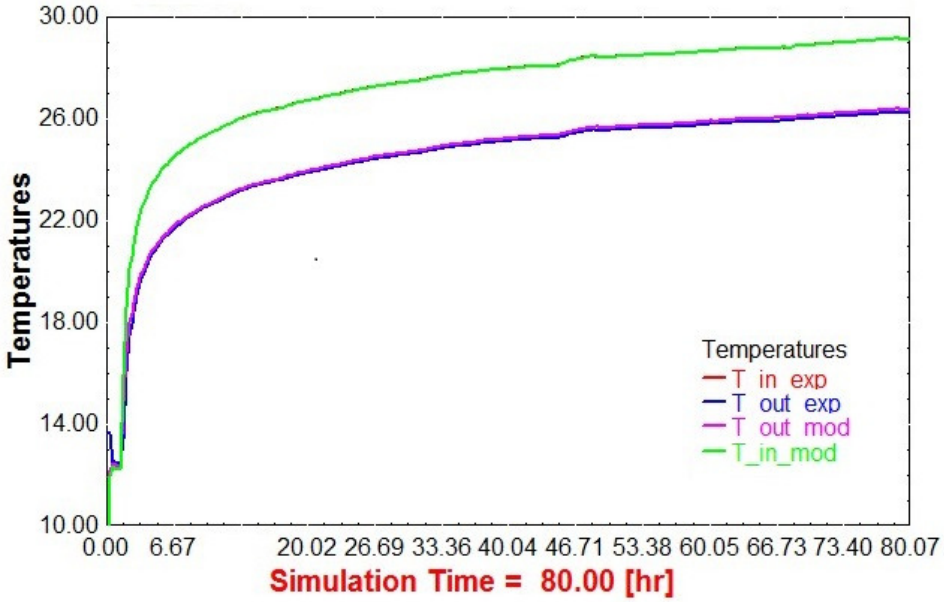

Figure 3-17: Temperature Profiles for TRT1 Leg1temeperature feed simulation using the determined values for K and R. Temperature in °C

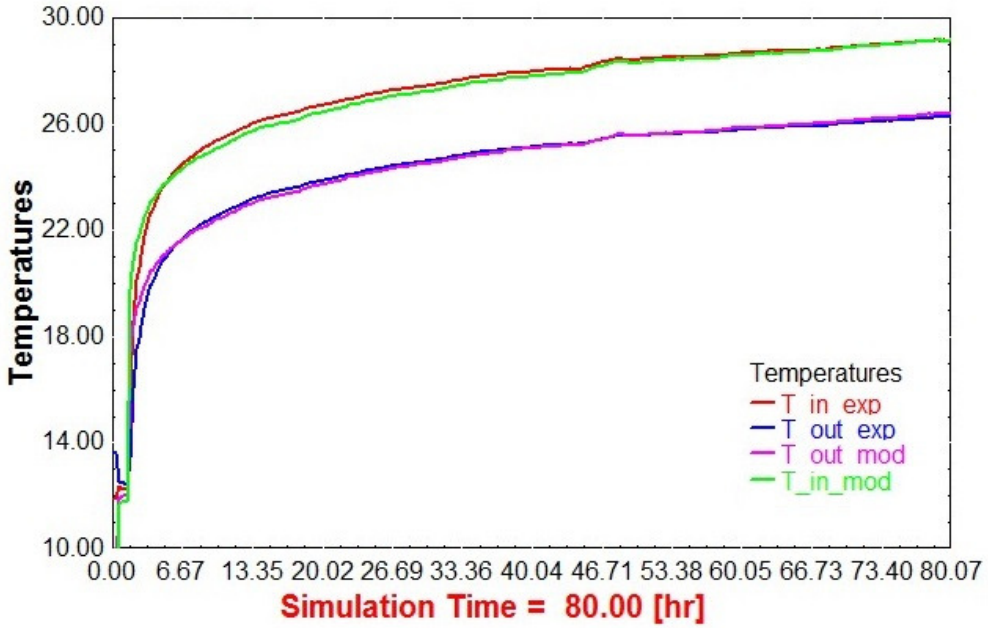

Figure 3-18: Temperature Profiles for TRT1 Leg1 Heat rate data feed simulation using the determined values for K and R. Temperature in °C

Figure 3-19 and Figure 3-20 are the experimental and modeled temperature profiles for the temperature feed and heat rate feed simulations of the first borehole during the second TRT (TRT2) using the values for R and K determined with the error contours. The modeled output temperature profile for the temperature feed simulation is slightly higher than the experimental temperature profile. The heat rate feed profiles again have the initial overshoot and the delta T appears to be slightly smaller than the experimental profile. The discontinuity shown in the diagrams was the result of an interruption in the testing rig's power supply that resulted in heating being briefly stopped. This discontinuity is, in a way, representative of the types of messy data that transient simulations handle better than steady state analysis.

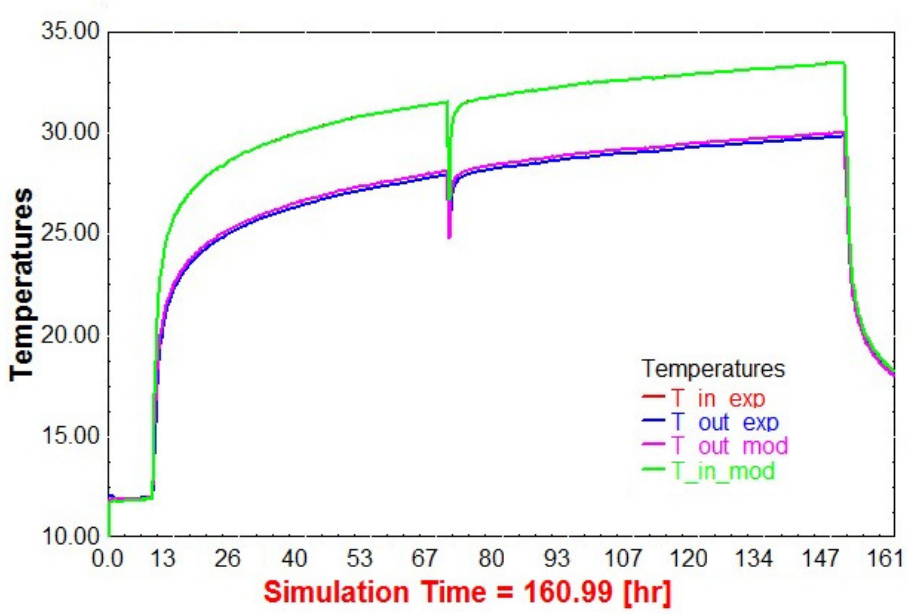

Figure 3-19: Temperature Profiles for TRT2Leg1temeperature feed simulation using the determined values for K and R. Temperature in °C

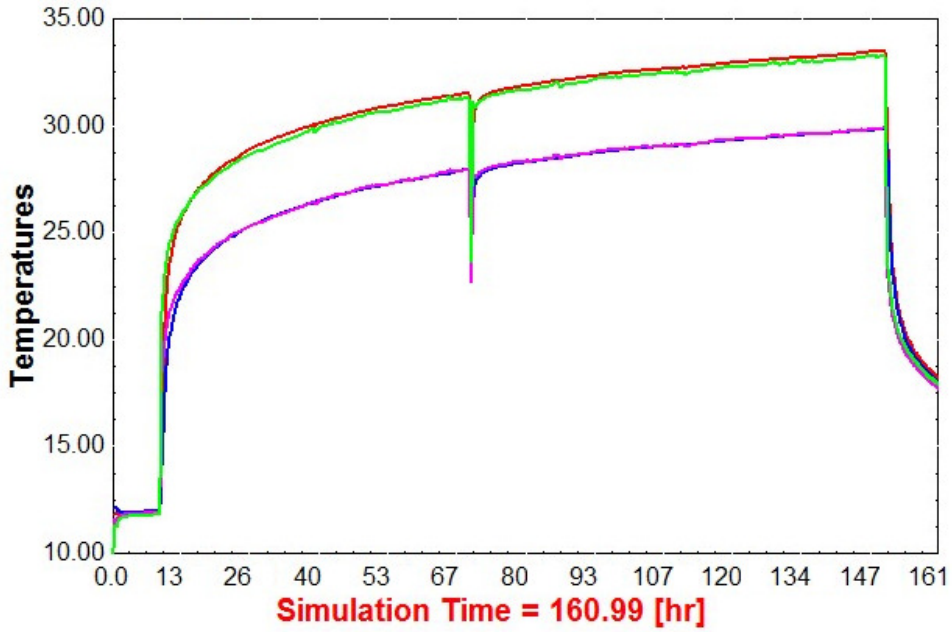

Figure 3-20: Temperature Profiles for TRT1 Leg2 Heat rate data feed simulation using the determined values for K and R. Temperature in °C

3.2.4.4 Other Analysis Methods Tested (LSM, TRNSYS Parameter Search, GPM)

3.2.4.4.1 LSM Model

The infinite line source model is the industry standard for TRT analysis. It is based on Kelvin's solution to an infinite line with constant heat flux in an infinite medium. The model greatly simplifies the geological formation and the borehole but for long test durations the LSM can deliver reasonably accurate measurements of the ground properties. However using the LSM model to provide accurate results still requires that the TRT have a near constant heat input to the borehole, the formation/borehole must be close to homogenous, and there can be no significant ground water flow. In this study, the LSM estimates of K_f for the first and second TRT are not quite representative of typical line source results due to the varying heat load applied to each leg of the bore field.

3.2.4.4.2 Geothermal Property Measurement Tool

Oak Ridge National Lab developed a numerical infinite cylinder borehole model and used it to create the Geothermal Property Measurement Tool (GPM). This tool uses a Nelder-Mead optimization function to search for an optimum set of formation conductivity (K_f) and borehole resistance (R_b) to match the model and a TRT data set. The cylinder source model has similar limits to the LSM in that it uses simple approximations of the geological formation and borehole. However the GPM cylinder source model is numerical and includes the borehole heat capacity and resistance allowing it to handle short time scale transients and unsteady heat inputs fairly well. The parameters estimated using GPM are typically lower than those from the line source model and higher than those generated from the TRNSYS DST based simulations.

3.2.4.4.3 TRNSYS Parameter Search Implementation

The TRNSYS parameter search implementation uses the MATLAB fminsearch function which is based on the same optimization algorithm as the GPM program. The error function that is minimized is also the same: the sum of the square of the difference between the experimental and modeled average borehole temperatures at each time step. The difference lies in the model being used to simulate the borehole: the TRNSYS DST component vs. the GPM numerical model. The TRNSYS model more accurately represents the geological formation, finite length of the boreholes, and environmental inputs (surface loses/gains) while the borehole itself is less accurate. The use of the DST borehole model results in parameter estimates being dependent on the data range selected. This dependence on data

range is also true of the GPM model and the parameters reported by the GPM model are taken after they converge later in the TRT and thus are less dependent on the early test data.

3.2.4.4.4 Impact of Exclusion of Early Data on Parameter Estimates

When analyzing the initial conductivity test (Ktest) data using the DST model, selecting only late time period data (after 20 hours) resulted in parameters that are closer to those estimated by LSM analysis. Selecting all data after the first hour results in parameters that are closer to those estimated by the crossed contour method. This relation is not as strong for the TRT1 and TRT2 data sets due to the effect of the deviation of testing conditions from those of an ideal semi steady state TRT on the LSM results. As shown in Figure 3-21 the TRNSYS optimization results for both R_b and K_f converge after about 20 hours of data are excluded. Figure 3-22 and Figure 3-23 show the temperature profile results when either early data (Figure 3-22) is included or only late data (Figure 3-23) is included in the optimization. As is expected, the inclusion of early data results in better matching between simulation and experiment during the initial rapid transient state at the expense of matching later in the data set. Likewise, the exclusion of the initial data results in better matching later at the expense of matching early in the simulation. With a perfect TRT, the LSM results would match the TRNSYS optimization results if only the later data is used. The TRNSYS DST model does not predict the short term behavior well and the TRNSYS optimization parameter estimation results presented in Table 3-2 below use the averaged results for 20, 30, and 40 hour start times.

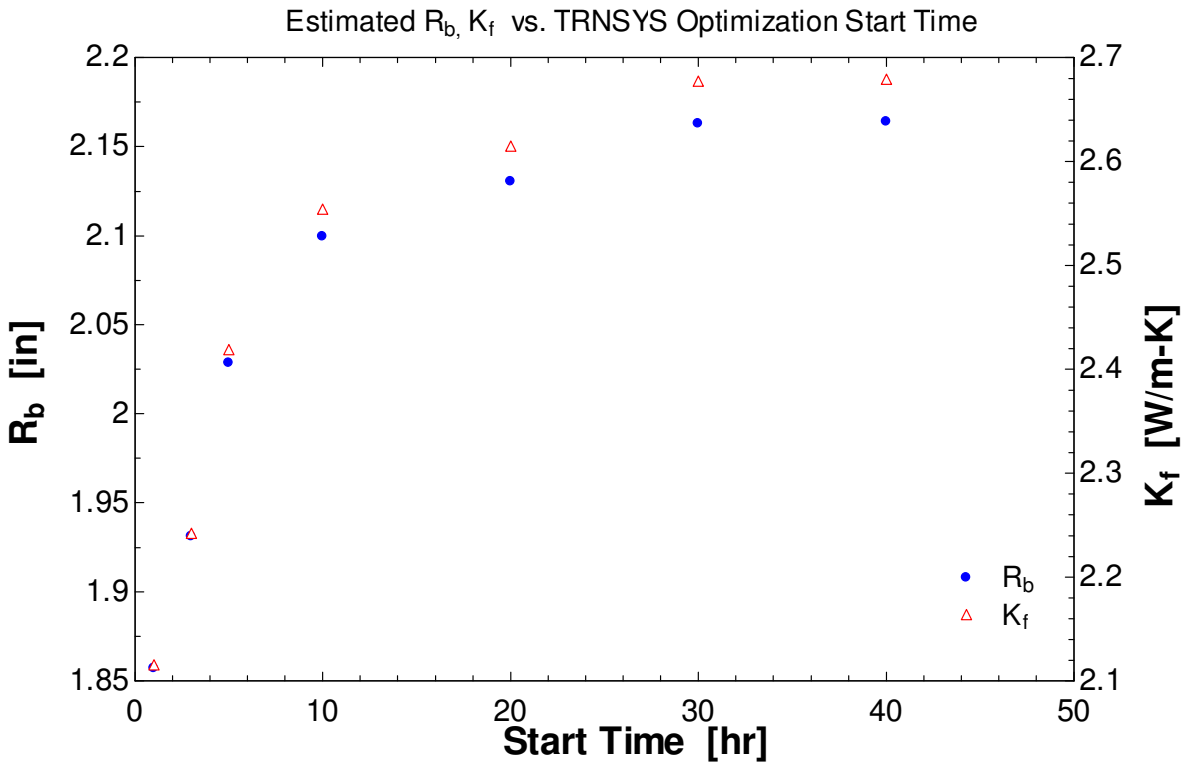

Figure 3-21: R_b and K_f estimated from TRT 1 Leg 1 using the TRNSYS optimization code. Start time is the length of initial data excluded.

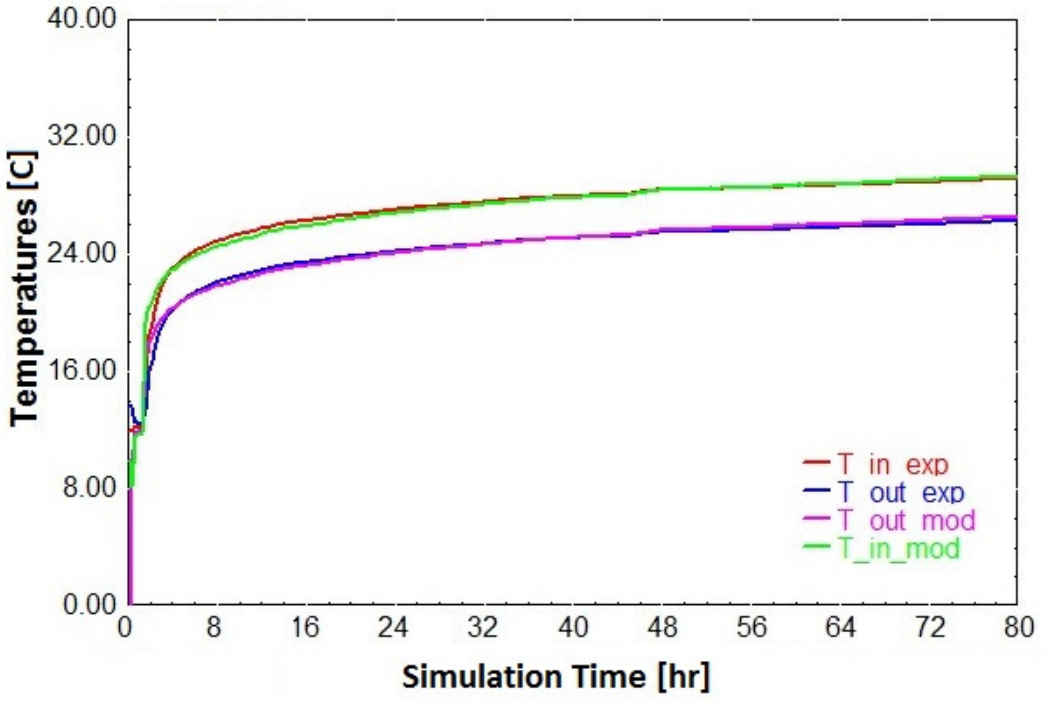

z

Figure 3-22: Plot of simulated and experimental temperature profiles for TRT1 Leg1. The simulation uses the parameters determined using the TRNSYS optimization code on all data after the first hour.

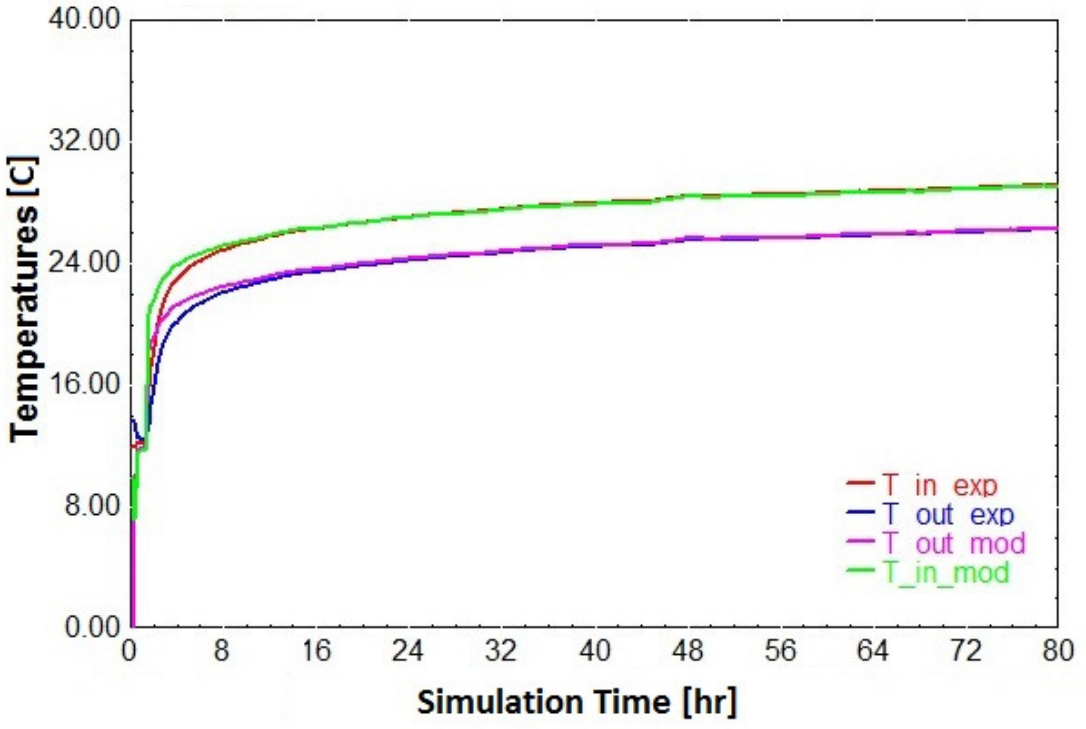

Figure 3-23: Plot of simulated and experimental temperature profiles for TRT1 Leg1. The simulation uses the parameters determined using the TRNSYS optimization code on all data after the first 40 hours.

It is also of interest to show the impact changing the start time of the data analysis has on the entering water temperature, a predictor of heat pump efficiency, of the borehole simulation over much longer time periods. Figure 3-24 shows the predicted maximum EWT for a series of models run based on the parameters estimated from a single data set, Leg 1 of the first TRT, using the TRNSYS parameter optimization code.

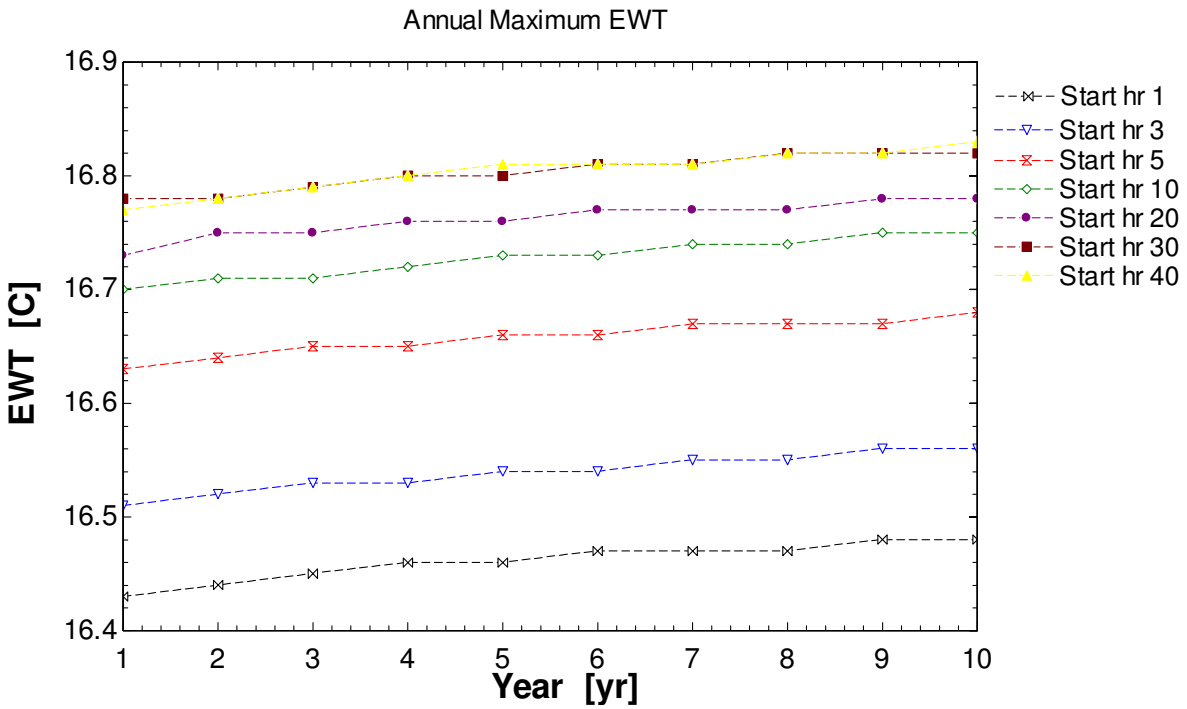

Figure 3-24: Plot of the maximum entering water temperature for each year of a ten year simulation using K_f and R_b estimated from the TRT1Leg1 TRNSYS parameter optimization. Each series represents the results from starting the parameter optimization at the given start time.

To demonstrate the difference that the initial parameter estimate can have on modeling results, Figure 3-25 shows the simulated maximum EWT in the tenth year as a function of the start time of the parameter estimate in the initial TRT data set. The total range is about 0.5 °C but the values converge as the start time of the parameter estimation is moved later and excludes more of the data from the TRT. This behavior is a result of the TRNSYS DST model's short time response behavior and its impact on the estimated parameters. In this way the TRNSYS parameter estimation is similar to LSM analysis, however the more accurate handling of transients in TRNSYS results in a more stable parameter prediction and less variation in the estimated parameters and thus in the predicted EWT.

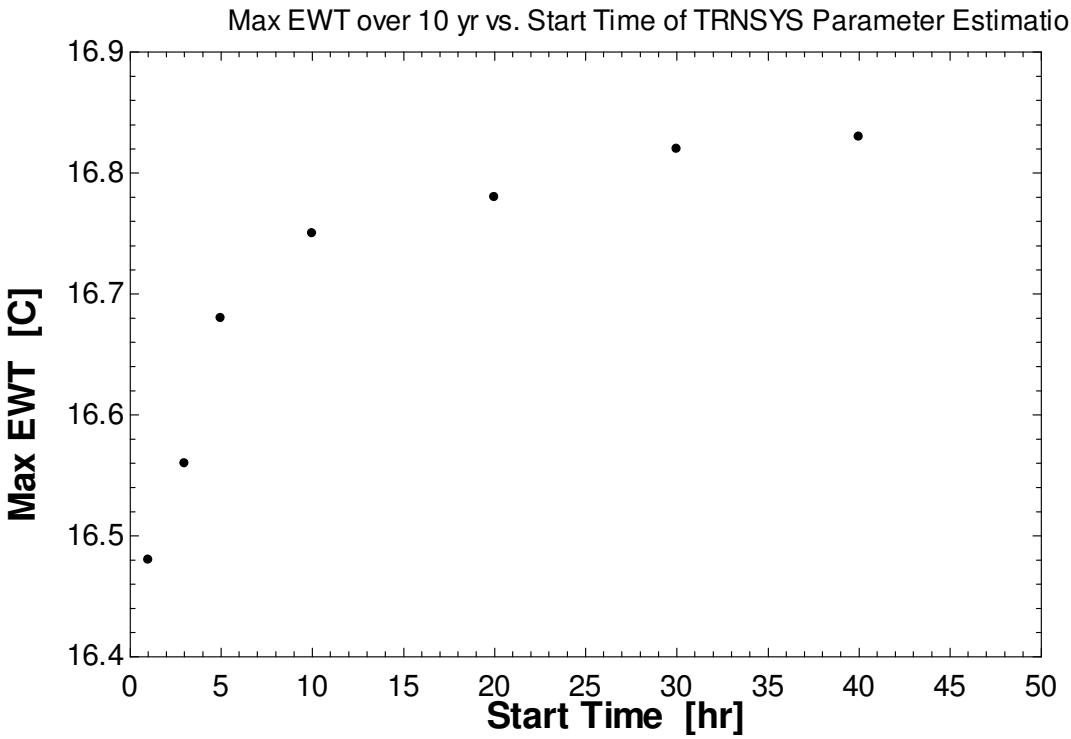

Figure 3-25: Plot of the maximum entering water temperature over 10 year simulation using K_f and R_b estimated from the TRT1Leg1 TRNSYS parameter optimization. Each point represents the results from starting the parameter optimization at the given start time.

3.2.4.5 Comparison of Crossed Contour Method to Other Optimization Methods

As a means of optimizing a model to fit the TRT data, the crossed contour method has several advantages: Simulating all of the data sets ahead of time allows them to be used in a manner similar to a look up table and the use of multiple time windows and contour plotting to smooth out the values reduces the number of runs required to estimate the parameters. The crossed contour method also provides a useful way of visualizing how the parameters affect the model accuracy at different time scales. With modern computers, the potential advantages in computation time are of little importance for borehole parameter estimation. However, it is interesting to note that a similar approach utilizing a database of parametric EnergyPlus simulations is being used by Oak Ridge National Laboratory's Building Technologies Research & Integration Center in an automated building simulation calibration project,

Autotune (Sanyal & New, 2013) and a similar method might be employed for more computationally intensive TRNSYS optimization projects.

All of the parameters estimated using the Crossed Contour method produce good fits between the modeled and experimental data. However the inclusion of early data in the analysis results in lower estimates of thermal conductivity and larger estimates of borehole radius. This behavior is due to the DST model over predicting the rate of change during transient events due to the lack of borehole thermal capacitance. The results from all the parameter estimation methods tested are outlined in the crossed contour columns of Table 3-2.

3.2.4.6 Summary of Estimated Ground Properties

The parameter estimates generated from each data set by every analysis method are outlined in Table 3-2. The estimates of R_b range from 1.85 [in] to 2.22 [in] for the initial conductivity test (with the nominal R_b being 2.25 [in]). The estimated values of K_f range from 1.73 [W/m-K] to 3.4[W/m-K]. Some of this variation appears to represent variations in the data itself: the initial conductivity test data yields a higher K_f value regardless of the method employed. Other variations appear to be between the methods: the TRNSYS Optimization consistently yields the highest K_f and lowest R_b values.

Table 3-2: Summary of Estimated Ground Properties

	LSM		Crossed Contour		TRNSYS Optimization		GPM	
Test Data Set	R_b **[in]**	K_f **[W/m-K]**	R_b **[in]**	K_f **[W/m-m]**	R_b **[in]**	K_f **[W/m-K]**	R_b **[in]**	K_f **[W/m-K]**
kTest	2.25	3.35	2.05	2.75	2.22	3.40	2.25	2.63
TRT 1 Leg 1	2.25	2.26	1.96	2.23	2.15	2.66	2.25	2.07
TRT 1 Leg 2	2.25	2.32	2.00	1.93	1.99	2.72	2.25	2.20
TRT 1 Leg 3	2.25	2.75	2.10	1.97	1.85	3.00	2.25	2.60
TRT 2 Leg 1	2.25	1.88	1.99	2.58	1.85	2.29	2.25	1.84
TRT 2 Leg 2	2.25	1.90	1.96	1.73	1.85	2.44	2.25	1.91
TRT 3 Leg 3	2.25	2.25	2.07	1.77	1.83	2.94	2.25	2.22

3.2.5 Ground Property Values for Future Modeling of the Test Facility

Though it is desirable to increase the accuracy of the predicted ground and borehole properties, there are significant variations between the properties estimated from the original conductivity test and the subsequent tests of Leg1 of the bore field which are in the same location. These results persist for each method of analysis, indicating more information about the borehole and ground conditions (water levels etc.) is needed than is currently available. It is unlikely that any further attempts to refine the parameter estimates without such information and/or a more detailed model would be helpful. However, the parameter estimates generated allow the ground models to match the test data to the best of the model's ability to accurately represent the system.

As the TRNSYS DST model uses one set of parameters for all boreholes within a bore-field, it is recommended that the median parameters predicted by all of the data analysis methods using the data from TRT1 and TRT2 be used in the coupled house model/ground loop simulations. This median excludes the data from the original conductivity test (Ktest) results. This data set is excluded due to the higher than average property predictions resulting from

this data and due to the nature of the Ktest borehole. The Ktest borehole is separate from the boreholes in the vertical GLHX, was twice as deep, potentially resulting in exposure to substantially different geological conditions and will not be in use as part of any of the Test Facility experiments. Thus the final values of borehole radius and formation thermal conductivity for use with the House Model are: **Rb 1.92 [in] and Kf 2.43 [W/m-K].**

3.3 Long Term Borehole Study

3.3.1 Long Term Sensitivity of the TRNSYS Model

A series of three long term simulations were performed to estimate the impact of differences in the estimated borehole parameters. Two Bore-field models were developed: one for direct application of the recorded load to the circulating fluid and one that included an intermediary heat pump. The single bore field simulation used in the parameter determination was altered to include three boreholes with identical parameters. The ground and borehole parameters were set to different combinations resulting from the different parameter estimation techniques and individual borehole data sets. The annual household HVAC thermal load requirement file from the TRNSYS House Envelope and Load Model documented in Chapter 2 and the matching TMY3 data file for Washington Dulles Airport were input into the simulations. The simulations were run over 10 and 60 year periods and the resulting entering water temperature predictions were processed in MATLAB.

3.3.1.1.1 Entering Water Temperature

The measure of performance chosen was the entering water temperature (EWT) which is the temperature of the working fluid exiting the ground heat exchanger and entering the heat pump. As EWT is the feed temperature for the heat-pump, it has the most direct impact on

heat-pump efficiency and capacity and manufacturers specify minimum and maximum entering water temperatures for nominal operation. The maximum EWT is of interest as the maximum cooling loads typically occur when the greatest heat pump capacity is required. Minimum EWT is also of interest as, in heating dominated location, it may occur when the greatest capacity is required (J. A. Shonder, Thornton, & Hughes, 2001).

3.3.1.1.2 Length of Long Term Simulations

If properly installed and maintained and no unexpected seismic incidents or accidents occur, the estimated life span of the ground loop heat exchanger is around 60 years (Liu, 2010). This longevity is due to the closed nature of the fluid flow which results in little buildup of contaminants and the resistance of the thermally joined polymer tubes to degradation in the absence of UV light. Thus the longest simulated time period was 60 years. As can be seen in Figure 3-30 the maximum EWT stabilizes well before 60 years and it was deemed sufficient to run the remainder of the simulations to 10 years.

3.3.1.2 Choice of Parameter Sets

The parameter sets (couples of R_b and K_f) used were all taken from the range of parameters estimated by the LSM, Crossed Contours, TRNSYS parameter optimization, and GPM methods. Thus the simulations represent the full range of estimated parameters for all of the different data sets and analysis methods.

Three parameter sets were chosen for the 60 year simulations. These parameter sets consisted of a minimum heat transfer case, a maximum heat transfer case, and the nominal R_b and K_f estimated from the original conductivity test using the LSM. These parameters are recorded

in Table 3-3. The minimum heat transfer case used a combination of the maximum (highest resistance) estimated R_b and the minimum estimated K_f. The maximum heat transfer case used a combination of the minimum (lowest resistance) estimated R_b and the maximum estimated K_f. The high and low heat transfer (HT) cases are more extreme than any of the predicted parameter sets as the optimization methods adjust the parameters relative to each other to match the data set given a specific heat input. Thus the high and low HT cases are used as external bounds on the estimated parameters.

The remaining seven parameter sets consist of the predicted parameter sets in which the minimum, maximum, and median values of R_b and K_f were found and the average of the predicted parameter sets, which will be used in future ground loop modeling.

Table 3-3: Parameter Sets Used in the Long Term Simulations

Case Name	Parameter Estimate Values From:	Rb [in]	Kf [W/m-K]	Description
High HT	Mixed	1.80	3.40	Combination of determined parameters with the lowest heat transfer (min K_f, max R_b).
Low HT	Mixed	2.22	1.71	Combination of determined parameters with the highest heat transfer (max K_f, min R_b).
LSM	Ktest LSM analysis	2.25	3.35	Original contractor reported values.
Min R	TRT 1 Leg3 Topt 50 hr	1.80	2.86	Parameter set with minimum R_b value.
Min K	TRT 2 Leg3 Xcon	2.05	1.70	Parameter set with minimum K_f value.
Med R	TRT 1 Leg1 Topt 3hr	1.93	2.24	Parameter set with median R_b value.
Med K	TRT 2 Leg2 Topt 20hr	1.87	2.46	Parameter set with median K_f value.
Max R	TRT 1 Leg1 Topt 40 hr	2.16	2.68	Parameter set with maximum R_b value.
Max K	TRT 1 Leg3 Topt 10 hr	1.92	3.27	Parameter set with Maximum K_f value.
In Use	Used for NZERTF model	1.92	2.43	Average of the predicted parameter sets

3.3.1.3 TRNSYS Bore-field Models Used

Two Bore-field models were developed: one for direct application of the recorded load to the circulating fluid and one which included an intermediary heat pump. Each model takes a simulated thermal load file from the house envelope and internal gain model and meets it via a vertical GLHX. The bore-field has three boreholes corresponding to the NZERTF vertical field (Building Sicence Corporation, 2012). The same TMY3 file for Washington-Dulles, 'Washington DC Dulles Int'l Ar [Sterling - ISIS]_724030TY.csv', that was used to generate the thermal load profile was repeated annually in the simulation. Thus the EWTs generated are representative of a typical year and not extreme years. All of the long term simulations studies used a 15 minute time step.

3.3.1.3.1 Direct Load Application Model

The direct application model shown in Figure 3-26 uses a heater to apply the load to the working fluid circulating through the borehole.

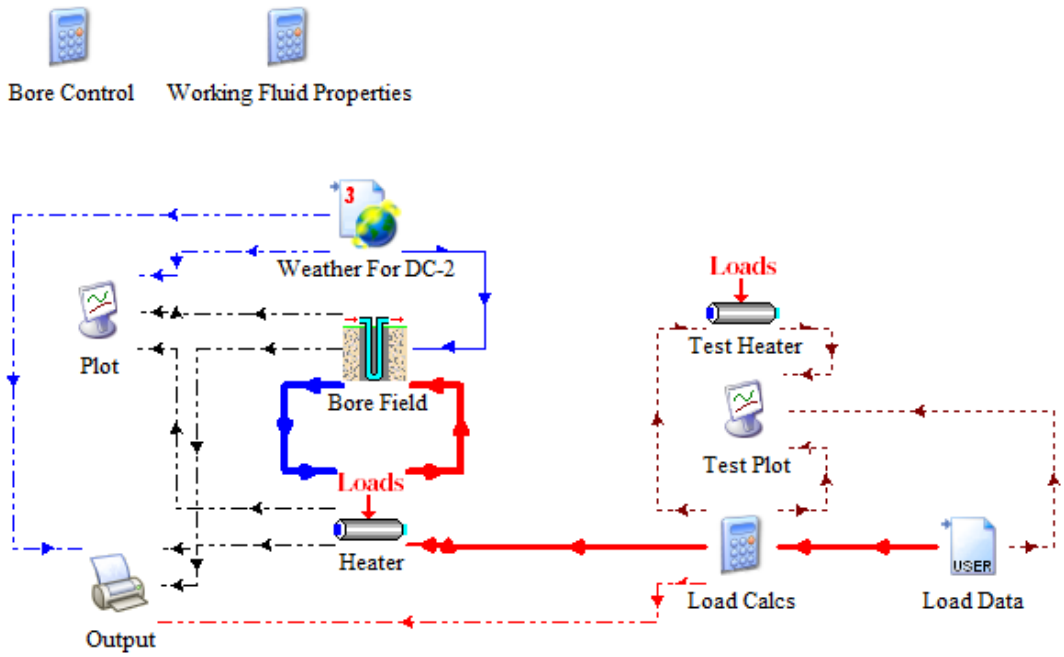

Figure 3-26: Original long term entering water model configuration.

3.3.1.3.2 Heat Pump Load Model

The direct application method does not include the amplifying impact that a heat-pump has on the minimum and maximum entering water temperatures due to the changes in heat-pump efficiency at the minimum and maximum temperatures. To test the impact that this effect would have on the minimum and maximum EWTs, a second simulation was developed that used a water source heat-pump to meet the thermal loads. This model is shown in Figure 3-27.

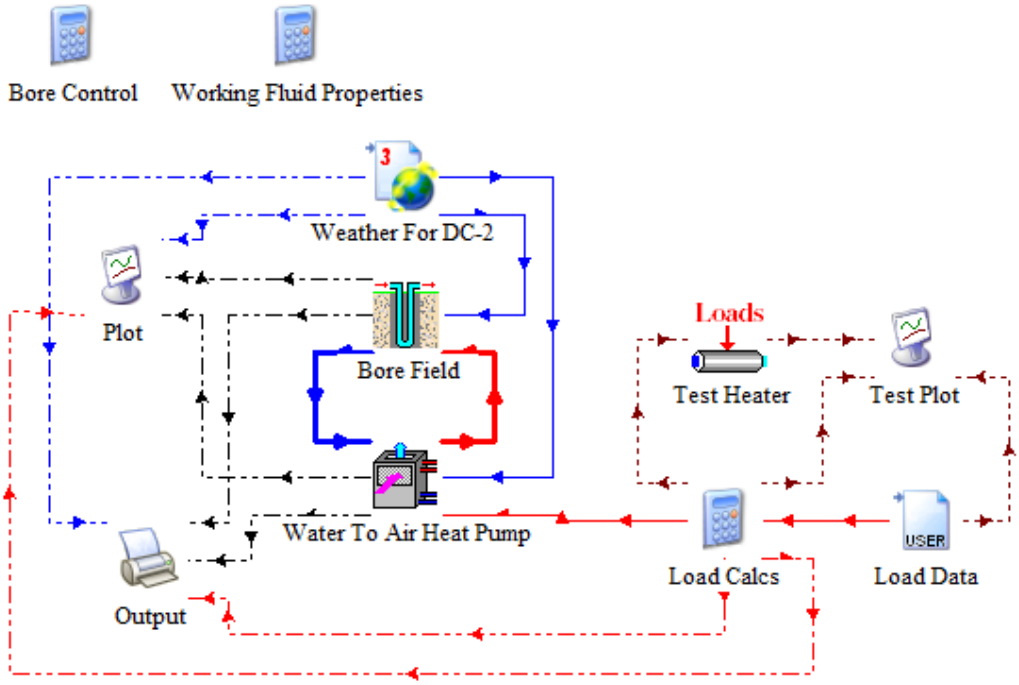

Figure 3-27: Long term entering water model with heat-pump

The TRNSYS TYPE 919 Water Source heat-pump was used. The parameters used in this component and reasoning behind them are documented in the 'GS HP (long study)' tab of the spread sheet 'TRNSYS model system parameters.xlsx' which is included in the electronic supplement. The parameters were determined from the *Water Furnace Specification Catalog 5 Series* (2013). The heat-pump was sized such that the cooling and heating capacities were equal to the maximum required cooling and heating capacities from the load file which was generated using energy control. The cooling and heating control signals were determined based on the load input file. The heat-pumps full cooling or heating capacity was applied to the air stream for the duration of the time step. The resulting thermal loads were applied to a water loop and sent to the bore-field. It should be noted that this load file was generated using TMY data and may be undersized relative to what is actually required to accommodate more extreme weather.

The resulting temperature profiles were output to a text file which was analyzed using the MATLAB script: LongStudy_Analysis1.m which can be found in the electronic supplement. This script reads the files in year-long segments and finds and records the minimum, average, and maximum EWT along with a number of other parameters. These values were then plotted in EES

3.3.1.3.3 High Load Simulations

The load profile was derived from the NZERTF TRNSYS envelope and load model and used in conjunction with a model of the bore field present at the NZERTF site. The use of this load profile resulted in lower loads per unit length of borehole relative to a typical residential installation. A series of simulations was run to test the impact of more typical, higher loads on both the direct application and heat pump models. The total load on the bore field was multiplied by three, resulting in a load profile approximately equal to the load a single borehole would be subjected to if it were isolated and used to meet the entire NZERTF demand. This loading scenario was chosen as it is possible to configure the NZERTF bore field in such a manner (Building Science Corporation, 2009).

3.3.2 Results of Direct Thermal Load Application

The results from the Direct Load Application Simulations indicate that the variations in the estimated parameters can result in noticeable changes in the minimum and maximum EWTs. Figure 3-28 and Figure 3-30 show the minimum and maximum temperatures, respectively. These temperatures change quickly in the first two years of the simulation and then slowly increase over the remaining time. The average EWT is shown in Figure 3-29 and increases over the course of the simulation; however, the scale of the change over time is on the order

of 0.1 °C. Thus increased thermal resistance between the working fluid and ground results in short term increases the temperature extremes around the borehole but leads to a minimal increase in the temperature of the formation as a whole. This situation changes as borehole density and loading increase and as dissipation is decreased.

For the parameter sets simulated, the minimum and maximum heat transfer cases are always to the outside of the distribution and the median R_b and K_f cases (Med R and Med K) are always close to the center, indicating that the high and low HT cases are indeed outer bounds. The total ranges of both the minimum and maximum EWT for the estimated sets varies by 1.2 °C. The impact these differences will have in heat pump efficiency can be determined by looking at the change in COP. For heating a space at 21 °C the lowest predicted EWT (8.2 °C) yields an ideal COP of 20.16 while the highest EWT (9.9 °C) yields an ideal COP of 23.25, a 13% increase. For cooling the predicted EWT never rises above 21 °C indicating that the heat pump system would only need to raise the temperature of the working fluid enough to ensure a sufficient heat transfer rate.

Table 3-4: Predicted EWT at 10 and 60 years

	Min EWT 10 yr. °C	Min EWT 60 yr. °C	Ave EWT 10 yr. °C	Ave EWT 60 yr. °C	Max EWT 10 yr. °C	Max EWT 60 yr. °C
Ktest LSM	9.14	9.18	12.69	12.72	16.80	16.84
Low HT	8.29	8.33	12.71	12.76	17.37	17.41
High HT	9.86	9.90	12.68	12.71	15.80	15.83
Min R	9.66	-	12.68	-	15.95	-
Min K	8.42	-	12.71	-	17.17	-
Med R	9.07	-	12.69	-	16.56	-
Med K	9.31	-	12.69	-	16.31	-

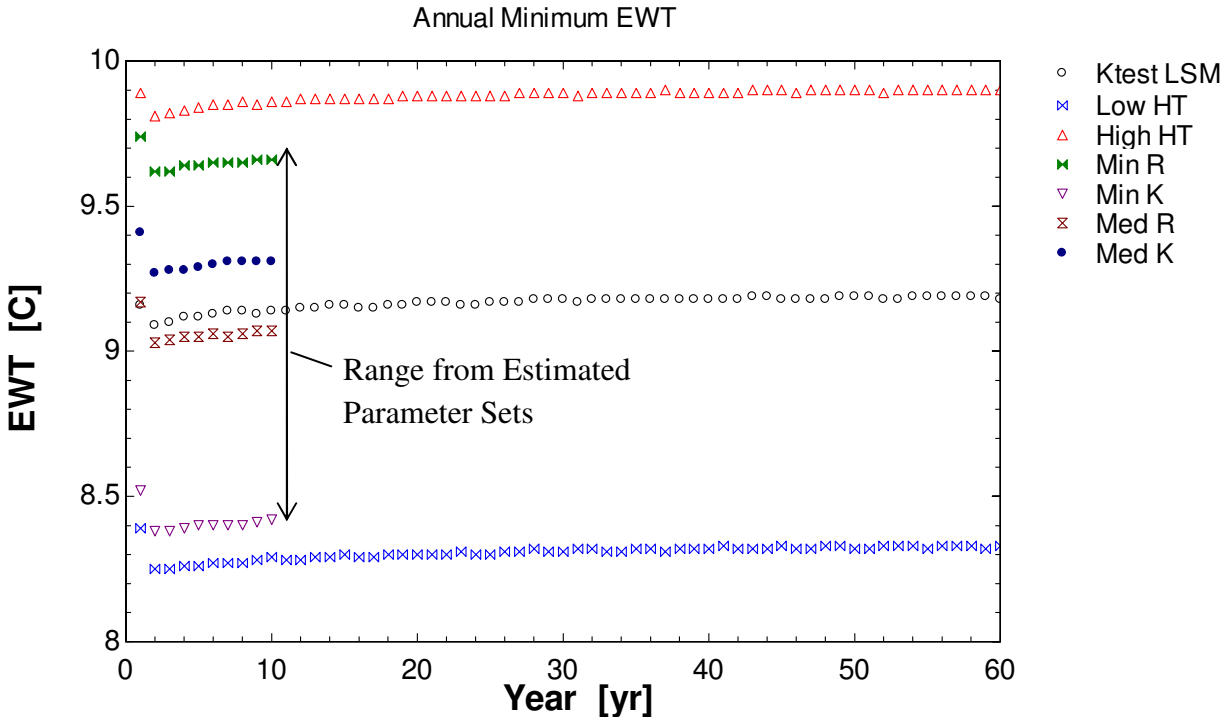

Figure 3-28: Plot of the minimum entering water temperature for each year for a series of simulations representing the range of estimated K_f and R_b values.

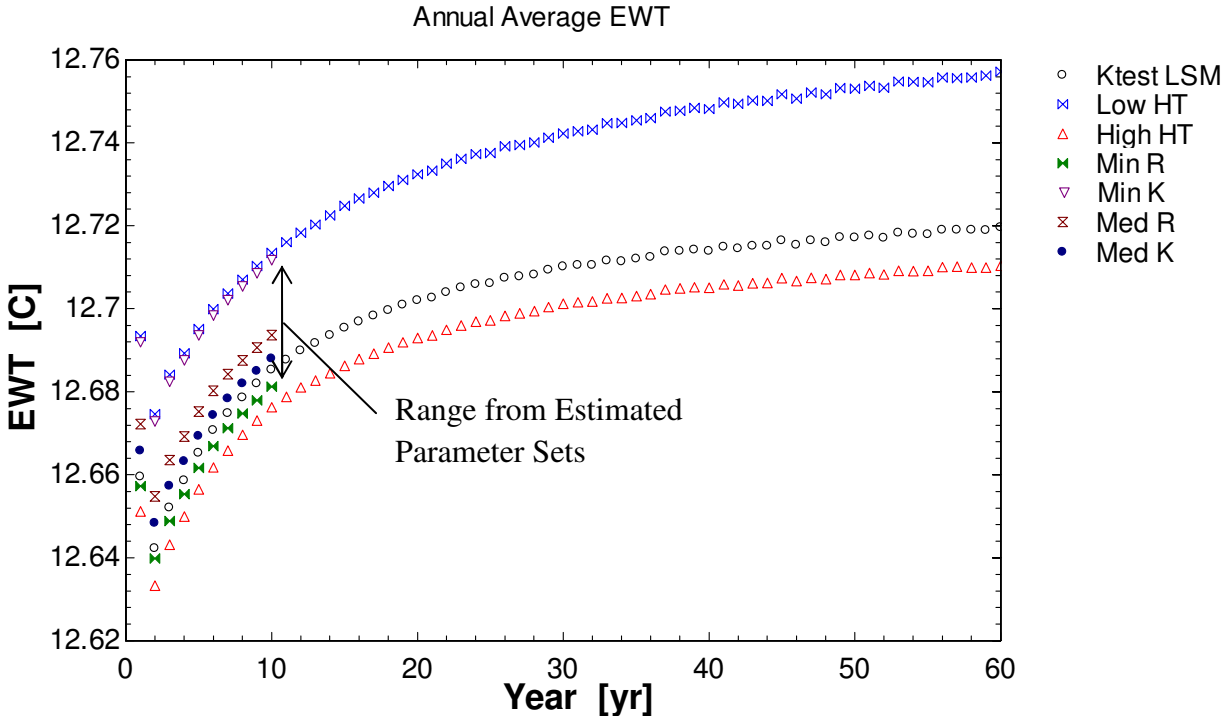

Figure 3-29: Plot of the average entering water temperature for each year for a series of simulations representing the range of estimated K_f and R_b values.

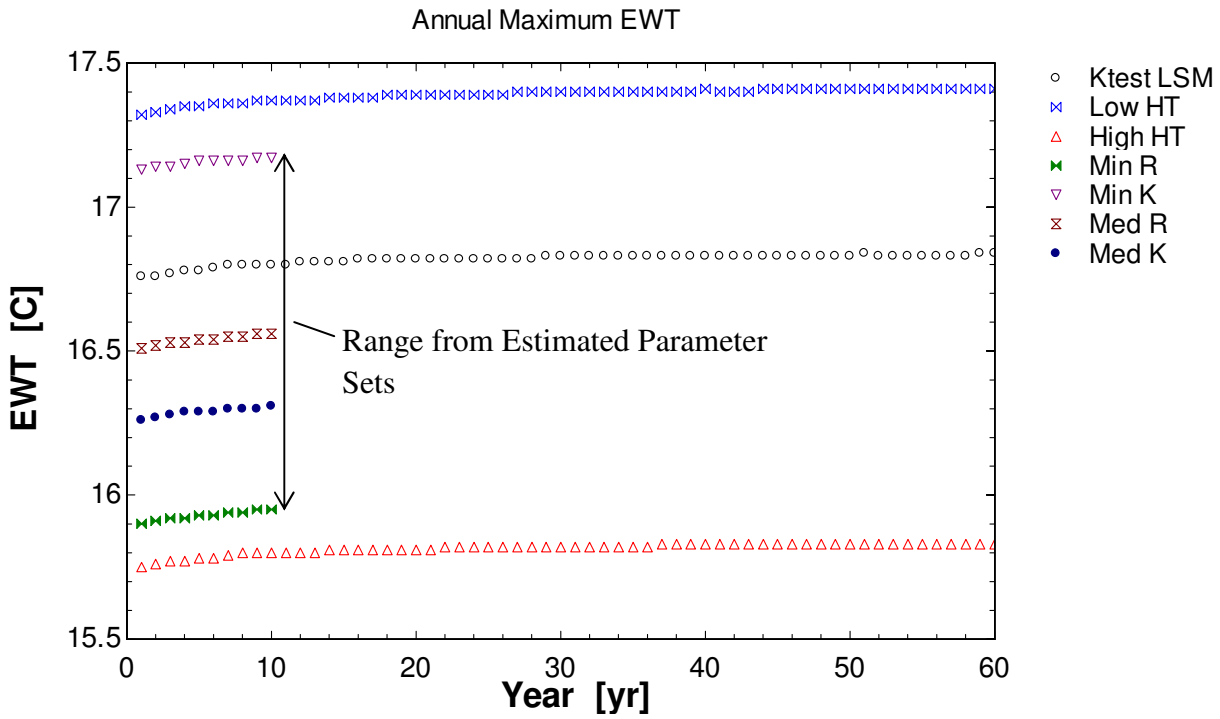

Figure 3-30: Plot of the maximum entering water temperature for each year for a series of simulations representing the range of estimated K_f and R_b values.

3.3.3 Results of Load Application through a Heat-Pump

It was found that the inclusion of the amplifying effect the heat-pump has on thermal loading of the bore-field resulted in significantly increased entering water temperature relative to the direct application of the house thermal load requirements to the borehole.

The heat-pump had a substantial impact on the EWTs as shown in Figure 3-31, Figure 3-32, and Figure 3-33. The direct input of the thermal load resulted in fairly stable EWTs as the thermal load is fairly small relative to the input from the surrounding ground and atmosphere. As a result equilibrium is reached after only a few years. With the heat-pump the efficiency changes as the temperature increases resulting in a feedback loop and greater variation in the temperatures over a ten year period relative to the direct input of the load. As the setting is cooling dominated the heat-pump had different effects on the minimum and maximum

entering water temperatures. The results after ten years for the minimum and maximum heat transfer parameter sets with and without the heat pump are shown in Table 3-6

The annual minimum entering water temperature (shown in Figure 3-31) occurs when the system is drawing heat from the ground. As each year results in a slightly higher formation temperature, the efficiency of the heat-pump increases and the heat being drawn from the working fluid decreases resulting in an increasing minimum entering water temperature. The minimum EWT is also affected by the subtraction of the heat-pumps electrical energy use from the energy extracted from the working fluid. As would be expected, the high heat transfer case resulted in increased minimum EWT for both the direct loading and heat-pump simulations as there was less resistance to heat entering the area around the borehole from the rest of the formation.

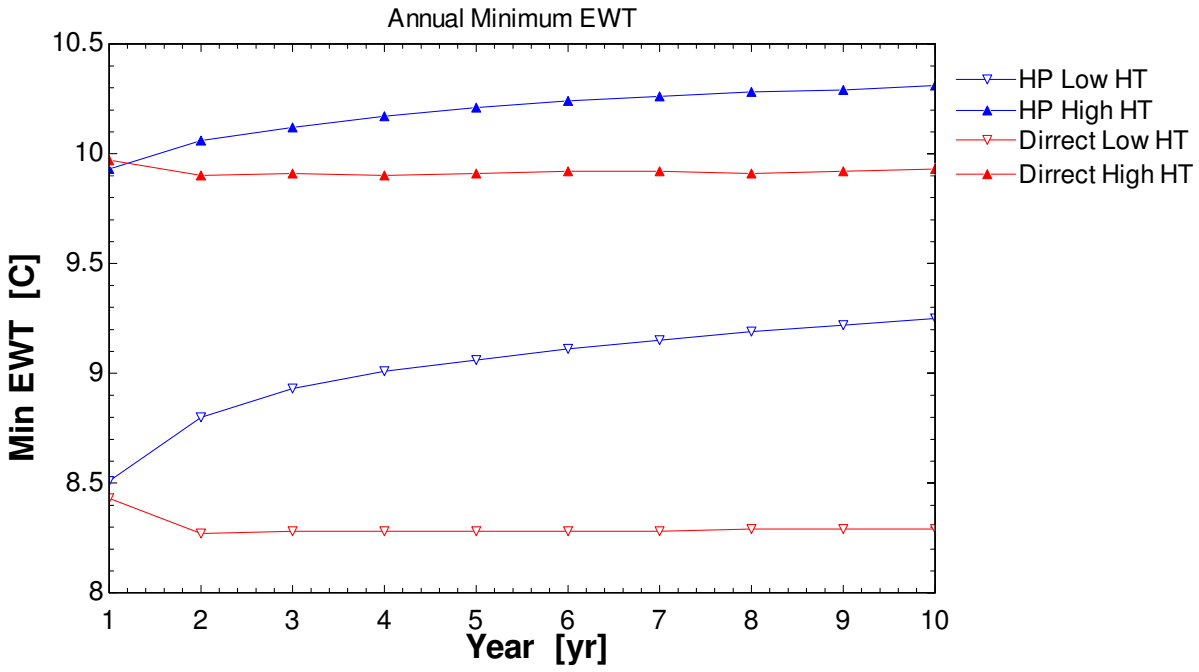

Figure 3-31: The Annual Minimum Entering Water Temperature

The annual maximum entering water temperature (shown in Figure 3-32) occurs when the system is rejecting heat to the ground. As the formation temperature increases each year, the efficiency of the heat-pump decreases and the heat being rejected to the working fluid increases resulting in an increasing maximum entering water temperature. The maximum EWT is also affected by the addition of the heat-pump's electrical energy use. As heat is being rejected into the well, the high heat transfer case resulted in decreased maximum EWT for both the direct loading and heat-pump simulations.

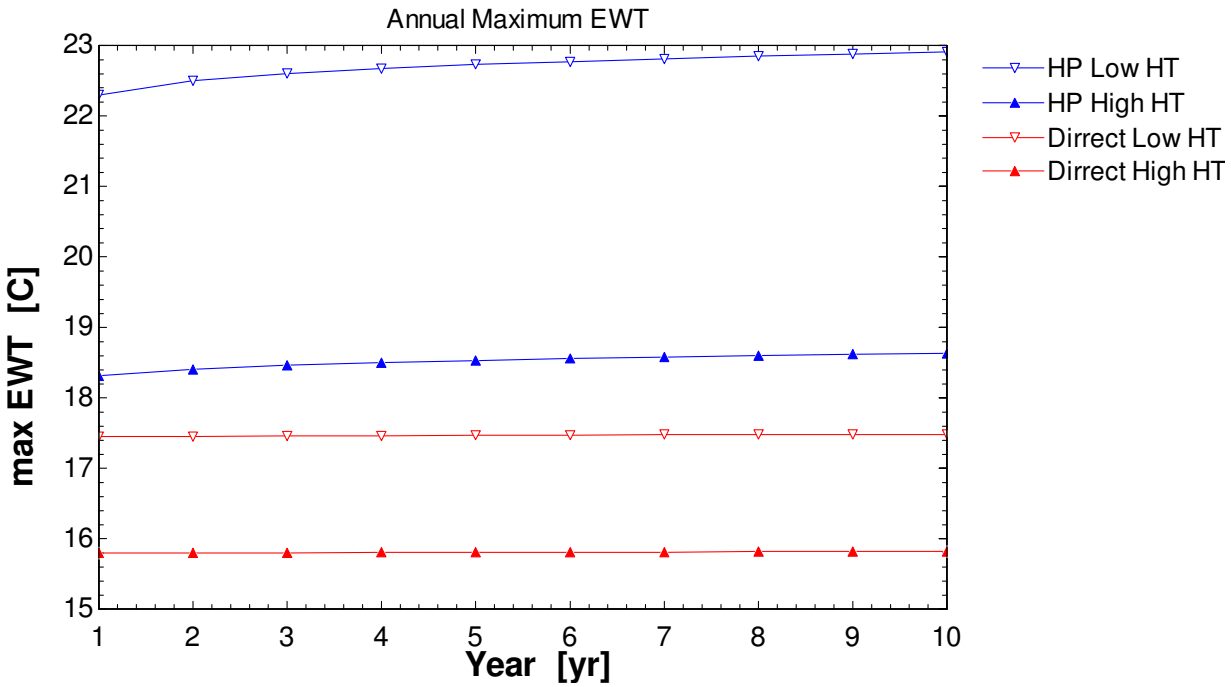

Figure 3-32: The Annual Maximum Entering Water Temperature

The average entering water temperature (shown in Figure 3-33) provides a measure of what is happening to the bore field over the course of each year. The direct loading simulations resulted in very slightly increasing averages. The low heat transfer case is slightly higher than the high heat transfer case. In contrast the heat-pump simulations have clearly visible increases in the annual average and a clear distinction between the low and high heat transfer

cases. As expected for a cooling dominated region, the annual average EWT is higher for the low heat transfer case than the high heat transfer case. This difference is a result of two effects: the decreased ability of heat to dissipate from around the borehole and the decreased heat-pump efficiency due to increased temperatures in the borehole resulting in total greater heat rejection.

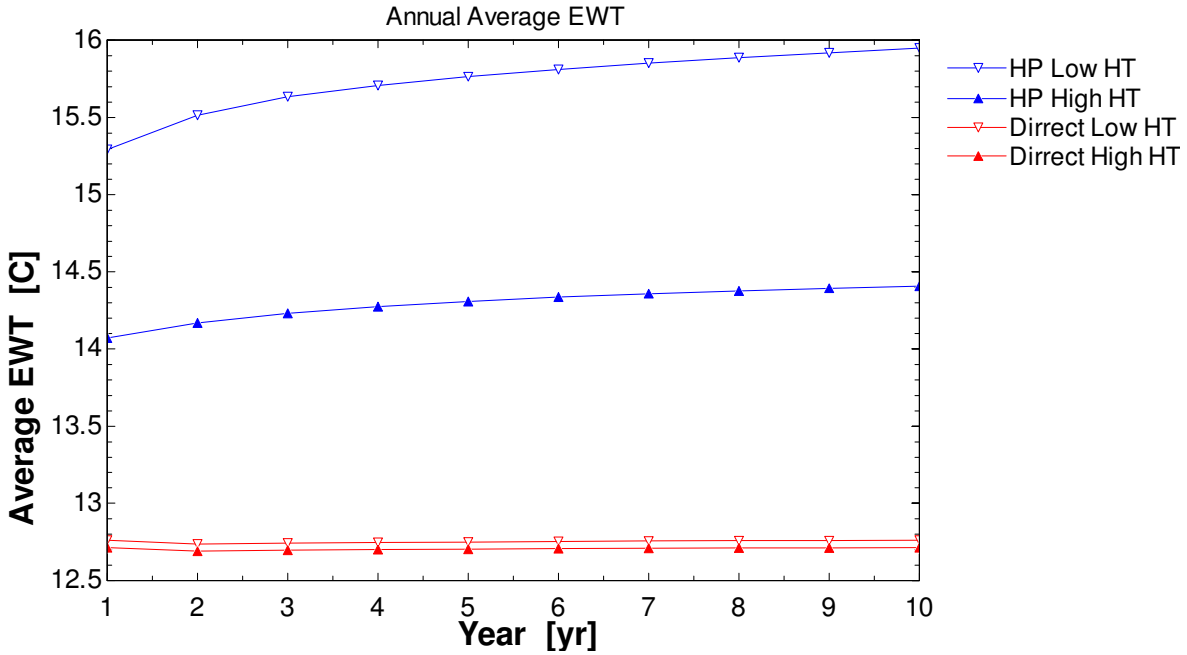

Figure 3-33: The Average Annual Entering Water Temperature

3.3.4 Results of Higher Thermal Loading

As expected, tripling the load resulted in substantial increases in the magnitude of the minimum and maximum EWTs. As the location of the Test Facility is cooling dominated, the load tripling increased the maximum EWTs more than it decreased the minimum EWTs. The increase in load also resulted in an increase in the average EWTs. The EWTs after ten years for the triple load simulations are included in Table 3-5. A comparison of the high and low heat transfer cases for direct loading and heat pump loading using both the original and triple load profiles is given in Table 3-6. The high and low heat transfer cases bound the results and

thus give a measure of the impacts of the variations in loading setup on the magnitudes of the results.

Table 3-5: Results of the Long Term Simulations Using the Tripled Loading (values for year 10)

Case	Min EWT 10 yr.		Ave EWT 10 yr.		Max EWT 10 yr.	
Name	°C	°F	°C	°F	°C	°F
High HT HP 3x	6.40	43.52	17.98	64.36	28.98	84.16
Low HT HP 3x	3.61	38.50	22.01	71.62	41.54	106.77
Min R HP 3x	5.96	42.73	18.70	65.66	31.97	89.55
Min K HP 3x	3.81	38.86	21.88	71.39	41.07	105.93
Med R HP 3x	4.89	40.80	20.11	68.20	36.12	97.02
Med K HP 3x	5.32	41.58	19.53	67.15	34.42	93.96
Max R HP 3x	4.82	40.68	19.59	67.26	35.04	95.07
Max K HP 3x	5.89	42.60	18.38	65.09	31.36	88.45
In Use HP 3x	5.14	41.25	19.68	67.42	34.93	94.87

Table 3-6: Comparison of Long Term Results for Different Loading Cases (values for year 10)

	Min EWT 10 yr.		Ave EWT 10 yr.		Max EWT 10 yr.	
	°C	°F	°C	°F	°C	°F
Direct Low HT	8.29	46.92	12.76	54.97	17.48	63.46
Direct High HT	9.93	49.87	12.71	54.88	15.82	60.47
HP Low HT	9.25	48.65	15.95	60.71	22.91	73.23
HP High HT	10.31	50.56	14.41	57.94	18.63	65.53
3x Load Direct Low HT	-0.53	31.05	12.95	55.31	26.85	80.33
3x Load Direct High HT	4.73	40.51	12.81	55.06	21.40	70.52
3x Load HP Low HT	3.61	38.50	22.01	71.61	41.54	106.77
3x Load HP High HT	6.40	43.52	17.98	64.36	29.98	85.96

The annual minimum entering water temperature, shown in Figure 3-34, occurs when the system is transferring energy from the ground. The minimum temperature profiles are significantly lower in the triple load case than in the single load case due to the increase in heating demand, which drives the lowest temperature profile towards freezing. This freezing

situation is somewhat alleviated as, like the previous study, each year results in slightly higher EWT as the annual rate of energy transfer to the ground is slightly greater than the rate at which energy is dissipated away from the borehole. The increase in EWTs increases the efficiency of the heat-pump during heating operation and decreases the heat being drawn from the working fluid resulting in an increasing annual minimum EWT. The annual minimum EWT is also increased by the subtraction of the electrical energy used by the heat-pump from the energy extracted from the working fluid to meet the heating load.

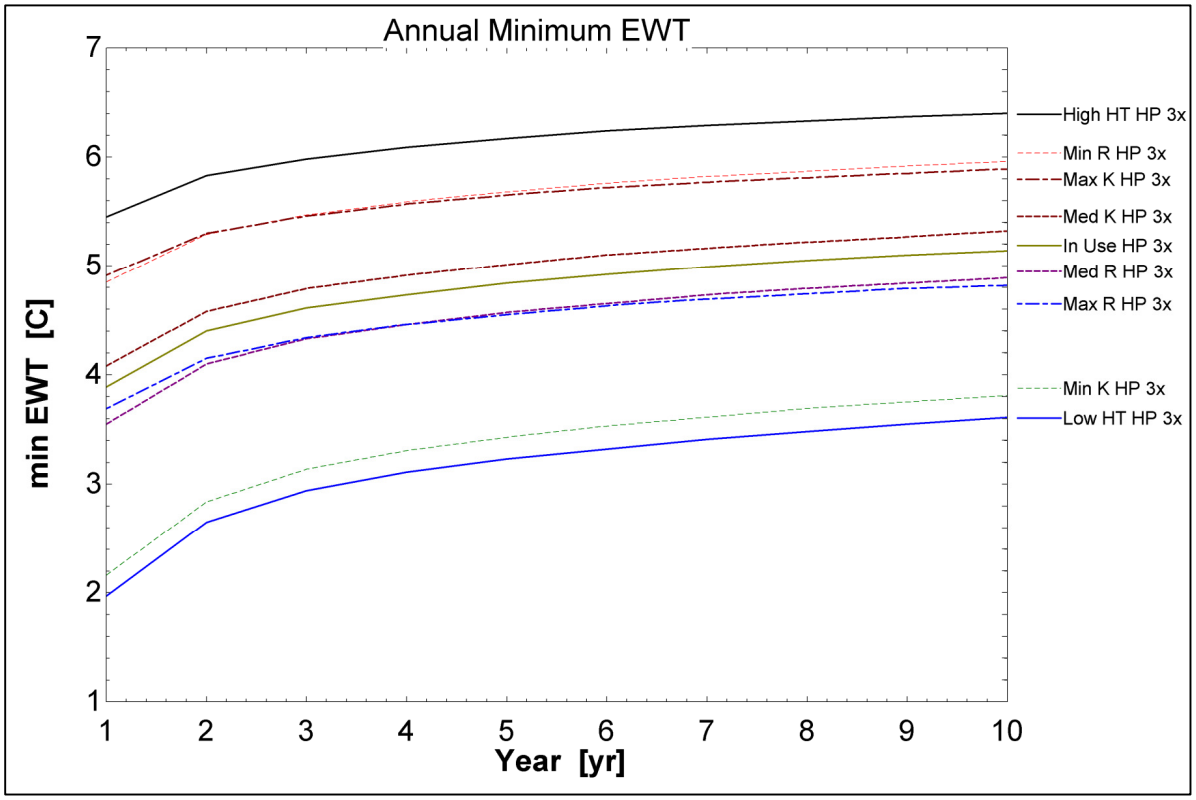

Figure 3-34: The Annual Minimum Entering Water Temperature

The annual maximum entering water temperature, shown in Figure 3-35, occurs when the system is rejecting heat to the ground. The maximum temperature profiles are higher and more widely spread out in the triple loading case as compared to the single loading case, which results in predicted temperatures in the 85 to 105 °F range, which are more typical of

residential bore fields. As with the single loading case, the average borehole temperature increases each year, decreasing the efficiency of the heat-pump in cooling mode and increasing the heat being rejected to the borehole. The increase in average borehole temperature combined with the decrease in cooling efficiency results in an increasing maximum EWT which is also affected by the need to reject the heat generated by the heat-pump's electrical energy use. As heat is being rejected into the well, the high heat transfer case resulted in decreased maximum EWT for both the direct loading and heat-pump simulations due to better dissipation of the thermal energy to the rest of the formation and eventually to the atmosphere.

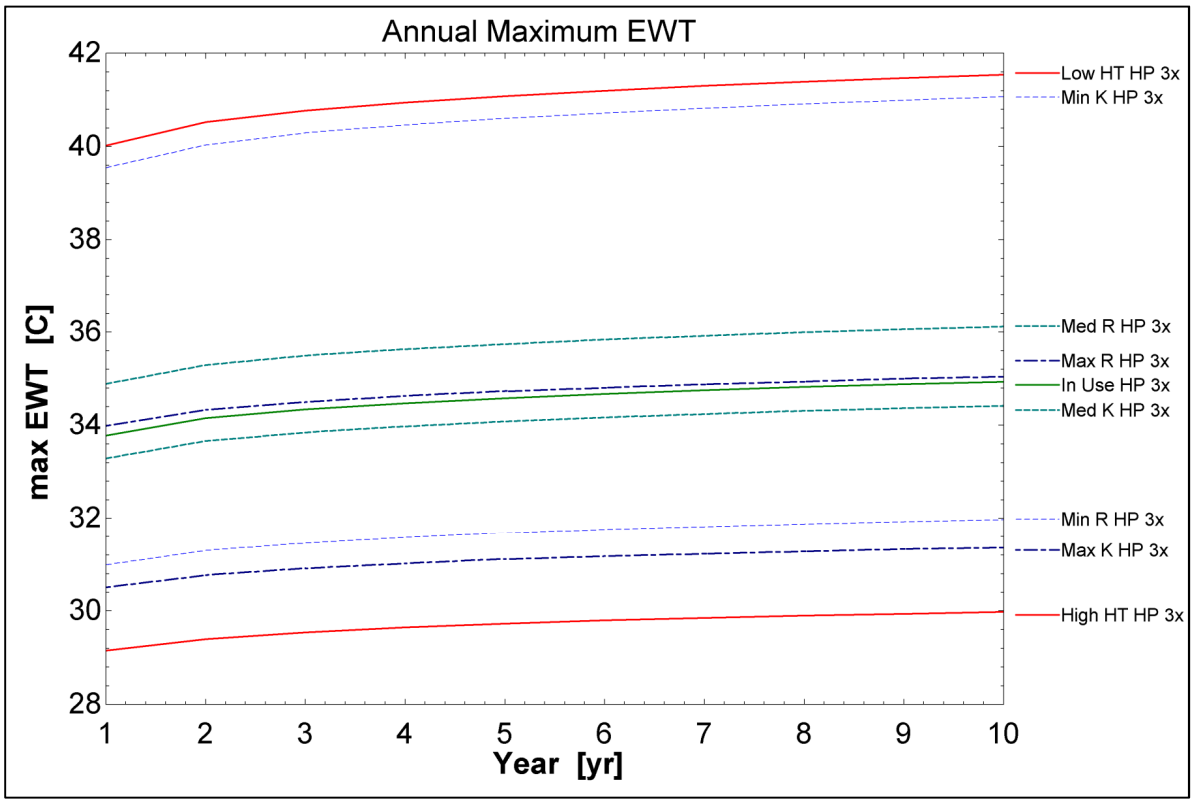

Figure 3-35: The Annual Maximum Entering Water Temperature

The average entering water temperature, shown in Figure 3-36, provides a measure of what is happening to the bore field over the course of each year. The average temperatures are higher

in the triple loading case relative to the single loading case. Much like the change from low to high heat transfer made only a small difference in the average EWT when the load was applied directly, the increase in the average EWT with the tripling of load is much greater with the inclusion of the heat pump.

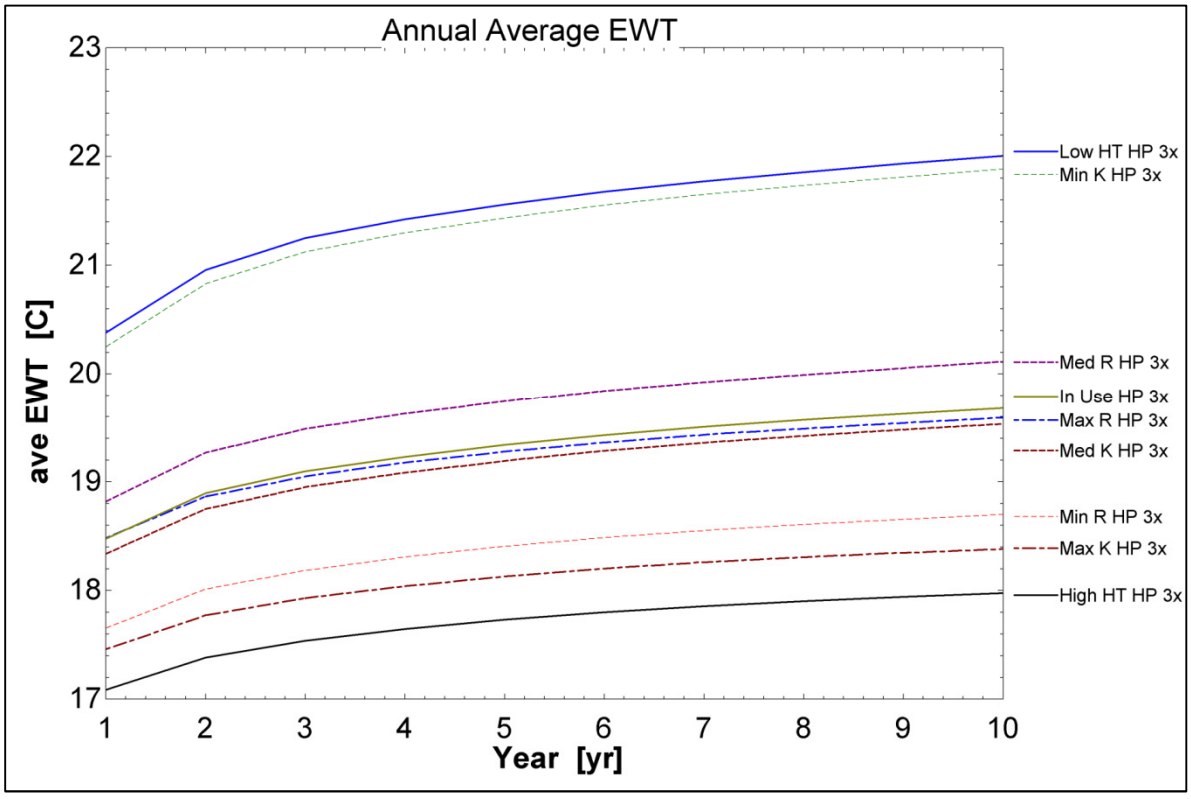

Figure 3-36: The Average Annual Entering Water Temperature

3.3.5 Conclusions

The direct application of the predicted Test Facility thermal load to the working fluid passing through the borehole resulted in predictions of a fairly small range of maximum EWTs resulting from the range of predicted borehole properties. Further the increase in EWT's over the course of ten years was predicted to be very small.

The addition of a heat-pump using the working fluid as a reservoir in order to meet the thermal load requirement resulted in an increase in the EWTs for a cooling dominated scenario. The inclusion of the heat pump increases the maximum entering water temperatures, the difference between low and high heat transfer cases, and the increase in maximum entering water temperature over the course of the simulations. Thus the addition of a heat pump has an amplifying effect on the changes in EWTs and results in greater variation of the EWTs with respect to the predicted formation and borehole thermal properties.

Much like the addition of the heat-pump, tripling the load being met by the heat-pump in order to more closely match a typical residential installation resulted in increased maximum and average EWTs and greater spread due to the properties used. The tripling of the load also decreased minimum EWTs as a result of the increase in heat being drawn from the borehole. Thus the impact of the borehole properties on the heat-pump efficiency and EWTs is dependent on the load being applied. While small variations in these properties may be negligible, the variations seen in the analysis of the NZERTF thermal response tests could result in significant variations in ground source heat pump performance depending on the total loading per linear foot of borehole.

Chapter 4: Baseline Full House Model

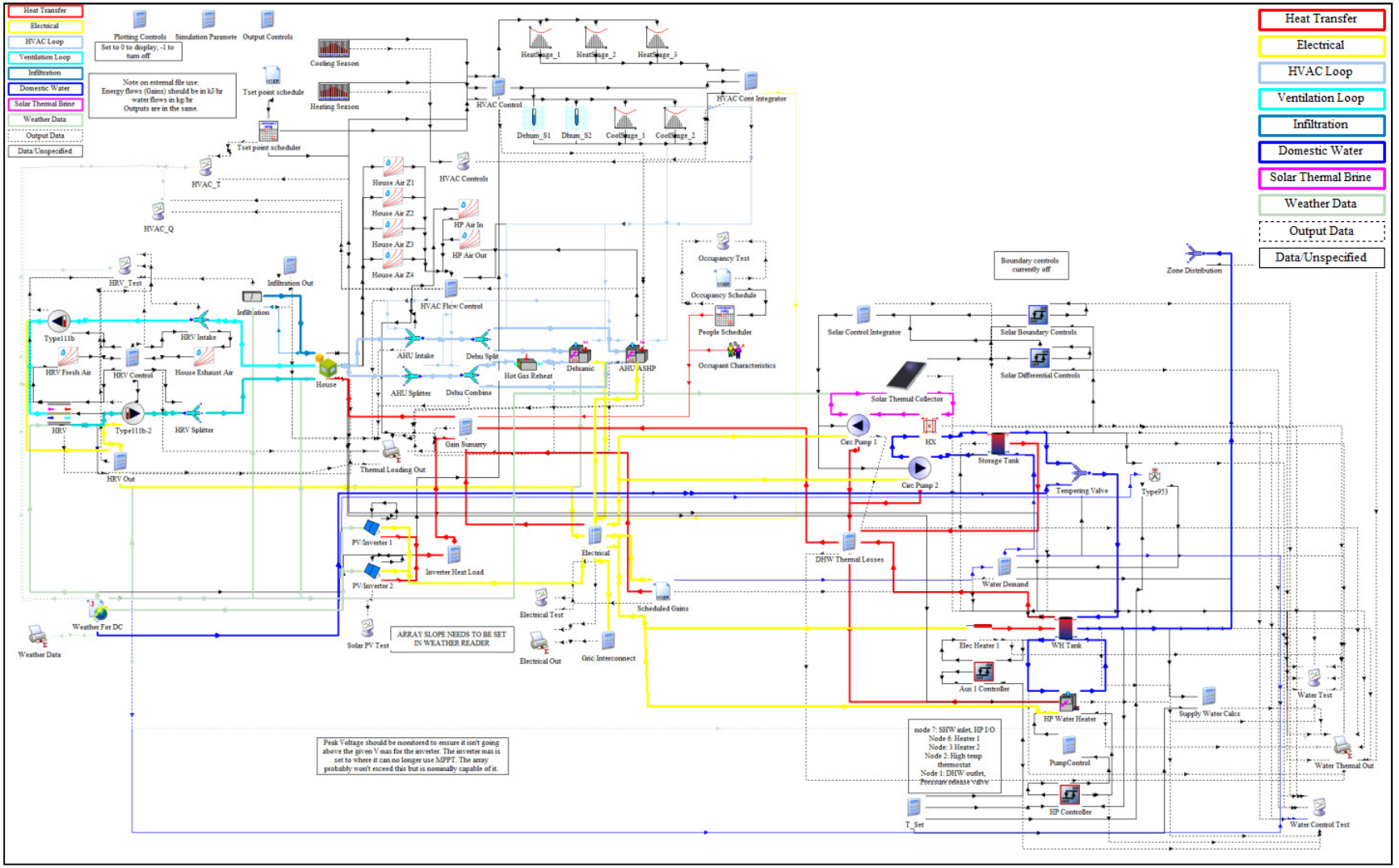

Figure 4-1: Diagram of the Baseline Full House Model

4.1 TRNSYS Baseline Full House Model Development

4.1.1 Changes to House Envelope and Loading Component

The TRNSYS TYPE 56 house component developed for the House Envelope and Load Model described in Chapter 2 was modified in several ways for the Full House Model. The original simple heating system, which was used to output the heating or cooling required for the first and second floors (zones 2 and 3) to meet specific temperature set points, was removed. Though this system was useful for determining heating and cooling requirements of the house, it was not compatible with the control strategy used in the actual system. The house component's inputs were expanded to include mass flow rates and air properties for the HVAC air loop and the ventilation air loop. The mass flow rates are set for each 'ventilation' type and heating zone and are assumed to be both the flow into and out of the zone.

4.1.1.1 Latent Load Tracking

Previously the house model did not track the scheduled latent loads. The house model has been modified to allow each zone to accept non-ventilation latent loading in kg/hr of water vapor. The scheduled loads and occupant loads were then modified to separate the latent and sensible loading. The TRNSYS occupant loading component, TYPE 574, provides the latent and sensible loading fractions for the occupants. The scheduled electrical loads were separated into sensible and latent loads assuming a value of 15% latent heat. The 15% value was determined by taking a weighted average of the latent load fractions used for the scheduled loads in the EnergyPlus Simulation. The latent loads are converted from kJ/hr to kg/hr water vapor in the gain summary equation block using the heat of vaporization of water

at 25 C, 1 atm. These loads are then applied to the appropriate zones in the house as was previously done with the sensible loading.

4.1.1.2 Load Schedule Modifications

After the initial envelope and load modeling was completed, several major modifications were made to the load schedules. All of the demand files were modified slightly to account for a missing minute at the end of the day that resulted in the demand profile shifting earlier in the day over the course of the simulation.

The water and electrical demand were taken from the schedule for a typical Monday and repeated every day. Unfortunately the typical Monday schedule does not include any of the washing machine and laundry dryer activity that makes up around 12% of the annual domestic hot water use and 25% of the appliance electrical demand. The demand schedule was modified to include a daily equivalent washing machine and dryer loads. The washing machine demand is made up of 5 cycles of 45 minute duration every week. These cycles are mostly scheduled in the evenings at around 8 pm. The daily load schedule used for the TRNSYS simulations was modified to include a 32 minute cycle with the same water use rate as the original cycle. These modifications results in a total domestic hot water (DHW) use that is very close to the water demand of the EnergyPlus model. However the new schedule has a more even demand in the evening. The dryer cycle was likewise changed from 5 cycles lasting 51 minute to 7 cycles lasting 37 minutes that were scheduled at daily 9 pm. The change in demand timing makes the TRNSYS schedule more favorable to the use of both the solar hot water system, as demand is at a time shortly after the solar hot water (SHW) storage tank has heated up for the day, and the heat pump as the washing machine

demand spike is shorter, allowing more of it to be met with the water supply in the tank. It has little impact on the solar PV demand as there is little generation during the evening. The impact on hypothetical electrical storage requirements is similar to the impact on solar hot water use: the smoothing out of demand from 5 to 7 days a week decreases the maximum daily demand and potentially decreases the required battery size. The battery Sizing program will be covered in Chapter 5.

It is also important to note that not all of the electrical energy used in the load files is delivered to the house in the form of heat. The non-thermal electrical use is estimated to be greatest for the dryer with only 20 % of the energy used being retained in the house as thermal energy. The other loads are estimated to deliver an average of 90% of their electrical use as thermal energy. The other 10% is estimated to be converted into non-thermal energy and lost from the house envelope. Electrical energy that is not retained as heat in the house is accommodated in the load files using the misc. load category. All loads in this category are added to the electrical energy demand but not to the thermal loading of any of the zones.

4.1.1.3 Time step Changes

All prior simulations were conducted using a time step of 15 minutes. While this time step allows a reasonable estimate for most of the processes involved in the house simulation, it is not fine enough to capture rapid changes in the controls. The lack of resolution was particularly problematic after the installed HVAC control scheme was implemented. This scheme involves time triggered controls with a minimum delay time of 10 minutes. To accurately simulate this system required a time step smaller than the minimum control delay time and preferably a factor of all of the other control delay times. Simulations were run with

time steps of 15, 5, and 1 minutes. For the trial model the results of these simulations are documented in Table 4-1 below. With these results it was decided that a 5 minute time step was sufficiently small for future simulations.

Table 4-1: Comparison of Different Time Steps Using Full_model_2013_4_21_house.tpf

Time Step Size	Convergence Failure	Electrical Consumption	Percent Difference	Run Time
[min]	% of time steps	kWhr	% 1 min Consumption	[min]
15	3 %	10760	2.087 %	4
5	1%	10610	0.664 %	10
1	0%	10540	0 %	45

4.1.2 Heat Recovery Ventilator Loop

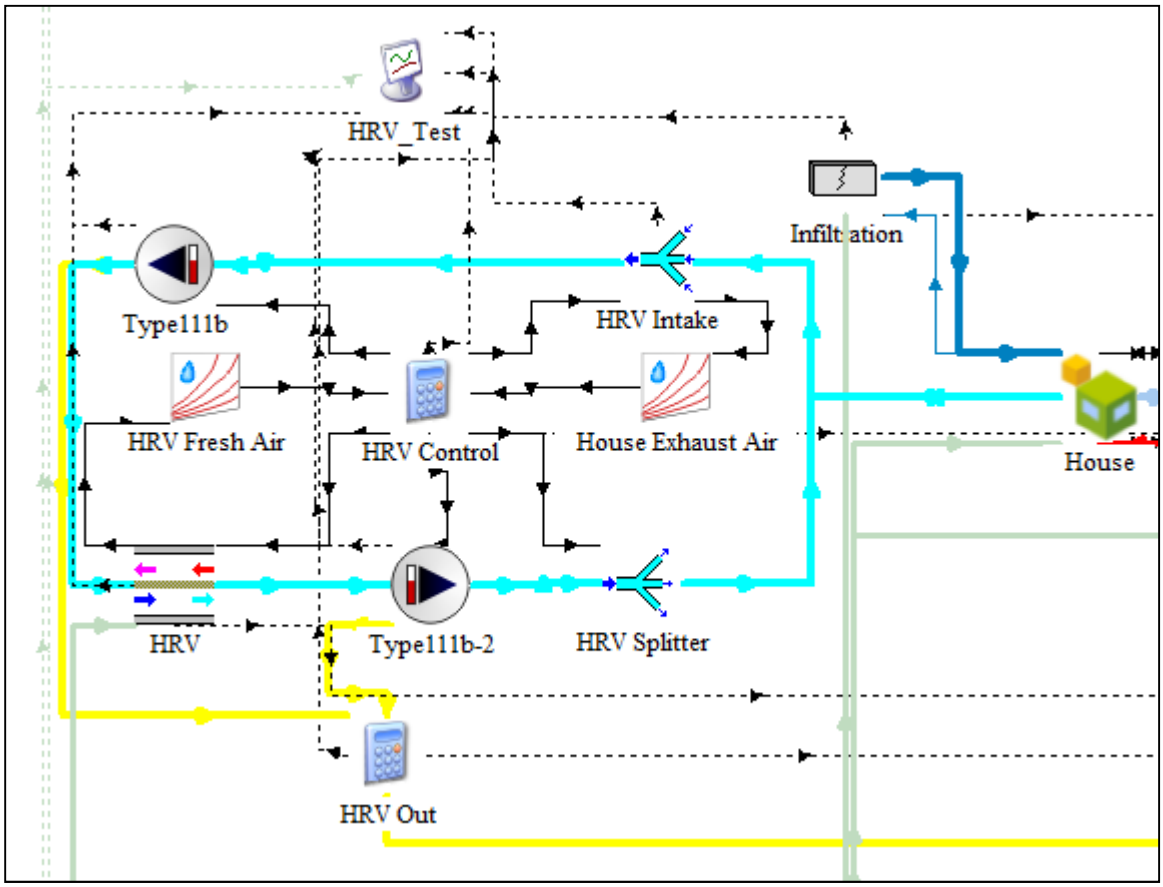

Figure 4-2: Ventilation Loop

The house currently has two separate air circulation systems: the ventilation loop and the HVAC loop. The ventilation loop, shown in Figure 4-2, draws 0.0205 [m^3/s] from zone 2 and 0.0187 [m^3/s] from zone 3, matching the values specified in the EnergyPlus model. The air is then passed through a Heat Recovery Ventilator (HRV) and exhausted. An equal volume of fresh air is taken in, passed though the HRV, and returned to zones 2 and 3. The system is set up such that the other zones may be added or the volume flow rates changed in the HRV Control equation block. The air flows are combined and split in the HRV intake component and the HRV splitter component. The HRV component is modeled after the installed Venmar AVS HRV EKO 1.5 and description of the parameters, reasoning, and sources can be found in the 'HRV' tab of the spread sheet 'TRNSYS model system parameters.xlsx' in the electronic supplement. The parameters are drawn from the *Venmar AVS HRV EKO 1.5 Heat Recovery Ventilator Specification Sheet* (2012) and the EnergyPlus model documentation (Kneifel, 2012a).

The HRV unit has two variable speed fans, one each for the exhaust and supply air streams, and a variable sensible effectiveness. The fans were modeled using the TYPE 111b Variable Speed Fan component. The performance of the two fans was determined using the specifications outlined by the manufacturer for the HRV. A normalized correlation between mass flow rate and power consumption was generated from the available data assuming that HRV power consumption is entirely due to the fans. A correlation between mass flow rate and sensible effectiveness was also generated using the same data. The calculations for these correlations may be found in the EES file 'HRV Performance Calcs.EES'. The sensible effectiveness correlation was input as an equation in the HRV controls equation block in

order to set the sensible effectiveness of the HRV component at each time step. The electrical use of the ventilation fans is calculated and sent to the electrical summary equation block. The thermal loading from the fans added to the exhaust and supply air streams.

The use of volume flow rates as opposed to the TRNSYS preferred mass flow rates required the addition of two property components that take in the temperature, pressure, and relative humidity of an air stream and output properties such as density and enthalpy. The densities of each stream were used in the HRV controls block to determine the mass flow rates of each stream. These mass flow rates are normalized with respect to the HRV's variable speed fans' maximum mass flow rate at the manufacturer's rating conditions. The normalized mass flow rates are passed to the fan components as control signals. The fans then set the mass flow rate of the loop as a fraction of the maximum mass flow rate with a control signal of zero corresponding to zero flow rate and a control signal of one corresponding to the maximum flow rate.

4.1.3 HVAC Loop

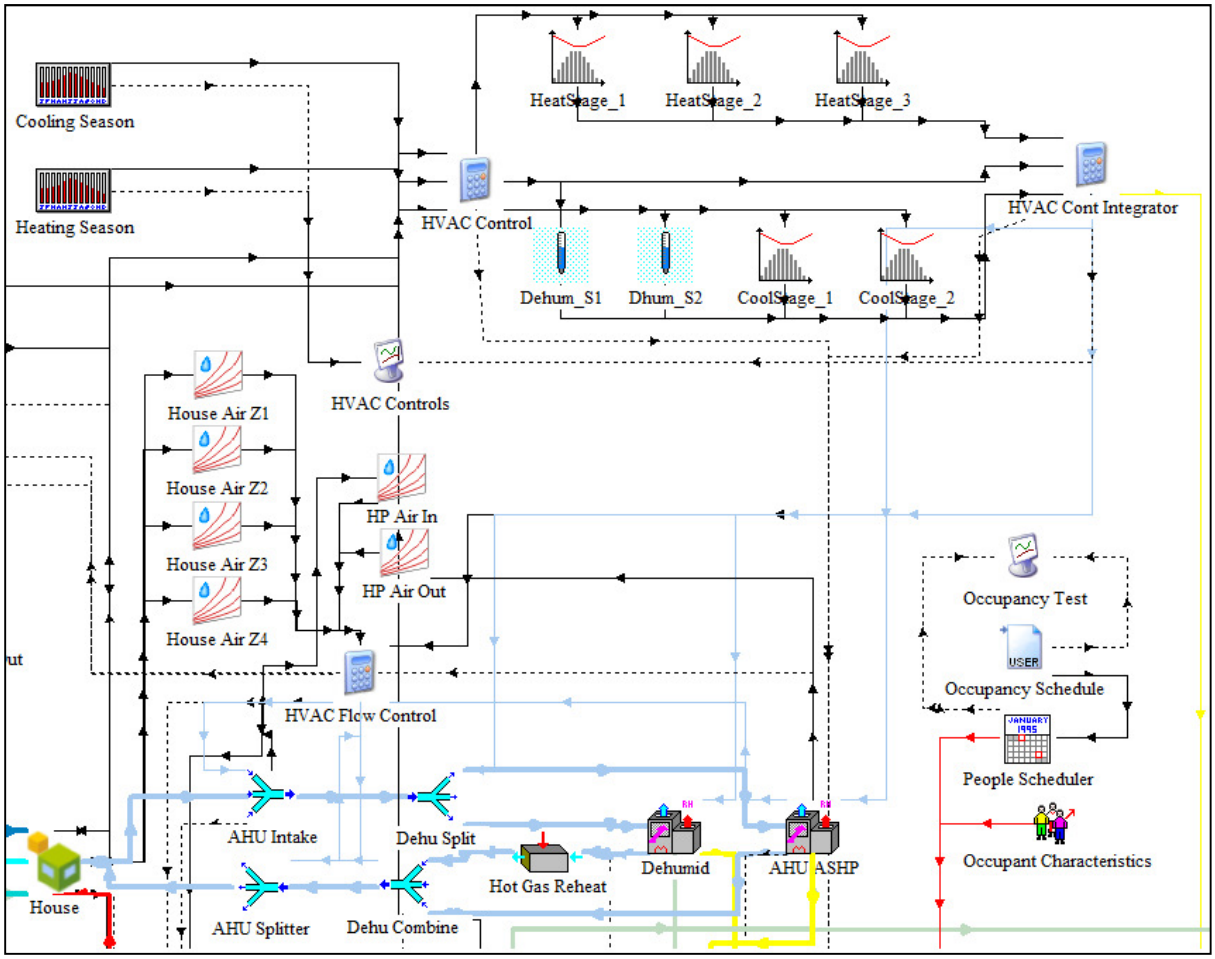

Figure 4-3: HVAC Loop and HVAC Controls

The HVAC loop and controls, shown in Figure 4-3, represent a parallel air circulation loop which is only responsible for heating, cooling, and dehumidification of the house. The HVAC loop is currently set to draw 55% of its air flow from zone 2 and 45% from zone 3. This ratio may be rebalanced later or additional zones included if it is found one zone is more regularly exceeding temperature set points or comfort limits. The total mass flow rate is set by the fan in the air-source heat-pump (ASHP) component and the ratios between the four zones are set in the HVAC control equation block. As with the HRV loop, the air flows are combined in the HVAC Intake component, passed through the ASHP component and then

split and supplied to the individual zones by the HVAC Splitter component. Heat lost from the ASHP fans and electronics are passed into the air stream and either decrease heating energy requirements or increase cooling energy requirements. It is assumed that none of the heat generated is passed into zone 1, the basement, where the HVAC heat-pump is located.

4.1.3.1 Air-Source Heat-Pump

The air-source heat pump (ASHP) model is based on performance data for the AAON F1-B-024-1-V-B air-source heat-pump. This is a two speed reversible heat-pump with supplemental electric resistance heating. Details of the parameters and inputs used may be found in the 'AA HP' tab of the spread sheet 'TRNSYS model system parameters.xlsx' in the electronic supplement. The parameter specifications were derived from a number of sources including the EnergyPlus model documentation, measured performance data from the NZERTF ("TOTAL _ Capacity _ Btu / h," 2013), the AHRI *Certificate of Product Ratings AAON F1B024**** (2014), the *AAON F1 Series Installation, Operation & Maintenance Manual* (2012), and conversations with AAON staff (*AAON*, 2014). The rated cooling and heating capacities and powers required by the TRNSYS heat-pump component are not the actual manufacturer ratings. Instead these values correspond to the heat-pump's performance at the rating conditions used in the performance map used by TRNSYS. To determine the rated capacities for the TRNSYS component the rating conditions, shown in Table 4-2, were entered into the empirical relations for heat pump performance vs. outdoor dry bulb temperature provided by NIST. The resulting output capacities and power consumptions were then used as the rated values for the TRNSYS component. The sensible cooling power was determined by assuming the TRNSYS default sensible heat ratio of 76 % of the rated

total cooling power as no other source of information was available. The generated values are shown in

TRNSYS Default Heat-Pump Rating Conditions	Vol Flow Fraction	In Door Wet Bulb Temperature	In Door Dry Bulb Temperature	Out Door Dry Bulb Temperature
	-	°C	°C	°C
Cooling Rating Conditions	1	19.444	26.667	35
Heating Rating Conditions	1	-	21.111	8.333

Table 4-3. The use of the modified TRNSYS default rating conditions also allows the possibility of using the TRNSYS default performance maps as drop in replacements for the hybrid performance maps generated from the NIST relations.

Table 4-2: TRNSYS Default Heat-Pump Rating Conditions

TRNSYS Default Heat-Pump Rating Conditions	Vol Flow Fraction	In Door Wet Bulb Temperature	In Door Dry Bulb Temperature	Out Door Dry Bulb Temperature
	-	°C	°C	°C
Cooling Rating Conditions	1	19.444	26.667	35
Heating Rating Conditions	1	-	21.111	8.333

Table 4-3: Modified Air-source Heat-pump Capacity and Power Ratings for TRNSYS Component

	TRNSYS Native		Given	
Parameter	Value	Unit	Value	Unit
Rated total cooling capacity - low speed	18671.04	kJ/hr	17697.67	btu/hr
Rated sensible cooling capacity - low speed	14376.7	kJ/hr	13627.2	btu/hr

Rated cooling power - low speed	5201.28	kJ/hr	1444.8	W
Rated total cooling capacity - high speed	24820.62	kJ/hr	23526.66	btu/hr
Rated sensible cooling capacity - high speed	19111.88	kJ/hr	18115.52	btu/hr
Rated cooling power - high speed	8190.054	kJ/hr	2275.015	W
Rated heating capacity - low speed	20633.59	kJ/hr	19557.91	btu/hr
Rated heating power - low speed	5133.521	kJ/hr	1425.978	W
Rated heating capacity - high speed	28966.93	kJ/hr	27456.8	btu/hr
Rated heating power - high speed	7570.564	kJ/hr	2102.934	W

4.1.3.2 HVAC Air Source Heat-Pump Performance Maps

The performance maps generated from the NIST relations are included in the spread sheet 'Curve Calculations.xlsx' in the electronic supplement. The Curve Calculations spread sheet also includes the original TRNSYS default performance maps as well as graphs and best fit curves showing the capacity and power vs OD DBT relations. These graphs use the rated heating and cooling capacities and powers derived from the NIST relations and the TRNSYS rating point making them directly comparable to those provided by NIST. The TRNSYS default performance maps significantly from the performance correlations provided by NIST in that they depend on the indoor dry bulb temperature, the indoor wet bulb temperature, and the normalized air flow rate, whereas the NIST correlation only depends on the outdoor air temperature. It was thus decided to generate performance maps that are hybrids of the NIST correlations and the TRNSYS default performance maps. The slopes of the new hybrid performance maps are based on the slopes of the TRNSYS default maps for all independent variables except the outdoor dry bulb temperature for which the slope is based on the NIST correlations.

To generate these hybrid performance maps, linear regressions of the normalized power consumption, total heat capacity, and, for cooling, the sensible heat capacity were generated

with respect to each of the independent variables of the TRNSYS default performance maps. These were then used in equation (4-4). Each of the dependent variables, total heat-pump capacity and power consumption, is normalized with respect to its value at the TRNSYS performance maps' rating conditions. As shown in equation (4-1), the dependent variables were then stated as functions of the sum of the value of the normalized dependent variable at the TRNSYS performance maps' rating conditions, K_0, and the change in the dependent variable as a function, ΔK, of the independent variables, out-door dry bulb temperature, indoor dry-bulb temperature, indoor wet-bulb temperature, and air flow rate. In equation (4-3), ΔK is broken into components related to the partial derivatives of the dependent variables with respect to each independent variable multiplied by the differential change in that independent variable. The differential changes were then approximated as a difference in the independent variables from the TRNSYS maps rating conditions, as shown in equation (4-3). The partial derivatives were approximated as the slopes of linear correlations of the dependent variable with respect to each independent variable as shown in equation (4-4). The difference and linear slopes were then combined in equation (4-5). For the slopes of the dependent variables with respect to the outdoor air temperature, the slopes of the NIST correlations were normalized and used in place of the TRNSYS value as shown in equation (4-6).

The new performance map was then generated by taking the difference of each independent variable from the rated conditions, multiplying it by the slope of the linear correlation of the dependent variable with respect to that independent variable and then adding it to the values generated by the same procedure for the other independent variables as shown in equations

(4-5) and (4-6). As the dependent variables are normalized, K_0 is equal to one. This procedure was repeated for every point in the TRNSYS performance map to yield a new normalized performance map of the same dimensions and with the same values of independent variables.

The equations used to generate a general hybrid map are as follows:

$$K = K(x, y, z) = K_0 + \Delta K(x, y, z) \tag{4-1}$$

$$K = K_0 + \frac{\partial K}{\partial x} * dx + \frac{\partial K}{\partial y} * dy + \frac{\partial K}{\partial z} * dz \tag{4-2}$$

$$K \approx K_0 + \frac{\partial K}{\partial x} * \Delta x + \frac{\partial K}{\partial y} * \Delta y + \frac{\partial K}{\partial z} * \Delta z \tag{4-3}$$

Linear correlations yield results of the form:

$$K(x) = m_x * (x - x_0) + b_x \text{ , where } m_x \approx \frac{\partial K}{\partial x} \tag{4-4}$$

Where x, y, and z are dependent variables such as outdoor temperature, humidity, and mass flow rate. The slopes determined by the linear correlations are then substituted into equation (4-3).

$$K \approx K_0 + m_x * (x - x_0) + m_y * (y - y_0) + m_z * (z - z_0) \tag{4-5}$$

For these performance maps this yields an approximate equation relating a performance property, K, to the slopes of a linear correlations with respect to

dependent variables x, y, and z. The linear correlations may be taken from different sources: in this case the NIST correlations and the TRNSYS default maps.

$$K_{Hybrid} \approx K_0 + m_{x,NIST} * (x - x_0) + m_{y,TRNSYS} * (y - y_0) + m_{z,TRNSYS} * (z - z_0) \quad (4\text{-}6)$$

The procedure above was modified slightly when determining the normalized sensible cooling capacity as a dependent variable. In order to couple the sensible cooling capacity to the NIST correlations for total cooling capacity, the ratio between the sensible cooling capacity and the total cooling capacity was used as the dependent variable rather than directly using the sensible cooling capacity. The ratio is determined from the TRNSYS performance map and the final value of the normalized sensible cooling capacity is determined by multiplying the hybrid map total cooling capacity by the ratio. The relation is then normalized by dividing by the rated sensible cooling capacity at the TRNSYS rating conditions. The equations for the sensible cooling capacity hybrid map are outlined below. The only difference from the general process previously outlined is that the function F, the ratio of sensible cooling capacity to total cooling capacity, is introduced in equation (4-7) in order to map from the function K, the total cooling capacity, to T, the sensible cooling capacity. F is then treated in equations (4-9) through (4-12) in the same manner as K was previously treated in equations (4-1) through (4-6). F and K are then multiplied to yield a hybrid function T in equation (4-13).

$$T(x, y, z) = F(x, y, z) * K(x, y, z) = F(x, y, z) * (K_0 + \Delta K(x, y, z)) \quad (4\text{-}7)$$

$$F \approx F_0 + \frac{\partial F}{\partial x} * dx + \frac{\partial F}{\partial y} * dy + \frac{\partial F}{\partial z} * dz \quad (4\text{-}8)$$

$$F \approx F_0 + \frac{\partial F}{\partial x} * \Delta x + \frac{\partial F}{\partial y} * \Delta y + \frac{\partial F}{\partial z} * \Delta z \quad (4\text{-}9)$$

Linear correlations yield results of the form:

$$F(x) = n_x * (x - x_0) + F_0, \text{ where } n_x \approx \frac{\partial F}{\partial x} \quad (4\text{-}10)$$

$$F \approx F_0 + n_x * (x - x_0) + n_y * (y - y_0) + n_z * (z - z_0) \quad (4\text{-}11)$$

$$F_{Hybrid} \approx F_0 + n_{x,NIST} * (x - x_0) + n_{y,TRNSYS} * (y - y_0) + n_{z,TRNSYS} * (z - z_0) \quad (4\text{-}12)$$

Where x, y, and z are dependent variables such as outdoor dry bulb temperature, humidity, and mass flow rate.

$$T_{Hybrid} \approx F_{Hybrid} * K_{Hybrid} \quad (4\text{-}13)$$

All of the calculations for the performance map generation may be found in the spread sheet ‘Curve Calculations Hybrid.xlsx’.

4.1.3.3 Dehumidification

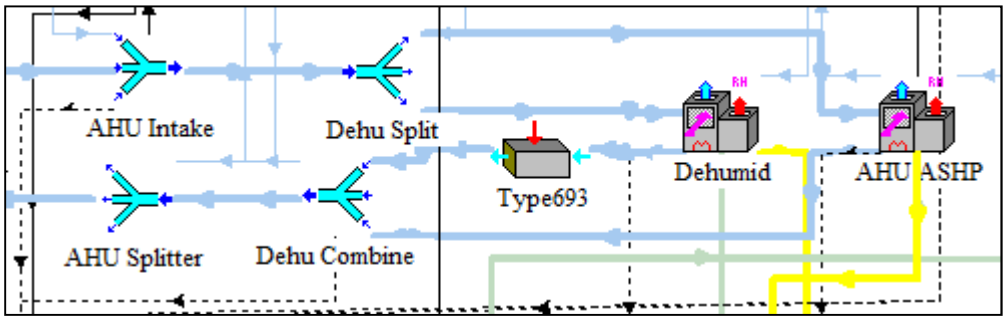

Figure 4-4: Addition of Dehumidification to the HVAC Heat Pump

The dehumidification system in the Test Facility relies on the central HVAC heat pump. The heat pump has two dehumidification modes that pass a reduced interior air flow over the cooling coils and then reheat the conditioned interior air with the condensing refrigerant. The air flow is reduced to 67% of the maximum air flow for the stage 1 dehumidification and 45% of the maximum air flow for stage 2 dehumidification.

The TYPE 922 Air Source Heat Pump component only allows two cooling settings. To work around this limitation, a second TYPE 922 component was added as a dehumidifier. This component uses the same performance maps as the main heating/cooling component and has the dehumidification settings in place of the cooling settings for fan speed. The hot gas reheat is implemented with a TYPE 693 fluid load component. The fluid load component takes the cooled air stream flowing out of the dehumidifier and heats it with the sensible load previously extracted from the air stream which results in a temperature about the same as the original air stream.

The air flow to and from the dehumidifier and the main HVAC HP is controlled by a series of TYPE 646 duct components that ensure that only the appropriate piece of equipment is

conditioning the air during any time step. Details of the parameters and inputs used in the dehumidification system may be found in the 'Dehumidifier' tab of the spread sheet 'TRNSYS model system parameters.xlsx' in the electronic supplement.

4.1.3.4 HVAC Controls

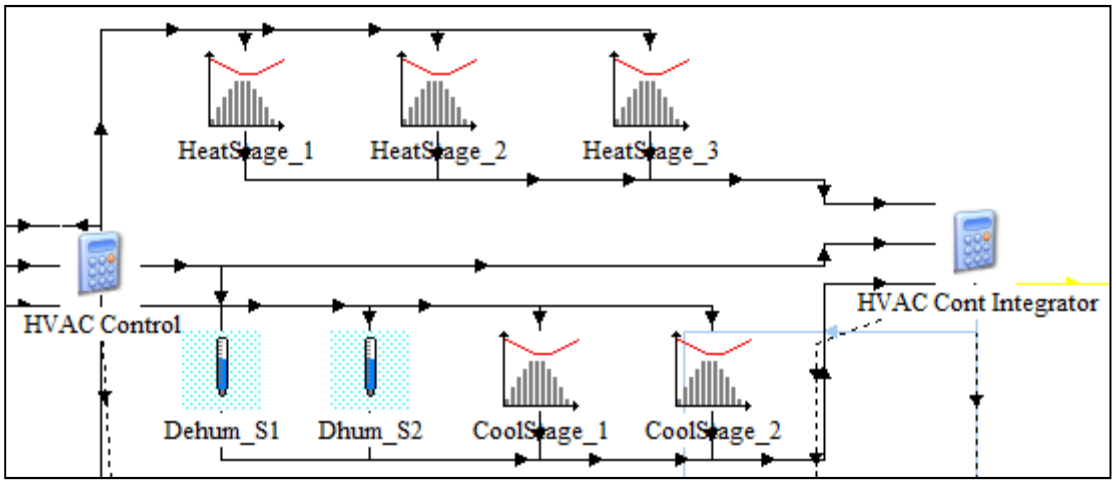

Figure 4-5: HVAC Control Thermostats and Humidistats

The Test Facility has a complex control scheme with time delay triggers in addition to temperature and humidity set point triggers. This control scheme was implemented in the TRNSYS Baseline Full House Model using 5 TYPE 974 Thermostats, 2 TYPE 1503 Humidistats, and 2 equation blocks.

Two of the TYPE 974 Thermostats control the cooling stages. The first thermostat activates stage 1 (low speed cooling) when the monitored zone temperature rises 1.1 C above the cooling temperature set point and turns stage 1 off when the monitored zone temperature reaches the temperature set point. If stage 1 remains on for 40 minutes, then stage 2 (high speed cooling) is automatically activated. The second cooling thermostat activates stage 2 if the temperature rises 2.8 C above the cooling set point.

Three TYPE 974 thermostats control the heating stages. The first thermostat activates stage 1 (low speed heating) when the monitored zone temperature drops 0.56 C below the heating set point. If stage 1 remains on for 10 minutes then stage 2 (high speed heating) is automatically activated. The second thermostat activates stage 2 if the zone temperature drops 1.1 C below the heating set point. If stage 2 remains on for 40 minutes then stage 3 (auxiliary electric heat) is automatically activated. The third thermostat activates stage 3 if the zone temperature drops 3.3 C below the heating set point. All of the thermostats deactivate their associated heating mode when the zone temperature rises above the set point.

The two TYPE 1503 humidistats control the stage 1 and stage 2 dehumidification modes. The first humidistat has a set point of 60 %RH with a 5 %RH dead band and activates stage 1 dehumidification when the humidity rises to 62.5 %RH and shuts off when the humidity drops below 57.5 %RH. The second humidistat has a set point of 70 %RH with a 5 %RH dead band and activates stage 2 dehumidification when the humidity rises to 72.5 %RH and shuts off when the humidity drops below 67.5 %RH.

The heating and cooling season schedulers read text files containing the heating and cooling season schedules and then output an on/off signal based on the simulation month. This effectively shuts down the cooling or heating when it is not the scheduled season. The Schedules are based on the heating and cooling schedules outlined in the EnergyPlus model documentation and described in Chapter 2.

The signals from the thermostats, humidistats, and season schedulers are sent to the HVAC Cont Integrator equation block. This equation block also accepts heating and cooling season indicators and indoor fan only control signals (not currently used) and outputs the combined

control signals for all heating, cooling, dehumidification, and indoor fan stages. The equation uses logical statements to activate each stage if other higher level conflicting stages are not being signaled and the appropriate season indicator is on. As an example, if the heating season indicator is on then the stage 1 heating will shut off if the stage 2 heating is activated but the stage 2 heating will remain on if the stage 3 heating is activated. Similarly, if the cooling season indicator is on then the dehumidification stages will only be activated if the cooling stages are off.

A description of the thermostat/humidistat component settings, along with the logical statements from the control integration equation block, can be found in the 'Thermostats (House)' tab of the spread sheet 'TRNSYS model system parameters.xlsx' in the electronic supplement.

4.1.3.5 EnergyPlus Comparison HVAC Controls

For comparison with the EnergyPlus simulations, a different control scheme was created based on the EnergyPlus model documentation. This control scheme is different from that used in the Test Facility and results in lower predicted power use and different deviations in zone temperatures from set-points as shown in Table 4-4.

Table 4-4: Initial Results of Control Scheme Variations

Control Scheme	**Total Power Consumption**	**1st Floor Deviation Above Cooling Set point**	**1st Floor Deviation Below Heating Set point**
	kWhr/yr	**C-day/yr**	**C-day/yr**
Test Facility Controls	12017	75	32
EnergyPlus Controls	10701	40	57

The EnergyPlus model based HVAC control system consists of the same components as the Test Facility based control scheme with many of the settings changed to imitate the less complex EnergyPlus Model Control Scheme. All of the time delay triggers in the control scheme were set to an extremely long time, 10000 min, in order to prevent the time delay triggers from being used. All of the heating and cooling thermostats were set to watch the temperature of zone 2 and to trigger, with different on and off dead bands, when the zone 2 temperature reaches the heating or cooling temperature set point. The Stage 1 heating thermostat was set to turn on 1 °C below and to turn off 1 °C above the heating set point. The Stage 2 heating thermostat was set to turn on 2 °C below the heating set point and to turn off at the heating set point. The Stage 3 heating thermostat was set to turn on 3 °C below the heating set point and to turn off at the heating set point. The Stage 1 cooling thermostat turns on 1 °C above and to turns off 1 °C below the cooling set point. The Stage 2 cooling thermostat turns on 2 °C above the cooling set point and to turns off at the cooling set point.

4.1.4 Solar PV System

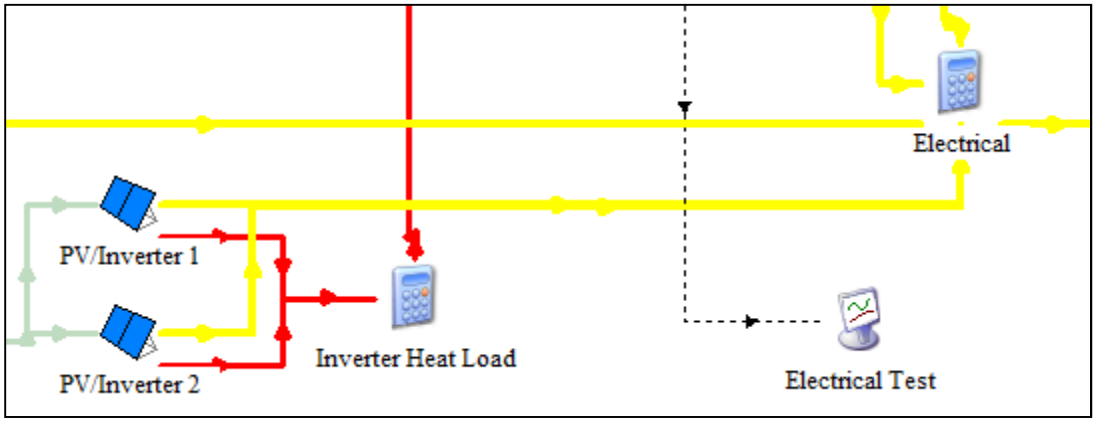

Figure 4-6: PV System and Electrical Equation Block

The Solar PV system consists of two identical TRNSYS TYPE 194b models combined solar array/maximum power point tracking inverter components. These components represent the

two 16 panel arrays which feed into separate inverters. This setup mimic the actual solar PV system and makes the simulation more flexible if it is decided to test the arrays separately as would happen if one array is used as a control. The parameters and inputs can be found on the 'PV MPP Inverter' tab of the spread sheet 'TRNSYS model system parameters.xlsx'. Each component feeds power to the Electrical equation block which also takes in energy demand from the load schedule and HVAC/HRV equipment. The night time power draw of the inverters was included in the total house hold power demand inside of the Electrical equation block. The heat given off by the inverters is included in the thermal gain for the attic space, zone 4.

The panels are SunPower SPR-320E-WHT-U's and are modeled using the 5 parameter model developed by DeSoto, Klein, Beckman, & De Soto (2006). The model parameters are determined from the manufacturer's specs via an EES function also developed by Klein (2013). The component then determines maximum power point (MPP) for the panels. The output for the combined panels is then determined and passed to a function that uses a lookup table of inverter efficiency to determine the total solar system output. The inverters are SunPower 5000m LUT's and the inverter parameters were taken from the *SunPower SPR-5000m, -6000m, -7000m and -8000m STRING INVERTERS Specification Sheet* (2010). The inverter efficiency table was read off of a chart in the manufacturer's specification sheet, Figure 4-7, using Google SketchUp and then formatted to a TRNSYS readable text file.

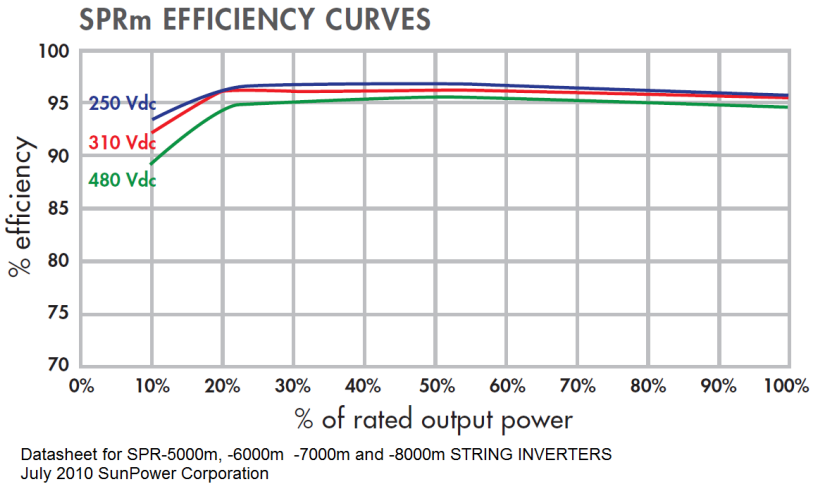

Figure 4-7: Manufacturer's Efficiency Curves for Solar PV Inverter

4.1.5 Solar Hot Water System

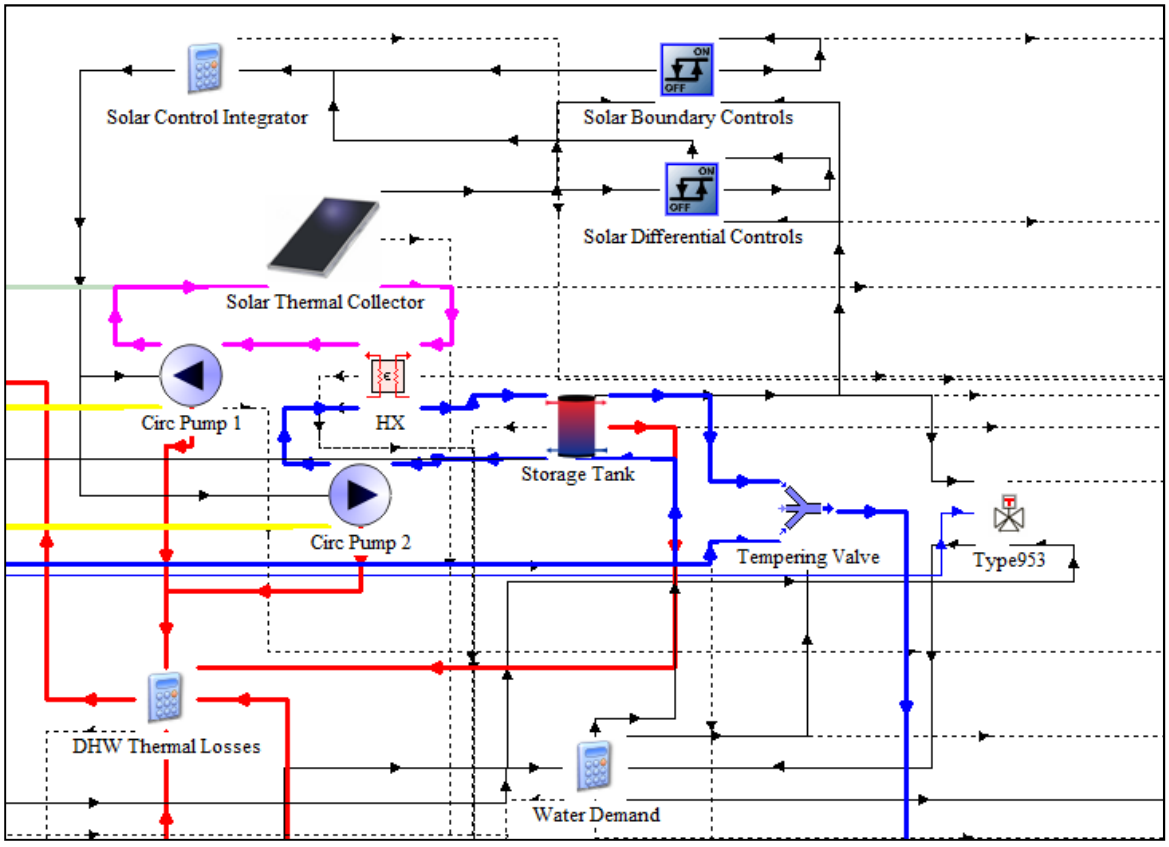

Figure 4-8: Solar Hot Water System

The Solar Hot Water system (SHW) preheats and stores water for the Domestic Hot Water system (DHW). The solar hot water system consists of a solar thermal collector array filled

with a propylene glycol brine mixture, a brine circulation pump, a counter flow heat exchanger, a water circulation pump, and a hot water storage tank.

4.1.5.1 Solar Thermal Collectors

The collectors are Heliodyne GOBI 406 001 flat plate collectors (Kneifel, 2012a). There are a total of 4 collectors installed on the NZERTF in two serial arrays of 2 collectors. Each array feeds into one of two separate storage tanks with only one array and tank set in use under the current setup. The collectors are located on the lower south facing roof of the house and are at the same 18.43 degree slope as the solar PV panels. As the thermal collectors are not subject to any additional shading, they receive the same solar radiation per unit area as the solar PV panels and the same surface calculations were used. These calculations are performed by the TYPE 15 Weather Data Processor File Reader component.

The collectors were modeled using the TYPE 539 glazed flat plate collector component. The model input parameters are mostly the values from the Solar Collector Certification and Rating Sheet (Solar Rating and Certification Corporation, 2011). The collector thermal capacitance was not included in the specifications and was estimated in EES assuming the collector had a full load of 2.3 L of 50% propylene glycol working fluid yielding a thermal capacitance of 8.437 [kJ/K] due to the retained working fluid. It was assumed that the 34 kg of collector dry mass had minimal impact on the effective collector capacitance as most of the aluminum and glass in the collector are insulated from the copper collector plate. The collector plate itself is made of copper and has a low thermal capacity. It was also found, as has been reported before (S. A. Klein, Duffie, & Beckman, 1974), that the thermal capacitance of the collector had a minimal impact on the annual solar fraction of the DHW

system. A comparison of three different capacitances is shown in Table 4-5. The largest capacitance is a median estimate for the thermal capacitance of the entire collector. The lowest capacitance assumes that the collector has no capacitance. The middle capacitance is the capacitance of the retained fluid. The collector capacitance calculations are contained in the EES file 'SHW Calculations.EES'. Details of the parameters and inputs used may be found in the 'Solar HW' tab of the spread sheet 'TRNSYS model system parameters.xlsx'.

Table 4-5: Impacts of Solar Thermal Collector Thermal Capacitance

Using: Full_model_2013_3_25_main	**High**	**Fluid**	**None**
Solar Thermal Collector Capacitance [kJ/K]:	24.35	8.437	0
	Annual Energy [kWhr]		
Solar Useful Energy Gain	3923	3968	3958
% of Zero capacitance case	-0.89%	0.26%	0.00%
Solar Brine Circulation Pump	25	26	26
Solar Water Circulation Pump	25	26	26
Heat Pump Hot Water Heater	1428	1411	1417
Auxiliary Electric Heater	10	10	12
Solar Storage Tank Losses	-396	-399	-397
Heater Storage Tank Losses	-235	-237	-236
Over Temperature Supply Losses	-582	-609	-607
Under Temperature Supply Requirement	30	29	30
Net Load:	4228	4226	423

4.1.5.2 Solar Thermal Circulation Pumps and Heat Exchanger

The Heliodyne HPAK heat exchanger system includes two circulation pumps and a high efficiency counter flow heat exchanger. Using the Heliodyne HPAK spec sheet and installation guide (Heliodyne, n.d.), the max collector area for the smallest heat exchanger, model 016, is 9 m^2 and the collector area feeding into a single tank area is 5 m^2. Thus the 016

unit was chosen. Due to lack of documentation the heat exchanger is assumed to have a constant effectiveness of 80% as assumed in the EnergyPlus model.

The pumps for the water and brine loops are identical models but have three speed settings. The brine pump is of more concern as it must overcome part of the head loss associated with the tubing to and from the panels. The second speed setting was used as the elevation to the base of the panels from the pump location is about 15 ft (4.572 m) which exceeds the recommended head rise for the first speed setting. Speed 2 is also the factory default setting. Using the pump head vs. flow rate and power charts in the installation manual the resulting pump flow rate is 1.5 gpm which is twice the recommended flow rate for 2 panels and is 95% of the value used in the EnergyPlus model. The corresponding power draw is indicated as 55 W at 1.5 GPM and speed 2. The water side pump has minimal change in height and a very short length of tubing loss so setting 1 should yield 8 gpm and a power consumption of 55 W. This setting results in a greater capacitance rate in the water loop with a ratio of 5.93 [-] between the water and brine loop capacitances. Details of the parameters and inputs used may be found in the 'SHW HX' and 'SHW Circ Pumps' tabs of the spread sheet 'TRNSYS model system parameters.xlsx'

4.1.5.3 Solar Hot Water Storage Tank

There are currently two solar hot water storage tanks installed in the NZERTF. The tanks have 80 and 120 gal capacities and are each connected to two of the solar thermal collectors. At the present time only the 80 gallon tank and attached collectors are in use. The 80 gal tank was modeled as a 7 node stratified storage tank using the TYPE 534 Cylindrical Storage Tank Component. The nodes are evenly distributed from top, node one, to bottom, node 7.

Flow to meet the house hot water demand, as determined by the tempering valve control, exits from the top node and an equivalent flow from the water mains enters in the bottom node. The solar collector water loop pump draws from the bottom node and returns to the third node about 18 inches from the top of the tank as outlined in the HPAK Installation Guide (Heliodyne, n.d.). As a specific tank was not specified, the skin loss coefficient, 0.86 W/m^2-K, calculated for the EnergyPlus model was used (Kneifel, 2012a). Details of the parameters and inputs used may be found in the 'SHW Tank 80gal' tab of the spread sheet 'TRNSYS model system parameters.xlsx'

4.1.5.4 Solar Hot Water Controls

The solar hot water system is controlled by two TYPE2 Aquastats. The first is the Solar Boundary Controller, which shuts off the solar collector circulation pumps if the temperature of the water entering the SHW heat exchanger from the bottom of the tank hits 80 °C. The second controller is the solar differential controller which turns the solar collector circulation pumps on if the temperature at the exit of the collector rises 10 °C above temperature of node 7 of the storage tank. The controller then shuts the pumps off if the temperature at the exit of the collector drops to 2 °C above the temperature of node 7.

4.1.5.5 Tempering System and Controls

In the baseline case, water demand is passed from the demand schedule to the Water Demand equation block. The Water Demand Equation block also accepts input from the TYPE953 tempering control and determines how much water to draw from the solar hot water storage tank and how much to draw directly from the water mains. The demanded mass flow rates are then mixed in the tempering valve, a TYPE649 Mixing Valve, and passed to the water

heater storage tank. The tempering control takes in the water mains temperature and the outlet temperature of the solar hot water storage tank and determines the appropriate fraction of each necessary to meet a set point temperature.

The solar hot water system can produce extremely hotwater, ~82 °C. While such high temperatures are acceptable in a thermal storage system, it is recommended by ASHRAE and OSHA that domestic water heater temperatures are kept below 140ºF (60 °C) in order to avoid the risk of scalding and first degree burns. For the EnergyPlus Comparison Model, the water from the solar storage tank is tempered down to 71.1 °C as specified in the EnergyPlus Model documentation. For the Baseline Full House Model the water from the solar storage tank is tempered down to 60 °C before it enters the hot water heater tank. The implementation of tempering control and the decrease in tempering temperature both resulted in a small increase in the hot water energy solar fraction due to the decrease in solar hot water demand relative to supply during warmer months.

4.1.6 Domestic Hot Water

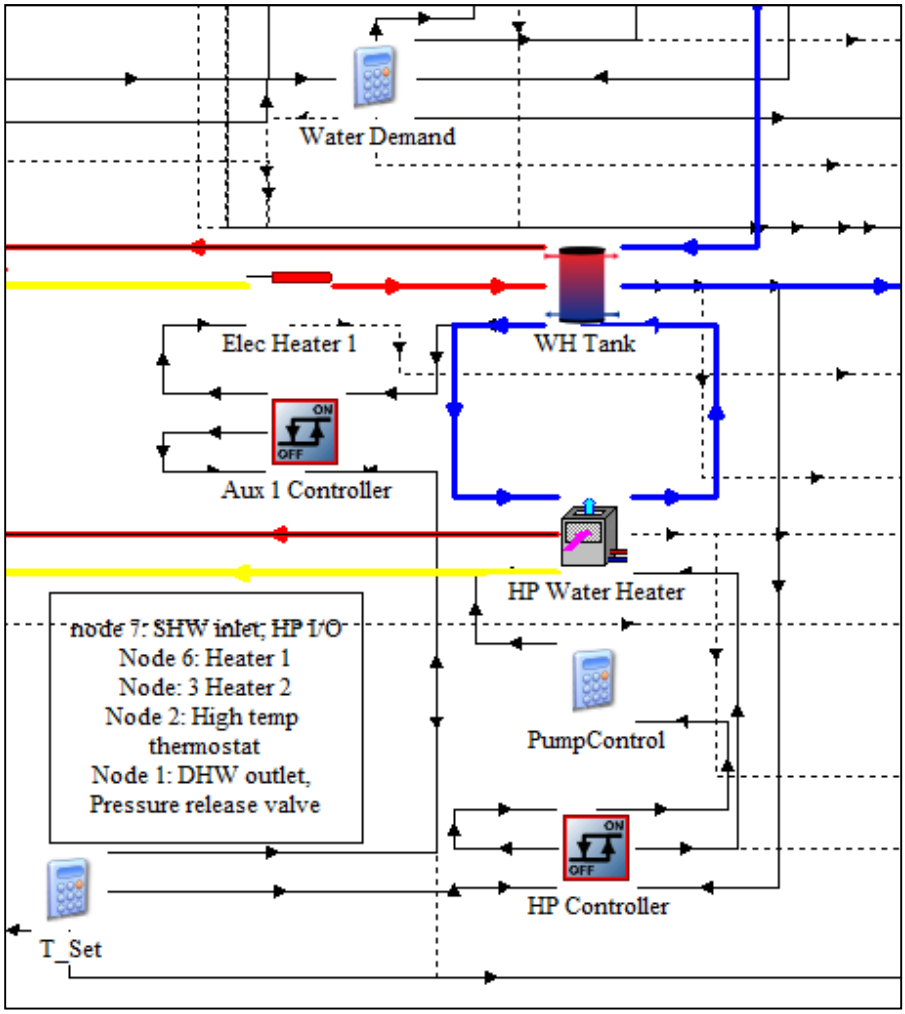

Figure 4-9: Domestic Hot Water System

The Domestic Hot Water system consists of a Heat Pump Water Heater (DHW HP), a storage tank, and an electric auxiliary heater.

4.1.6.1 Domestic Hot Water Heat Pump

The DHW HP is a Hubbell PBX 50SL and was modeled with a TYPE938 Heat Pump Water Heater component. The TRNSYS default performance maps for this component was used along with the heat-pump manufacturer's rated performance (HUBBELL, 2012). The TRNSYS rated performance was calculated by dividing the manufacturer's rated

performance by the normalized performance values of the TRNSYS performance map at the manufacturer rating conditions. The blower power was also separated out of the overall power consumption of the heat pump using the manufacturers specification sheet. The high blower power is recommended except when low noise operation is desired and results in a blower power of 148.5 W relative to a compressor power of 531.5 W at the manufacturer rated conditions. The water flow rate through the heat pump was left at the TRNSYS default of 1000 kg/hr resulting in a ratio of 4.6 between the water and air flow capacitances. These calculations may be found in the file 'DHW HP Calculations.EES'. The electrical demand of the water pump power was not considered separately from the compressor. The dehumidifying effect of the heat pump on the basement was also not considered. The net result is an annual average COP of about 2.7 vs. the rated COP of 2.6. The TRNSYS simulated performance is under the conditions found in the basement as opposed to the manufacturer or TRNSYS rated conditions and, as it is calculated from simulated energy use and delivery, it varies with the controls used. The manufacturer rated conditions are also worse for efficiency than the normal operating conditions of the heat pump during the simulation. The rating condition supply temperature set point temperature is 57.5 °C (135 °F) vs. the simulation supply temperature set point of 60 °C (140 °F). The rated room temperature is set to 19.7 °C (67.5 °F) whereas the simulation room temperature varies and is typically lower than 19.7°C. However when the room temperature during winter is low, the entering water temperature for the heat pump is much lower than the rating condition entering water temperature. Details of the parameters and inputs used may be found in the 'DHW HP' tab of the spread sheet 'TRNSYS model system parameters.xlsx'.

The heat pump hot water storage tank is in an integrated 50 gallon Hubbell PBX storage tank. Like the solar hot water storage tank, it was also modeled as a 7 node stratified storage tank using the TYPE 534 Cylindrical Storage Tank Component. The nodes are evenly distributed from top, node one, to bottom, node 7. Flow to meet the total house hot water demand exits from the top node and an equivalent flow from the tempering valve enters in the bottom node. While counter intuitive, the heat pump both draws from and discharges to the bottom node as noted in the manufacturer's specifications (HUBBELL, 2012). It is of interest to note that the current mixing set up in the event of a temperature inversion is to have the two relevant fluid nodes instantly and adiabatically mix. There are two auxiliary electric heaters included in the tank of which only the top one is used with the current operating mode. The auxiliary electrical heater in use is modeled as a heat addition to the third node from the top of the tank. The skin loss coefficient, 1.476 W/m^2-K, calculated for the EnergyPlus model was used. Details of the parameters and inputs used may be found in the 'DHW Tank' tab of the spread sheet 'TRNSYS model system parameters.xlsx'.

4.1.6.2 Heat Pump and Auxiliary Heater Controls

The heat pump is controlled by a TYPE2 Aquastat component. The aquastat monitors the temperature in the top node of the water heater storage tank and turns the DHW HP on if the temperature drops below the set point temperature. The heat pump is turned off once the temperature in the top node of the tank rises 5 °C above the set point. For the Baseline full house model the DHW HP storage tank set point is 60 °C. For the EnergyPlus Comparison Model the set point is 49 °C. The aquastat will also shut off if the temperature rises to the safety shutoff of 71.1 °C though this should be unnecessary with the other controls,

The 4500 [W] auxiliary heater is controlled by another TYPE2 Aquastat component which also monitors the temperature in the top of the heat pump storage tank. This aquastat turns on the auxiliary heater if the temperature drops 10 °C below the set point temperature. The heater is turned off once the temperature in the tank rises back to the set point. This aquastat will also shut off if the temperature rises to the safety shutoff of 71.1 °C.

The differences between the tempering and water heater set point temperatures of the EnergyPlus Comparison Model and the Baseline Full House Model resulted in a 0.12 increase in the solar fraction and a decrease of 1047 kWhr/year in the domestic water heater energy use for a savings of 42% of the total hot water demand.

4.1.7 Validation of the Solar Hot Water and Domestic Hot Water Systems

The DHW and SHW systems have been compared with the direct electrical heating requirements, the solar fraction using the F-Chart method (Duffie & Beckman, 2012), and the results from the EnergyPlus model. The direct electrical heating requirement is the amount of energy required to take water from the mains temperature to the end use set point temperature.

The F-Chart method is a way of estimating the annual performance of solar thermal systems given average monthly values for weather and solar data. In order to make a performance estimate that was relevant to the simulation and EnergyPlus model, the TMY3 weather file being use in the simulation was processed to get the relevant monthly variables. These variables were then used to calculate the monthly load requirement, total intercepted solar radiation, and the fraction of the loading being met by the thermal energy delivered after

taking into account thermal losses, heat exchanger efficiencies, and thermal storage capacity. The results for every month are then summed to yield annual results. The calculations for the direct heating requirements and F-Chart estimate can be found in the spread sheet 'FCHART Weather.xlsx' and 'FCHART DHW Calculations.EES' in the electronic supplement.

The monthly solar fraction for the TRNSYS simulation of the DHW system was calculated by dividing the useful energy gain from the solar collectors by the sum of the useful energy gain, the heat loss to the fluid from the circulation pumps, the heat input from the heat pump hot water heater, and the heat input from the auxiliary hot water heater. The total annual DHW heating load, the solar input to the system, and the solar fraction, are summarized for the F-Chart estimate, the EnergyPlus estimate, and the TRNSYS baseline case in Table 4-6.

Table 4-6: Comparison DHW Load and Solar Fractions

Source:	Total Annual Load [kWhr]	Solar Contribution [kWhr]	Solar Fraction [-]
Direct Electrical Annual Ave Data	4175	0	0
Direct Electrical Monthly Ave Data	4092	0	0
F-Chart w/ 49.9 °C set-point	4092	2933	0.72
EnergyPlus	3630	2577	0.71
TRNSYS w/ 49.9 °C set-point	4091	2961	0.72
F-Chart w/ 60 °C set-point	5310	3334	0.63
TRNSYS w/ 60 °C set-point	6498	3364	0.62

Note that the total annual load for the TRNSYS baseline does not include the losses from the storage tanks or the 'lost' energy from supplying water above the system set point. The total annual losses from losses from supplying hotter than set point water were calculated along with the additional energy required to meet the set point temperature all the time by determining how often and by how much the water supply was below the set point

temperature. The energy losses from both tanks and the gains from the circulation pumps and auxiliary heater were also calculated. Table 4-7 summarizes the gains and losses to the DHW system along with the TRNSYS simulations net load requirement. Due to thermal losses, the TRNSYS simulation's net load requirement for a hot water heater tank set point of 49.9 °C, 4228 [kWhr], is closer to the estimated minimum load requirement, 4092 [kWhr], than the TRNSYS simulation's total delivered energy, 5435 [kWhr]. Similarly for a hot water heater tank set point of 60 °C the net load requirement of 5579 [kWhr] is closer to the minimum required, 5310 [kWhr], than the total delivered energy of 6498 [kWhr].

Table 4-7: TRNSYS Baseline Simulation Solar and Domestic Hot Water System Gains and Losses

	Annual Energy T_set = 49.9 °C [kWhr]	**Annual Energy T_set = 60 °C [kWhr]**
Solar Useful Energy Gain	3923	4028
Solar Brine Circulation Pump	25	25
Solar Water Circulation Pump	25	25
Heat Pump Hot Water Heater	1430	2295
Auxiliary Electric Heater	10	124
Solar Storage Tank Losses	-396	-400
Heater Storage Tank Losses	-235	-286
Over Temperature Supply Losses	-583	-315
Under Temperature Supply Requirement	29	82
Net Load Requirement:	**4228**	**5579**

4.1.7.1 Initial observations on the Hot Water Heating Control System

The triggering temperatures are extremely important. Anything that can be done to prevent the auxiliary electric heater from turning on is helpful. The heat pump hot water heater's default setting even deactivates the auxiliary heaters. A larger HW heater storage tank or more sensitive auxiliary heating controls could eliminate the small amount of under set-point

temperature water supply. However, eliminating this small amount of under temperature supply would come at the expense of less efficient heating or greater tank losses to the basement. As can be seen in Figure 4-10, the additional energy carried out of the DHW system by water supplied at a temperature hotter than the set point temperature is greatest in summer when the SHW system is most effective and supplies water exceeding the set point to the DHW HP. The loss of energy due to the supply temperature exceeding the set-point persists during winter when the SHW system often does not meet the set point temperature due to the DHW HP control system overshooting the supply temperature when heating the tank. The lower-than set point water delivery mostly occurs during winter as the heat pump struggles to keep up with the heating requirements.

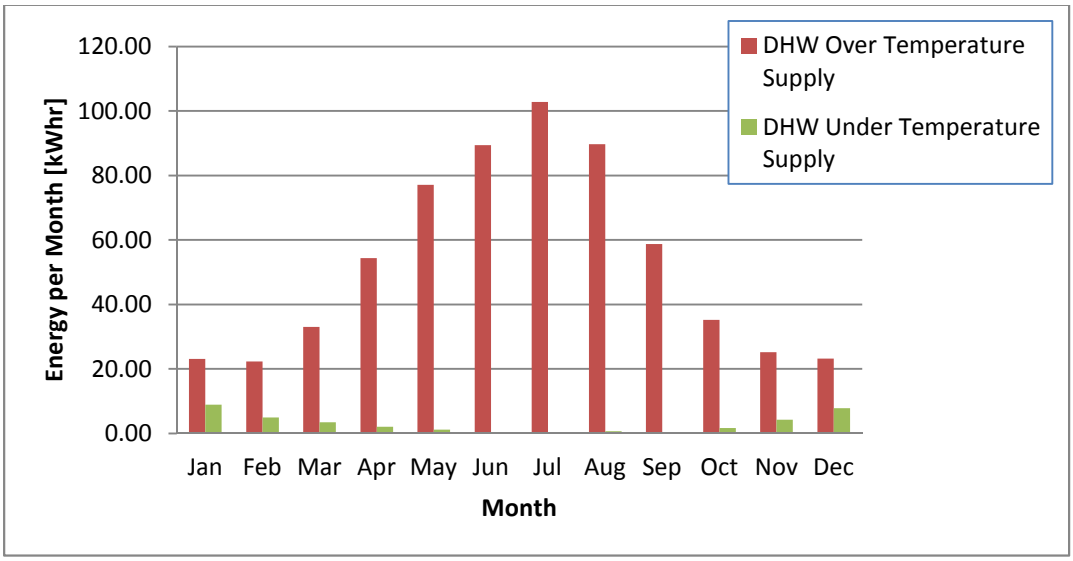

Figure 4-10: DHW End Use Deviation of Energy Supplied Relative to Set Point Temperature (49.9 °C)

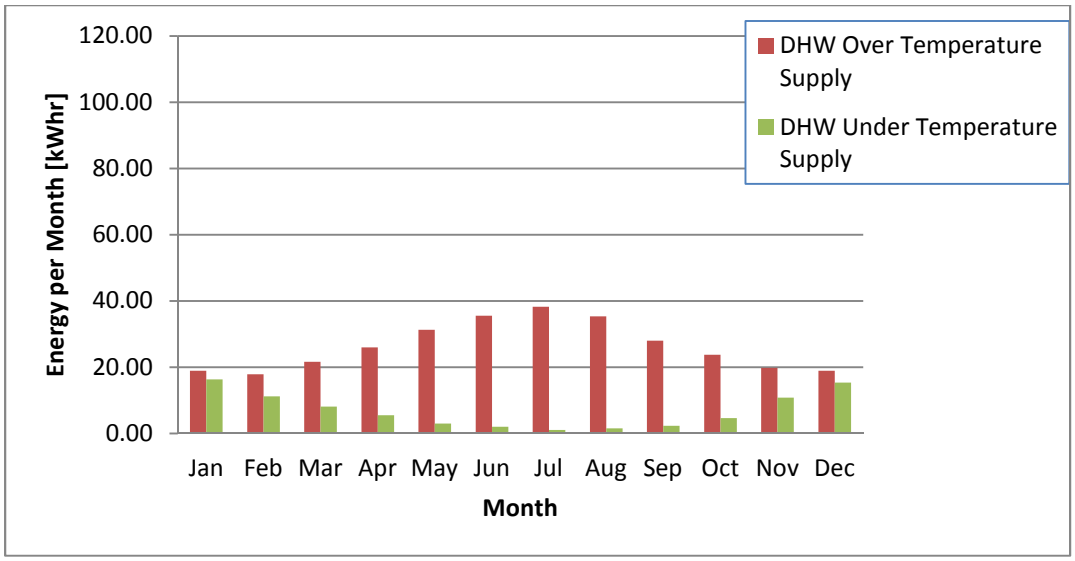

Figure 4-11: DHW End Use Deviation of Energy Supplied Relative to Set Point Temperature (60 °C). Note the decrease in over temperature supply energy and the increase in under temperature supply energy relative to the 49.9 °C tank set-point.

4.1.8 Output Structure

The model output structure now has 8 TYPE 65d online plotters for troubleshooting and four TYPE 46f Printegrators for result output. The printegrators each produce an output file with all of the selected variables at each time step of the simulation. These output files are then read into MATLAB for processing. The printegrators also produce a monthly output file with all of the selected variables integrated over each month of the simulation. The monthly results are copied into an EXCEL spread sheet which then generates graphs similar to those from the EnergyPlus model report (Kneifel, 2012a). The printegrators cover four areas: Weather, HVAC, Electrical,

4.2 Comparison of Baseline Full House Model with EnergyPlus Model

4.2.1 Setup of Baseline Model Comparison with EnergyPlus Model

Comparing the TRNSYS full house model to the EnergyPlus Simulation is important for validation of the TRNSYS model and may be useful in evaluating the relative strengths and weaknesses of the two models. The comparison simulation used a 5 minute time step and one year duration. This comparison simulation deviates from the baseline full house model simulation in several ways: the weather data, the HVAC system control settings, and the domestic hot water system control settings. The weather file consists of the typical meteorological year file for the Washington Dulles meteorological station: 'Washington Dc Dulles Int'l Ar [Sterling - ISIS]_724030TY.csv'. The HVAC controls used are described in the 'EnergyPlus Comparison HVAC Controls' section of Chapter 4. The domestic hot water controls used are also described in the domestic hot water control section of Chapter 4 and differ from the Baseline House Model only in the tempering and set point temperatures.

4.2.2 Results of Baseline Model Comparison with EnergyPlus Model

4.2.2.1 Overview

Table 4-8shows the electrical consumption results from the TRNSYS simulation and the EnergyPlus simulation for the full length of the TMY weather data file. Over the comparison period, the TRNSYS simulation predicted that the total energy consumed would be 6.84% less than the amount predicted by the EnergyPlus simulation. The TRNSYS simulation predicted that the total energy generated by the solar PV system would be 3.35% less than the amount predicted by the EnergyPlus simulation. The TRNSYS simulation predicted a net generation of 4249 kWhr while the EnergyPlus simulation predicted a net generation of

3982, a difference of 6.71 %. These predicted net generations represent 28.4 % and 25.7 % of the total predicted consumption of the TRNSYS and EnergyPlus simulation respectively.

The largest contributors to the difference in the demand were the HVAC heating system and the solar hot water system pumps, as seen in Table 4-8. The Solar PV generation also had a large absolute difference, 519 kWhr, which is 4.52% of the EnergyPlus simulations predicted consumption. The largest percentage errors for individual systems were seen in the heating HVAC performance and the solar hot water heater pumps. The solar PV night time tare load was also off but the total size of this load is such that it is of little importance.

Table 4-8: Electrical Energy Consumption and Generation over the Washington-Dulles TMY Data File

	TRNSYS Simulation	EnergyPlus Simulation	Error	Percent Error	Error Percent of Total Consumed
	kWhr	kWhr	dkWhr	-	-
Heating	1947	1708	239	14.01%	2.08%
Cooling	1820	1886	-66	-3.49%	-0.57%
Heat Recovery	468	472	-4	-0.95%	-0.04%
Fans	0	519	-519	-	-
Interior Lighting	483	486	-3	-0.67%	-0.03%
Interior Equipment	4724	4767	-43	-0.90%	-0.37%
Water Systems	480	506	-26	-5.14%	-0.23%
Pumps	298	78	220	282.12%	1.92%
Generators	0.872	3	-2	-70.94%	-0.02%
Consumed	10703	11489	-786	-6.84%	-6.84%
Generated	14952	15471	-519	-3.35%	-4.52%
Net Generation	4249	3982	267	6.71%	2.33%

4.2.2.2 Monthly Overview

The monthly power consumption and solar PV generation is shown in Figure 4-12. The EnergyPlus and TRNSYS simulations are generally quite close. The electrical consumption of the TRNSYS simulation varies more than that of the EnergyPlus simulation and predicts higher consumption during winter due to greater heating electrical use and during summer due to greater solar hot water pump electrical use.

4.2.2.2.1 Total Electrical Demand and Generation

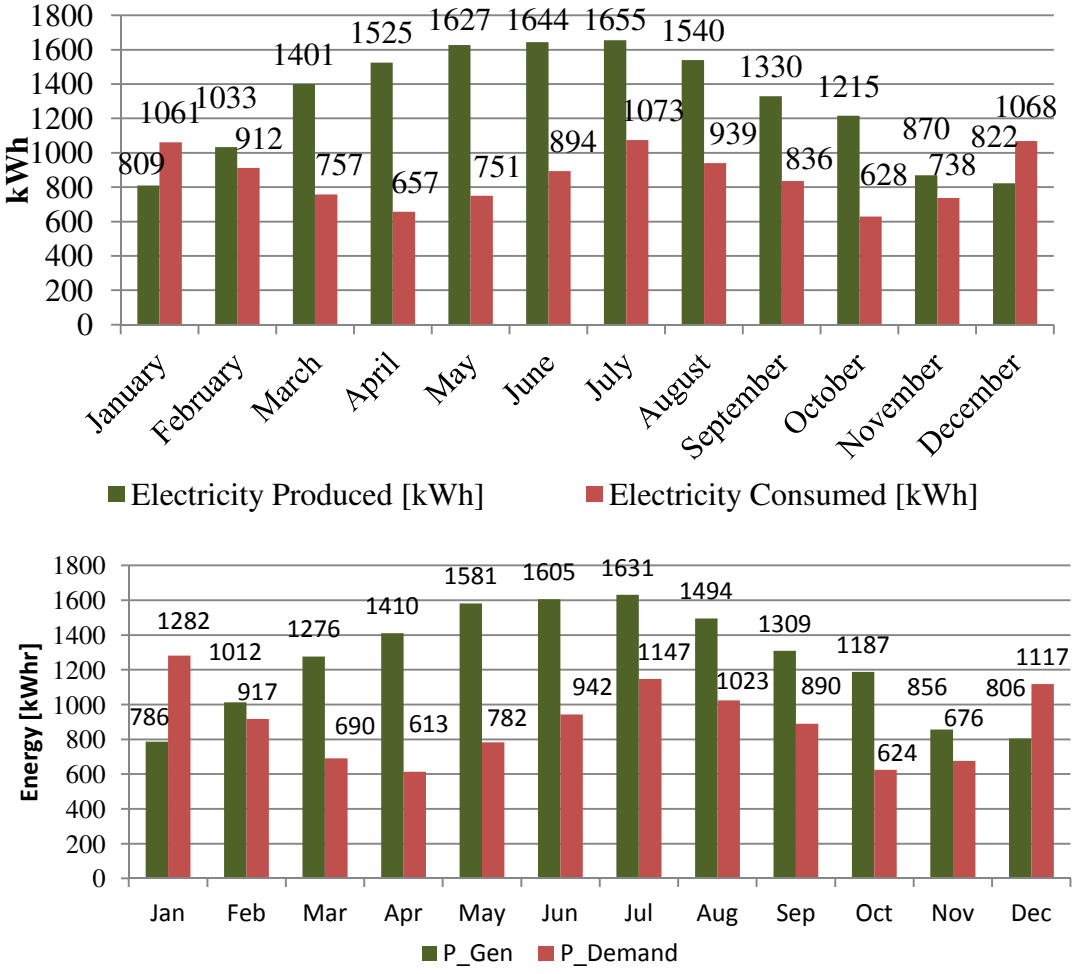

Figure 4-12: Comparison of Total Electrical Consumption and PV Production in [kWhr]. The top graph is "Figure 5-15 Total Electricity Consumption and Solar PV Production (kWh) – Monthly" (Kneifel, Sep. 2012) and the bottom graph displays results from the TRNSYS Baseline Full House model.

4.2.2.2.2 Scheduled Loads

The internal heat gains for the 1st floor of the EnergyPlus NZERTF model and the TRNSYS Baseline Full House model are shown below in Figure 1. The top figure is "Figure 5.13 Internal Heat Gains by Category (kWh) – 1st Floor" (Kneifel, Sep. 2012). The overall values of the heat gains are quite close: the EnergyPlus model averages 323 [kWh/month] and the TRNSYS model averages about 6.8% higher at 345 [kWh/month]. The differences in gains are due to the TRNSYS model using a different electric gain schedule which does not include variations for the different days of the week and particularly the relatively energy intense weekend which is made up for with an equivalent base load demand.

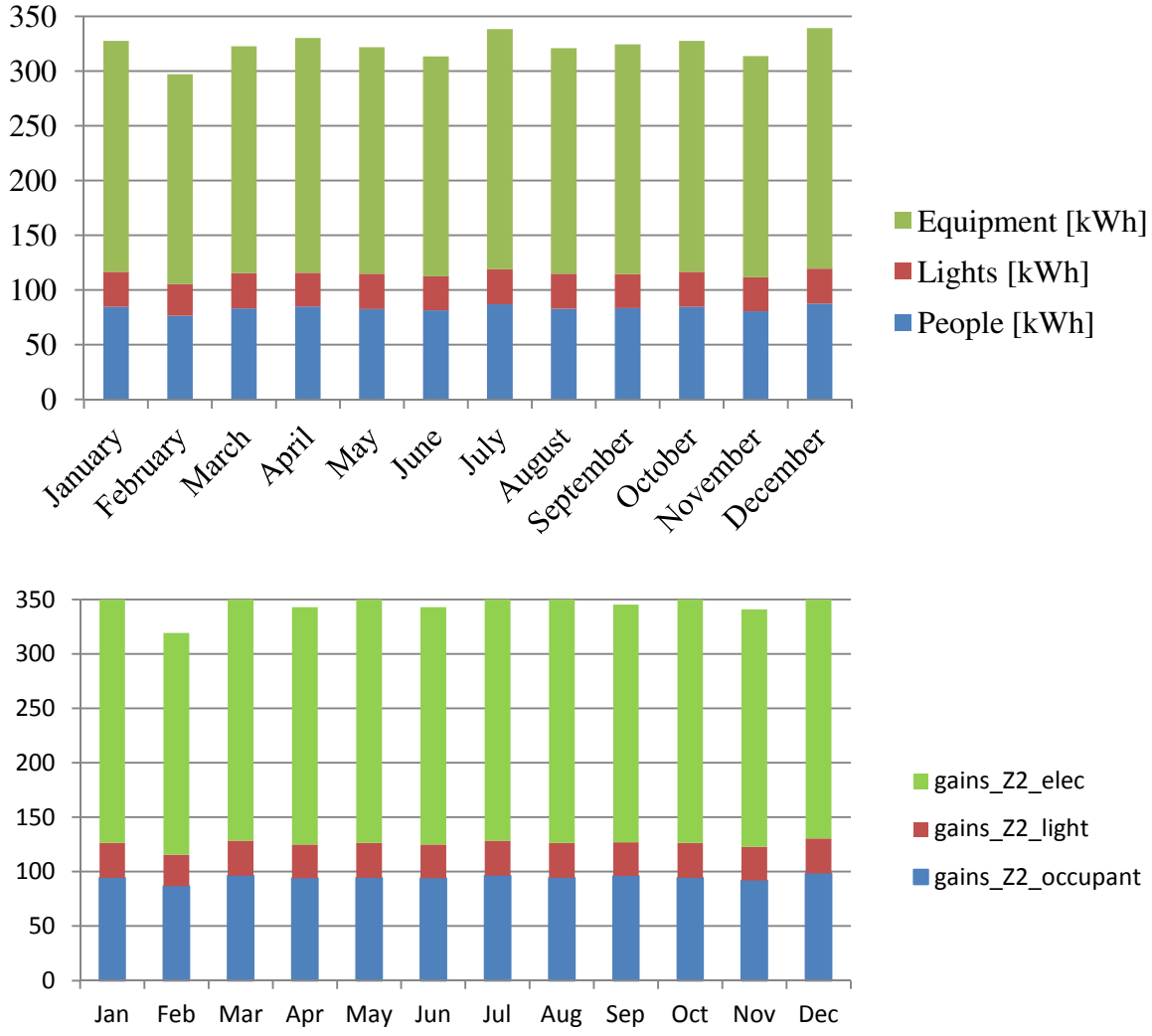

Figure 4-13: Comparison of Internal Heat Gains 1st Floor [kWhr].
The top graph is "Figure 5 13 Internal Heat Gains by Category (kWh) – 1st Floor" (Kneifel, Sep. 2012) and the bottom figure are results of the TRNSYS Baseline Full House model.

The internal heat gains for the 2nd floor of the EnergyPlus NZERTF model and the TRNSYS Baseline Full House model are shown below in Figure 2. The top figure is "Figure 5.14 Internal Heat Gains by Category (kWh) – 2nd Floor" (Kneifel, Sep. 2012). The overall values of the heat gains are very close with the EnergyPlus model averaging around 200[kWh/month] and the TRNSYS model averaging 205 [kWh/month].

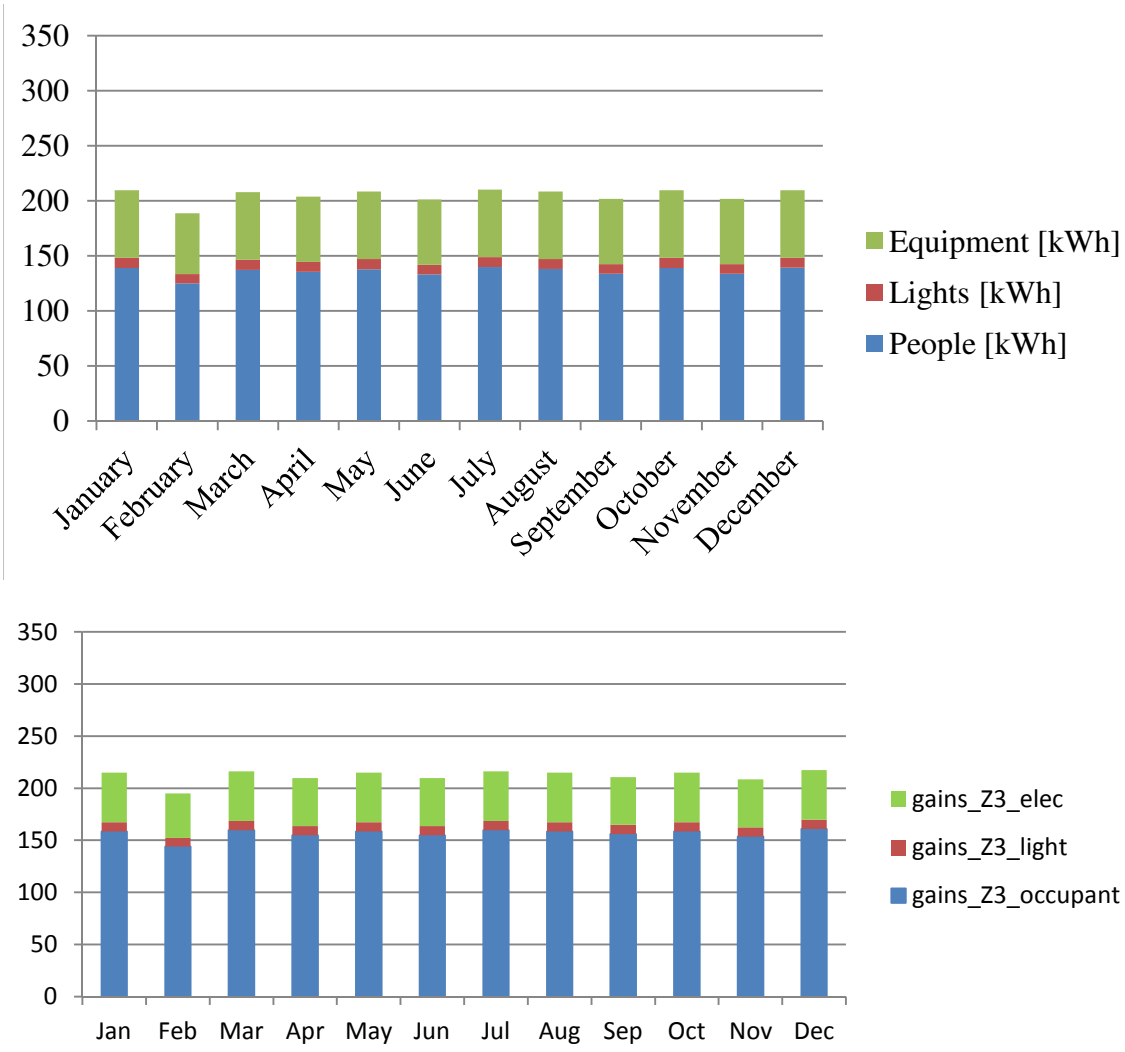

Figure 4-14: Comparison of Internal Heat Gains 1st Floor [kWhr].
The top graph is "Figure 5.14 Internal Heat Gains by Category (kWh) – 2nd Floor" (Kneifel, Sep. 2012) and the bottom figure is from the results of the TRNSYS Baseline Full House model.

4.2.2.2.3 Solar and Domestic Hot Water Systems

The predicted electrical demand from the solar and domestic hot water systems differs significantly as shown in Figure 4-15. The EnergyPlus model hot water heat pump total electrical consumption is 584 [kWh] and the TRNSYS model total is 533% higher at 778 [kWh]. Most of the difference between the EnergyPlus simulation to the TRNSYS simulation is due to a 282% greater solar hot water pump electrical consumption. The TRNSYS simulation has a slightly lower hot water heat pump heater energy demand which is offset by the solar thermal hot water pumps. The EnergyPlus simulation also never employs the electrical resistance auxiliary heaters though the use of these heaters is only a small portion of the TRNSYS simulation's hot water system annual electrical consumption. It is interesting to note that though the TRNSYS simulation predicts a greater electrical consumption, the fraction of the total thermal energy delivered to the domestic hot water supplied by the solar collectors is almost the same in both simulations and matches with an estimate made using the F-chart method as shown in Table 4-6.

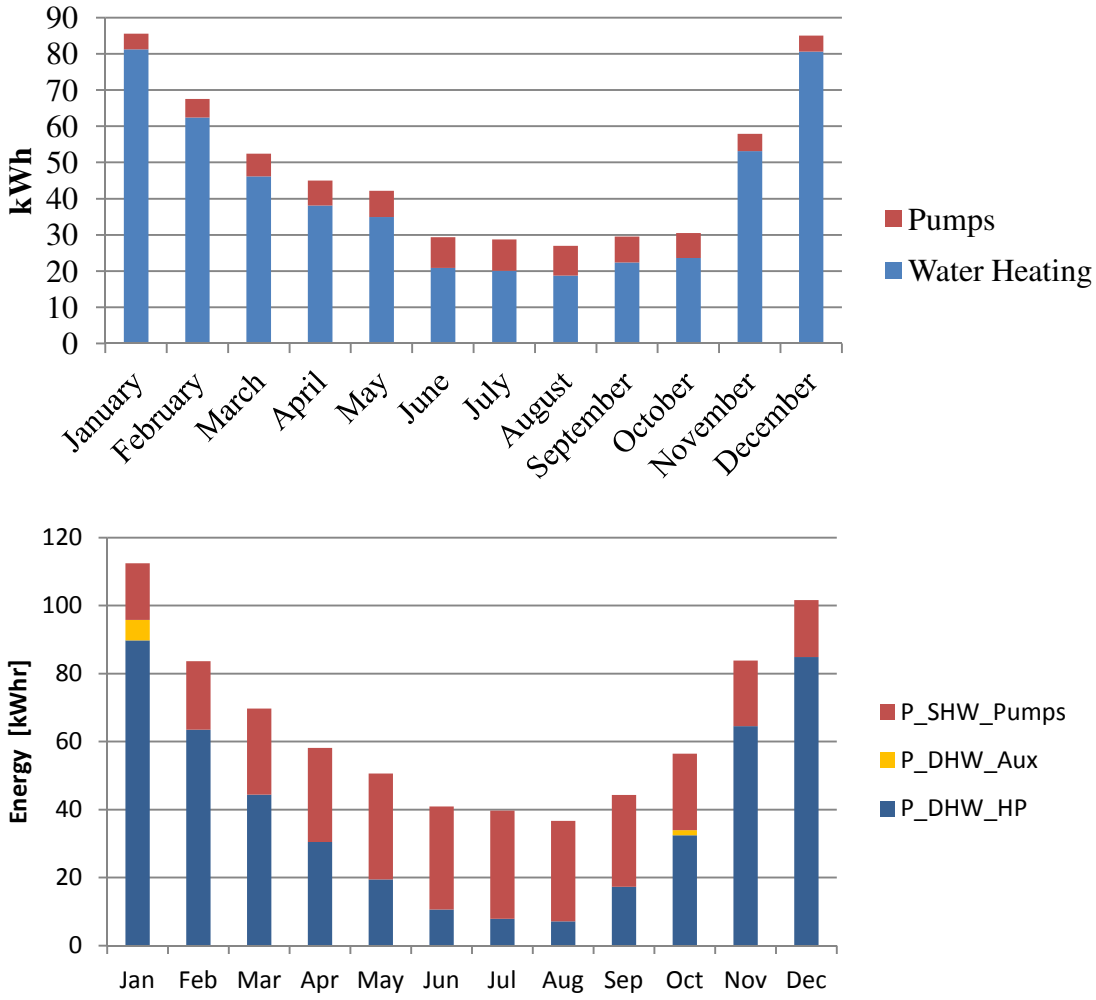

Figure 4-15: Comparison of Domestic Hot Water Monthly Electricity Use in [kWhr].
The top graph is "Figure 5-16 Heat Pump Water Heater and Pump Electricity Use (kWh) – Monthly" (Kneifel, Sep. 2012) and the bottom graph displays results from the TRNSYS Baseline Full House model.

The mains supply and water heater tank average temperatures are almost identical in both simulations which makes sense as the mains temperature is derived from the weather file using the same correlation and the water heater tank temperature is kept near the set point temperature. The solar storage tank temperatures are more dependent upon the solar thermal collector system and the tank losses.

4.2.2.2.4 Infiltration

The monthly average infiltration rate for the 1st and 2nd floors of the EnergyPlus NZERTF model and the TRNSYS model are shown in Figure 4-16. The top graph is "Figure 5.27 Infiltration Rate by Floor - ACH" (Kneifel, Sep. 2012). The TRNSYS model results were quite similar in shape but were consistently about 0.1 ACH greater than the EnergyPlus results. Identical wind shielding and stack coefficients were provided to the TRNSYS infiltration model indicating that the difference is caused either by the infiltration model itself or differences in an interaction between other elements of the models such as increases in internal pressure due to the HVAC system.

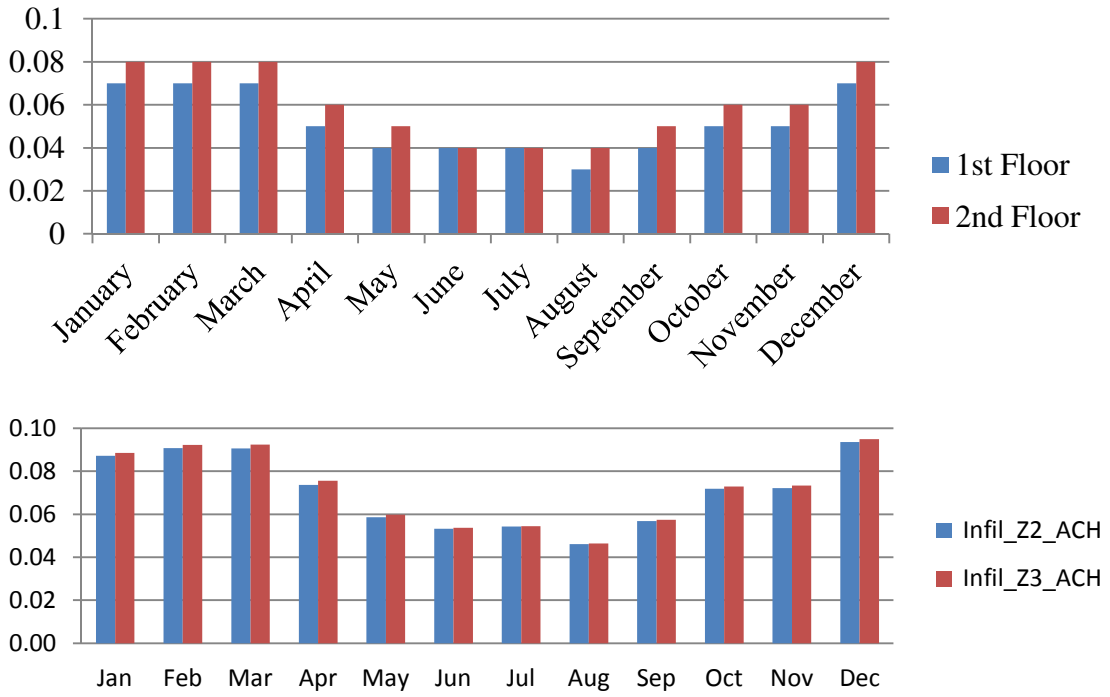

Figure 4-16: Comparison of Monthly Average Infiltration Rate in Air changes/hr
The top graph is "Figure 5.27 Infiltration Rate by Floor - ACH" (Kneifel, Sep. 2012) and the bottom figure is from the results of the TRNSYS Baseline Full House model.

The sensible heat transfer due to infiltration for the 1st floor of the EnergyPlus NZERTF model and the TRNSYS Baseline Full House model are shown in Figure 4-17. The top figure

is “Figure 5.28 Infiltration Sensible Heat Transfer – 1st Floor (kWh)” (Kneifel 2012). The TRNSYS model results in very similar but slightly greater infiltration heat gains and losses than were reported for the EnergyPlus model.

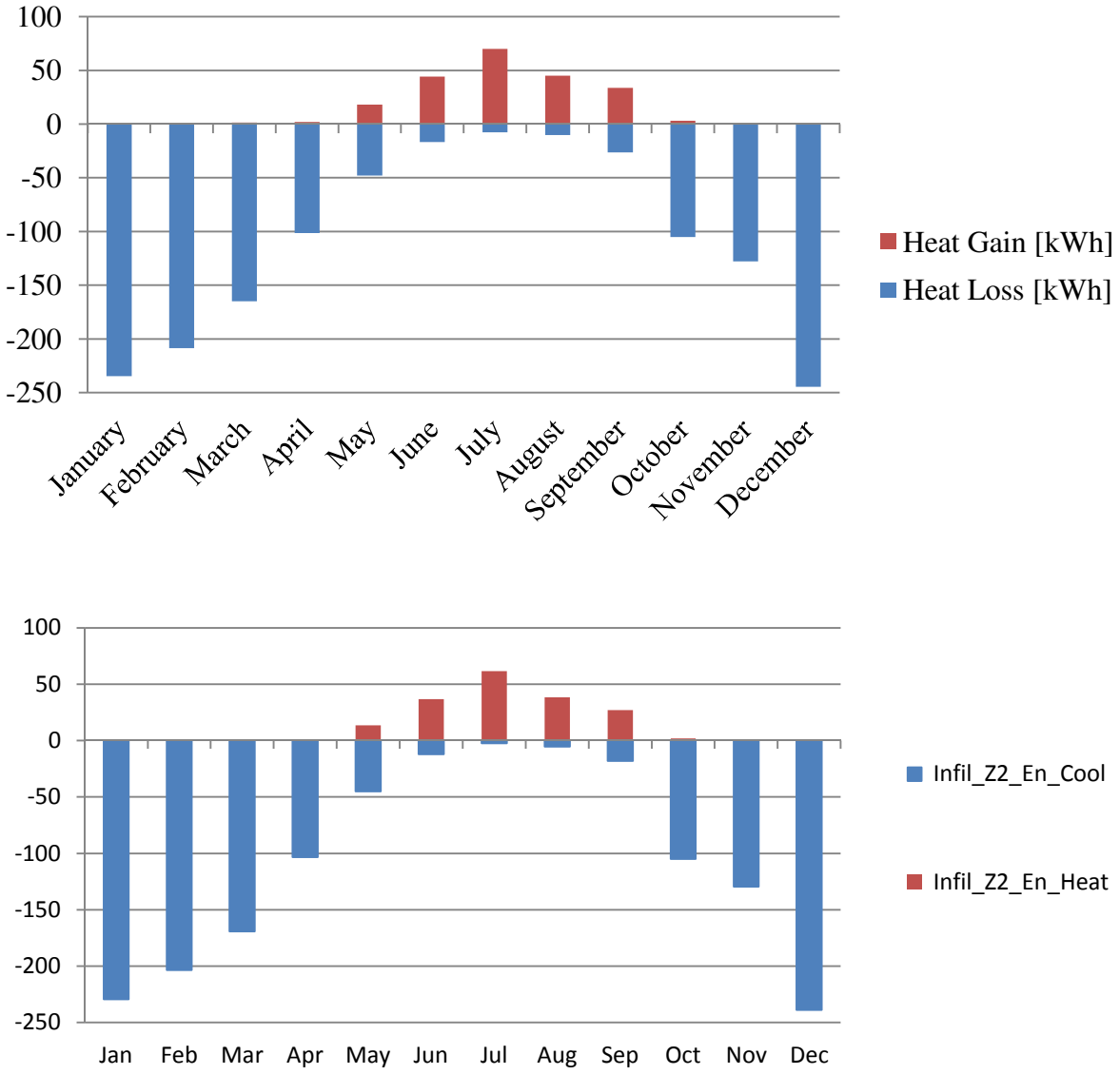

Figure 4-17: Comparison of Infiltration Heat Gains and loses 1st Floor. Thermal Energy [kWhr] The top graph is “Figure 5.28 Infiltration Sensible Heat Transfer – 1st Floor (kWh)” (Kneifel, Sep. 2012) and the bottom figure is from the results of the TRNSYS Baseline Full House model.

4.2.2.2.5 Heat Recovery Ventilator

The TRNSYS simulation predicted the heat recovery ventilation system annual electrical use within 1% of the EnergyPlus simulation's predicted value. Figure 4-18 shows how similar the total predicted heat transfer in the simulated HRV systems were. Neither simulation models the HRV's defrost/freeze protection cycle and thus it is expected that the actual energy use will be slightly higher.

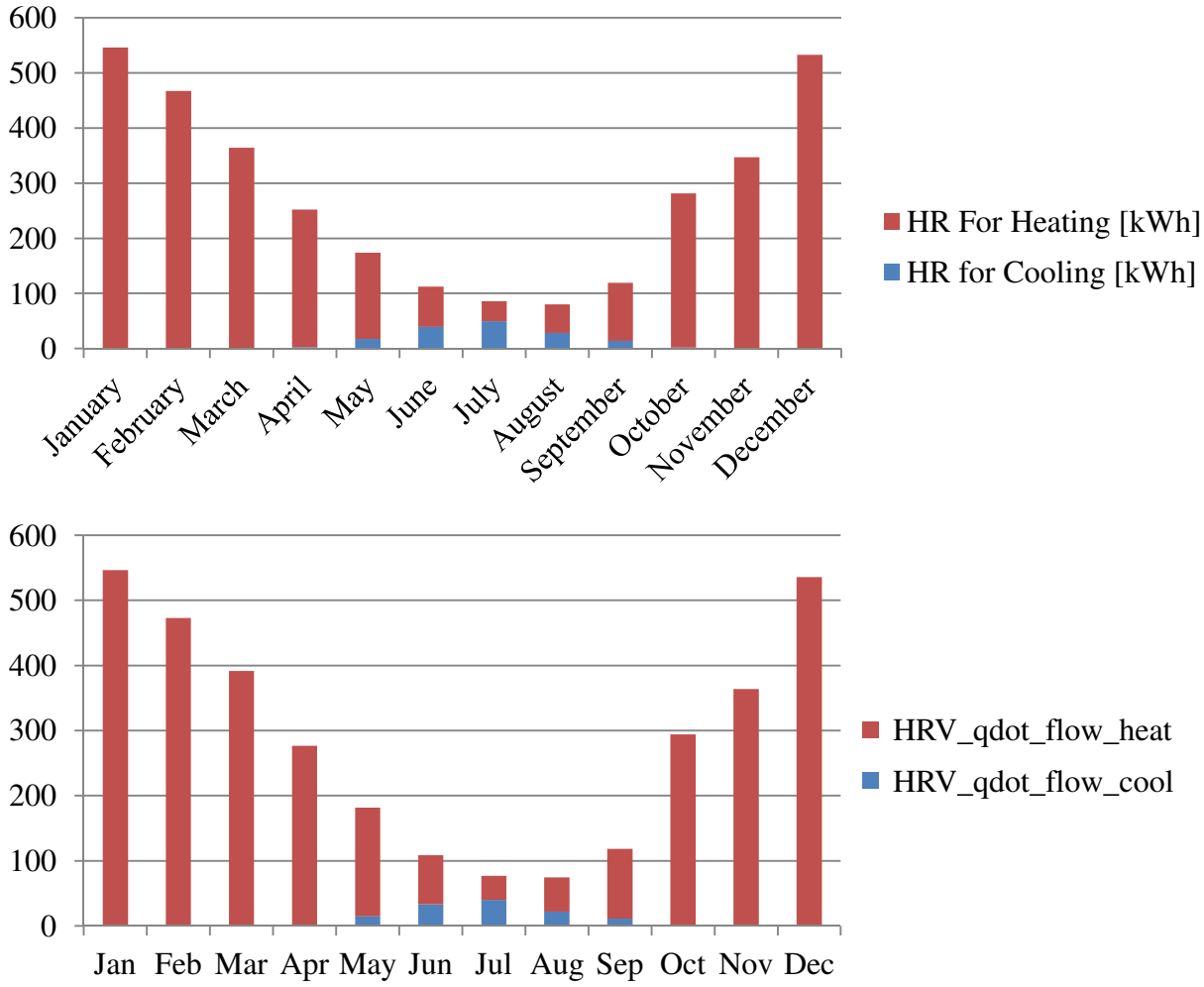

Figure 4-18: Comparison of HRV Monthly Heat Transfer. Thermal Energy [kWhr]
The top graph is "Figure 5 7 HVAC Heat Exchanger Energy Transfer (kWh) – Monthly" (Kneifel, Sep. 2012) and the bottom graph displays results from the TRNSYS Baseline Full House model.

4.2.2.2.6 HVAC System

The monthly cooling and heating thermal loads for the EnergyPlus NZERTF model and the TRNSYS Baseline Full House model are shown in Figure 4-19 and Table 4-9. The top figure is "Figure 5.10 HVAC Energy Load by Coil (kWh) – Monthly" (Kneifel, Sep. 2012). The TRNSYS model had higher heating requirements during winter than the EnergyPlus model. It is interesting to note that the heat pump thermal output is almost identical while the electric resistance auxiliary heater contributes much more to the TRNSYS simulation total. The cooling requirements during summer months are almost identical between the models with the TRNSYS model being slightly higher during the spring and fall transition months.

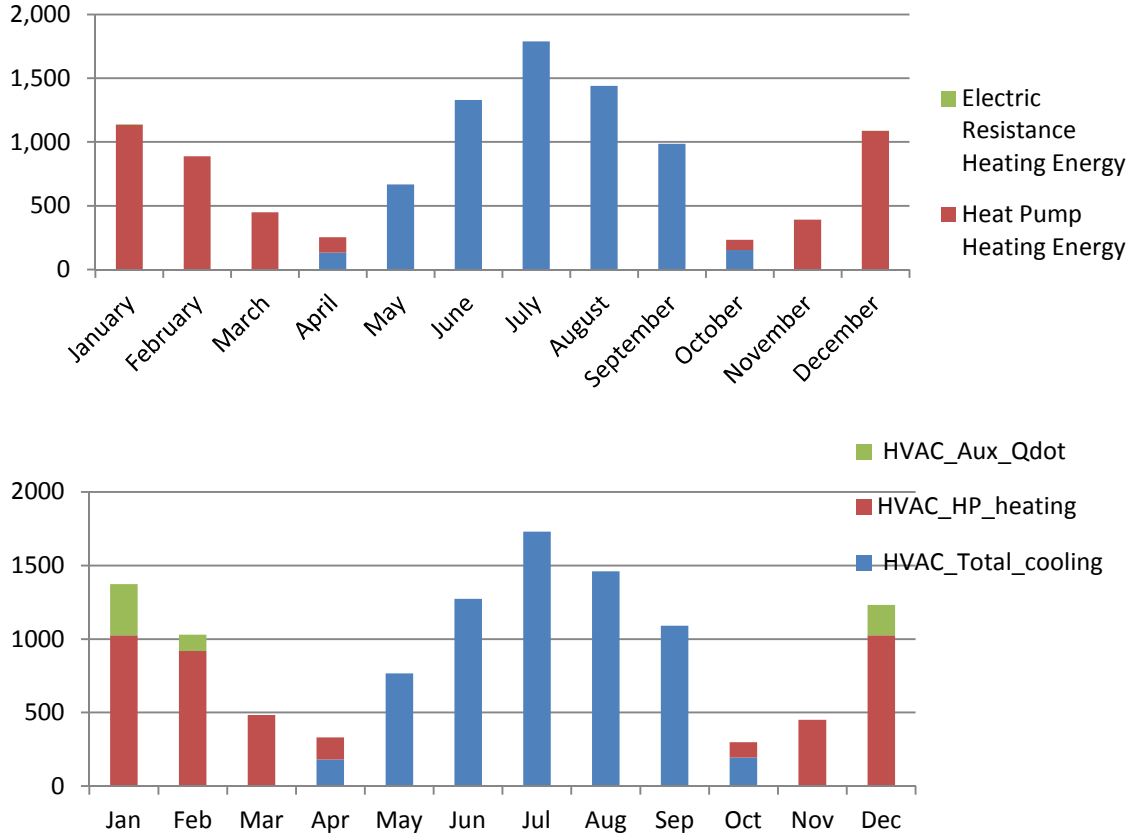

Figure 4-19: Comparison of Heating and Cooling Loads 1st Floor Thermal Energy [kWhr]
The top graph is "Figure 5.10 HVAC Energy Load by Coil (kWh) – Monthly" (Kneifel, Sep. 2012) and the bottom figure is from the results of the TRNSYS Baseline Full House model.

Table 4-9: Comparison of HVAC Heat Pump Thermal Output Heating and Cooling

	Eplus Model		Current TRNSYS Model	
Month	Heating [kWh]	Cooling [kWh]	Heating [kWh]	Cooling [kWh]
Jan	1134	0	1373	0
Feb	888	0	1028	0
Mar	449	0	483	0
Apr	121	133	148	182
May	0	667	0	765
Jun	0	1329	0	1273
Jul	0	1788	0	1729
Aug	0	1440	0	1459
Sep	0	985	0	1091
Oct	79	154	105	195
Nov	392	0	451	0
Dec	1086	0	1232	0
Annual	4148	6496	4819	6694

The monthly cooling and heating electrical energy use for the EnergyPlus NZERTF model and the TRNSYS Baseline Full House model are shown below in Figure 4-20. The top figure is “Figure 5-11 HVAC Electricity Use (kWh) – Monthly” (Kneifel, Sep. 2012) . As would be expected from the total thermal outputs and greater reliance on the electrical resistance heater, the heating electrical energy use during winter is much higher, almost 30%, in the TRNSYS simulation. The cooling electrical energy use during summer is slightly lower indicating that the heat pump in the TRNSYS simulation is operating a little more efficiently than the EnergyPlus simulation predicts.

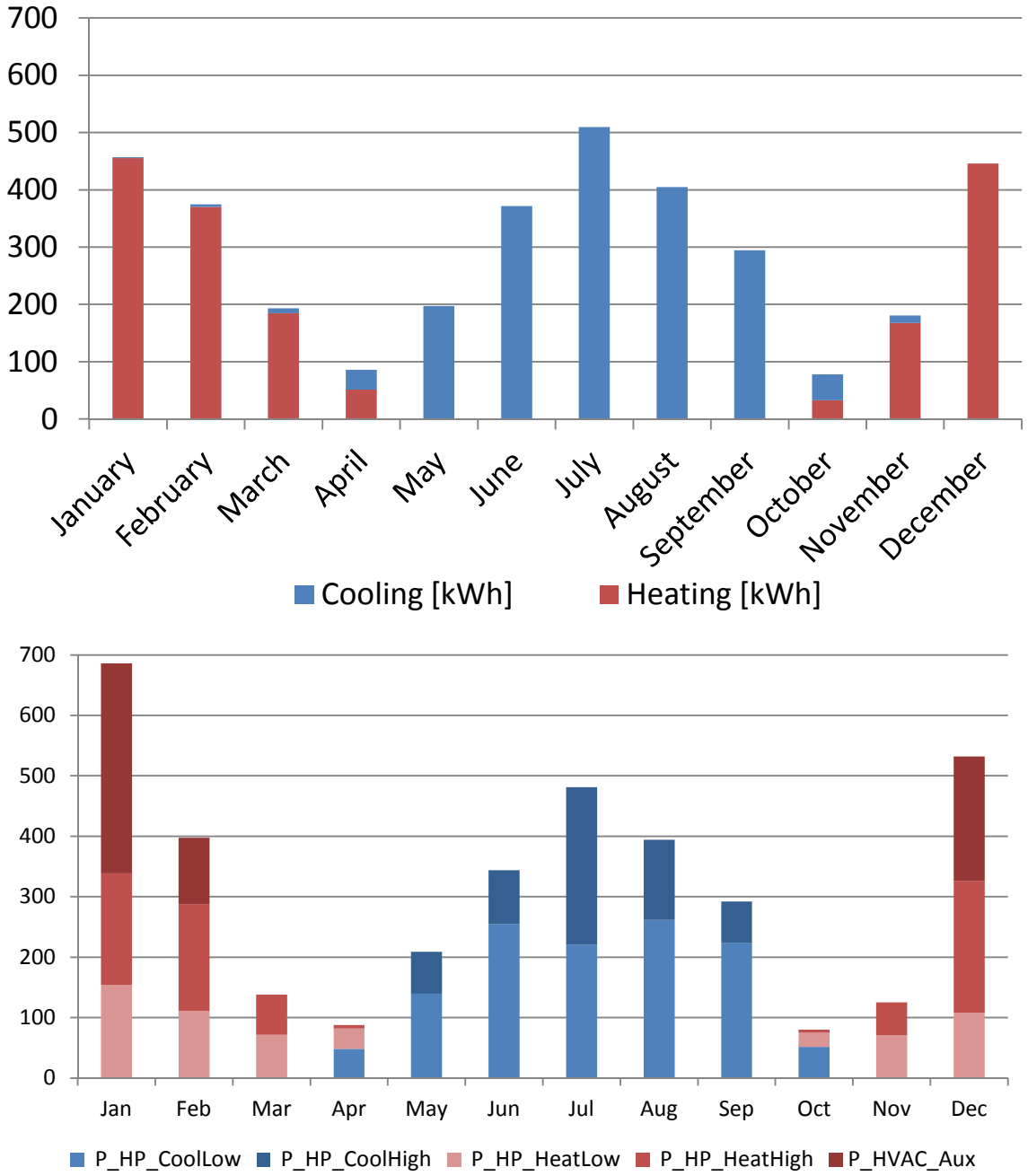

Figure 4-20: Comparison of HVAC Monthly Electricity Use [kWhr].
The top graph is "Figure 5-11 HVAC Electricity Use (kWh) – Monthly" (Kneifel, Sep. 2012) and the bottom graph displays results from the TRNSYS Baseline Full House model.

4.2.2.3 Conclusion

The TRNSYS simulation results are generally very close to the EnergyPlus simulation results leading to the conclusion that the TRNSYS model is performing well. The systems with the

greatest deviation in electrical use such as the pumps and HVAC systems result from differences in model parameters. In the case of the solar thermal collector system the pumps in the TRNSYS simulation were modeled after the manufacturer's specification while the EnergyPlus simulation uses an auto sizing function. Likewise the TRNSYS simulation's HVAC heat pump performance map uses manufacturers and recorded data. Whether the EnergyPlus model or the TRNSYS model is more accurate in matching the Test Facility results will likely depend on the degree of tuning carried out on either model. A comparison of the unturned TRNSYS Baseline Full House Model follows in section 4.3.

4.3 Comparison with Recorded Data

4.3.1 Setup of Baseline Model Comparison with Recorded Data

4.3.1.1 Simulation Setup

The comparison simulation used a 5 minute time step and one year duration. The weather file consists of hourly data from the Washington Dulles meteorological station provided by Matthew Boyd (Boyd, 2014). The weather data covers from January 2013 to the end of December 2013. The Washington Dulles recorded weather was used in the simulation because the weather data that was recorded on site is currently unavailable. All parameters and settings were as described in Chapter 4 for the Baseline Full House Model.

4.3.1.2 Considerations Concerning the Recorded Data

The experimental data recorded from the Test Facility covers a time period from July 2013 to April 2014. The data set is missing 17 days in April and 5 days in August. Because of the difference in covered time periods and the missing data in April and August the comparison

between the model and Test Facility was done for July, September, October, November, and December of 2013.

The weather file used in the simulation was recorded at Washington-Dulles Airport, which is about 20 miles away from the Test Facility. As can be seen in Figure 4-21 and Figure 4-23, some differences are evident in the temperature profiles at each site. While the daily average temperatures are fairly close, the minimum and maximum recorded temperatures, shown in Figure 4-22 and Figure 4-24, vary by up to 6 °C. This difference is particularly notable in the maximum temperatures recorded in July: the Test Facility recorded maximum temperature is typically about 5 C greater than the maximum temperature from the Washington-Dulles weather data. While this variation may be a result of recording and reporting differences and not actual variation in the temperatures, the simulation is dependent on the weather data files and will be affected.

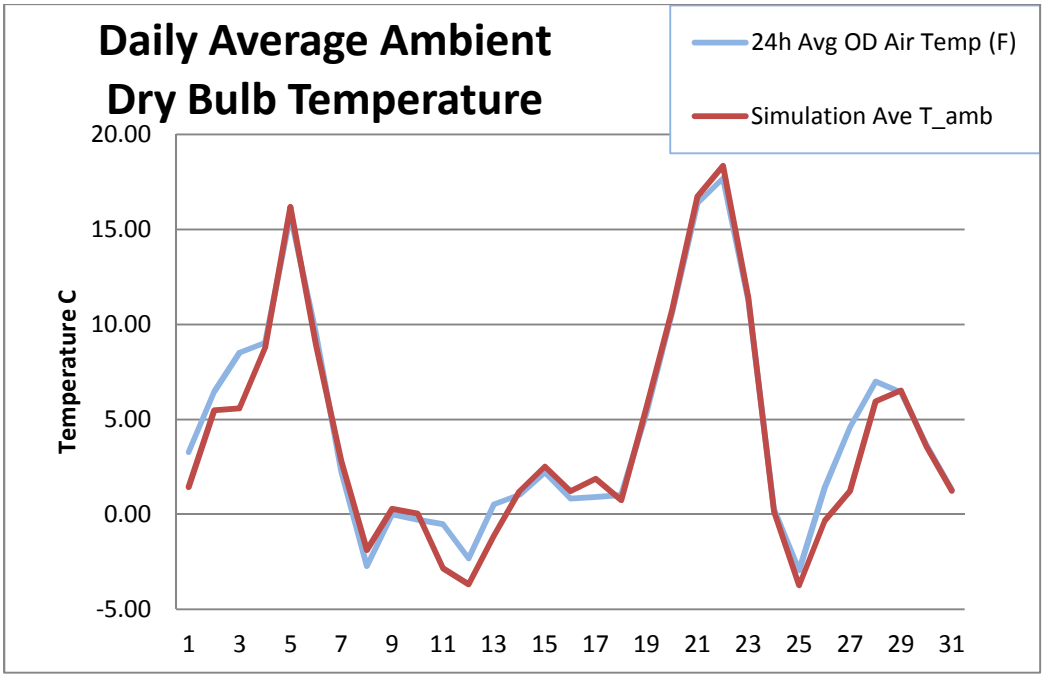

Figure 4-21: Daily Average Temperature Profiles for December 2013 at Washington-Dulles airport (Simulation) and the Test Facility (24H)

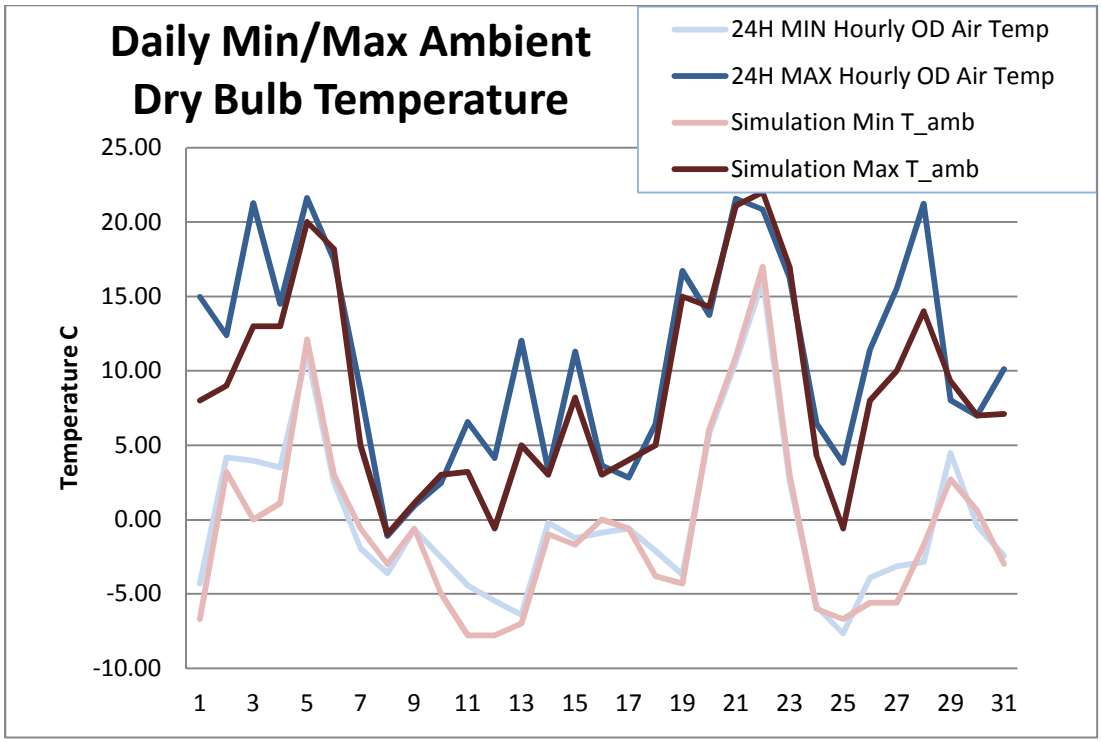

Figure 4-22: Daily Maximum and Minimum Temperature Profiles for December 2013 at Washington-Dulles airport (Simulation) and the Test Facility (24H)

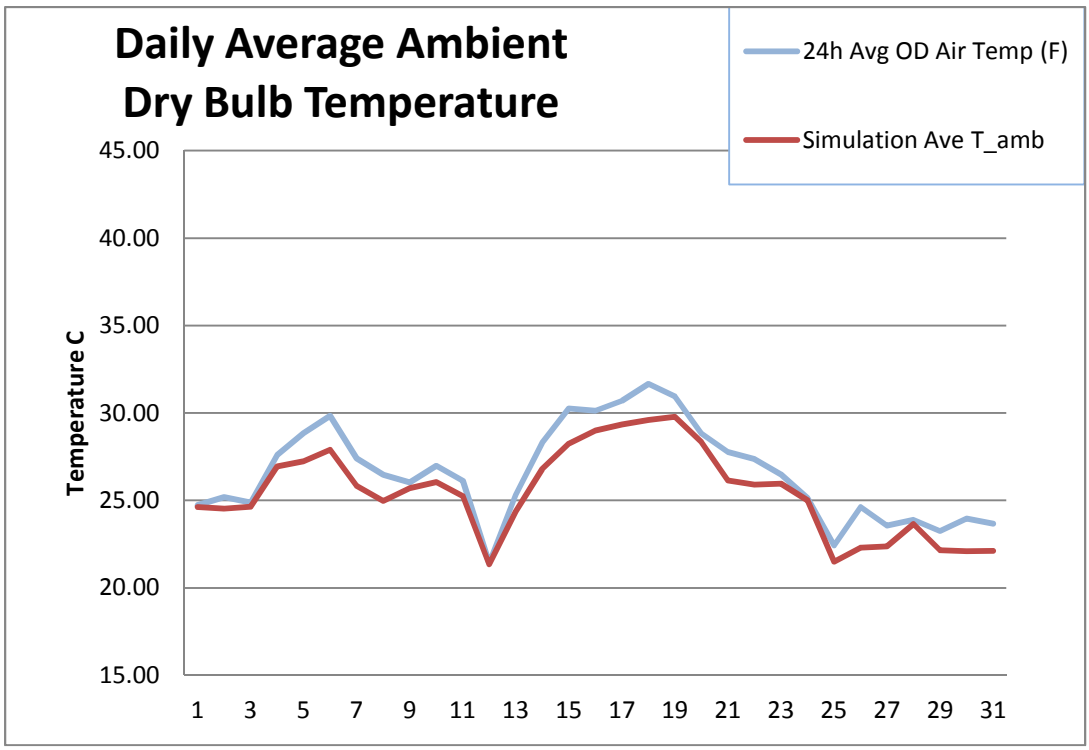

Figure 4-23: Daily Temperature Profiles for July 2013 at Washington-Dulles airport (Simulation) and the Test Facility (24H)

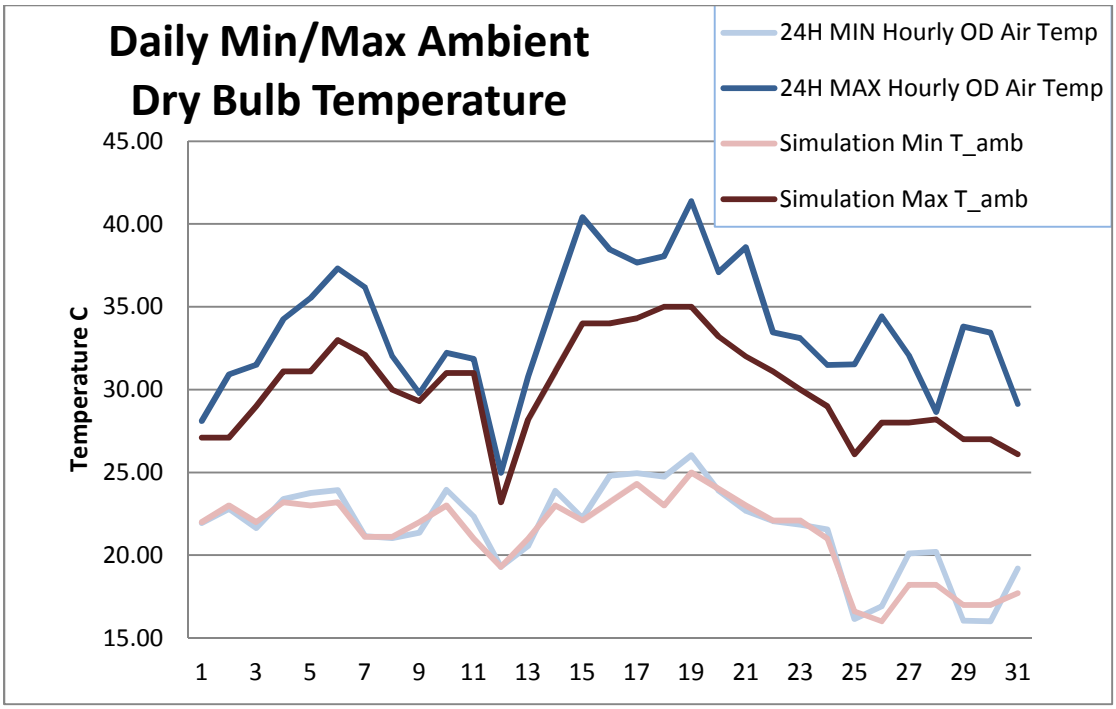

Figure 4-24: Daily Minimum and Maximum Temperature Profiles for July 2013 at Washington-Dulles airport (Simulation) and the Test Facility (24H)

The difference between the simulation and recorded weather files also results in a significant difference in the amount and timing of cloud coverage, fog, haze, rain, and snow. The impact of this difference is evident in Figure 4-25 and Figure 4-26, which show the solar PV output of the TRNSYS simulation, and the recorded data from the test facility. The graphs also show the recorded cloud cover at Washington Dulles airport and Reagan International Airport. The simulated PV outputs both correspond quite closely to the cloud and snow cover at Washington-Dulles, as would be expected. The experimental data corresponds to the data measured at Washington-Dulles but exhibits significant departures due to variations in cloud cover at the house location. The impact of snow fall and ground snow depth can be seen clearly in Figure 4-27. It is interesting to note that snow cover seems to persist longer (as indicated by near zero recorded PV production) on the test facility than at either airport location.

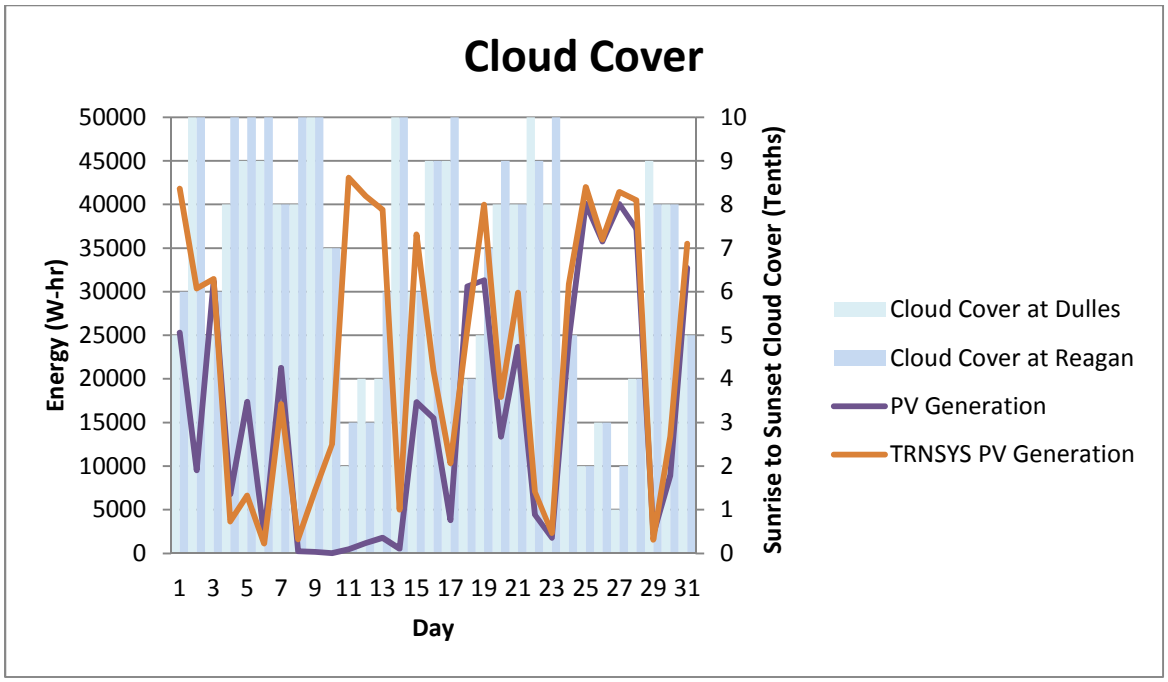

Figure 4-25: PV Generation and Cloud Cover December 2013

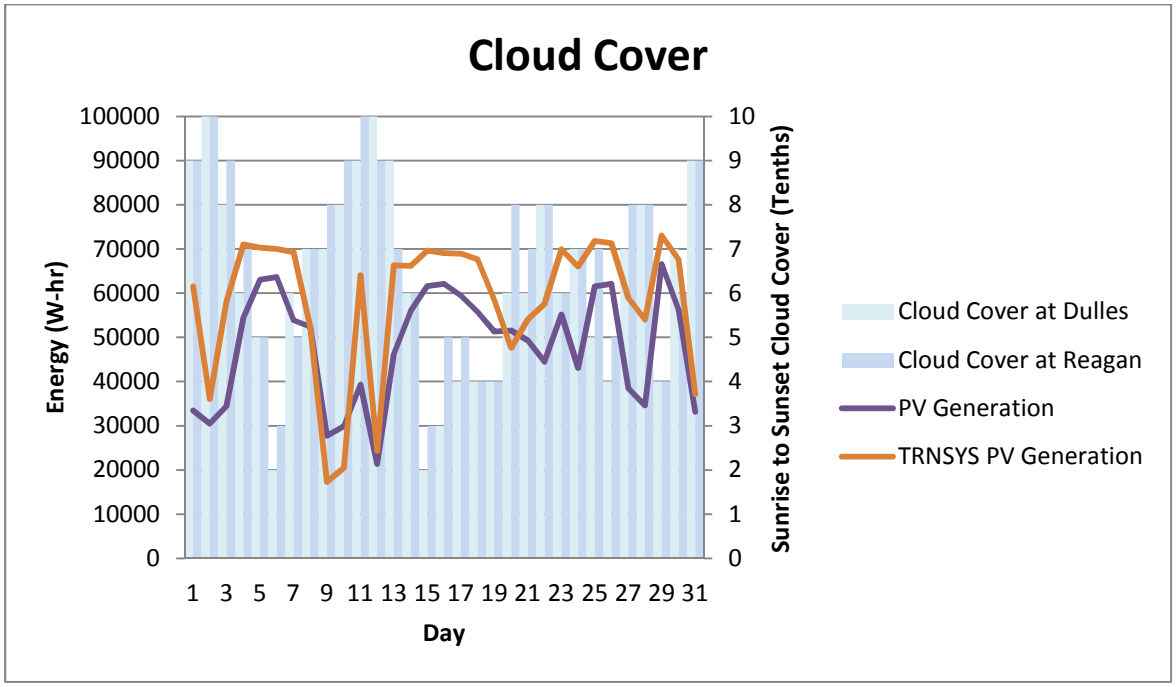

Figure 4-26: PV Generation and Cloud Cover July 2013

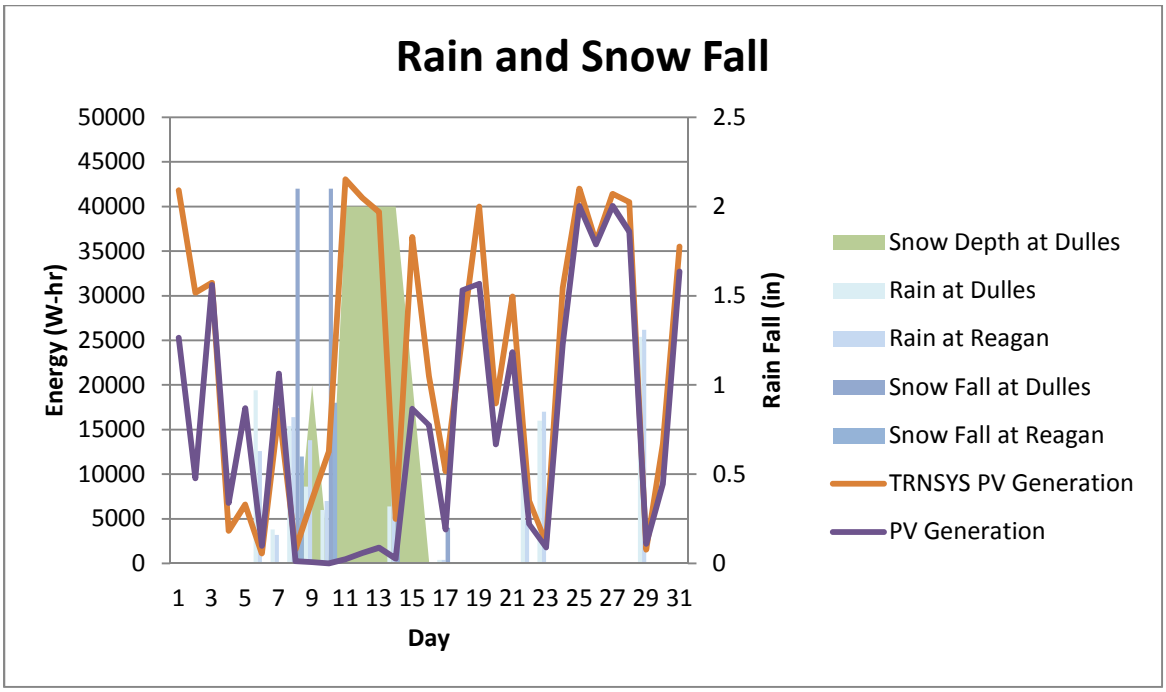

Figure 4-27: PV generation, Snow Fall, and Snow Depth December 2013

4.3.1.3 Set up of the Graphing and Recording Spread Sheets

The graphs presented in this report were generated using a series of three Excel workbooks. The graphs showing only the TRNSYS results were generated using the work book 'Ouputs4.xlsx'. The graphs showing monthly plots comparing the TRNSYS results with the test facility recorded data were generated using the work book 'Monthly Comparison Graphs.xlsx'. The results showing daily values over the course of a month were generated using the 'Daily Comparison Graphs.xlsx'. To generate new plots, the TRNSYS simulation output files are copied into the indicated cells in each spread sheet. Some basic calculations such as unit conversions and heat pump COP determination are then performed within the spread sheets. All of the recording and graphing spread sheets may be found in the electronic supplement.

4.3.2 Results of Baseline Model Comparison with Recorded Data

4.3.2.1 Overview

Table 4-10 shows the results from the TRNSYS Simulation and the Test Facility for July, September, October, November, and December of 2013. Over the comparison period, the simulation predicted that the total energy consumed would be 3.42% less than the amount recorded for the Test Facility. The simulation predicted that the total energy generated by the solar PV system would be 19.91% greater than the amount recorded. The contrary differences in these two predictions results in the TRNSYS simulation over predicting the margin by which the Test Facility achieves net zero status by a factor of 8. The simulation predicted a net generation of 1209 kWhr or 24% of the recorded energy consumption over the comparison period while the recorded net generation over the same period was 165 kWhr or 3.3% of the recorded energy consumption.

The largest contributors to the absolute difference in the demand were the HVAC system and the domestic hot water system, as seen in Table 2. The interior equipment demands were overestimated by 8.56 % and this decreased the difference between the predicted and recorded demand. The largest percentage errors were seen in the domestic hot water system and the solar PV.

Table 4-10: Electrical Energy Consumption and Generation over the Comparison Period

	TRNSYS Simulation	NIST Recorded Data	Error	Percent Error	Error Percent of Total Consumed
	kWhr	kWhr	dkWhr		
HVAC	1992	2209	-217	-9.81%	-4.30%
Heat Recovery	195	217	-22	-10.34%	-0.45%
Interior Lighting	202	184	18	9.86%	0.36%
Interior Equipment	1980	1824	156	8.56%	3.10%
Water Systems	384	475	-91	-19.10%	-1.80%
Pumps	114	132	-17	-13.23%	-0.34%
Consumed	4870	5042	-172	-3.42%	-3.42%
Generated	6244	5207	1037	19.91%	20.56%
Net Generation	1374	165	1209	731.12%	23.98%

4.3.2.2 Monthly Overview

The monthly power consumption is broken down in Figure 4-28. During warmer months (e.g., July), the predicted power consumption is very close to the recorded power consumption. During November and December there is a significantly larger difference between the predicted and recorded power consumptions. This difference is largely due to the lack of a HVAC heat pump defrost cycle in the TRNSYS simulation which accounts for 56% of the HVAC error over the comparison period.

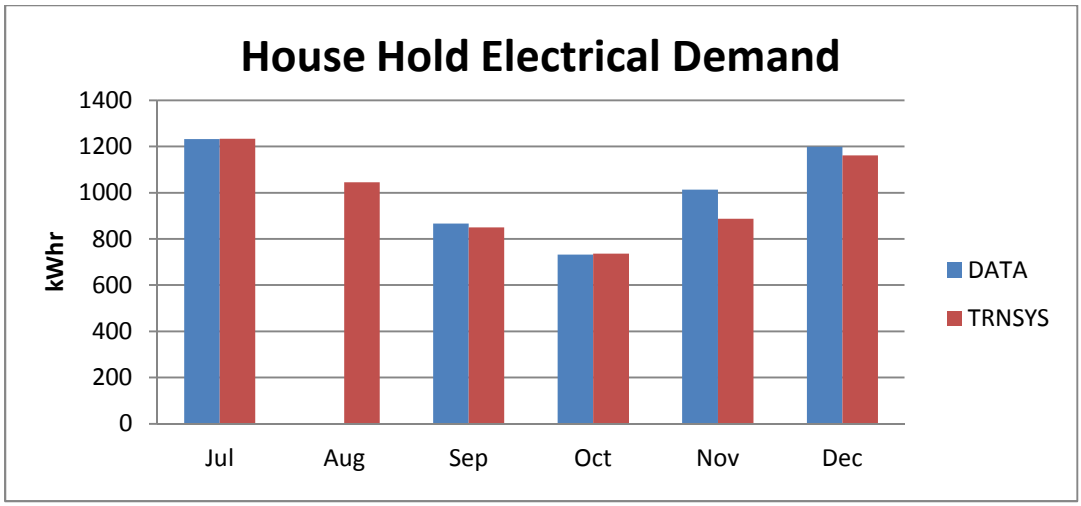

Figure 4-28: Monthly Total Electrical Demand

4.3.2.2.1 Scheduled Loads

The Scheduled Loads are shown in Figure 4-29 and the differences between the Test Facility and the TRNSYS Simulation are shown in Figure 4-31. The monthly values for the TRNSYS simulation are on average 8.56 % greater than the values recorded at the Test Facility and the differences also are fairly consistent month to month. The scheduled loads are being set as a forcing function in the simulation so a tuned model could use a scheduled load that more closely corresponds to the recorded data.

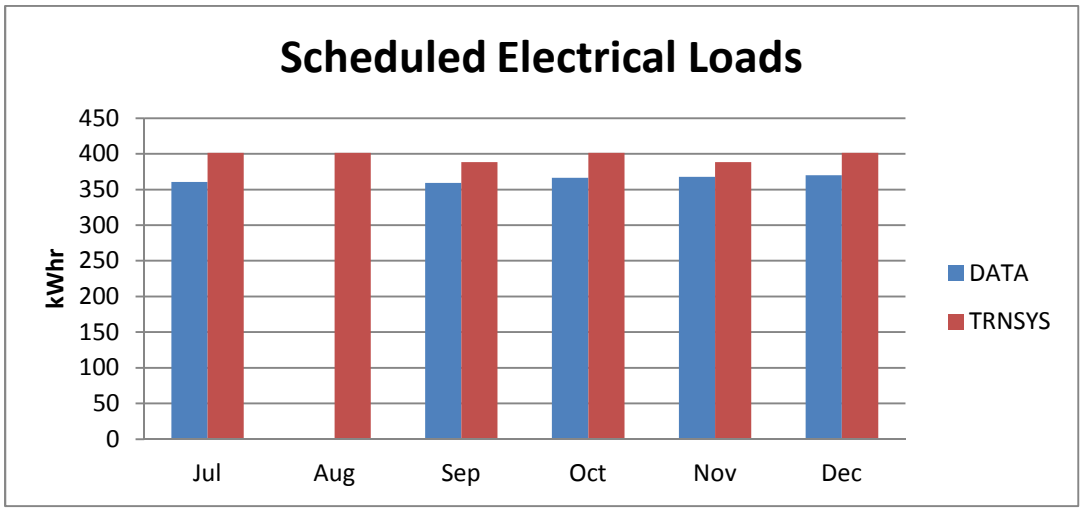

Figure 4-29: Comparison of monthly scheduled electrical appliance and plug loads 2013

The lighting demand is shown in Figure 4-30 and the differences between the Test Facility and the TRNSYS Simulation are shown in Figure 4-31. The monthly values for the TRNSYS simulation are on average 9.86 % greater than the values recorded at the Test Facility. As with the scheduled loads, the lighting power demand is a set function and could be altered in a tuned model to more closely match the recorded data.

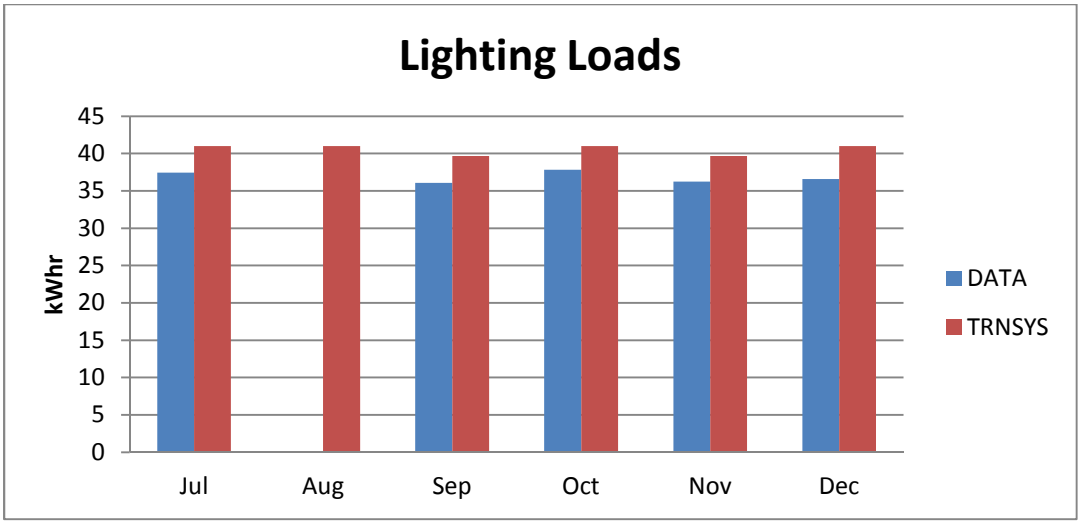

Figure 4-30: Comparison of monthly lighting loads 2013

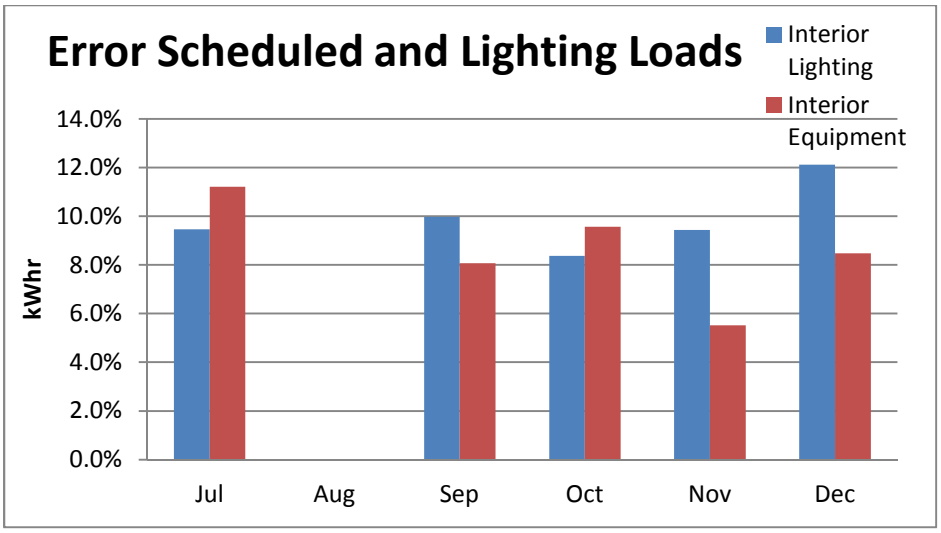

Figure 4-31: Percent error of the scheduled electrical and lighting loads, recorded data as baseline.

4.3.2.2.2 HVAC Hp

About half of the difference between the HVAC heat pump performance during winter can be attributed to the lack of a defrost cycle in the TRNSYS simulation. During October, November and December of 2013 this accounted for 121 kWhr of energy use in the Test Facility and about 56% of the difference between the recorded HVAC demand data and TRNSYS simulation results. A comparison of the monthly heating power and load is shown in Figure 4-32. Figure 4-33 shows the HVAC power requirements without the HVAC heat pump defrost energy usage. When the defrost energy is subtracted, the TRNSYS simulation HVAC power requirements are within 5% of the Test Facility's requirements.

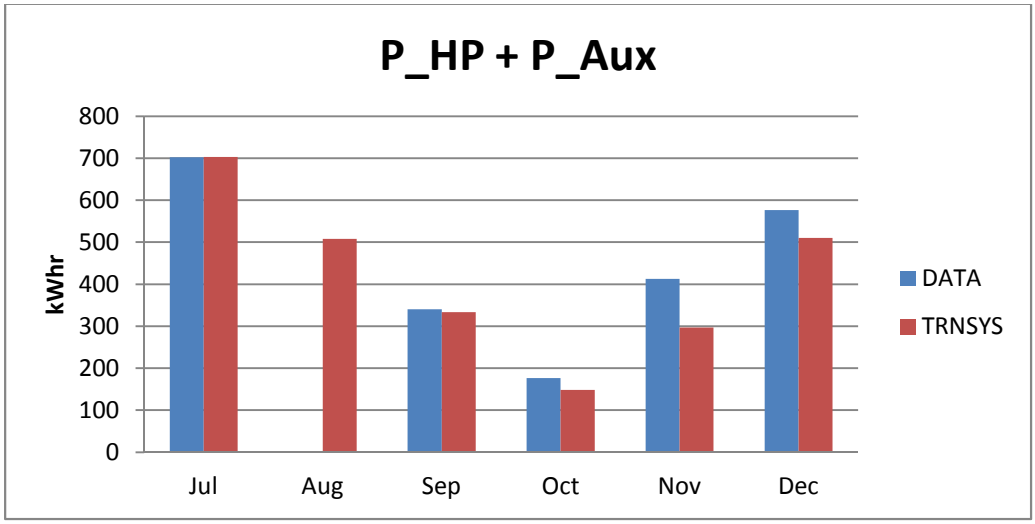

Figure 4-32: Comparison of the monthly HVAC power usage, 2013

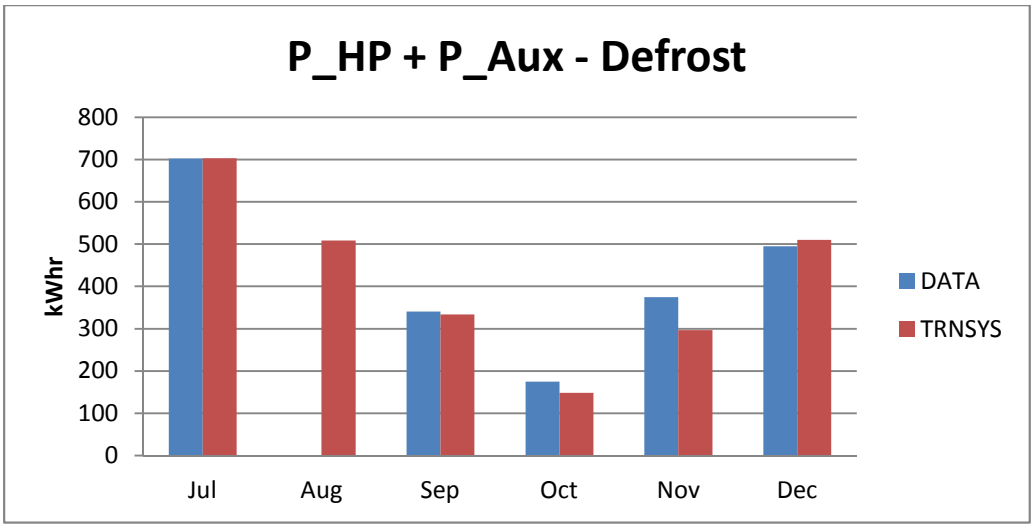

Figure 4-33: Comparison of the monthly HVAC power usage excluding the main HVAC Heat Pump defrost energy, 2013

Figure 4-34 shows the monthly average HVAC heat-pump COPs for heating and cooling. The TRNSYS values come much closer to the rated cooling and heating efficiency of the heat pump which suggests that there may be potential for significant gains in heat pump efficiency. The Heat-pump was also significantly worse at both heating and cooling during the fall when the lower temperature difference between indoors and outdoors should make both operations more efficient. This decrease in performance may be the result of partial loading, short run times, or potentially lower efficiency in low speed operation.

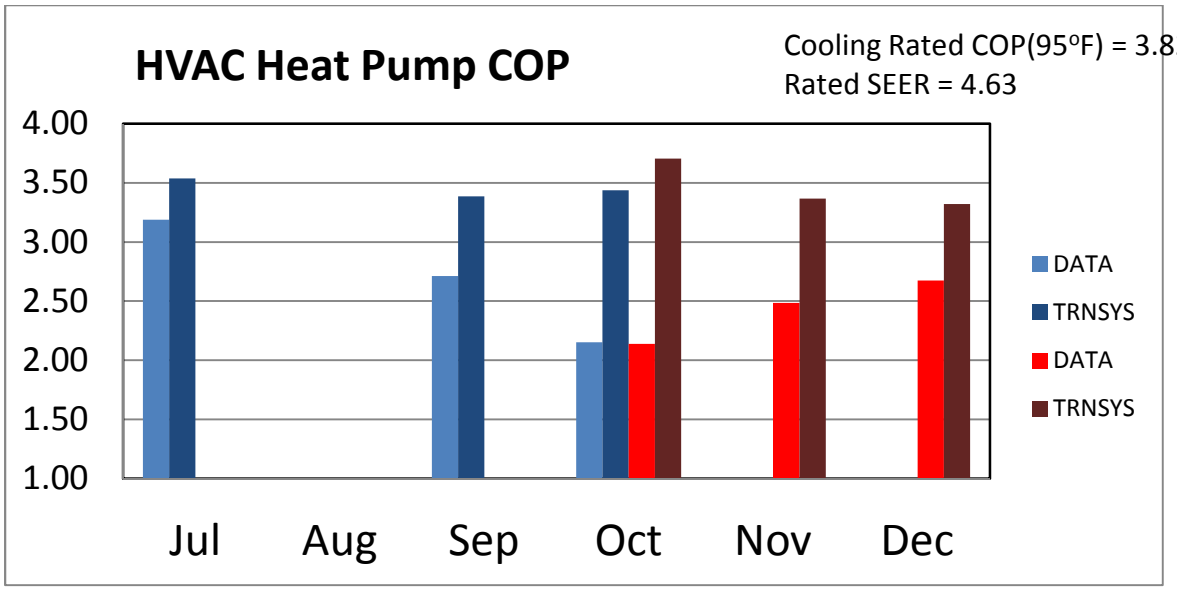

Figure 4-34: Comparison of the HVAC heat pump COP without the Electrical Resistance heater. Cooling is in blue, heating is in red.

Figure 4-35 shows the monthly average HVAC heat-pump COPs for heating and cooling with and without the addition of the auxiliary resistance heating energy. The relative change in the values indicates that the TRNSYS simulation is using the auxiliary heater more frequently than the Test Facility with the exception of October.

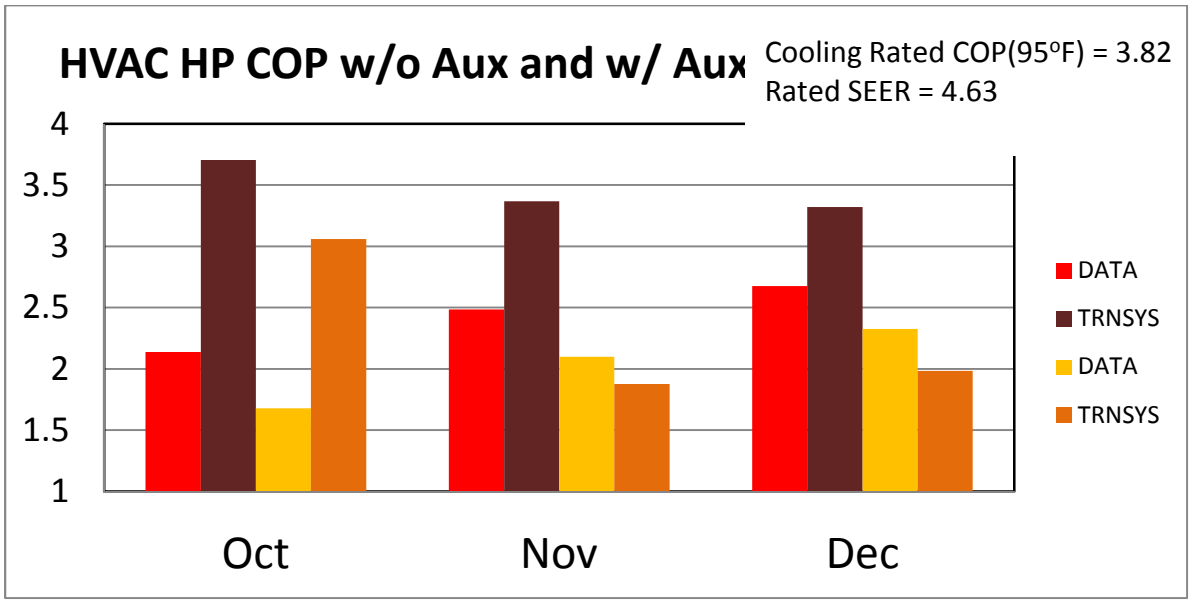

Figure 4-35: Comparison of the HVAC heat pump heating COP including Auxiliary resistance heat (red) and without auxiliary resistance heat (orange)

4.3.2.2.3 House Envelope loads

Figure 4-36 and Figure 4-37 show the daily HVAC Heat-pump and Resistance heater load (thermal output) and power consumption for the December 2013. The simulation loads and power consumption are usually slightly lower than those recorded at the Test Facility. There are also significant deviations that are likely the result of differences in the triggering of the resistance heater. As the resistance heater has higher capacity but lower efficiency than the heat-pump, small changes in its controlled operation can result in significant deviation in energy consumption and thermal output.

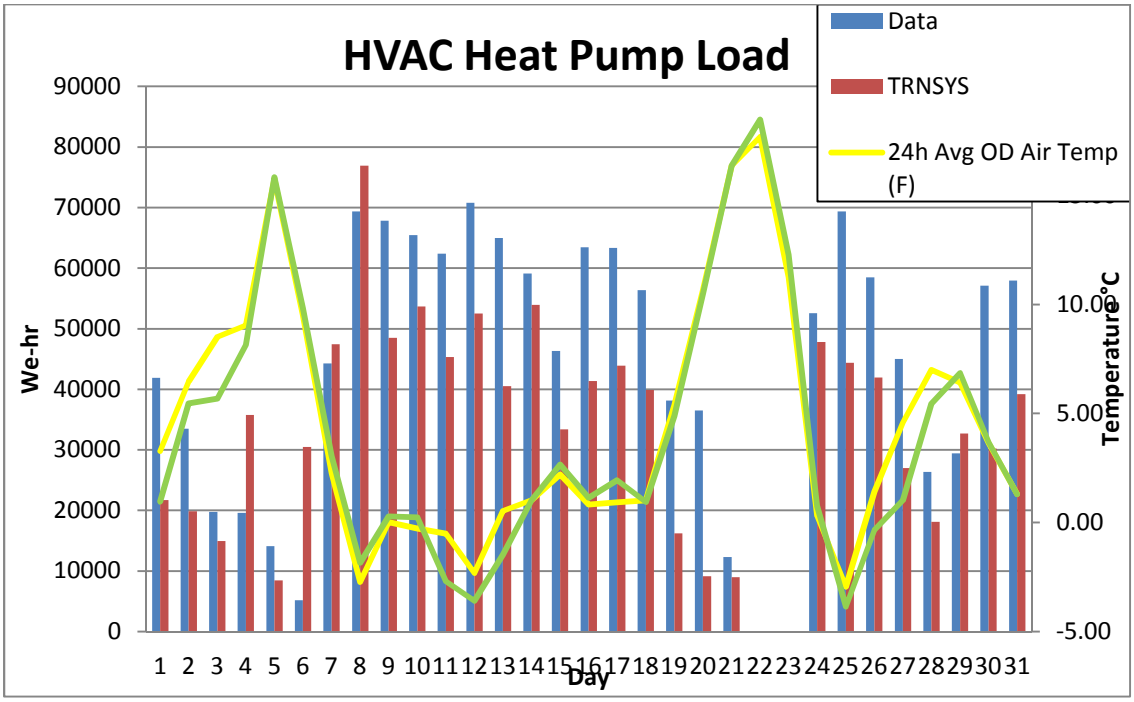

Figure 4-36: Comparison of daily HVAC system thermal energy output (bars) and daily average temperature (lines) for December 2013

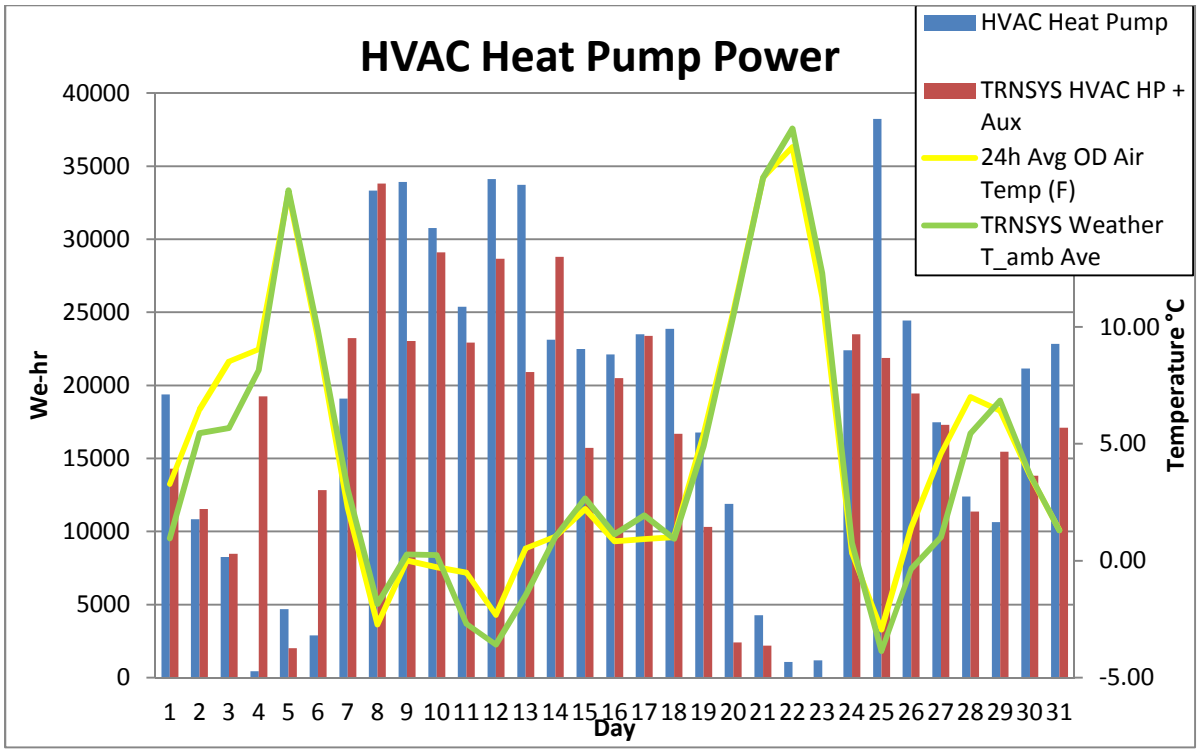

Figure 4-37: Comparison of daily HVAC electrical power demand (bars) and daily average temperature (lines) for December 2013

Figure 4-38 shows the recorded daily run times for the indoor fan, which is taken to be equivalent to the total air handling unit (AHU) run time, and the simulation AHU run time during December. The TRNSYS simulation predicts about half of the total run time recorded at the test facility. It also shows a significantly greater run time for the auxiliary heater which is further evidence of a difference in the control of the resistance heater. The heat pump has two speed settings that are not currently differentiated in the recorded data. Figure 4-39 shows the daily run times for the auxiliary electric resistance heater. The simulation is overestimating the amount of resistance heat use, countering the lower estimate for heat pump use.

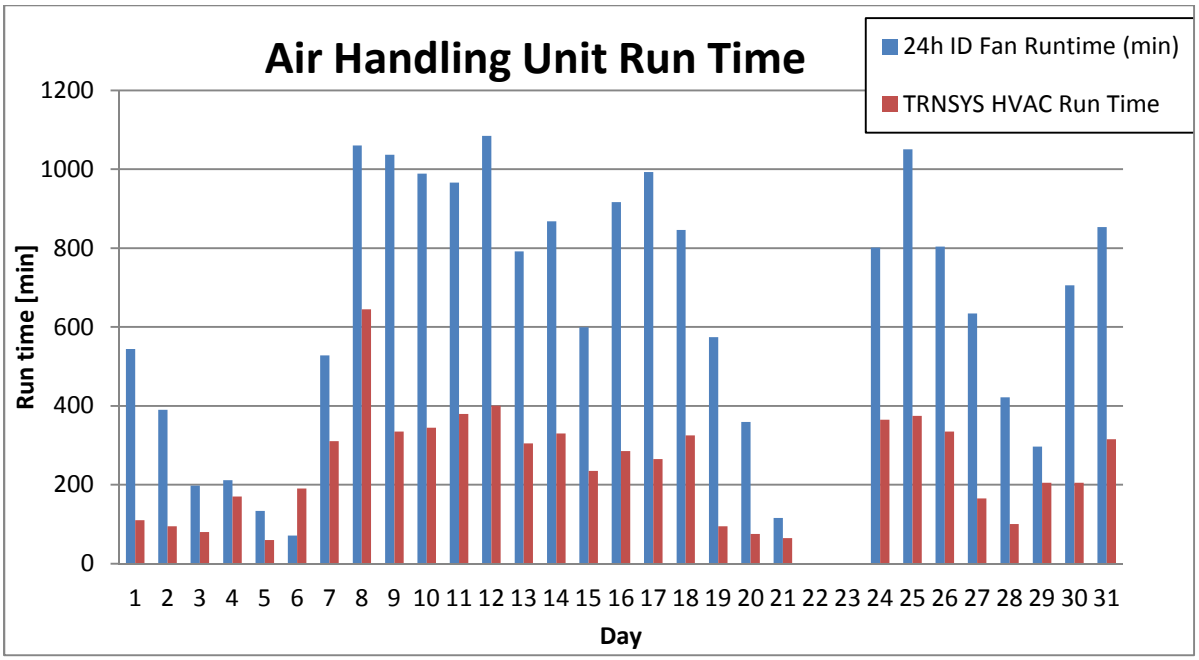

Figure 4-38: Comparison of daily HVAC air handling unit run times for December 2013

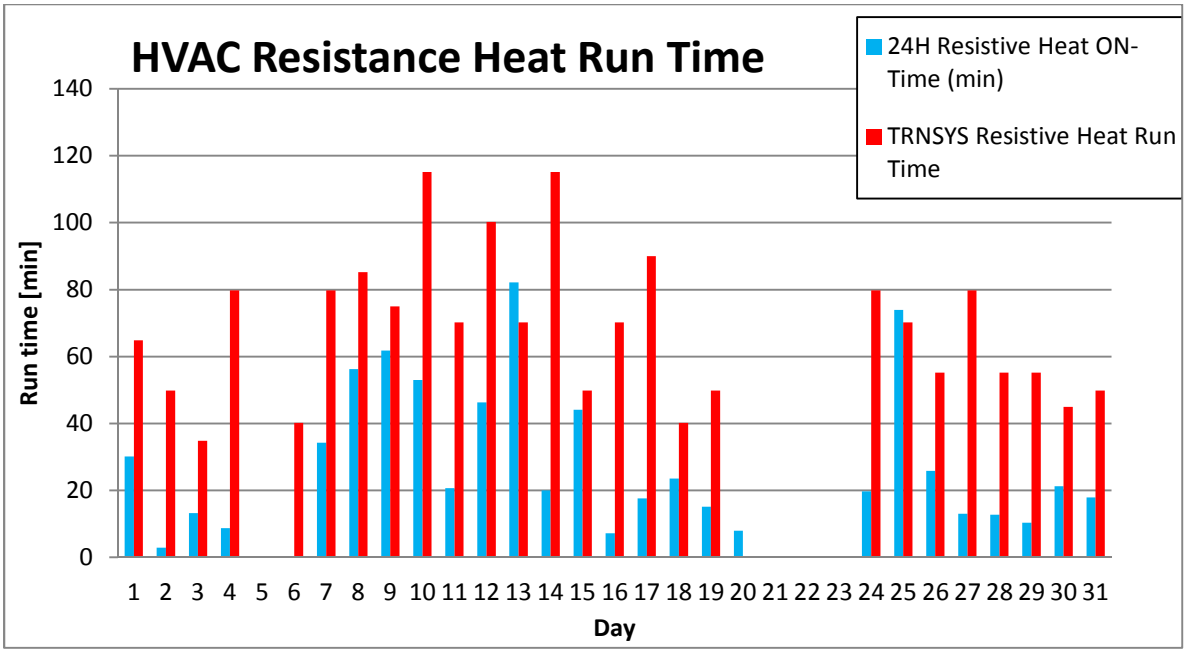

Figure 4-39: Comparison of daily HVAC auxiliary heater run times for December 2013

Figure 4-40 and Figure 4-41 show the daily HVAC Heat-pump and Resistance heater load (thermal output) and power consumption for the July 2013. The simulation loads are quite close to the recorded data and calculated power consumption is usually slightly lower than the recorded data.

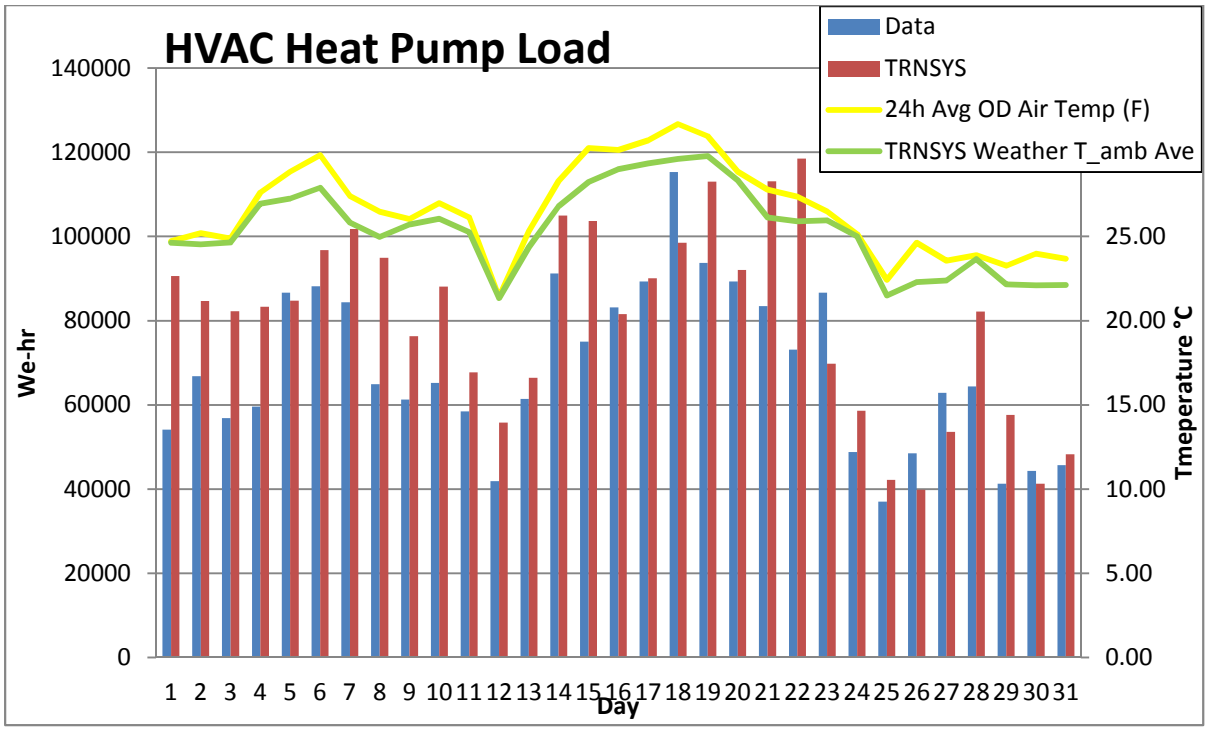

Figure 4-40: Comparison of daily HVAC system thermal energy output (bars) and daily average temperature (lines) for July 2013

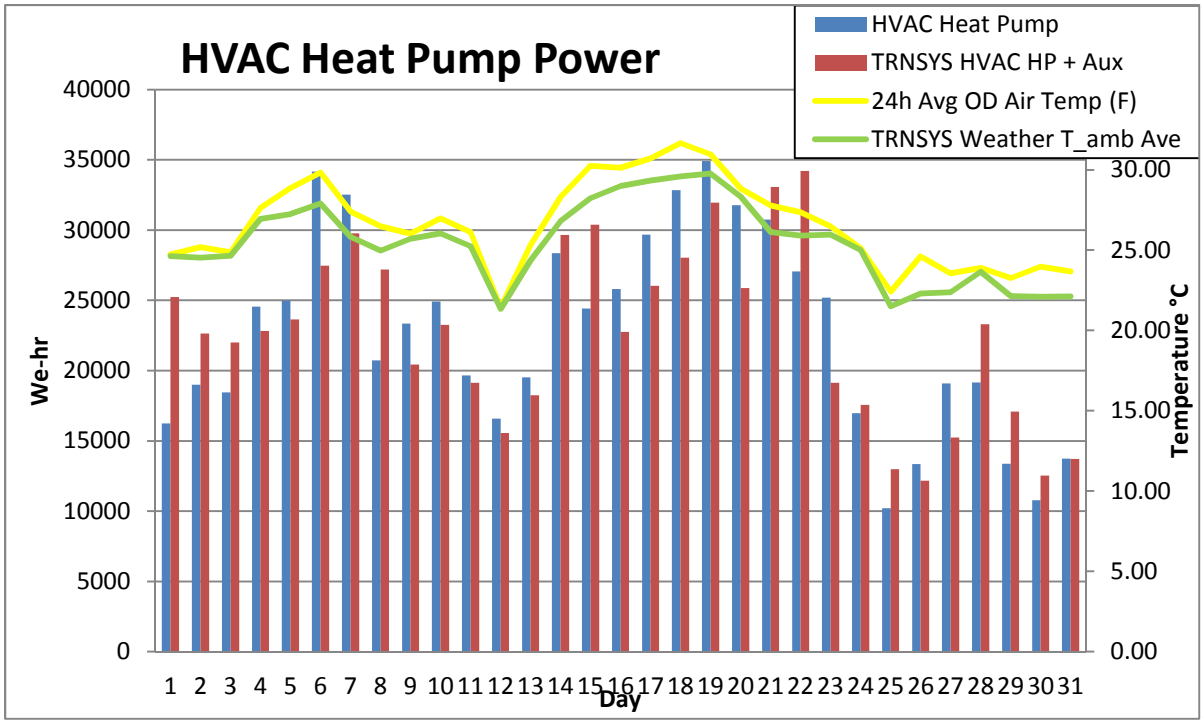

Figure 4-41: Comparison of daily HVAC electrical power demand (bars) and daily average temperature (lines) for July 2013

Figure 4-42 shows the daily run times for the HVAC heat-pump and dehumidification system during July. The TRNSYS simulation predicts about 80% of the total run time that is recorded at the test facility. The dehumidification system run time is also lower than the recorded data. Combined with the loading and the power consumption, this result indicates that the HVAC simulation heat-pump cooling modes are more efficient than indicated in the data. This higher predicted efficiency is also shown by the cooling COP in Figure 4-34.

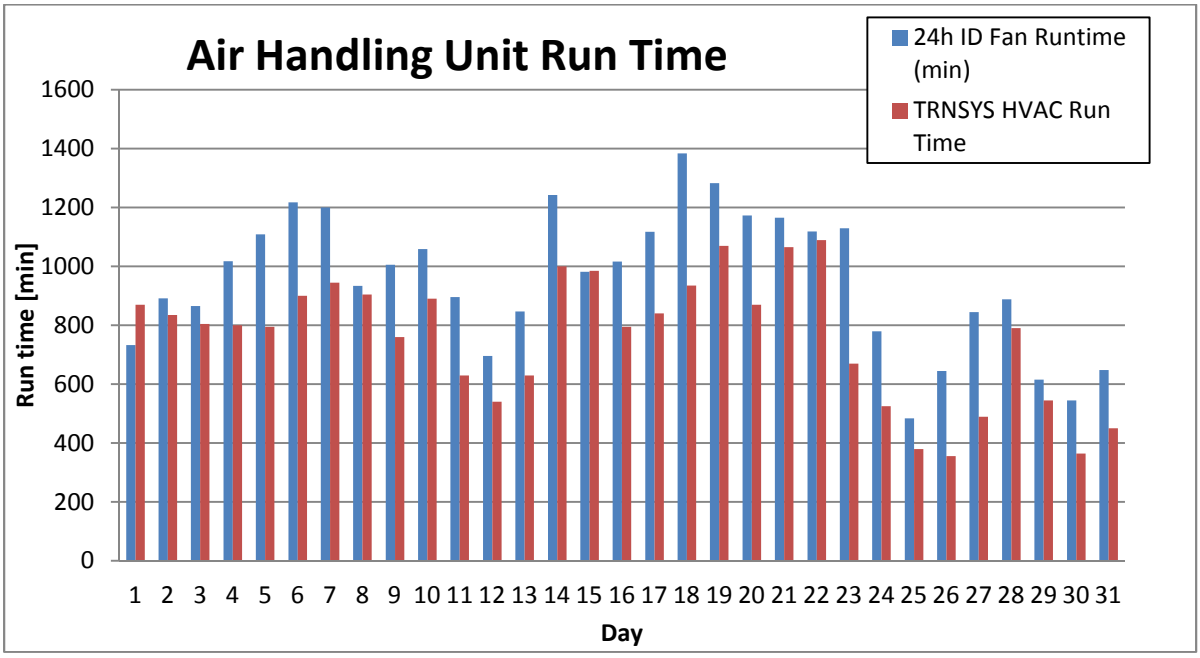

Figure 4-42: Comparison of daily HVAC stage run times for December 2013

4.3.2.3 HVAC Heat Recovery Ventilator

As shown in Figure 4-43 the simulation HRV system uses less power than the experimental data records. The difference over the entire comparison time period is 22 kWhr which is 10.3% of the recorded HRV demand and 0.45 % of the total recorded household demand. Potential reasons for this difference include changes in ventilation settings between the EnergyPlus model documentation and the Test Facility and differences in the performance of the HRV unit from the manufacturer's specifications. The lack of a defrost setting in the

HRV simulation may also play a part in the lower energy consumption as the difference between the simulation and recorded data is slightly higher during winter months.

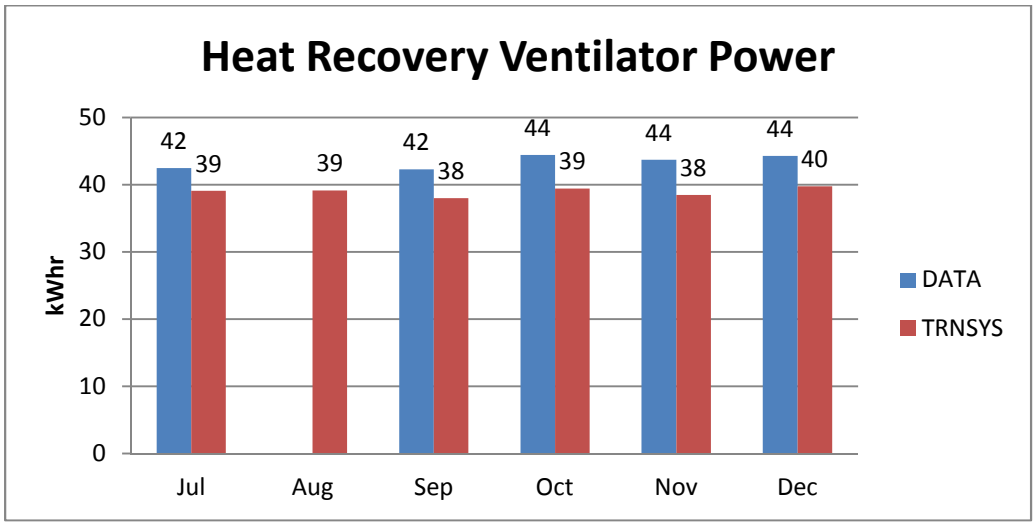

Figure 4-43: Comparison of the monthly total heat recovery ventilartor power demand. 2013

4.3.2.4 DHW solar

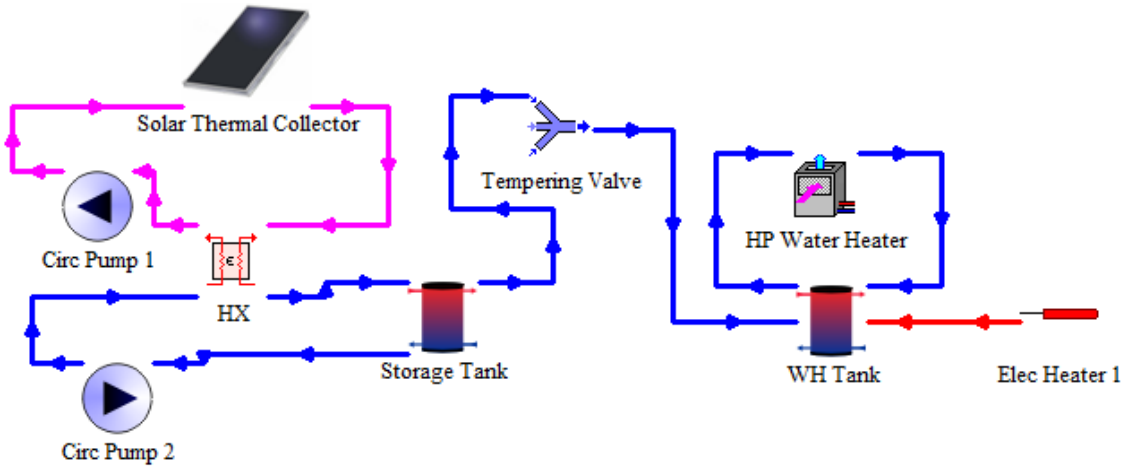

Figure 4-44: Diagram of the Domestic Hot Water System

The solar thermal collection system pumping power consumption is shown in Figure 4-45 and the error is shown in Figure 4-46. The Test Facility uses more power than the TRNSYS model predicts. The difference over the entire comparison time period is 17 kWhr which is

13.2% of the recorded solar collector pump power demand and 0.34% of the total recorded household demand. This difference is likely due to variations in the pump performance resulting from either different pumping efficiency or flow resistances. The deviation might also be due to differences in the solar collector control scheme resulting in lower pump run times in the simulation.

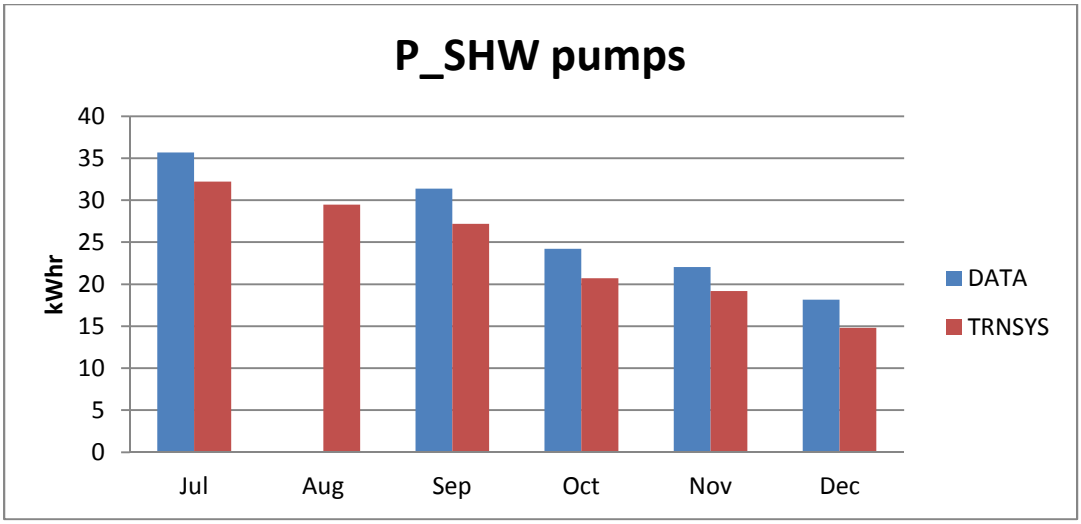

Figure 4-45: Comparison of the electrical demand of the solar thermal water heater pumps. 2013

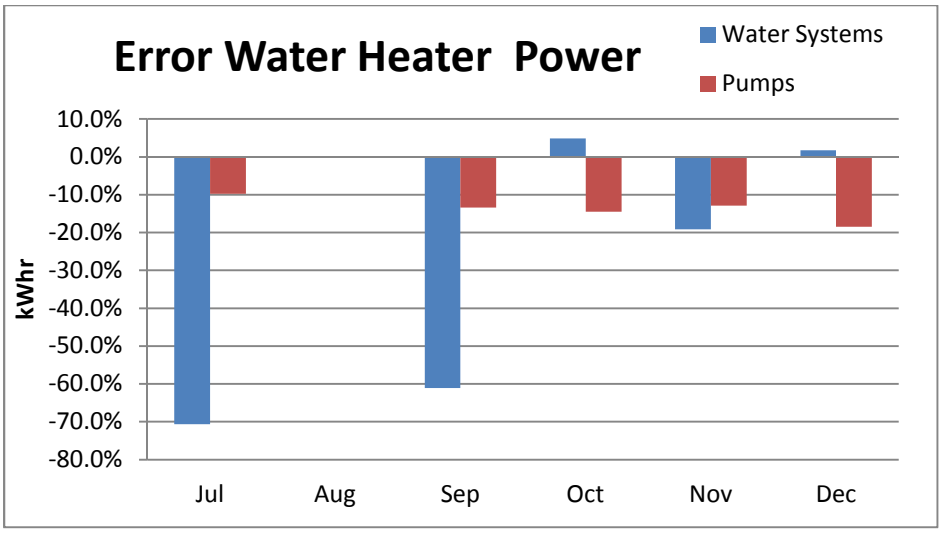

Figure 4-46: Percent error of the electrical demand of the solar thermal pumping system and the hot water heat-pump, Recorded data used as the baseline. 2013

4.3.2.5 DHW HP

As shown in Figure 4-47 the simulated domestic hot-water heater uses about 80% of the power that the actual hot water heater uses. The error over the entire comparison time period is 91 kWhr which is 19.1% of the recorded water heater demand and 1.8% of the total recorded household demand. Potential reasons for this difference include deviation of the simulated water heater efficiency from the actual water heater, differences in temperature set-points and tempering, and differences in the triggering of the electrical resistance strip heaters. It is also possible that the solar thermal hot water system is not as efficient as the simulation predicts and is thus feeding the hot water heater with colder water. Lower solar thermal performance could be a result of dirt on solar thermal collectors or the heat exchanger underperforming. It is also likely that the snow coverage seen during the analysis of the solar PV system also affects the solar thermal collectors. Snow would last longer on the solar thermal collectors as they are specifically insulated and designed to remove heat.

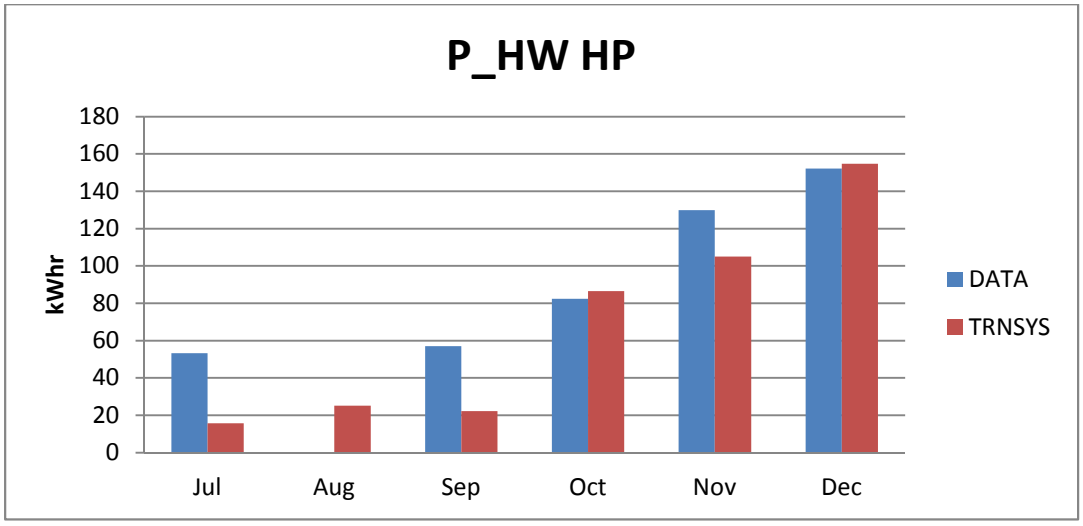

Figure 4-47: Comparison of the monthly total domestic hot water heat-pump water heater power demands. 2013

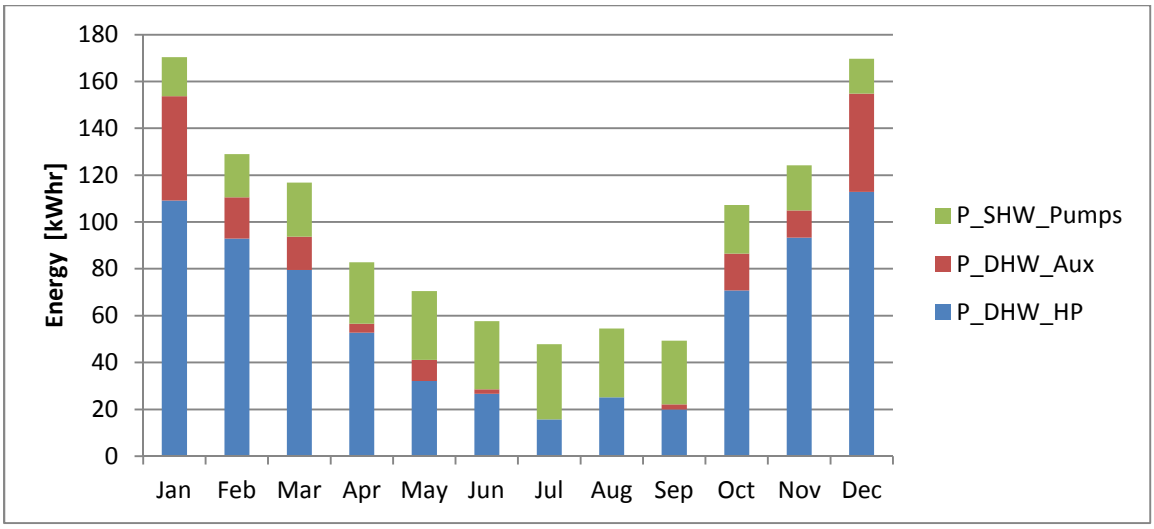

Figure 4-48: TRNSYS simulation monthly electrical power demand of the domestic hot water system. 2013

4.3.2.6 Solar PV

The monthly solar PV generation is shown in Figure 4-49. The TRNSYS model predicts more power generation than was recorded at the test facility. The difference over the entire comparison time period is 1037 kWhr, which is 19.9% of the recorded PV generation and 20.6% of the recorded household demand. Some of the difference in PV generation is likely attributable to the difference between the weather at the Test facility and the weather record used in the simulations. The effect of the weather difference is demonstrated clearly in Figure 4-51 and Figure 4-52

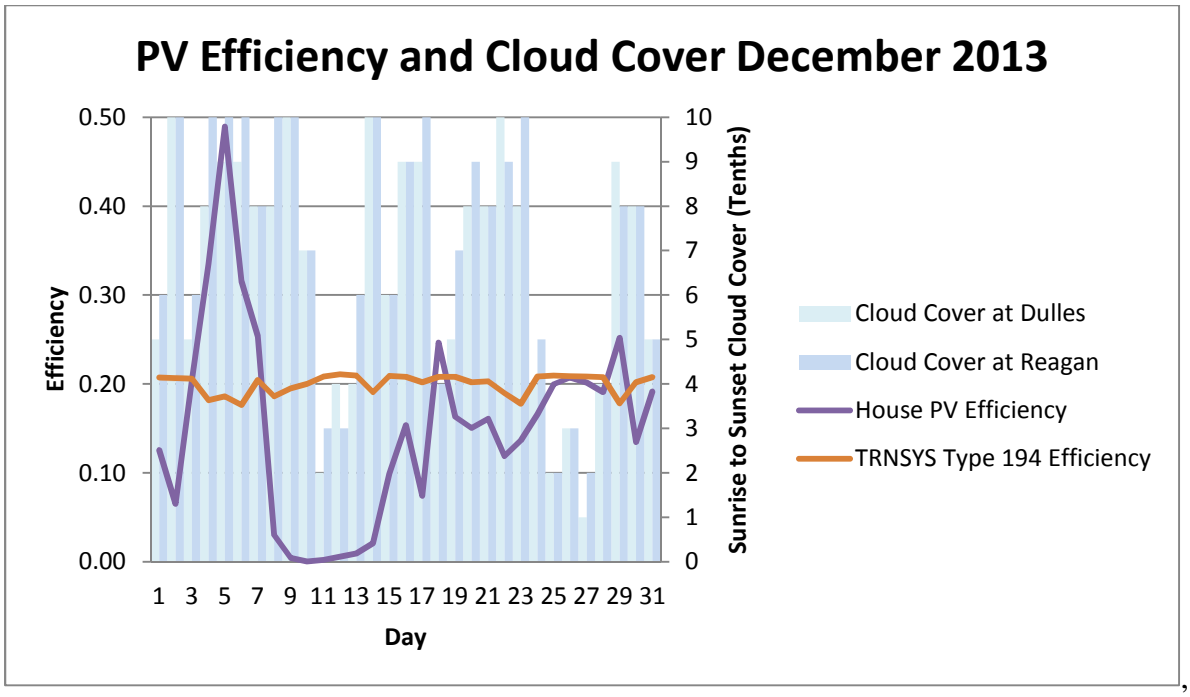

,

which show the simulated and recorded solar PV generation and efficiency for December of 2013. In December, the TRNSYS simulation shows almost zero production corresponding with snow falls and snow cover at Washington-Dulles airport. The PV production recorded at the Test Facility shows some relation to the snow fall in the weather file but also indicates that there was additional snow fall at the Test Facility and that snow lasted longer on the Test Facility panels before melting. Figure 4-54 and Figure 4-55 show the solar PV generation and efficiency for July as well as the sky cloud cover fraction. The data corresponds fairly well, though there are still a few days where the PV efficiency relative to the available sunlight in the Weather file exceeds realistic values (29%) indicating that the Test Facility is receiving more sunlight than the Washington-Dulles weather file records. Over the comparison period, the recorded PV generation is lower than the amount predicted by the simulation and this discrepancy holds even on relatively clear days when the two results should be close. This observation indicates that the actual PV array is operating at a lower efficiency than the predicted. Potential reasons for this include higher operating cell

temperatures due to differences in ventilation setup, unanticipated shading, dust on the panels, and other issues with the PV equipment performance.

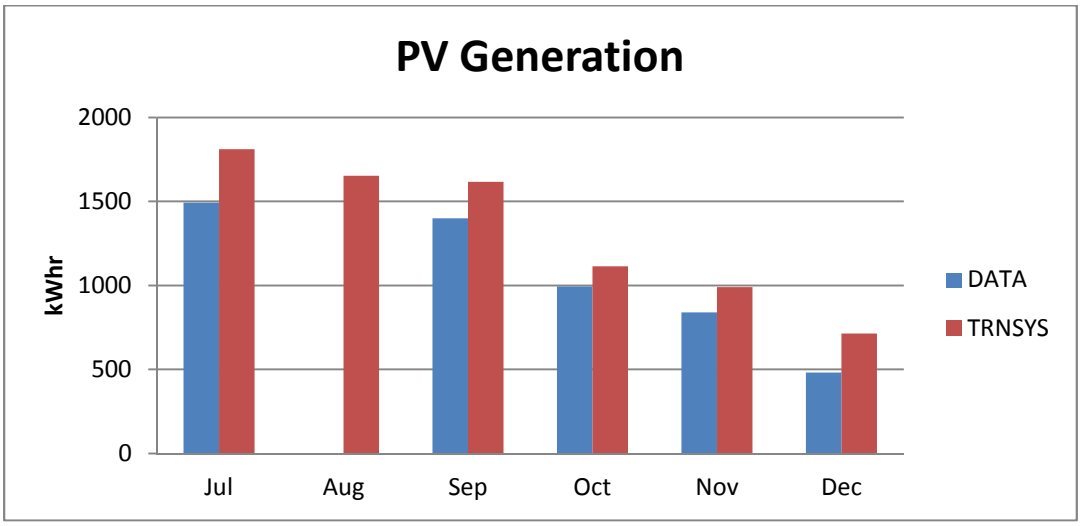

Figure 4-49: Comparison of the monthly total solar PV generation, 2013

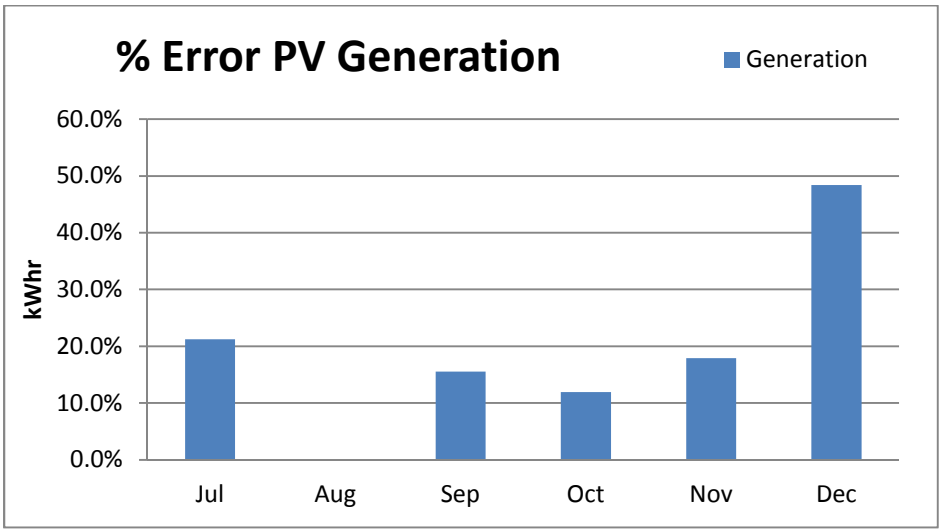

Figure 4-50: Percent error of the monthly solar PV generation. 2013. The recorded data is used as the baseline.

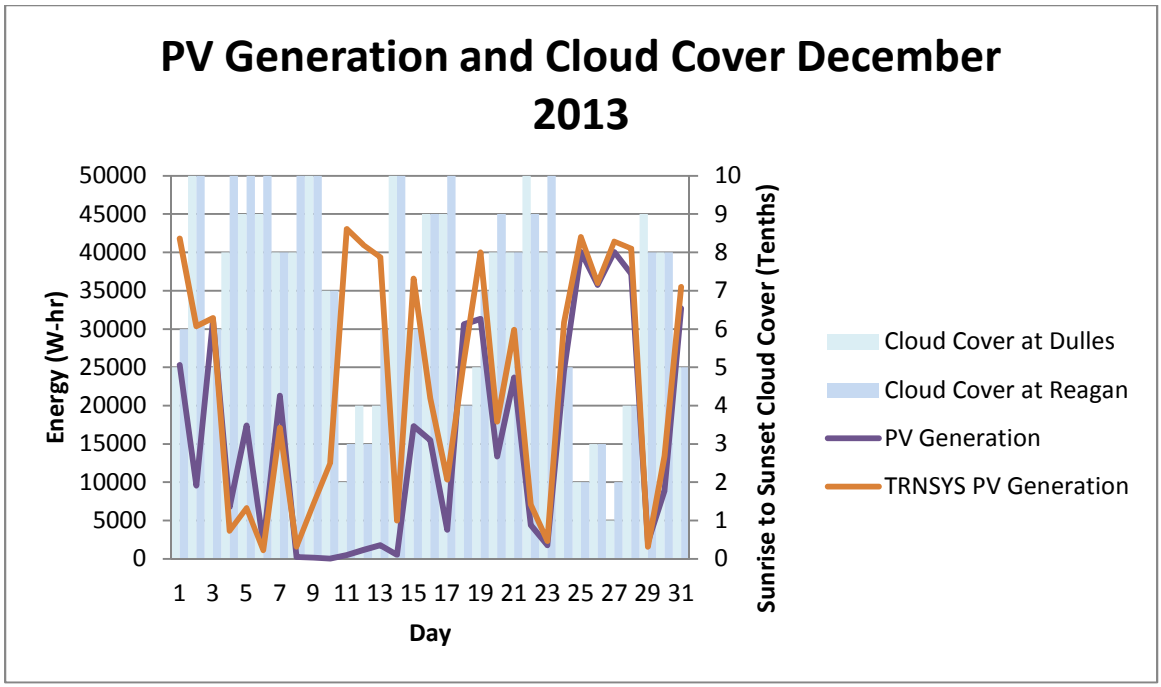

Figure 4-51: Daily total solar PV generation (lines) and cloud cover at nearby airports (bars) for December 2013

For the lowest cloud cover day, Dec 27 in Figure 4-52, the difference in efficiency is 1.7%, 19.1 % recorded vs 20.8 % predicted. If the efficiency is 19.1% then this accounts for 18% of the error for December.

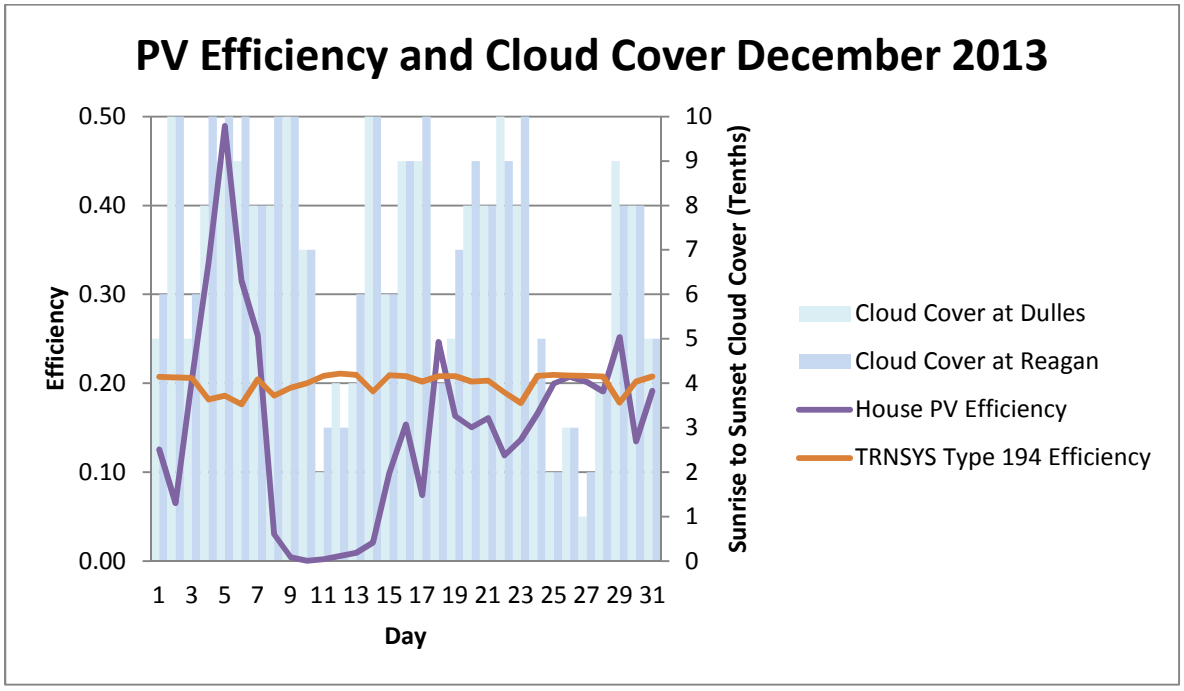

Figure 4-52: Daily average solar PV efficiency (lines) and cloud cover at near by airports (bars) for December 2013. The available solar energy was determined from the simulation weather file.

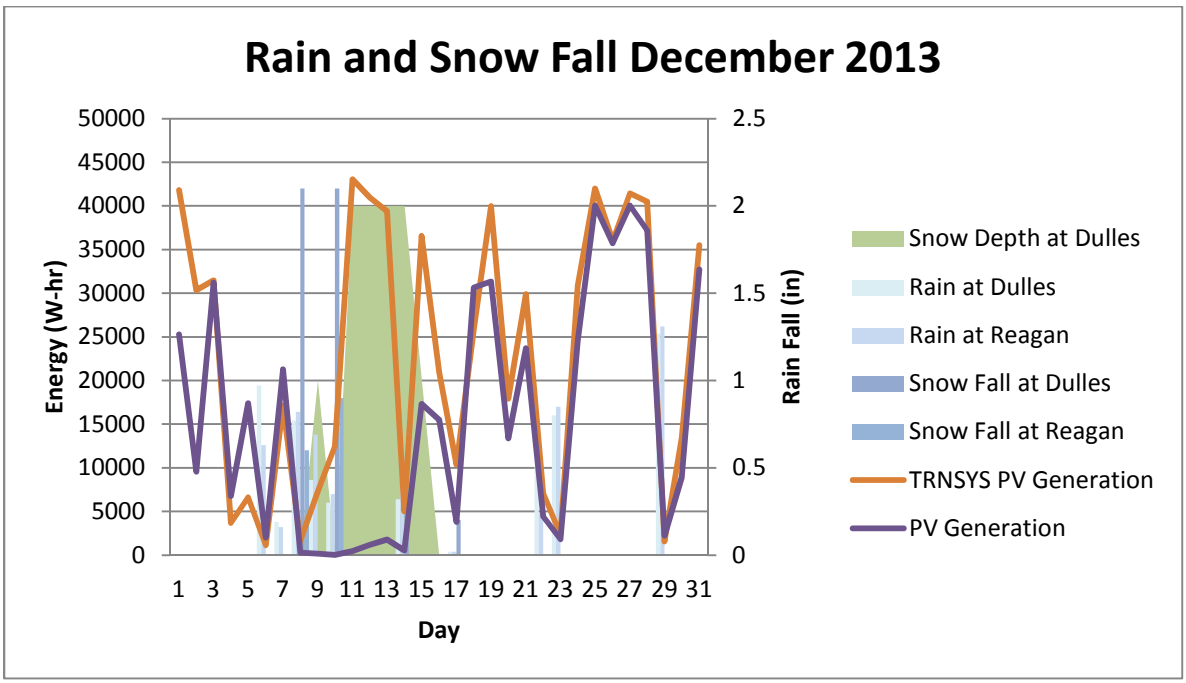

Figure 4-53: Solar PV Array Generation and Rain/Snow Fall for December 2013

As can be seen in Figure 4-53, it appears that snow cover from the 7th to the 13th severely affected the recorded PV generation but not the recorded solar irradiation data at Washington-Dulles or the simulated generation. Assuming that the actual efficiency is the 19.1 % found on the clearest day in December, this 5 day loss of generation accounts for 138 kW-hr of missed generation. The lost generation from this instance alone accounts for 58% of the error for December. Adjusting for the lost generation and efficiency errors leaves only 27 kWhr of error in December unexplained. This unexplained error is about 5.6% of the recorded PV generation.

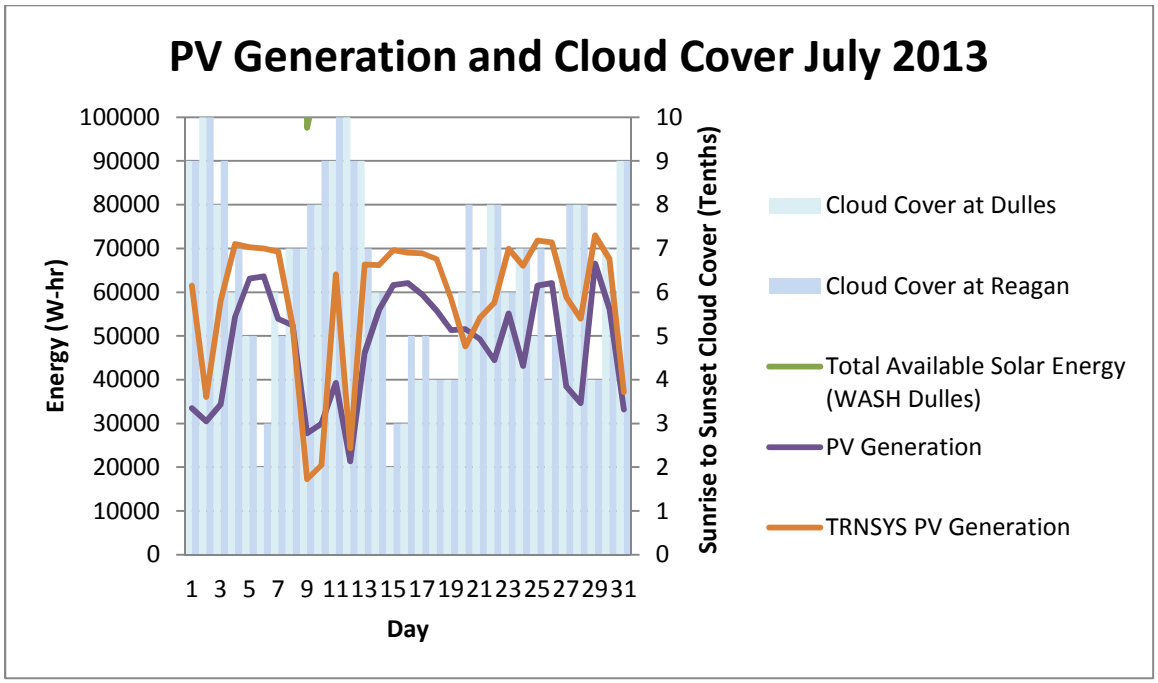

Figure 4-54: Daily total solar PV generation (lines) and cloud cover at nearby airports (bars) for July 2013

Again using the clearest day from the Washington Dulles and Reagan National records, July 6th in Figure 4-55, the difference in efficiency is 1.7%, 17.2 % recorded vs 18.9 % predicted. If the efficiency is 17.2 for the entirety of July then this accounts for 50% of the error for July. Adjusting for the efficiency error leaves 157 kW-hr of error unaccounted for. This is about 11% of the recorded generation.

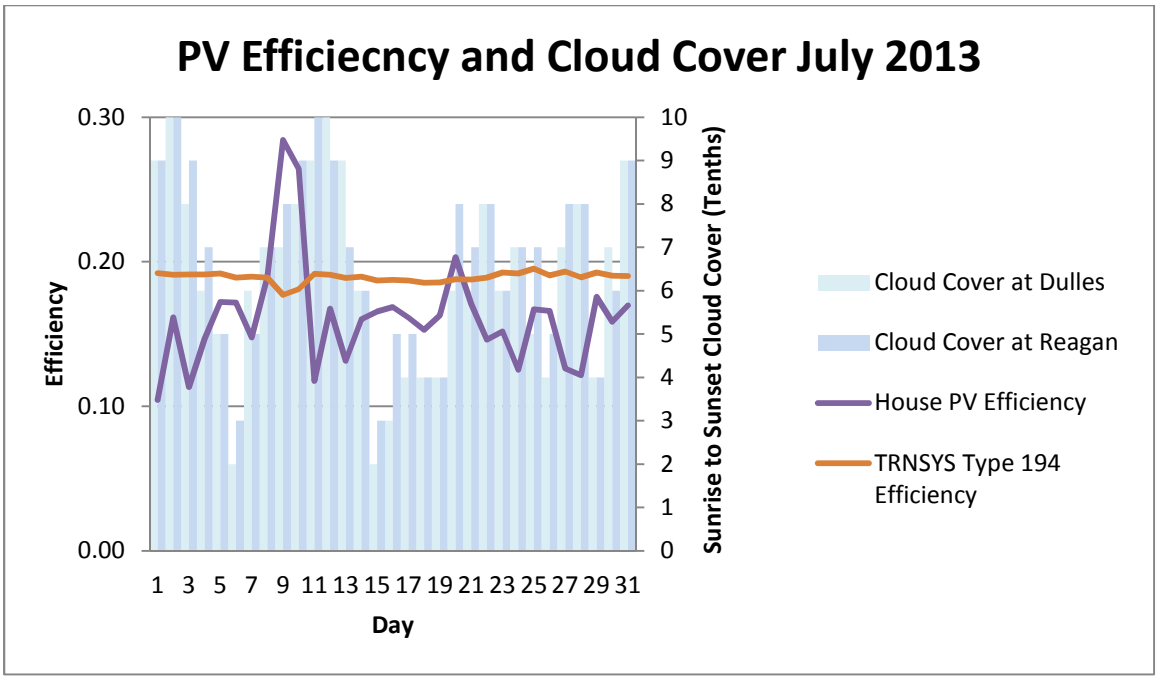

Figure 4-55: Solar PV Array Efficiency and Cloud Cover for July 2013

As can be seen in
Figure 4-52 and Figure 4-55 there are instances where the solar irradiance at the Test Facility was significantly greater than the solar irradiance in the weather file being used for the simulations. This results in greater than realistic solar conversion efficiencies. It is easy to see such differences when the test facility significantly more or less, as with snow cover in December, solar energy. However, without further data it is impossible to distinguish the effects of small differences in available energy from any other factor effecting the solar PV generation at the test facility. If there is a persistent effect such as slightly greater cloud cover or higher temperature then these would be difficult to separate and account for with the current data.

Figure 4-56 shows the modeled efficiency with respect to cell temperature of the PV panels in use at the Test Faclity. An efficiency drop of 1.7% requires a 20°C increase in cell temperature. While it is likely that the cells at the test facility are running hotter than

predicted by the TRNSYS model it seems likely that other factors such as dust, lower than rated PV performance, or greater than anticipated inverter losses are contributing to the decreased efficiency.

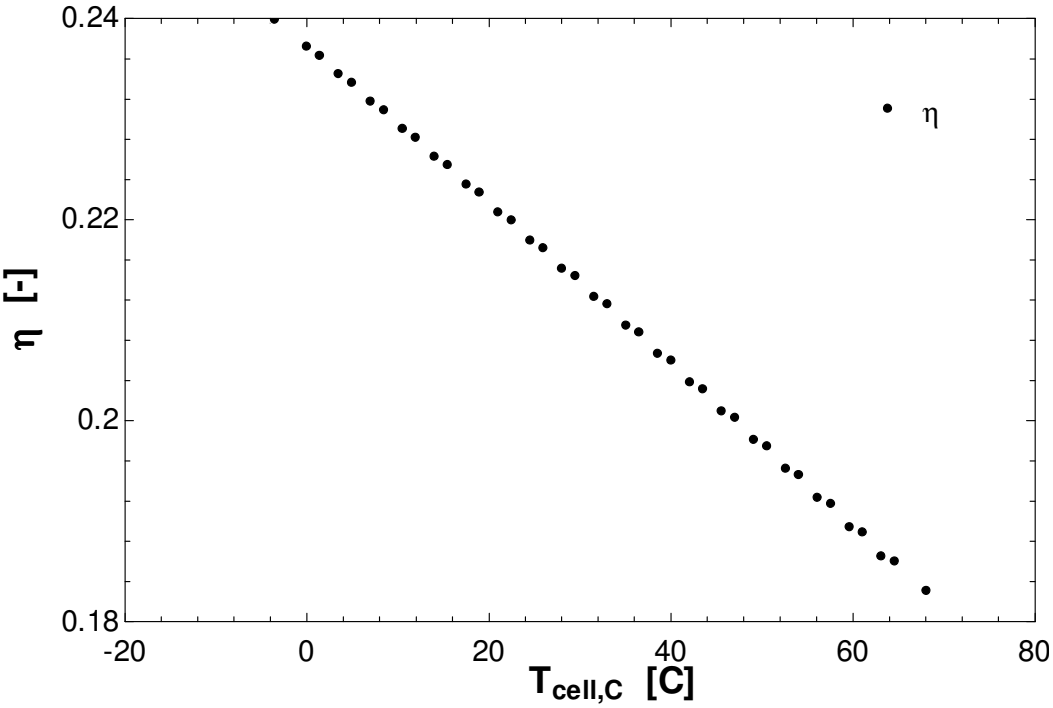

Figure 4-56: PV efficiency vs Cell Temperature. Note does not include Inverter Efficiency

It is interesting to note that the differences in heat transfer models between the EES and TRNSYS models are solely responsible for the differences in cell temperature and thus efficiency shown in Figure 4-57. This demonstrates the potential impact of cell temperature on efficiency and generation.

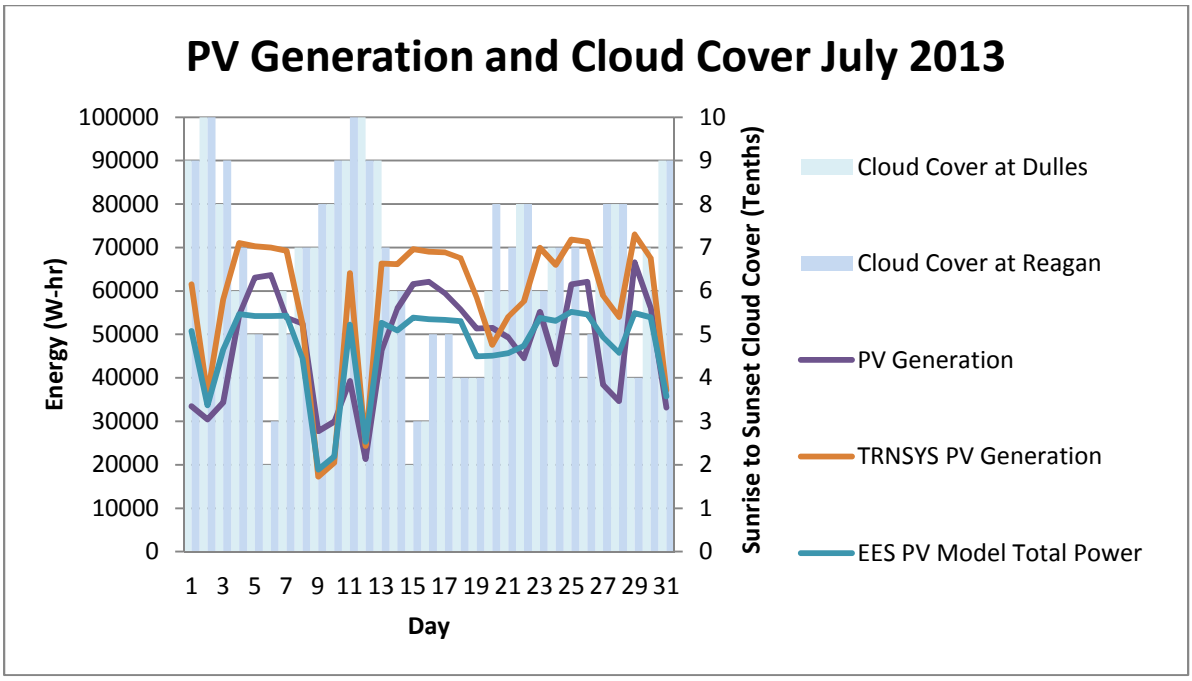

Figure 4-57: Solar PV Array Generation and Cloud Cover for July 2013

4.4 Tuned House Model

Several changes were made to the Schedule Load and Lighting files in order to more closely match the Baseline house model to the recorded data. These changes match the total electrical energy consumption of the TRNSYS simulation to that of the recorded data over the comparison time period.

The predicted interior lighting electrical power consumption is 9.86% greater than the recorded power consumption over the comparison period. To correct for this the lighting loads, which are included in the simulation as constant base loads, were decreased by 13.9kJ/hr for the first floor and by 3.9 [kJ/hr] for the second floor resulting in new loads of 140.9 kJ/hr and 39.6 kJ/hr respectively.

The predicted internal equipment electrical power consumption was 8.56% greater that the recorded power consumption over the comparison period. To correct for this the internal

equipment was adjusted in the load file by reducing the Base Load Correction from 125 W to 82 W for a total reduction of 8.56 % of the total daily load file.

These changes resulted in the predicted electrical demand from the internal equipment demand and lighting loads matching the recorded electrical consumption. The changes in the all of the electrical demands are shown in Table 2. The reduced internal thermal loading resulted in increased heating requirements and decreased cooling energy requirements.

Table 4-11: Tuned Baseline House Model Electrical Energy Consumption and Generation over the Comparison Period

	TRNSYS Simulation	NIST Recorded Data	Error	Percent Error	Error % of Total Consumed
	kWhr	kWhr	dkWhr		
HVAC	1903	2209	-306	-13.86%	-6.07%
Heat Recovery	195	217	-22	-10.35%	-0.45%
Interior Lighting	184	184	0	0.00%	0.00%
Interior Equipment	1833	1824	9	0.49%	0.18%
Water Systems	365	475	-110	-23.19%	-2.18%
Pumps	110	132	-22	-16.66%	-0.43%
Consumed	4588	5042	-454	-9.00%	-9.00%
Generated	6244	5207	1037	19.91%	20.56%
Net Generation	1656	165	1491	901.55%	29.56%

The Tuned Baseline House model was used as the basis for the HVAC and Domestic Hot Water variations presented in Chapter 5.

Chapter 5: Baseline House Model Variations

A series of model variants were created and run in order to predict the performance of each technology, control scheme, and system variation. These variants were based on the tuned house model file with appropriate changes made for each model as documented in this chapter. All of the simulations presented here were run with a one minute time step and used the same 2013 weather data file for Washington-Dulles Airport that was used in the Baseline House Model.

5.1 Domestic Hot Water System Variations

5.1.1 Electric Tankless Hot Water Heater

A tankless electric resistance heater was first used to bypass the conventional hot water heater and hot water heater storage tank in order to determine the energy savings of the heat pump hot water heater and tank system. This model is shown in Figure 5-1. Note that the solar thermal hot water system is still in use.

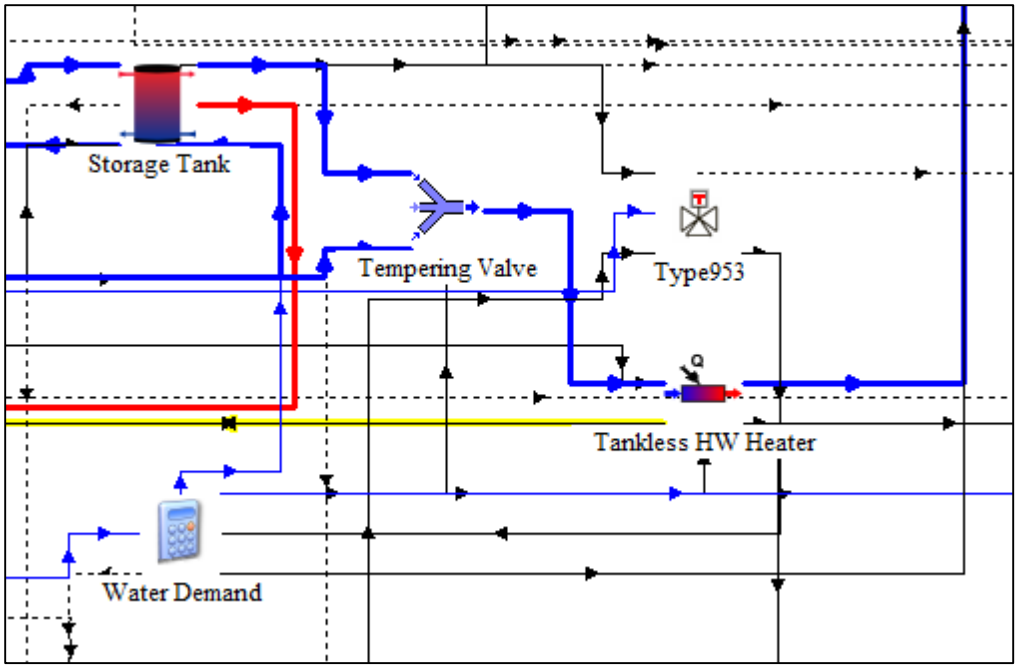

Figure 5-1: Replacement of the Heat Pump Hot Water Heater with Tankless Electrical Resistance Heater

The tankless heater was then used to bypass the entire DHW system in order to determine how much energy was necessary to meet the DHW demand through purely electric resistance heating. This model is shown in Figure 5-2. Note that the entire solar hot water system has been removed and that all hot water heating is being provided by the tankless hot water heater.

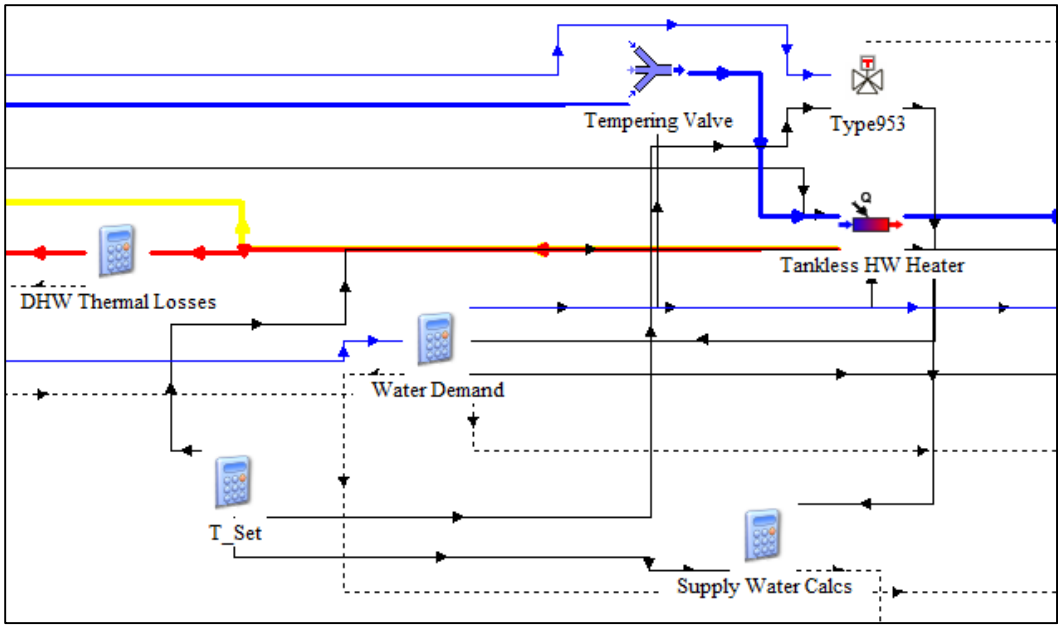

Figure 5-2: Replacement of Solar and Heat Pump Hot Water Systems with a Tankless Hot Water Heater

In each configuration it was assumed that the heater is 99% efficient in transferring heat to the water flow with 1% being lost to the surroundings. The heater's total heating capacity was set to 20x the Baseline system's auxiliary electric hot water heater in order to ensure that the tankless heater was capable of meeting the hot water temperature set point at all times. It was also assumed that the tankless hot water heater was able to precisely match the hot water supply set point temperature. This assumption is justified by the capability of commercial models to match the desired supply temperature within 1 ℃.

5.1.2 Electric Storage Tank Hot Water Heater without Solar Thermal Water Heater

This simulation eliminated the solar thermal hot water heater system and used the heat pump hot water heater from the baseline house model. Note that the tempering valve is not attached to the solar hot water system and feeds directly to the water heater storage tank (Figure 5-3). This heat pump/tank combination may be less than ideal as the heater was sized to be

operated in conjunction with the solar thermal system and thus employs the auxiliary electric heat more frequently than a larger hot water heat pump/storage tank system might. However this system is also capable of coming close to meeting the Test Facility's hot water demand during winter when the solar thermal system is severely underperforming.

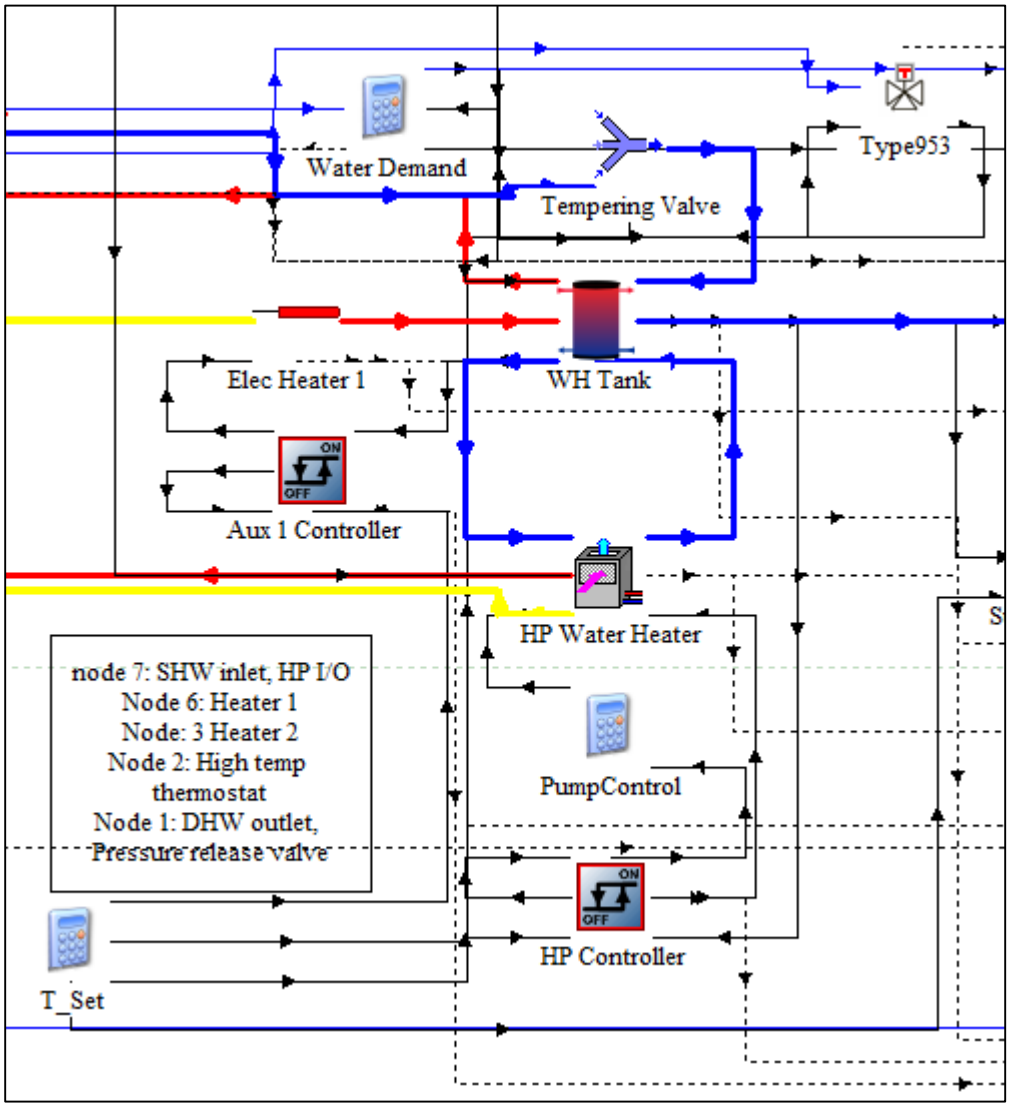

Figure 5-3: Use of only the Heat Pump Hot water System. I.e. elimination of the Solar Thermal System.

5.1.3 Baseline with Larger Solar Hot Water Storage Tank

In this simulation the Baseline House Model's 80 gallon solar thermal hot water storage tank was replaced with a 120 gallon tank similar to the secondary solar thermal hot water system installed in the Test Facility.

5.1.4 Results of Domestic Hot Water System Variations

The annual results for the water system variant simulations are documented in Table 5-1.

The use of a tankless electric resistance heater alongside the solar thermal hot water system resulted in an 89% increase in the DHW electrical demand which translates to an 8.9% increase in the total house hold electrical demand. This increase in demand is due to the use of a less efficient electrical resistance heater to supply the non-solar fraction the water heating. It is interesting to note that the use of the tankless heater resulted in the water supply always being at or above the set point temperature. This system still provides water over the set point temperature during parts of summer as the solar hot water system is being tempered down to a safety temperature that is higher than the set point temperature.

The use of only a tankless electric resistance heater resulted in the highest hot water system electrical demand of all the combinations investigated: 5380 kWhr or 381% over the baseline simulation. The high demand resulted in a 38.7% increase in the total house hold electrical consumption and a shift from the HVAC system to the water system being the largest load source. These results were expected due to the exclusive use of the least efficient heating method. However this method does provide very good temperature control and eliminates all water supplied over and under the set point temperatures. In real life the temperature controls

would be less accurate and the tankless hot water heater would likely be slightly under sized to optimize costs.

The use of only the heat pump hot water heater and auxiliary electric heater resulted in a hot water system caused an electrical demand increase of 1549 kWhr, 139%, over the Baseline simulation. However the use of the heat pump required about 50% of the electrical power required by the tankless hot water heater. The heat pump only simulation uses 26% more energy than the solar thermal and tankless hot water heater simulation.

The addition of the larger solar thermal hot water storage tank resulted in a 1.5% decrease in the annual water system electrical demand. The decreased demand was accompanied by a slight decrease in both the energy lost due to supplying water hotter than the desired set point temperature and the amount of water supplied under the set point temperature. Thus the added storage capacity allowed more solar energy to be utilized and it increased the adherence to the set point temperature. The increased adherence to the set points is partly the result of a decrease in DHW heat pump run time: the heat pump increases the temperature of the water supply over the desired set point.

Table 5-1: Annual Results of Water System Variants

	Electrical Demand	% Diff.	Water System Demand	% Diff.	Over Temp. Supply	Under Temp. Supply	Ave Temp.
Simulation Variant	**kWhr**	**-**	**kWhr**	**-**	**kWhr**	**kWhr**	**C**
Tuned Baseline House Model	10971	0.0%	1118	0.0%	382	76	**62.53**
Baseline w/120 gal SHW Tank	10950	-0.2%	1101	-1.5%	344	72	**62.25**
Tankless DHW Heater + SHW	11950	8.9%	2116	89.3%	391	0	**63.22**

Tankless DHW Heater Only	15214	38.7%	5380	381%	0	0	**60.00**
Heat Pump DHW Heater + Aux	12513	14.0%	2667	139%	198	243	**59.53**

5.2 HRV with Enthalpy Exchanger Core

In this simulation the Heat Recovery Ventilator, HRV, was changed to an Enthalpy Recovery ventilator, ERV, by modification of the performance equations in the HVR Control equation block. Unlike the HRV the ERV recovers both latent and thermal energy. In the actual test facility, this change would be accomplished by swapping out the heat exchanger core of the HRV unit for a drop in energy recovery core. Two correlations were generated using the manufacturer's data for the ERV core: one for mass flow rate and sensible effectiveness and another for mass flow rate and latent effectiveness. The calculations for these correlations may be found in the EES file 'ERV Performance Calcs.EES'. The effectiveness correlations were then input as equations in the HRV controls equation block. In average sensible effectiveness of the ERV core is 0.65 vs. the HRV core at 0.72. However the ERV core has an average latent effectiveness of 0.55 vs. the HRV core latent effectiveness which is necessarily equal to 0.

5.3 HVAC Control Variations

5.3.1 Blocking the HVAC Auxiliary Heater

This simulation is identical to the Baseline House Model only with the HVAC auxiliary resistance heater control set to zero. This change in controls prevents the auxiliary heater from being triggered.

5.3.2 Blocking the HVAC Auxiliary Heater Timed Triggers

This simulation is identical to the Baseline House Model only with the HVAC auxiliary resistance heater time trigger control set to zero. This change in controls prevents the auxiliary heater from being triggered as a result of the second stage HVAC heat pump running for more than 40 minutes. The auxiliary heater will still be triggered as a result of the control zone temperature dropping sufficiently below the set point. Note that the temperature differences are the same as in the Baseline House model.

5.3.3 Blocking all of the HVAC Timed Triggers

This simulation is identical to the Baseline House Model but with all of the HVAC time trigger controls set to zero. This change in controls prevents the second cooling and heating stages and the auxiliary heating stage from being triggered as a result of the lower stages being on for sufficiently long. All of the stages will still turn on if the control zone temperature deviates sufficiently from the temperature set points. Note that the temperature differences are the same as in the Baseline House model.

5.4 HVAC Ground Loop and Heat Pump

5.4.1 Model Set Up

5.4.1.1 Ground Source Heat Pump Implementation

The ground source heat pump is modeled after a Water Furnace 5-D-V-026-G-1-1. This model of ground source heat pump was selected because it is a 2 [ton] (24000 [btu/hr]), variable speed system making it a close match to the existing AAON Air-Air HP. The core of the TRNSYS GSHP model employs two TYPE 919 Water to Air heat pump components in order to model the low and high speed cooling and heating stages of the actual heat pump.

The high speed component also has an auxiliary electric resistance heating stage. Note that dehumidification is still performed by the air source heat pump component described in the baseline model in Chapter 4. The selected Water Furnace heat pump does not have a specific dehumidification setting and the air source heat pump component acts as a whole house dehumidifier.

The parameter specifications were derived from the manufacturer specification catalog ("Specification Catalog," n.d.). Details of the parameters and inputs used may be found in the 'GS HP stage1' and 'GS HP stage2' tabs of the spread sheet 'TRNSYS model system parameters.xlsx' in the electronic supplement. The rated cooling and heating capacities and powers required by the TRNSYS heat-pump component were included in the manufacturer ratings: these values correspond to the heat-pump's performance at the rating conditions used in the performance map used by TRNSYS. The rating conditions are shown in Table 4-2 and the rated capacities are shown in Table 5-3. Currently the TRNSYS default performance maps for the GSHP component are being used.

Table 5-2: TRNSYS Ground Source Heat-Pump Rating Conditions

TRNSYS Heat-Pump Rating Conditions	Frac. Fluid Flow	Frac. Air Flow	In Door Wet Bulb Temperature	In Door Dry Bulb Temperature	Entering Water Temperature
	-	-	°C	°C	°C
Cooling Conditions	1	1	19.44	26.67	21.10
Heating Conditions	1	1	-	21.11	10

Table 5-3: Ground Source Heat-pump Capacity and Power Ratings for TRNSYS Component

Parameter	TRNSYS Native Value	Unit	Given Value	Unit
Rated total cooling capacity - low speed	23878	kJ/hr	22633.3	btu/h
Rated sensible cooling capacity - low speed	16485	kJ/hr	15625.5	btu/h
Rated cooling power - low speed	2988	kJ/hr	830	W
Rated total cooling capacity - high speed	30472	kJ/hr	28883.5	btu/h
Rated sensible cooling capacity - high speed	20981	kJ/hr	19887	btu/h
Rated cooling power - high speed	4860	kJ/hr	1350	W
Rated heating capacity - low speed	16978	kJ/hr	16092.8	btu/h
Rated heating power - low speed	3960	kJ/hr	1100	W
Rated heating capacity - high speed	23029	kJ/hr	21828	btu/h
Rated heating power - high speed	5688	kJ/hr	1580	W

The two ground source heat pump components and the air source heat pump/dehumidifier were combined using a series of air flow splitters, 'Dehu Split' and 'Stage Split', and a plenum, 'Dehu Combine' as shown in Figure 5-4. The flow in these splitters is controlled by the HVAC Cont Integrator and GSHP Flow equation blocks according to which stage of heating, cooling, or dehumidification is called for. Similarly the two ground source heat pump components are connected to the working fluid loop circulating through the ground loop heat exchanger component using a mixing valve, Stage Output which feeds into the GLHX, and flow splitter, Stage Input which returns fluid to the HP as shown in Figure 5-4. The mass flow rate of brine in the GLHX loop is set by the GSHP Flow equation block to match the manufacturer recommended highest efficiency flow rate for each heat pump stage. When stage 1, the low speed stage, is activated, the flow rate is set to 7 GPM. When stage 2, the high speed stage, is activated the flow rate is set to 8 GPM.

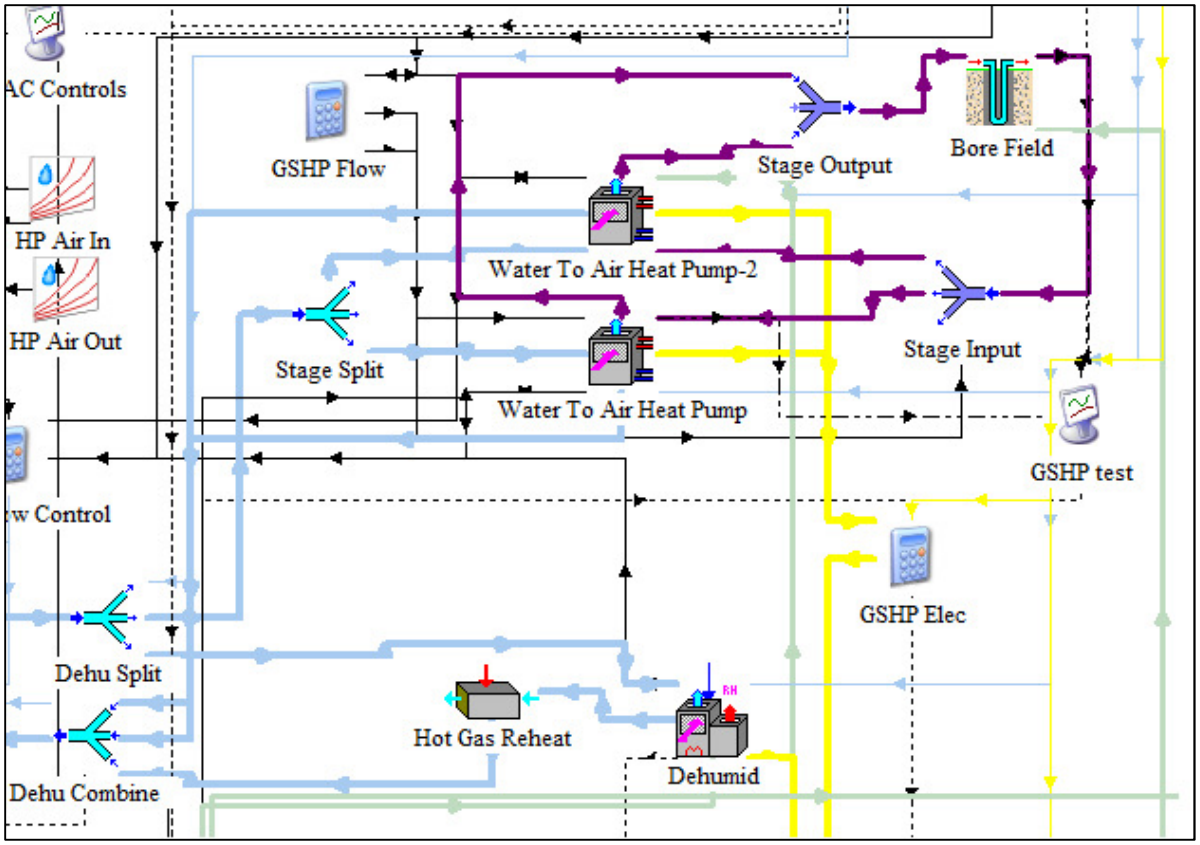

Figure 5-4: Ground Source Heat Pump and GLHX Model

The electrical and thermal output from the two heat pump stages and the control signals from the HVAC Control Integrator block are processed in the GSHP Elec equation block to combine the outputs of the two components. Using this equation block allows the outputs to match the expected inputs of the thermal and electrical output files.

The ground source heat pump is controlled using the same control scheme as outlined in the Baseline System Model for the air-source heat pump. This control scheme is functional as the same number of heat and cooling stages are present and the stage capacities are similar between the GSHP and the ASHP.

5.4.1.2 Ground Loop Heat Exchanger

The heat transfer fluid is a water/ethanol brine based on the Environol 1000 formula. The Environol brine is specified as 70% water, 25% ethanol, and 5% isopropanol. The TRNSYS simulation used a brine with 70% water and 30% ethanol. The properties for this mixture were calculated in EES and the WaterFurnace specification guide includes correction tables for heating capacities and power consumption with a 70/30 water/ethanol mixture at 25°C. The TRNSYS GLHX component doesn't calculate the fluid properties at each time step. Instead it uses one set of fluid properties along with a rated flow rate at the beginning of the simulation to determine the heat transfer and pressure drop coefficients in the pipe and then uses these coefficients for the rest of the simulation. Likewise the water to air HP model only takes in one set of properties for the fluid side.

The Ground Loop Heat Exchanger model is based on the vertical bore field installed at the Test Facility. The TRNSYS model uses the same TYPE 557a Duct Storage Model Implementation as the ground loop studies presented in Chapter 3. The borehole geometries are identical to those used in the optimization studies and the Ground Thermal Properties and borehole radius are the Rb 1.92 [in] and Kf 2.43 [W/m-K] determined using those studies. In these simulations the number of boreholes in the bore-field was varied from 1 to 4. These boreholes are assumed to be identical and the heat transfer in the pipes connecting the boreholes and the heat pumps is ignored.

5.4.2 Results of the HVAC Variations

The annual results for the HVAC system and HVAC control variant simulations are documented in Table 5-4 and Table 5-5.

The Enthalpy Recovery Core simulation resulted in a 2.5 % decrease in the HVAC Electrical demand. This decrease resulted from a combination of different effects. The enthalpy recovery core is less efficient at sensible heat transfer and there was a 5% increase in heating electrical requirements. The cooling electrical demand decreased by 2.5% as the increased latent heat transfer made up for the decrease in sensible heat transfer. Similarly the dehumidification electrical demand was reduced by 41.3% and was where the bulk of the energy savings were made. The ERV core had little impact on the HVAC systems ability to maintain the temperature set points. Due to the seasonal nature of the energy savings it might be economical to use the HRV core during the cooling season and the ERV core during the heating season.

The ground source heat pump system energy savings varied substantially with the number of boreholes in the vertical ground loop heat exchanger. The entering water temperature decreased as the number of boreholes increase and thus the efficiency of the heat pump increased with the number of bore holes. The increase in efficiency decreases and the pumping cost increases as the number of boreholes rises. The single borehole system resulted in a 3.6 % increase in the HVAC electrical demand relative to the baseline simulation. The two and three borehole systems resulted in 11.3% and 17.5% decreases relative to the baseline. The four borehole system resulted in a 20.4% decrease in the HVAC electrical demand. The four borehole system is particularly interesting as this system is similar to the Test Facility in terms of total length of heat exchanger piping. It is interesting to note that energy savings during cooling operation for all the GSHP simulations are greater than the energy savings during heating operation. As with the HRV to ERV change, the swap from

the baseline ASHP to the GSHP system resulted in minimal change to the HVAC systems ability to maintain the set point temperatures.

The control system variations all resulted in significant energy savings over the baseline simulation. Most of these savings were the result of decreased use of the auxiliary electric resistance heaters. Elimination of the use of the aux. heater resulted in a 20.5% reduction in HVAC electrical demand while only turning it on as a result of low control zone temperature, vs. with a timed trigger, resulted in a 19.2% reduction. Eliminating all of the timed triggers so that the stages are only triggered by the difference between the control zone and the set point temperatures resulted in a 22.1% reduction in HVAC energy use. This reduction is due to reduced use of the less efficient high speed heating and cooling stages and greatly reduced use of the auxiliary heater. It is interesting to note that eliminating the timed triggers also reduced the dehumidification energy use even though the dehumidification stages are only controlled by humidity level. This energy reduction does come at some cost to comfort level, a 30% increase in the degree days below the heating temperature set point, but it is mostly the result of replacing short bursts of auxiliary heat with longer use of the HVAC heat pump.

The control variations had a greater impact on the HVAC systems ability to follow the heating temperature set points due to the reduced use of the Auxiliary heater. In the most extreme case, elimination of the auxiliary heater resulted in an 8.2 C-day increase in the zone temperature difference below the heating temperature set point which is an increase of 30.4% over the baseline simulation. However the total, 36.8 C-day, is still below the baseline control zone temperature difference above the cooling set point temperature of 83.0 C-day.

Table 5-4: Annual Results of HVAC System and HVAC Control Variants

	Total Electrical Demand	% Diff.	HVAC Electrical Demand	% Diff.	Heating Diff. Zone vs Set point	Cooling Diff. Zone vs Set point
Simulation Variant	**kWhr**	**-**	**kWhr**	**-**	**C-Day**	**C-Day**
Tuned Baseline House Model	10971	0.0%	4578	0.0%	28.2	83.0
Enthalpy Recovery Core	10855	-1.1%	4465	-2.5%	29.0	81.7
GSHP 1 Borehole	11137	1.5%	4743	3.6%	29.9	82.3
GSHP 2 Borehole	10456	-4.7%	4062	-11.3%	29.2	82.1
GSHP 3 Borehole	10166	-7.3%	3773	-17.6%	28.8	81.1
GSHP 4 Borehole	10038	-8.5%	3643	-20.4%	28.6	80.8
Control Aux. Elec. Off	10031	-8.6%	3638	-20.5%	36.8	82.9
Control Aux. Elec. Timed Trigger Off	10091	-8.0%	3698	-19.2%	35.1	82.9
Control All Timed Triggers Off	9959	-9.2%	3567	-22.1%	35.3	83.6

For Table 5-4, the Heating and Cooling Differences Zone vs. Set point are calculated by taking the difference between control zone temperature and the heating or cooling temperature set point at each time step. For the heating difference, all negative values, where the zone temperature is below the heating set point, are summed over the course of the simulation. For the cooling difference, all positive values, where the zone temperature is above the cooling set point, are summed over the course of the simulation.

Table 5-5: Annual Results for HVAC Control Variants Continued

	Heating Electrical Demand	% Diff.	Cooling Electrical Demand	% Diff.	Dehum. Electrical Demand	% Diff.
Simulation Variant	**kWhr**	**-**	**kWhr**	**-**	**kWhr**	**-**
Tuned Baseline House Model	2328	0.0%	1817	0.0%	433	0.0%
Enthalpy Recovery Core	2445	5.0%	1766	-2.8%	254	-41.3%
GSHP 1 Borehole	2570	10.4%	1770	-2.6%	403	-6.9%
GSHP 2 Borehole	2357	1.2%	1300	-28.5%	405	-6.4%
GSHP 3 Borehole	2263	-2.8%	1109	-39.0%	401	-7.4%
GSHP 4 Borehole	2213	-4.9%	1025	-43.6%	405	-6.5%
Control Aux. Elec. Off	1388	-40.4%	1817	0.0%	433	0.0%
Control Aux. Elec. Timed Trigger Off	1448	-37.8%	1817	0.0%	433	0.0%
Control All Timed Triggers Off	1459	-37.3%	1686	-7.2%	422	-2.5%

5.5 Battery Sizing Program

A small program, 'BatterySizer.m', has been developed in MATLAB, which analyses the TRNSYS simulation output files to determine the required capacity and power output of a backup electrical source, such as a battery, which would allow the Test Facility to operate independent of the electrical grid. The program outputs four variables: The maximum power output requirement, the simulation hour at which the maximum power is required, the maximum energy storage capacity requirement, and the simulation hour at which the maximum capacity is required. The MATLAB code for this program may be found in the electronic supplement.

The maximum power is determined by finding the maximum instantaneous net power demand from the simulation. The net power demand is one of the output variables of the TRNSYS House model and is calculated by subtracting the 'instantaneous' solar PV

generation from the ‘instantaneous’ total household power demand. These values are not actually instantaneous as they are calculated over the length of the simulation time step. Thus for a 1 minute simulation the ‘instantaneous’ power is actually the one minute average power demand. A 1 minute level or resolution is acceptable when excluding the transient power surges associated with inductive loads such as AC engines. For these simulations the maximum power demand is usually the result of a combination of high scheduled loads, hot water heater loads, and HVAC loads and, simultaneously, low solar PV generation. This combination of loads usually occurs during a dark, cold day in winter.

The maximum energy storage capacity requirement is calculated by determining the cumulative net power demand at each time step. This value increases for time steps where demand is greater than generation and power would be drawn from the grid and decreases for time steps where demand is less than generation and power would be supplied to the grid. The storage capacity required for the simulation to be grid independent is the maximum instantaneous cumulative net power demand over the course of the simulation. For these simulations the maximum energy storage capacity demand is usually the result of a long period of decreased Solar PV generation and increased HVAC and hot water loads. Again this combination usually occurs during winter after several weeks of low solar input.

5.5.1 Results of the Battery Sizing Program

The results of the Battery Sizing program analysis of the model variations are documented in

The time of day at which the simulation predicts maximum power varies based on whether the HVAC or DHW system is dominating the power use. However the maximum power is always at night when there is no solar PV generation and often in the early hours of the morning when the occupant loads become active. The time of day when the maximum storage capacity is required does not vary and is always shortly after dawn when the solar PV generation equals the total household power demand.

Table 5-6. The first column is the maximum power output required over the course of the simulation. The second column is the simulation time that the maximum power was required. The simulation time is measured from midnight on January 1st. The third column is the time of day that the maximum occurs. The fourth column is the maximum battery capacity required during the simulation. The fifth column is the time at which the maximum battery capacity is required. Another way of looking at this time is that it is when a storage system of the maximum required capacity would be drawn to zero before starting to recharge. The sixth column is the time of day the maximum capacity is required.

The Baseline simulation required maximum power, 0.99 kW, and capacity, 277.6 kWhr. This much storage capacity is equivalent to 11.6 Nissan Leaf 24 kWhr battery packs at a price of $63,800 (Nissan, 2014) or 4.6 Tesla Model S 60 kWhr battery packs at a cost of $46,000 (Tesla, 2014). In terms of lead acid batteries this is equivalent to 116 deep cycle 2.4 kWhr Key Power storage batteries for an estimated cost of $22,000 (Keypower Battery, 2014). Both requirements are necessary in December of 2013 and are heavily dependent on the HVAC loads. As these results are so heavily dependent on the HVAC loads, the addition of

more solar thermal hot water capacity in the Baseline w/120 gal SHW Tank simulation had no impact.

For the Tankless DHW Heater + SHW, Tankless DHW Heater Only, and Heat Pump DHW Heater + Aux simulations the maximum power and capacity become more dependent on the domestic hot water system. The increased dependence is due to the large increase in water system electrical requirements. This effect is particularly notable in the maximum power requirements for the Tankless DHW Heater + SHW and Tankless DHW Heater Only simulations which at 2.44 kW and 2.48 kW are almost 250% larger than the maximum power requirement of the Baseline simulation.

The Enthalpy Recovery Core simulation is nearly identical to the baseline simulation but has a 1.6% larger battery capacity requirement. This larger battery requirement is due to the decreased heat recovery efficiency relative to the energy recovery core. Thus while the ERV core reduces annual energy demand it increases the necessary battery capacity.

The single borehole ground source heat pump simulation has a higher HVAC loading and auxiliary heater use resulting in increased power and capacity requirements, 1.11 kW and 313 kWhr, relative to the baseline. The other GSHP simulations show identical maximum power requirements of 0.95 kW and decreasing maximum capacity requirements from 297.4 to 285.7 kWhr.

All three of the control variations investigated resulted in almost identical battery requirements, 0.87 kW and 209 kWhr. These requirements are significantly lower than for the Baseline simulation as a result of the near elimination of auxiliary HVAC use. Along

with the Tankless DHW simulations, this shows the importance of energy efficient and low power equipment in reducing energy storage requirements.

The time of day at which the simulation predicts maximum power varies based on whether the HVAC or DHW system is dominating the power use. However the maximum power is always at night when there is no solar PV generation and often in the early hours of the morning when the occupant loads become active. The time of day when the maximum storage capacity is required does not vary and is always shortly after dawn when the solar PV generation equals the total household power demand.

Table 5-6: Annual Battery Sizing Results of Water and HVAC Variants

	Max Power Requirement	Simulation Time	Time of day	Max Capacity Requirement	Simulation Time	Time of day
Simulation Variant	**kW**	**hr**	**24 hr**	**kWhr**	**hr**	**24 hr**
Tuned Baseline House Model	0.99	558.7	6.7	277.6	416.2	8.2
Baseline w/120 gal SHW Tank	0.99	558.7	6.7	277.4	416.2	8.2
Tankless DHW Heater + SHW	2.44	414	6	359	584	8
Tankless DHW Heater Only	2.48	414	6	514	584	8
Heat Pump DHW Heater + Aux	1.15	559	7	304.8	584.4	8.4
Enthalpy Recovery Core	0.99	558.7	6.7	282	416.2	8.2
GSHP 1 Borehole	1.11	6.8	6.8	313	416.2	8.2
GSHP 2 Borehole	0.95	558.7	6.7	297.4	416.2	8.2
GSHP 3 Borehole	0.95	558.7	6.7	289.4	416.2	8.2
GSHP 4 Borehole	0.95	558.7	6.7	285.7	416.2	8.2
Control Aux. Elec. Off	0.87	381.3	21.3	209.9	416.2	8.2
Control Aux. Elec. Timed Trigger Off	0.87	381.3	21.3	209.3	416.2	8.2
Control All Timed Triggers Off	0.87	381.3	21.3	209.3	416.2	8.2

Chapter 6: Summary of Results and Recommendations for Future Work

6.1 Summary of Ground Loop Heat Exchanger Studies

6.1.1 House Envelope

A model of the house envelope and load was needed to generate realistic thermal loading files for ground loop heat exchanger studies (GLHX). A 3D model of the NZERTF was created in TRNSYS3d based upon the 'As Built' architecture documentation (Corporation, n.d.) and then used to generate a TRNSYS TYPE 56 Multizone Building component in TRNBuild. This building component was combined with TMY3 data file for Washington DC Dulles International Airport, the initial Monday NZERTF internal load files, occupant schedules, set point temperature schedules, an infiltration model, and a basic placeholder HVAC system to form the TRNSYS House Envelope and Load Model. This model ran yearlong simulations at a 15 minute time step and output thermal loading data to a text file for use with the GSHP and GLHX models.

The TRNSYS House Envelope and Load Model was compared with the NIST EnergyPlus NZERTF model (Kneifel, 2012). The internal gains of both models were matched, however the TRNSYS model resulted in greater wind, stack effect, and pressure driven infiltration heat losses (50-75%) during winter months than were reported for the EnergyPlus model. The heat gains during summer months are almost identical. The total HVAC thermal requirements were broken down into heating and cooling components. Though the patterns were very similar, the TRNSYS model had a lower heating requirement of 4148 kWhr vs. 4986 kWhr, in spite of the higher infiltration losses, and higher cooling requirement, 6496

kWhr vs. 5654 kWhr. This difference shows the effects of the EnergyPlus model including the forced ventilation system, slightly different wall construction, and varying zone temperatures. This difference was deemed to be close enough for the ground loop studies and the predicted building thermal load file was used for those studies. The House Envelope and Load Model was later updated to make the Baseline House model.

6.1.2 Ground Loop Study

The thermal properties of the ground formation around a ground loop heat exchanger, and the geometric properties of such heat exchangers have a large impact on their effectiveness. As such it is desirable to know these properties to avoid over or under sizing the ground loop heat exchanger. The performance of the GLHX is determined via a thermal response test. For the NIST NZERTF vertical GLHX (bore field) three such tests were performed: one by the drilling contractor on a test borehole, and two by Harrison Skye on the final GLHX. These test data sets were evaluated using the industry standard Line Source Model (LSM), the Geothermal Property Measurement Tool (GPM), and the TRNSYS TYPE 557a Bore field Component. The TRNSYS Borefield Component is based on the Duct Storage Model (HellStrom, 1989) and was combined with a two MATLAB based optimization functions. The first function used the built in Nelder-Mead optimization function, fminsearch. The second was a parametric optimization function called the crossed Contour Method which developed during this project.

The models and optimization functions were used to determine the ground formation thermal conductivity and the borehole radius. The ground formation heat capacity was found to have little impact over relevant time scales and was assumed to be the drilling contractors

estimate. The borehole geometry was assumed to be the nominal geometry except for the borehole radius which was used as a proxy for all factors which affect the borehole thermal resistance. Each test, model, and optimization method yielded slightly different results and the final values chosen for the formation thermal conductivity, 2.43 [W/m-K], and borehole radius, 1.92 [in], were averages. The range of property estimates generated was tested in the long time scale GLHX study to determine if the variation seen was relevant.

6.1.3 Long Time Scale GLHX Study

A series of long term bore field simulations were performed in order to estimate the efficiency impacts of the ground and borehole property variations found in the Ground Loop Study. The simulations done for these studies used the thermal load file from the House Envelope and Load Model and the TMY data file for Washington-Dulles. Initially the simulations were run with hour long time steps for either 10 or 60 years. It was determined that the 10 year time span was sufficiently long and the remaining simulations were run for 10 years. The heat transfer to and from the working fluid circulating through the borehole was determined by the load file but was modified to make four models. In the first model the load file was applied directly to the working fluid. For the second model the load was applied using a heat-pump with the nominal capacities of the NZERTF HVAC heat pump. The third and fourth models tripled the applied loads and then applied them directly or through the heat pump. Each model was then tested with a range of estimated properties representing low and high heat transfer; minimum, median, and maximum values of formation conductivity and borehole radius; and the averaged properties used in the House Model GLHX simulations.

The performance measure for these studies was the Entering Water Temperature (EWT). This is the temperature of the working fluid entering the heat pump after leaving the GLHX and it has a large impact on the heat-pump's efficiency and ability to meet the load. For this climate and facility the loads are cooling dominated and maximum EWT, when heat is being rejected to the borehole, is of greatest interest.

The direct application of the predicted Test Facility thermal load to the working fluid passing through the borehole resulted in predictions of a fairly small range of maximum EWTs resulting from the range of predicted borehole properties. Further the increase in EWT's over the course of ten years was predicted to be very small.

The addition of a heat-pump resulted in an increase in the maximum entering water temperatures, the difference between low and high heat transfer cases, and the increase in maximum entering water temperature over the course of the simulations. Thus the addition of a heat pump has an amplifying effect on the changes in EWTs and results in greater variation of the EWTs with respect to the predicted formation and borehole thermal properties.

Tripling the load being met by the heat-pump in order to more closely match a typical residential installation resulted in increased maximum and average EWTs and greater spread in EWT for the different properties cases. The tripling of the load also decreased the minimum EWTs as a result of the increase in heat being drawn from the borehole.

The impact of the borehole properties on the heat-pump efficiency and EWTs is dependent on the load being applied: while small variations in these properties may be negligible, the variations seen in the analysis of the NZERTF thermal response tests could result in

significant variations in ground source heat pump performance depending on the total loading per linear foot of borehole.

6.2 Summary of NZERTF Modeling and Comparisons

6.2.1 Baseline House Model

The House Envelope and Load Model was updated and expanded to create the Baseline House Model. The Baseline Model was created to match the Test Facility while still providing flexibility to simulate modifications to the existing equipment and control schemes. The TRNSYS Baseline model was compared to both the NIST EnergyPlus model and the initial data collected from the test facility. Several variations of the TRNSYS Baseline model were also generated and run to test hot water system, HVAC, and HVAC control modifications.

The changes made to create the Baseline House Model include changing the scheduled internal load files, addition of latent load tracking, and shortening of the simulation time step to accommodate timed HVAC controls. Additions to the model were the heat recovery ventilation, HVAC system, solar hot water system, heat pump hot water system, and solar PV system. The heat recovery ventilation system consisted of the heat exchanger core, inlet fan, outlet fan, inlet and outlet plenums, and the control system. The HVAC system consisted of an air source heat pump, dehumidifier, inlet and outlet plenums, and the HVAC control system. The HVAC control system uses a combination of HVAC stage run time and temperature set points to trigger 3 heating, 2 cooling, and 2 dehumidification stages. The solar hot water system consists of the solar thermal collector array, a brine pump, a water pump, a heat exchanger, the solar hot water storage tank, a tempering valve and the solar

thermal control system. The domestic hot water system consists of an air to water heat pump, a hot water storage tank, an electric resistance auxiliary heater, and the domestic hot water control system. The solar PV system consists of two solar PV panel arrays and two inverters.

6.2.2 Eplus Comparison

The comparison between the NIST EnergyPlus Model and the TRNSYS Baseline House model required changes to the Baseline hot water system and HVAC controls, which were designed to match what was implemented in the Test Facility after the creation of the EnergyPlus Model. The HVAC controls used are described in the 'EnergyPlus Comparison HVAC Controls' section of Chapter 4. The domestic hot water controls used are also described in the domestic hot water control section of Chapter 4 and differ from the Baseline House Model only in the tempering and set point temperatures. This model also used the TMY weather data file for Washington-Dulles and the comparison was made over the full, year long, length of this data.

Over the comparison period, the TRNSYS simulation predicted that the total electrical energy consumed and generated by the Test Facility would be 6.84% and 3.35% less than the amounts predicted by the EnergyPlus simulation. These values yield a predicted a net generation of 4249 kWhr for the TRNSYS Simulation while the EnergyPlus simulation predicted a net generation of 3982, a difference of 6.71 %. These predicted net generations represent 28.4 % and 25.7 % of the total predicted consumption of the TRNSYS and EnergyPlus simulation respectively.

The largest contributors to the difference in the demand were the HVAC heating system and the solar hot water system pumps. The Solar PV generation also had a large absolute difference, 519 kWhr, which is 4.52% of the EnergyPlus simulations predicted consumption. The largest percentage errors for individual systems were seen in the heating HVAC performance and the solar hot water heater pumps.

The TRNSYS simulation results are generally very close to the EnergyPlus simulation results leading to the conclusion that the TRNSYS model is performing well. The systems with the greatest deviation in electrical use, the pumps and HVAC system, use different model parameters which maybe closer to the equipment installed in the Test Facility than the EnergyPlus simulation's equivalent parameters. In the case of the solar thermal collector system the pumps in the TRNSYS simulation were modeled after the manufacturer's specification while the EnergyPlus simulation uses an auto sizing function. Likewise the TRNSYS simulation's HVAC heat pump performance map uses manufacturers and recorded data vs. EnergyPlus defaults. Whether the EnergyPlus model or the TRNSYS model is more accurate in matching the Test Facility results will likely depend on the degree of tuning carried out on either model.

6.2.3 House Data Comparison

6.2.3.1 Setup and Weather Data

The comparison between the NIST the TRNSYS Baseline House model and the NIST Test Facility Data used the Baseline House Model as described in Chapter 4.1 for the Baseline Full House Model. This model used the 2013 recorded weather data file from Washington-Dulles Airport meteorological station provided by Matthew Boyd (Boyd, 2014). The

comparison simulation used a 1 minute time step and one year duration. The weather data covers from January 2013 to the end of December 2013. The Washington Dulles recorded weather was used in the simulation because the weather data that was recorded on site is currently unavailable.

The experimental data recorded from the Test Facility covers a time period from July 2013 to April 2014. The data set is missing 17 days in April and 5 days in August. Because of the difference in covered time periods and the missing data in April and August the comparison between the model and Test Facility was done for July, September, October, November, and December of 2013.

The weather file used in the simulation was recorded at Washington-Dulles Airport, which is about 20 miles away from the Test Facility. As a result some differences are evident in the temperature profiles at each site. While the daily average temperatures are fairly close, the minimum and maximum recorded temperatures vary by up to 6 °C. This difference is particularly notable in the maximum temperatures recorded in July: the Test Facility recorded maximum temperature is typically about 5 °C greater than the maximum temperature from the Washington-Dulles weather data. While this variation may be a result of recording and reporting differences and not actual variation in the temperatures, the simulation is dependent on the weather data files and will be affected.

The difference between the simulation and recorded weather files also results in a significant difference in the amount and timing of cloud coverage, fog, haze, rain, and snow. The simulated PV outputs correspond quite closely to the cloud and snow cover at Washington-Dulles, as would be expected. The experimental data corresponds to the data measured at

Washington-Dulles but exhibits significant departures due to variations in cloud cover at the house location. The impact of snow fall and ground snow depth can be seen clearly in the experimental data and it is interesting to note that snow cover seems to persist longer (as indicated by near zero recorded PV production) on the test facility than at either airport location.

6.2.3.2 Summary of Experimental Data Comparison Results

6.2.3.2.1 Overview

Over the comparison period, July, September, October, November, and December of 2013, the TRNSYS Baseline simulation predicted that the total energy consumed would be 3.42% less than the amount recorded for the Test Facility. The simulation predicted that the total energy generated by the solar PV system would be 19.91% greater than the amount recorded. These two predictions result in the TRNSYS simulation over predicting the margin by which the Test Facility achieves net zero status by a factor of 8. The simulation predicted a net generation of 1209 kWhr or 24% of the recorded energy consumption over the comparison period while the recorded net generation over the same period was 165 kWhr or 3.3% of the recorded energy consumption.

The largest contributors to the absolute difference in the demand were the HVAC system and the domestic hot water system. The interior equipment demands, which were input to the model based on the initial schedule for the Test Facility, were overestimated by 8.56 % and this decreased the difference between the predicted and recorded demand. The largest percentage errors were seen in the domestic hot water system and the solar PV.

During warmer months (e.g., July), the predicted power consumption is very close to the recorded power consumption. During November and December there is a significantly larger difference between the predicted and recorded power consumptions. This difference is largely due to the lack of a HVAC heat pump defrost cycle in the TRNSYS simulation which accounts for 56% of the HVAC error over the comparison period.

The Scheduled Loads and Lighting Demand predicted by the simulation are on average 8.56 % and 9.86 % greater than the values recorded at the Test Facility. These differences are fairly consistent month to month implying a systemic offset. The simulation scheduled loads and lighting demand are set as forcing functions based on the anticipated Test Facility Load Schedule and are thus subject to tuning. The result of a tuned model with more closely corresponding loads is presented at the end of Chapter 4.

6.2.3.2.2 HVAC and Heat Recovery Ventilation System Results

About half of the difference between the HVAC heat pump performance during winter can be attributed to the lack of a defrost cycle in the TRNSYS simulation. During October, November and December of 2013 this accounted for 121 kWhr of energy use in the Test Facility and about 56% of the difference between the recorded HVAC demand data and TRNSYS simulation results. When the defrost energy is subtracted, the TRNSYS simulation HVAC power requirements are within 5% of the Test Facility's requirements.

The monthly average HVAC heat-pump COPs for heating and cooling indicate that the TRNSYS simulation comes much closer to the rated cooling and heating efficiency of the heat pump which suggests that there may be potential for significant gains in heat pump

efficiency. The Heat-pump was also significantly worse at both heating and cooling during the fall when the lower temperature difference between indoors and outdoors should make both operations more efficient. This decrease in performance may be the result of partial loading, short run times, or potentially lower efficiency in low speed operation.

The TRNSYS simulation's daily HVAC Heat-pump and Resistance heater load (thermal output) and power consumption for the December 2013 are usually slightly lower than those recorded at the Test Facility. There are however significant deviations that are likely the result of differences in the triggering of the HVAC auxiliary resistance heater.

The recorded daily run times for the indoor fan, which are taken to be equivalent to the total air handling unit (AHU) run time, and the simulation AHU run time during December show significant deviation. The TRNSYS simulation predicts about half of the total run time recorded at the test facility and a significantly greater run time for the auxiliary heater which is further evidence of a difference in the control of the resistance heater. The simulation is thus overestimating the amount of resistance heat use and under estimating the heat pump use. This counters the decreased heat-pump efficiency in the Test Facility.

The TRNSYS simulation's daily HVAC Heat-pump and Resistance heater load (thermal output) and power consumption for the July 2013 are quite close to the recorded data and calculated power consumption. The TRNSYS simulation predicts about 80% of the total run time that is recorded at the test facility. The dehumidification system run time is also lower than the recorded data. Combined with the loading and the power consumption, this result indicates that the HVAC simulation heat-pump cooling modes are more efficient than indicated by the recorded data.

The TRNSYS simulation's Heat Recovery Ventilation system uses less power than the experimental data records. The difference over the entire comparison time period is 22 kWhr which is 10.3% of the recorded HRV demand and 0.45 % of the total recorded household demand. Potential reasons for this difference include changes in ventilation settings between the EnergyPlus model documentation and the Test Facility and differences in the performance of the HRV unit from the manufacturer's specifications. The lack of a defrost setting in the HRV simulation may also play a part in the lower energy consumption as the difference between the simulation and recorded data is slightly higher during winter months.

6.2.3.2.3 Domestic Hot Water and Solar Hot Water Systems

The solar thermal collection system pumping power consumption in the Test Facility is greater than the TRNSYS model predicts. The difference over the entire comparison time period is 17 kWhr which is 13.2% of the recorded solar collector pump power demand and 0.34% of the total recorded household demand. This difference is likely due to variations in the pump performance resulting from either different pumping efficiency or flow resistances. The deviation might also be due to differences in the solar collector control scheme resulting in lower pump run times in the simulation.

The TRNSYS simulation's domestic hot-water heater uses about 80% of the power that the actual hot water heater uses. The error over the entire comparison time period is 91 kWhr which is 19.1% of the recorded water heater demand and 1.8% of the total recorded household demand. Potential reasons for this difference include deviation of the simulated water heater efficiency from the actual water heater, differences in temperature set-points and tempering, and differences in the triggering of the electrical resistance strip heaters. It is also

possible that the solar thermal hot water system is not as efficient as the simulation predicts and is thus feeding the hot water heater with colder water. Lower solar thermal performance could be a result of dirt on solar thermal collectors or the heat exchanger underperforming. The relation between the solar thermal performance and heat exchanger effectiveness was further investigated and found to have minimal impact down to an effectiveness of 20%. It is also likely that the snow coverage seen during the analysis of the solar PV system also affects the solar thermal collectors. Snow would last longer on the solar thermal collectors as they are specifically insulated and designed to remove heat.

6.2.3.2.4 Solar PV

The TRNSYS model predicts more power generation than was recorded at the test facility. The difference over the entire comparison time period is 1037 kWhr, which is 19.9% of the recorded PV generation and 20.6% of the recorded household demand. Some of the difference in PV generation is likely attributable to the difference between the weather at the Test facility and the weather record used in the simulations.

In December, the TRNSYS simulation shows almost zero production corresponding with snow falls and snow cover at Washington-Dulles airport. The PV production recorded at the Test Facility shows some relation to the snow fall in the weather file but also indicates that there was additional snow fall at the Test Facility and that snow lasted longer on the Test Facility panels before melting. Over the comparison period, the recorded PV generation is lower than the amount predicted by the simulation and this discrepancy holds even on relatively clear days when the two results should be close. This observation indicates that the actual PV array is operating at a lower efficiency than the predicted. Potential reasons for this

include higher operating cell temperatures due to differences in ventilation setup, unanticipated shading, dust on the panels, and other issues with the PV equipment performance.

In December it appears there is a drop in the solar PV efficiency of 1.7% of the total received energy: 19.1 % recorded vs 20.8 % predicted. This 1.7% difference in efficiency accounts for 18% of the error in PV generation for December. Snow cover from the 7th to the 13th severely affected the recorded PV generation but not the recorded solar irradiation data at Washington-Dulles or the simulated generation. Assuming that the actual efficiency in December was the 19.1 %, this 5 day loss of generation accounts for 138 kW-hr of missed generation and 58% of the error for December. Adjusting for the lost generation and efficiency errors leaves only 27 kWhr of error in December, 5.6% of the recorded PV generation, unexplained. In July the apparent difference in the solar PV efficiency is again 1.7% of the total received energy: 17.2 % recorded vs 18.9 % predicted. This difference accounts for 50% of the error for July leaving 157 kW-hr of error in July, 11% of the recorded generation, unaccounted for.

The modeled efficiency with respect to cell temperature of the PV panels in use at the Test Faclity indicates that an efficiency drop of 1.7% requires a 20°C increase in cell temperature. While it the cells at the test facility are almost certainly running hotter than predicted by the TRNSYS model, it seems likely that other factors such as dust, lower than rated PV performance, or greater than anticipated inverter losses are contributing to the decreased efficiency.

6.2.3.3 Tuned House Model

Several changes were made to the Schedule Load and Lighting files in order to more closely match the Baseline house model to the recorded data. These changes resulted in the predicted electrical demand from the internal equipment demand and lighting loads matching the recorded electrical consumption. The reduced internal thermal loading resulted in increased heating requirements and decreased cooling energy requirements. The Tuned Baseline House model was used as the basis for the HVAC and Domestic Hot Water variations presented in Chapter 5.

6.3 Summary of Baseline House Model Variations

6.3.1 Domestic Hot Water Variations

Five variations of the domestic hot water system were simulated: The baseline system (solar thermal + heat pump), the baseline system with a larger solar storage tank, the baseline solar thermal with a tankless hot-water heater, a tankless hot water heater, and the baseline heat pump hot water heater with electric back up.

The baseline system was predicted to consume 10971 kWhr electric per year while losing 382 kWh in water supplied at a temperature hotter than the set point and failing to supply 76 kWhr to water delivered at a temperature under the set point. The baseline with larger solar storage tank was predicted to be the best option as it consumed 1.5% less energy while reducing the over temperature water supply losses to 344 kWhr and the under temperature water supply requirement to 72 kWhr.

The other three systems had significantly worse energy performance. The tankless hot water heater + solar thermal system faired best with an 89.3% increase in water heating electrical consumption and the elimination of under set point temperature water supply. The heat pump + aux system resulted in a 139% increase over the baseline and a tripling of under set point temperature water supplied. The tankless hot water only system performed the worst from an energy stand point with a predicted consumption of 381% of the baseline system. However the tankless system did result in the elimination of water supplied over and under the set point temperature.

6.3.2 Heat Recovery Ventilator vs. Enthalpy Recovery Ventilator

The use of an Enthalpy Recovery Core in place of a heat recovery core was predicted to result in a 5% increase in heating electrical demand, a 2.5% decrease in cooling electrical demand, and a 41.3% decrease in the dehumidification electrical demand. These changes resulted in a 2.5% decrease in total HVAC electrical demand and a slight shifting of demand towards the winter months. The ERV core had little impact on the HVAC systems ability to maintain the temperature set points.

6.3.3 HVAC Control Variations

Four HVAC control system variations were simulated: the baseline, no use of the auxiliary heater, no timed triggering of auxiliary heat (low temperature set point trigger only), and no timed triggering of any systems (set points only). In the baseline system all heating stages available to be turned on either by temperature set points or if a prior stage runs for sufficient time.

The control system variations all resulted in significant energy savings over the baseline simulation, mostly as a result of decreased use of the auxiliary electric resistance heater. Elimination of the use of the auxiliary heater resulted in a 20.5% reduction in HVAC electrical demand while only turning it on as a result of low control zone temperature, vs. with a timed trigger, resulted in a 19.2% reduction. Eliminating all of the timed triggers so that the stages are only triggered by the difference between the control zone and the set point temperatures resulted in a 22.1% reduction in HVAC energy use.

This energy reduction does come at some cost to comfort level but it is mostly the result of replacing short bursts of auxiliary heat with longer use of the HVAC heat pump. The control variations had a greater impact on the HVAC systems ability to follow the heating temperature set points, vs. cooling set points, due to the reduced use of the Auxiliary heater. In the most extreme case, elimination of the auxiliary heater resulted in an 8.2 C-day increase in the zone temperature difference below the heating temperature set point which is an increase of 30.4% over the baseline simulation. However the total, 36.8 C-day, is still below the baseline control zone temperature difference above the cooling set point temperature of 83.0 C-day.

6.3.4 HVAC Ground Source Heat Pumps

A ground source heat pump simulation was created and tested with 1, 2, 3, and 4 boreholes matched to those in the test facilities vertical ground loop heat exchanger. The test facility has three boreholes but the four borehole system is of interest because it is similar to the Test Facility in terms of total length of heat exchanger piping.

The ground source heat pump system energy savings varied substantially with the number of boreholes in the vertical ground loop heat exchanger. The single borehole system resulted in a 3.6 % increase in the HVAC electrical demand relative to the baseline simulation. The two and three borehole systems resulted in 11.3% and 17.5% decreases relative to the baseline. The four borehole system resulted in a 20.4% decrease in the HVAC electrical demand. The change from the baseline ASHP to the GSHP system resulted in minimal change to the HVAC systems ability to maintain the set point temperatures.

6.3.5 Battery Sizing Program Results

The results of all of the Baseline house model variations were analyzed using a MATLAB script 'BatterySizer.m' to determine the maximum power output required over the course of the simulation, the simulation time that the maximum power was required, the time of day that the maximum power occurs, the maximum battery capacity required during the simulation, the time at which the maximum battery capacity is required, and the time of day the maximum capacity is required.

The Baseline simulation required maximum power, 0.99 kW, and capacity, 277.6 kWhr. This much storage capacity is equivalent to 11.6 Nissan Leaf 24 kWhr battery packs at a battery cost of $63,800 (Nissan, 2014) or 4.6 Tesla Model S 60 kWhr battery packs at a battery cost of $46,000 (Tesla, 2014). In terms of lead acid batteries this is equivalent to 116 deep cycle 2.4 kWhr (200 Ahr, 12 V) Key Power storage batteries for an estimated battery cost of $22,000 (Keypower Battery, 2014).

Both the maximum power and maximum capacity requirements are necessary in December of 2013 and are heavily dependent on the HVAC loads. As these results are so heavily dependent on the HVAC loads, the addition of more solar thermal hot water capacity in the Baseline w/120 gal SHW Tank simulation had no impact. For the Tankless DHW Heater + SHW, Tankless DHW Heater Only, and Heat Pump DHW Heater + Aux simulations the power and capacity requirements increased substantially: the maximum power requirements for the Tankless DHW Heater + SHW and Tankless DHW Heater Only simulations were almost 250% larger than the maximum power requirement of the Baseline simulation.

The Enthalpy Recovery Core simulation is nearly identical to the baseline simulation but has a 1.6% larger battery capacity requirement. The single borehole ground source heat pump simulation has resulted in increased power and capacity requirements, 1.11 kW and 313 kWhr, relative to the baseline. The other GSHP simulations show identical maximum power requirements of 0.95 kW and decreasing maximum capacity requirements from 297.4 to 285.7 kWhr. All three of the control variations investigated resulted in almost identical battery requirements, 0.87 kW and 209 kWhr. These requirements are significantly lower than for the Baseline simulation.

The time of day at which the simulation predicts maximum power varies based on whether the HVAC or DHW system is dominating the power use. However the maximum power is always at night when there is no solar PV generation and often in the early hours of the morning when the occupant loads become active. The time of day when the maximum storage capacity is required does not vary and is always shortly after dawn when the solar PV generation equals the total household power demand.

6.3.6 Recommendation for Decreasing Test Facility Energy Use

In order to achieve the largest energy reduction in the Test Facility, the recommendations from this study is to use the 120 gal solar hot water storage tank, swap the core of the heat recovery ventilator for the enthalpy recovery core, use the full vertical ground loop heat exchanger, and eliminate the timed controls from the HVAC control system. The largest, and presumably easiest, savings are predicted to result from eliminating the timed triggers from the HVAC system and only using temperature set point triggers. The next largest savings are from switching to a ground source heat pump and vertical bore field. Due to drilling costs this option is much more expensive in new construction. Swapping the HRV core, though small in impact, is also likely to be economical.

6.4 Future Work

The overall objective of this project is to investigate energy saving equipment configurations and control strategies for high efficiency residential buildings and specifically ones which can be implemented in the NZERTF. The following plan outlines the future research activities and how they will contribute to that goal.

6.4.1 House Model Tuning

Though the TRNSYS Baseline House model does a fairly good job of predicting the electrical energy demands of the NZERTF, there are several aspects which could be significantly improved in order to match the Test Facility better. The scheduled load and lighting files should be changed to the recorded scheduled load and lighting power consumption data. The HRV and HVAC heat-pump performances could be modified to match the recorded data from the test facility. These two systems could also be updated to

include their respective defrost cycles. The HVAC control system could then be better tuned to match the simulation and experimental HVAC system run times. The Solar PV array model could be improved but this would require additional information about the weather at the test facility, solar cell temperature data corresponding with the weather data, and a change to the solar PV model to include the effects of persistent snow cover. The domestic hot water and solar hot water systems could also be tuned but this requires more detailed data on equipment run times and water temperatures in the system.

6.4.2 House Envelope Model Additions

The Test Facility has a number of additional systems and potential system variations which were not modeled or studied in this project. The basement, Zone 1, has a currently unused radiant heating system installed in the floor which could be added to the TRNBuild model and then the TRNSYS Multizone Building component. The radiant heating system would be connected to the domestic hot water system and would likely change the utility and economics of the solar hot water collectors. The attic and basement, zones 4 and 1, are also subject to some conditioning through air exchange with the other zones which is currently not modeled.

There are also a number of potential equipment configurations which could be of interest. These include switch from an air source heat pump to a ground source heat pump and GLHX, electric or gas heating and independent air conditioner, and use of the heat-pump de-superheater to supply some of the domestic hot water heating requirement.

6.4.2.1 Additional Ground Loop Heat Exchanger Models

The Test Facility currently has three ground loop heat exchangers installed: the vertical bore-field, the horizontal field, and the slinky. Only the vertical bore field was examined in this project. The development of simulations of the ground heat exchangers and calibration with data from the ground thermal conductivity test and ground response tests performed at the Test Facility would allow these GLHXs to be tested in Baseline house model variations to explore their impacts on the HVAC energy consumption. The process of calibrating GLHX TRNSYS models is now documented in Chapter 3.

6.4.2.2 Changes to the HVAC control System

The HVAC control system currently in place at the Test Facility is not necessarily the ideal system and, even in its current form, could likely be optimized to better balance energy consumption and comfort levels. This effort would require modification of the Thermostat Algorithms to allow external modification by MATLAB or TRNOpt and better comfort level tracking. Once these were implemented the exact time delays and temperature set-points could be automatically optimized. Variations in the form of the control system, such as independent zone temperature control and occupant triggered heating and cooling, could also be explored. Another interesting use of the HVAC and hot water control system is demand response and peak energy shaving. In this configuration the control systems would attempt to maintain the house or water supply at comfortable comfort levels while using the thermal mass of the house or water storage tanks as storage to shift the time of energy consumption away from either the grid's peak power demand or towards the Test Facilities peak solar production.

References

Air, I., & Units, H. (n.d.). F1 Series.

Austin, W. A. (1995). Thesis: DEVELOPMENT OF AN IN SITU SYSTEM FOR MEASURING GROUND THERMAL PROPERTIES.

Austin, W. A. (2000). Paper: Development of an In-Situ System and Analysis Procedure for Measuring Ground Thermal Properties, *106*(1), 365–379.

Bandos, T. V., Montero, Á., Fernández de Córdoba, P., & Urchueguía, J. F. (2011). Improving parameter estimates obtained from thermal response tests: Effect of ambient air temperature variations. *Geothermics*, *40*(2), 136–143. doi:10.1016/j.geothermics.2011.02.003

Beier, R. a., Smith, M. D., & Spitler, J. D. (2011). Reference data sets for vertical borehole ground heat exchanger models and thermal response test analysis. *Geothermics*, *40*(1), 79–85. doi:10.1016/j.geothermics.2010.12.007

Borinaga-Treviño, R., Pascual-Muñoz, P., Castro-Fresno, D., & Blanco-Fernandez, E. (2013). Borehole thermal response and thermal resistance of four different grouting materials measured with a TRT. *Applied Thermal Engineering*, *53*(1), 13–20. doi:10.1016/j.applthermaleng.2012.12.036

Boyd, M. (2014). *2013 NZERTF Simulation Weather Data File*. Gaithursburg Md.

Bozzoli, F., Pagliarini, G., Rainieri, S., & Schiavi, L. (2011). Estimation of soil and grout thermal properties through a TSPEP (two-step parameter estimation procedure) applied to TRT (thermal response test) data. *Energy*, *36*(2), 839–846. doi:10.1016/j.energy.2010.12.031

Building Science Corporation. (2007). Guide to Insulating Sheathing.

Building Science Corporation. (2009). *Net Zero Energy Residential Test Facility As Built Architectural Plan*.

Building Science Corporation. (2011). Strategy Guideline: Advanced Construction Documentation Recommendations for High Performance Homes.

Certificate of Product Ratings. (2014), 5548167.

Design, R., Range, E. P., Use, C., Efficiency, H., Cost, R. I., & Aesthetics, A. (n.d.). STRING INVERTERS Reliable and Robust Design.

Duffie, J. A., & Beckman, W. A. (2012). *Solar Engineering of Thermal Processes* (4th ed.). Wiley. Retrieved from http://books.google.com/books/about/Solar_Engineering_of_Thermal_Processes.html?id=w0QzhrBV21gC

Engineering Toolbox. (2009). *Material characteristics*.

Eskilson, P. (1987). *Thermal analysis of heat extraction boreholes*. University of Lund.

Fujii, H., Okubo, H., Nishi, K., Itoi, R., Ohyama, K., & Shibata, K. (2009). An improved thermal response test for U-tube ground heat exchanger based on optical fiber thermometers. *Geothermics*, *38*(4), 399–406. doi:10.1016/j.geothermics.2009.06.002

Gehlin, S. (2002). Thermal Response Test. *Lulea University Of Technology*, (DOCTORAL THESIS), 1402–1544.

Gelder, G. J. Van, Spitler, J. D., & Witte, H. J. L. (2002). In Situ Measurement of Ground Thermal Conductivity : A Dutch Perspective. *ASHRAE*, *108*.

Grimsrud, S. M. (1980). Measurement of Infiltration Using Fan Pressurization and Weather Data, *October*.

Gupta, H. K. (ed. . (2011). *"Encyclopedia of Solid Earth Geophysics."* Springer.

Gustafsson, A.-M., & Westerlund, L. (2011). Heat extraction thermal response test in groundwater-filled borehole heat exchanger Investigation of the borehole thermal resistance. *Renewable Energy*, *36*(9), 2388–2394. doi:10.1016/j.renene.2010.12.023

Heliodyne. (n.d.). HPAK SYSTEMS INSTALLATIION GUIDE v2.1.1.

HellStrom, G. (1989). *Duct ground heat storage model manual for computer code*. University of Lund.

HUBBELL. (2012). *Installation, Operation, and Maintenence Manual for BASE MODEL " PBX ."* STRATFORD, CT. Retrieved from http://www.hubbellheaters.com/ --

Katsura, T., Nagano, K., & Takeda, S. (2008). Method of calculation of the ground temperature for multiple ground heat exchangers. *Applied Thermal Engineering*, *28*(14-15), 1995–2004. doi:10.1016/j.applthermaleng.2007.12.013

Klein, S. (2013). PV Reference Parameter Determination.

Klein, S. A., Duffie, J. A., & Beckman, W. A. (1974). Transient Considerations of Flat-Plate Solar Collectors. *J. Eng. Gas Turbines Power*, (96), 109–113.

Klein, S A, Beckman, W. A., Mitchell, J. W., Duffie, J. A., Thornton, J W, Mitchell, J. C., et al. (2012). TRNSYS, A Transient System Simulation Program, User's Manual. Solar Energy Laboratory, University of Wisconsin.

Kneifel, J. D. (2012a). Annual Whole Building Energy Simulation of the NIST Net Zero Energy Residential Test Facility Design.

Kneifel, J. D. (2012b). NIST NZE HOUSE EnergyPlus Simulation.

Lamarche, L., & Beauchamp, B. (2007). A new contribution to the finite line-source model for geothermal boreholes. *Energy and Buildings*, *39*(2), 188–198. doi:10.1016/j.enbuild.2006.06.003

Lamarche, L., Kajl, S., & Beauchamp, B. (2010). A review of methods to evaluate borehole thermal resistances in geothermal heat-pump systems. *Geothermics*, *39*(2), 187–200. doi:10.1016/j.geothermics.2010.03.003

LIOS. (2013). *State-of-the-art Temperature Measurement System*. *Lios Technology*. Retrieved from http://www.lios-tech.com/Menu/Technology

Liu, X. (2010). *Assessment of National Benefits from Retrofitting Existing Single-Family Homes with Ground Source Heat Pump Systems*. Energy and Transportation Science Division Oak Ridge National Laboratory.

NREL. (n.d.). TMY Data File for Washington-Dulled.

Oak Ridge National Lab: Building Technologies Research & Integration Center. (n.d.). *Autotune*. Retrieved from http://rsc.ornl.gov/autotune/?q=content/autotune

Pertzborn, A. (2012). Understanding DST.

Products, A. C. (2014). AAON Coil Products , Inc ., (903).

Raymond, J., Therrien, R., Gosselin, L., & Lefebvre, R. (2011). A review of thermal response test analysis using pumping test concepts. *Ground Water*, *49*(6), 932–45. doi:10.1111/j.1745-6584.2010.00791.x

Robertson, E. C. (1988). THERMAL PROPERTIES OF ROCKS. *UNITED STATES DEPARTMENT OF THE INTERIOR GEOLOGICAL SURVEY*.

Roth, P., Georgiev, A., Busso, A., & Barraza, E. (2004). First in situ determination of ground and borehole thermal properties in Latin America. *Renewable Energy*, *29*(12), 1947–1963. doi:10.1016/j.renene.2004.02.014

Sanyal, J., & New, J. (2013). Simulation and big data challenges in tuning building energy models. *2013 Workshop on Modeling and Simulation of Cyber-Physical Energy Systems (MSCPES)*, 1–6. doi:10.1109/MSCPES.2013.6623320

SCHNABEL ENGINEERING. (2010a). *Conductivity Test MD-Gaithersburg-4-9-10-RawData.xls*.

SCHNABEL ENGINEERING. (2010b). GEOTECHNICAL REPORT Geothermal Test Results Net Zero Energy Residential Test Facility National Institute of Standards and Technology (NIST).

SCHNABEL ENGINEERING. (2010c). GEOTECHNICAL REPORT REVISION NO . 1 NET ZERO ENERGY RESIDENTIAL TEST FACILITY NATIONAL INSITUTE OF STANDARDS AND TECHNOLOGY (NIST), (1).

Shonder, J. A., & Beck, J. V. (2000). *A New Method to Determine the Thermal Properties of Soil Formations from In Situ Field Tests*.

Shonder, J. A., Thornton, J., & Hughes, P. J. (2001). Selecting the Design Entering Water Temperature for Vertical Geothermal Heat Pumps in Cooling-Dominated Applications. *ASHRAE*, *Annual Mee*.

Signorelli, S., Bassetti, S., Pahud, D., & Kohl, T. (2007). Numerical evaluation of thermal response tests. *Geothermics*, *36*(2), 141–166. doi:10.1016/j.geothermics.2006.10.006

Skye, H. (2013). 2013-01-25 and 2013-04-01 Vertical-Loop-TRT-Test_Rev-23 (simplified).

Skye, H., & NIST. (2012). Narrative Schedule Monday V2.

Solar Rating and Certification Corporation. (2011). SOLAR COLLECTOR CERTIFICATION AND RATING 2010115A.

SotoW., D., Klein, S. a. A., Beckman, W. a. A., & De Soto, W. (2005). Improvement and validation of a model for photovoltaic array performance. *Solar Energy*, *80*, 78–88. doi:10.1016/j.solener.2005.06.010

Specification Catalog. (n.d.), 2–6.

Taylor, P., House, M., Street, M., Wt, L., Rainieri, S., Bozzoli, F., & Pagliarini, G. (2011). Modeling approaches applied to the thermal response test : A critical review of the literature. *HVAC&R Research*, (June 2013), 37–41. doi:10.1080/10789669.2011.610282

Thermal Energy System Specialists LLC. (2012). TRNSYS: Transient System Simulation Software.

TOTAL _ Capacity _ Btu / h. (2013), (July), 32471.

Venmar. (2014). Heat recovery ventilator, 4–5.

Witte, H. J. L. (2013). Error analysis of thermal response tests. *Applied Energy*, *109*, 302–311. doi:10.1016/j.apenergy.2012.11.060

Yang, H., Cui, P., & Fang, Z. (2010). Vertical-borehole ground-coupled heat pumps: A review of models and systems. *Applied Energy*, *87*(1), 16–27. doi:10.1016/j.apenergy.2009.04.038

Yavuzturk, C. (1999). A Transient Two-Dimensional Finite Volume Model for the Simulation of Vertical U- Tube Ground Heat Exchangers. *ASHRAE Transactions*, *M*(2), 465–474.

Appendix A. Vertical Bore-field Diagrams

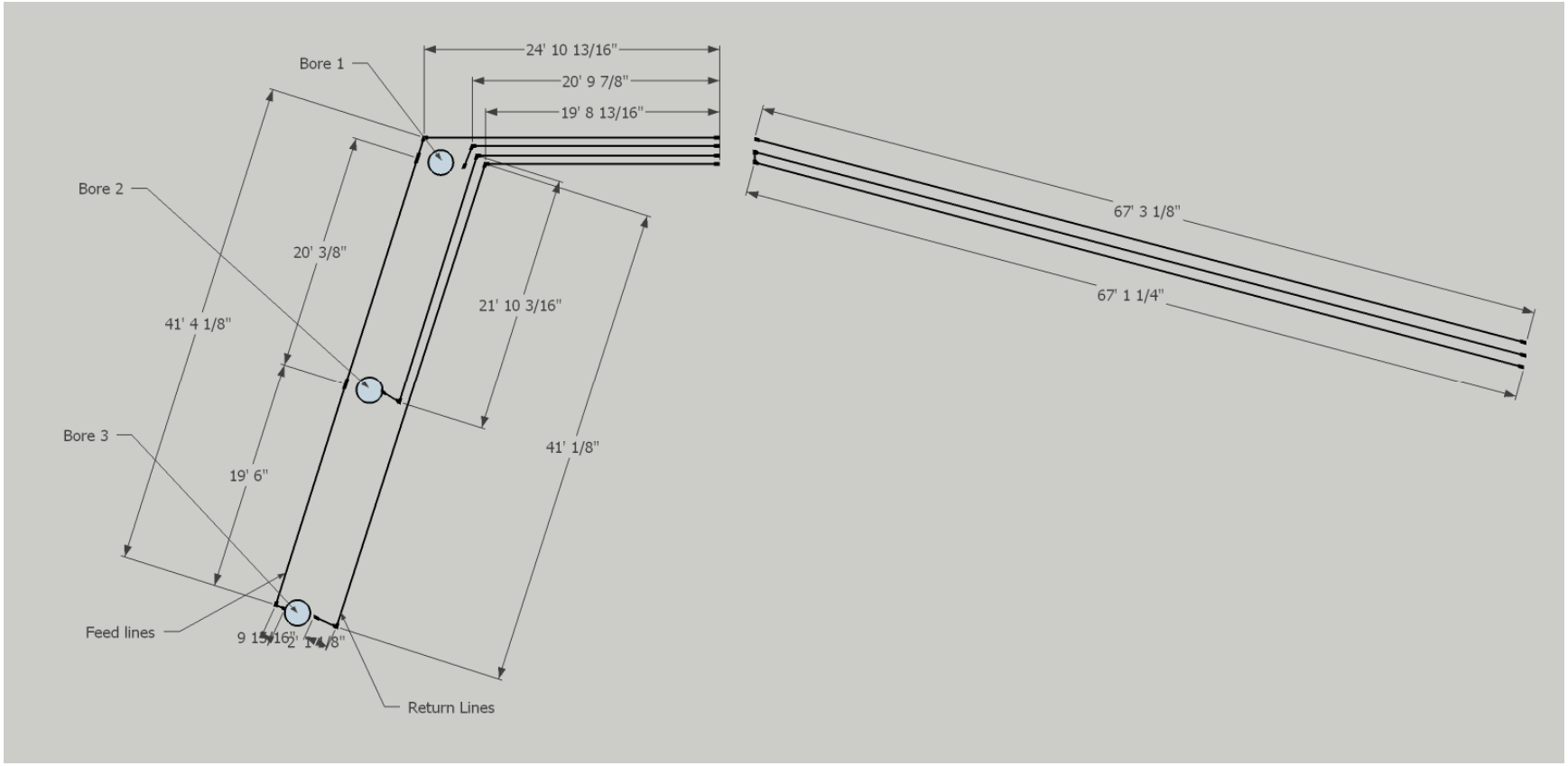

Figure A-1: Borefield Lengths diagram (generated from As Built diagrams using Google Sketchup)

Appendix B. Vertical Bore-field Diagrams Cont.

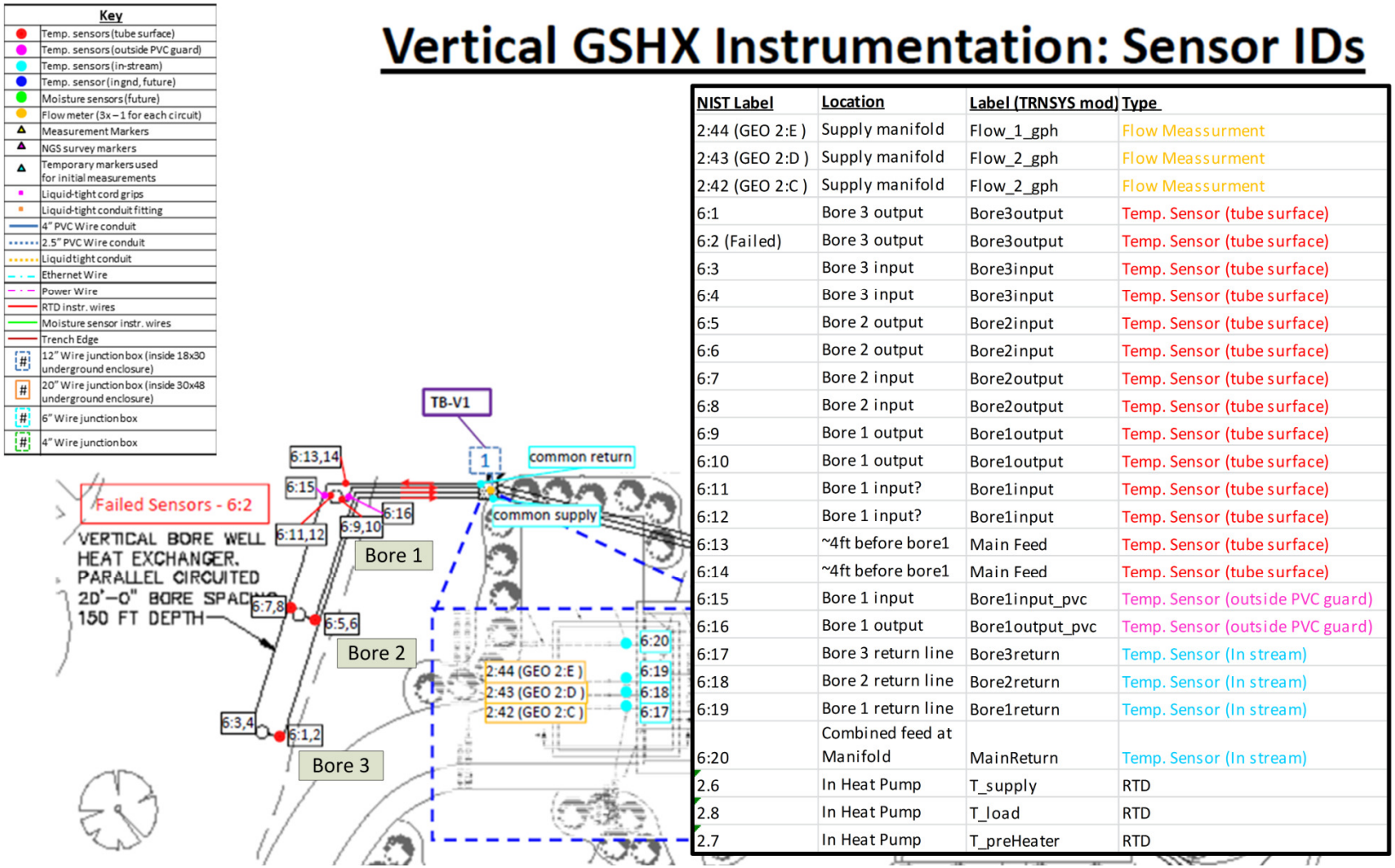

NIST Label	Location	Label (TRNSYS mod)	Type
2:44 (GEO 2:E)	Supply manifold	Flow_1_gph	Flow Meassurment
2:43 (GEO 2:D)	Supply manifold	Flow_2_gph	Flow Meassurment
2:42 (GEO 2:C)	Supply manifold	Flow_2_gph	Flow Meassurment
6:1	Bore 3 output	Bore3output	Temp. Sensor (tube surface)
6:2 (Failed)	Bore 3 output	Bore3output	Temp. Sensor (tube surface)
6:3	Bore 3 input	Bore3input	Temp. Sensor (tube surface)
6:4	Bore 3 input	Bore3input	Temp. Sensor (tube surface)
6:5	Bore 2 output	Bore2input	Temp. Sensor (tube surface)
6:6	Bore 2 output	Bore2input	Temp. Sensor (tube surface)
6:7	Bore 2 input	Bore2output	Temp. Sensor (tube surface)
6:8	Bore 2 input	Bore2output	Temp. Sensor (tube surface)
6:9	Bore 1 output	Bore1output	Temp. Sensor (tube surface)
6:10	Bore 1 output	Bore1output	Temp. Sensor (tube surface)
6:11	Bore 1 input?	Bore1input	Temp. Sensor (tube surface)
6:12	Bore 1 input?	Bore1input	Temp. Sensor (tube surface)
6:13	~4ft before bore1	Main Feed	Temp. Sensor (tube surface)
6:14	~4ft before bore1	Main Feed	Temp. Sensor (tube surface)
6:15	Bore 1 input	Bore1input_pvc	Temp. Sensor (outside PVC guard)
6:16	Bore 1 output	Bore1output_pvc	Temp. Sensor (outside PVC guard)
6:17	Bore 3 return line	Bore3return	Temp. Sensor (In stream)
6:18	Bore 2 return line	Bore2return	Temp. Sensor (In stream)
6:19	Bore 1 return line	Bore1return	Temp. Sensor (In stream)
6:20	Combined feed at Manifold	MainReturn	Temp. Sensor (In stream)
2.6	In Heat Pump	T_supply	RTD
2.8	In Heat Pump	T_load	RTD
2.7	In Heat Pump	T_preHeater	RTD

Figure B-1: Temperature Sensor Labeling Chart

Appendix C. Sensor/TRNSYS Variable Naming Chart

NIST Label	Old TRNSYS Label	NIST Name	New TRNSYS Label	Type
2:44 (GEO 2:E)	Flow_1_gph	Flow Rate Leg 3	Flow_Leg3_gph	Flow Meassurment
2:43 (GEO 2:D)	Flow_2_gph	Flow Rate Leg 2	Flow_Leg2_gph	Flow Meassurment
2:42 (GEO 2:C)	Flow_3_gph	Flow Rate Leg 1	Flow_Leg1_gph	Flow Meassurment
6:1	Bore3output	In Ground Leg 1 Supply	T_Leg1_Supply	Temp. Sensor (tube surface)
6:2 (Failed)	Bore3output	In Ground Leg 1 Supply	T_Leg1_Supply	Temp. Sensor (tube surface)
6:3	Bore3input	In Ground Leg 1 Return	T_Leg1_Return	Temp. Sensor (tube surface)
6:4	Bore3input	In Ground Leg 1 Return	T_Leg1_Return	Temp. Sensor (tube surface)
6:5	Bore2input	In Ground Leg 2 Supply	T_Leg2_Supply	Temp. Sensor (tube surface)
6:6	Bore2input	In Ground Leg 2 Supply	T_Leg2_Supply	Temp. Sensor (tube surface)
6:7	Bore2output	In Ground Leg 2 Return	T_Leg2_Return	Temp. Sensor (tube surface)
6:8	Bore2output	In Ground Leg 2 Return	T_Leg2_Return	Temp. Sensor (tube surface)
6:9	Bore1output	In Ground Leg 3 Supply	T_Leg3_Supply	Temp. Sensor (tube surface)
6:10	Bore1output	In Ground Leg 3 Supply	T_Leg3_Supply	Temp. Sensor (tube surface)
6:11	Bore1input	In Ground Leg 3 Return	T_Leg3_Return	Temp. Sensor (tube surface)
6:12	Bore1input	In Ground Leg 3 Return	T_Leg3_Return	Temp. Sensor (tube surface)
6:13	Main Feed	In Ground Common Return	T_Common_Return	Temp. Sensor (tube surface)
6:14	Main Feed	In Ground Common Return	T_Common_Return	Temp. Sensor (tube surface)
6:15	Bore1input_pvc	In Ground Leg 3 Return Uninsulated	T_Leg3_Return_PVC	Temp. Sensor (outside PVC guard/uninsulated)
6:16	Bore1output_pvc	In Ground Leg 3 Supply Uninsulated	T_Leg3_Supply_PVC	Temp. Sensor (outside PVC guard/uninsulated)
6:17	Bore3return	Header Box Leg 1 Supply	T_Leg1_Supply_Header	Temp. Sensor (In stream)
6:18	Bore2return	Header Box Leg 2 Supply	T_Leg2_Supply_Header	Temp. Sensor (In stream)
6:19	Bore1return	Header Box Leg 3 Supply	T_Leg3_Supply_Header	Temp. Sensor (In stream)
6:20	MainReturn	Header Box Leg Common Return	T_Common_Return_Header	Temp. Sensor (In stream)
2.6	T_supply	In Heat Pump	T_Field_Supply	RTD
2.8	T_load	In Heat Pump	T_Field_Return	RTD
2.7	T_preHeater	In Heat Pump	T_preHeater	RTD

Figure C-1: Temperature Sensor Labeling Chart.

Appendix D. Diagram of GLHX Parameter Determination Code

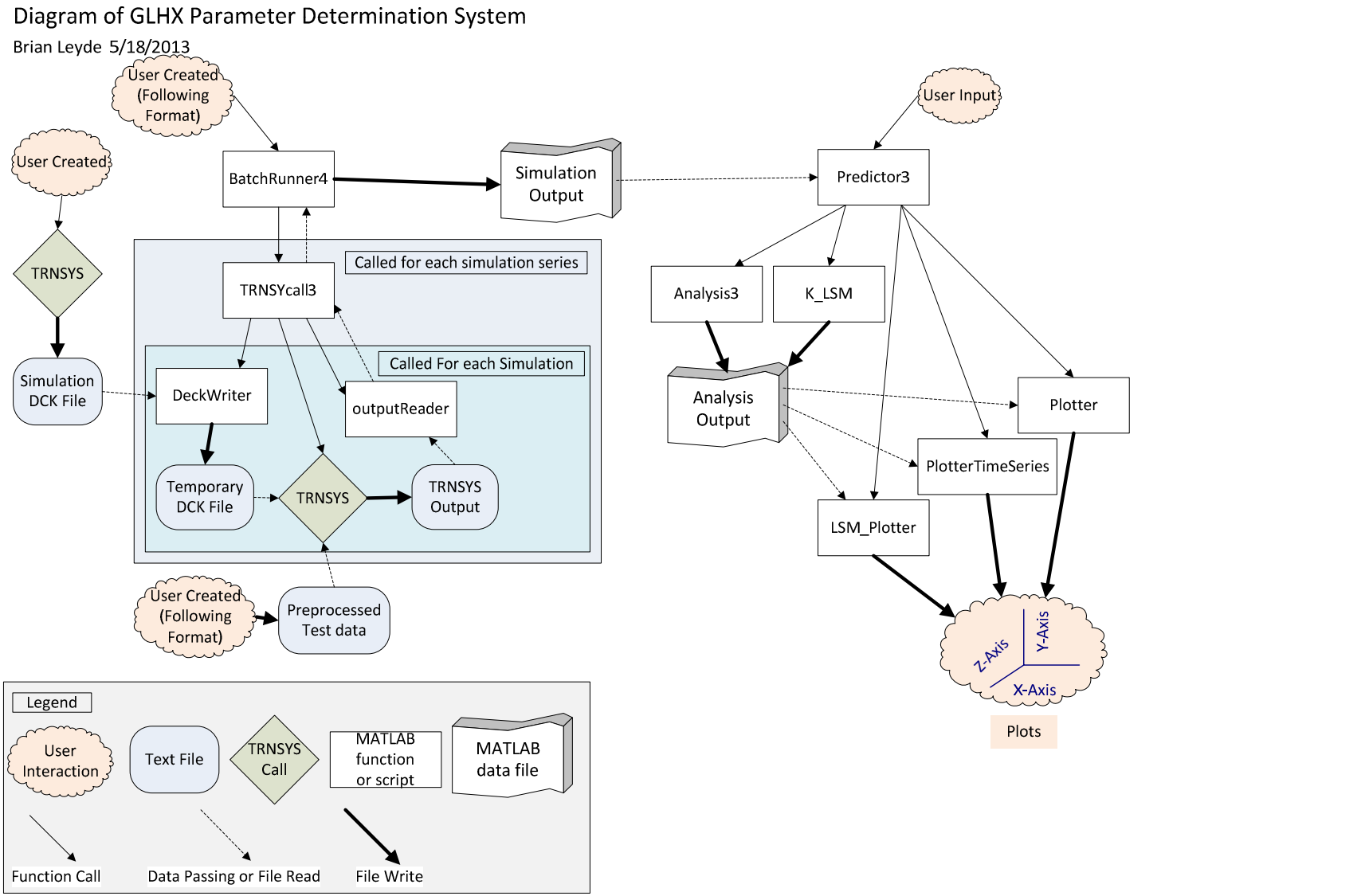

Appendix E. Sample Weekly temperature profile

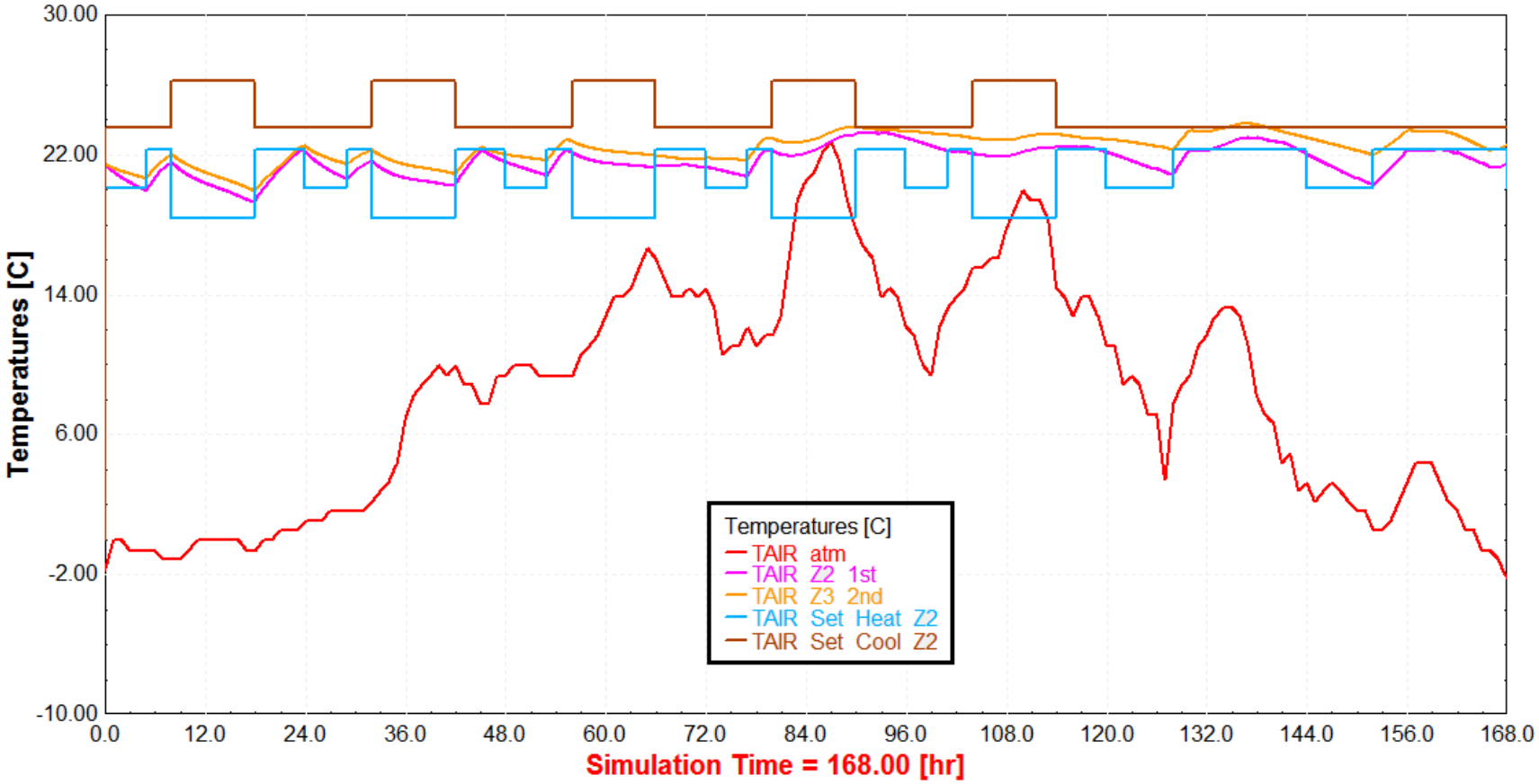

Figure E-1: Temperature Profiles and Heating Rate (negative value indicates heating) for modeled first week of January.

It is interesting to note the response rates of the temperatures on each floor as this is a potential calibration tool.

Appendix F. Description of MATLAB Files

Name	Description
Initial Ground Loop Studies	
Analysis3.m	This function takes the experimental data, the simulated data, which columns in the simulated date to look at, and the time range/time step. It runs all of the error computations and stores them in another MATLAB variable: AnnOutput
BatchRunner4.m	This script allows multiple parametric simulations runs to be done one after the other in order to facilitate overnight simulations. The first section section specifies the simulation time step, the variables being changed, the argument range for those variables, the file paths for input and output and the number of header lines in the input file (uses outputReader.m). The second section specifies specific parametric runs. The section specifies the TRNSYS simulation Name, time step, and the run number (run) which is used to keep the output files separate.
DeckWriter.m	DeckWriter takes in the name of a TRNSY dck file (or any other text file really…), a set of variable names, and matching set of variable arguments. It then find the variable assignment statement (var name = value) and changes the variable value.
K_LSM.m	This script determines the line source model predicted formation conductivity value for the original experimental data and the simulated data from each run of a parameteric set of TRT simulations.
Keep.m	This Function clears all variables except those specified to be kept. I downloaded this one from then MATLAB data base.
LSM_Plotter.m	This script takes the variables ArgsOut, which is stored in the workspace as the output from Batchrunner.m, Var1 and Var2, which are set in plotting section of Predictor.m, k_lsm which is generated in K_LSM_script.m, and tStart, tEnd, tLength which are set by Predictor.m as to determine time windows. It outputs a series of surface meshes plotting the Line Source model K prediction error. (Each simulation run's LSM K value vs Experimental LSM K Value)

outputReader.m	This function reads off a tab delimited text file with a text header lines and numerical data. The file can have a variable number of header lines. All instances of outputReader should be updated to outputReader2.m
outputReader2.m	This function reads off a tab delimited text file with a text header lines and numerical data. The file can have a variable number of header lines, a specified line containing the variable names, and a specified end line.
Plotter.m	This script takes the variables ArgsOut, which is stored in the workspace as the output from Batchrunner.m, Var1 and Var2, which are set in plotting section of Predictor.m, AnnOutput, which is generated in Predictor.m by a call to Analysis.m, and tStart, tEnd, tLength which are set by Predictor.m as to determine time windows. It outputs surface mesh, overlapping contours, one for each time window, centered around zero, and auto-spaced contours.
PlotterTimeSeries.m	This script takes the variables ArgsOut, which is stored in the workspace as the output from Batchrunner.m, Var1 and Var2, which are set in plotting section of Predictor.m, AnnOutput, which is generated in Predictor.m by a call to Analysis.m, and tStart, tEnd, tLength which are set by Predictor.m as to determine time windows. It outputs a series of surface meshes showing how the temperature profiles vary with time and Variable 1 (Var1)
Predictor3.m	This script takes the output file from BatchRunner4.m and calls analysis3.m to calculate error meassures, and then a series of plotting functions to display the error meassures calculated. The first section specifies settings for different TRNSYS models and TRT data sets and can be turned on and off via commenting.
TRNSYScall3.m	TRNSYScall3, generates a linear distribution of input values (2d grid for 2 variables, 3d grid for 3, etc) calls the other functions, runs TRNSYS, processes the output and the returns a matrix of values run and results. It takes in the names of the TRNSYS deck file to be run, a vector with the names of the variables to be changed, vectors of the minimum and maximum values for each variable and the number of divisions within that range to run. It also takes in the column positions of the desired data in the output file and the number of header lines. The function generates a series of all the combinations of the variable values.

TRNSYS Optimization Program	
TRNSYS_GLHX_ObjFunc.m	This function is the objective function for the TRNSYSoptimization routine. It is a wrapper for TRNSYSrunner and a sum of sqare errors calculation. The function takes in model arguments from the optimizer and outputs the error measurement.
TRNSYSoptimizer.m	This function uses the MATLAB fminsearch function and the TRNSYS_GLHX_ObjFunc.m to minimize the sum square of errors (set in the objective Function) between a TRNSYS simulation and a set of experimental data. Runs optimization function and returns optimum parameters.
TRNSYSoptimizer_batch.m	This script is set up to iterate through all 7 TRT test models and optimize their model parameters using the TRNSYSoptimizer function.
TRNSYSrunner.m	This function takes inputs similar to TRNSYScaller: fNameIn, vars, Args, headerline. It then calls deck writer to make a new .dck file, calls TRNSYS through windows to run the .dck, calls the reader to read off the results, formats the results and passes them back.
Long Time Scale Gound Loop Studies	
LongStudy_Analysis1.m	This script reads through the TRNSYS borehole simulation output file in order to determine the max, min, and ave entering water temperatures for that simulation.
HVAC Studies	
BatterySizer.m	This Script loads the electrical.out file. Finds the column for total net power consumption and uses that data to determine the max electrical power and capacity requirements as well as the simulation time at which they occur.
DataIntegrator.m	This script loads the processed daily heat pump data files from the test facilities HVAC HP and then averages and sums the data for every minute. The resulting averaged and summed data sets are then loaded into the variable 'output' for use with the outputWriter funciton.
DataLoader.m	This script loads all of the data in Electrical.out, Water.out, Thermal Loads.out, and WeatherData.out into the variables Header_Elec, Data_Elec, Header_Water, Data_Water, Header_Therm, Data_Therm, Header_Weather, and Data_Weather.
End_Sim_Script.m	This Script runs in order: DataLoader, outputCutter, and BatterySizer
linecount.m	This Function determines the number of lines in a text file

ouputCutter.m	This Script takes the variables Header_Elec, Data_Elec, Header_Water, Data_Water, Header_Therm, Data_Therm, Header_Weather, and Data_Weather and samples the first days of december and july. The sampling periods are adjustable (ie can get the middle week of october etc) and the samples are saved as new output files with names following the form of Electrical_cutjul.out.
outputWriter.m	This function takes a header variable and a matching data variable such as Header_elec and Data_elec and writes them to a tab delimited text file. This allows samples of larger data sets to be copied into the Excel Spreed sheets used for graphing without modifying the variable order or spacing of the excel sheets.